Impact assessment of global change on wetland-catchment interactions in a tropical East African catchment

Dissertation
zur
Erlangung des Doktorgrades (Dr.rer.nat.)
der
Mathematisch-Naturwissenschaftlichen Fakultät
der
Rheinischen Friedrich-Wilhelms-Universität Bonn

vorgelegt von

Kristian Näschen
aus
Gummersbach, Deutschland
Bonn, Dezember 2019

Angefertigt mit Genehmigung der Mathematisch-Naturwissenschaftlichen Fakultät der Rheinischen Friedrich-Wilhelms-Universität Bonn

1. Gutachter	:Prof. Dr. Bernd Diekkrüger
2. Gutachterin	:Prof. Dr. Mariele Evers
Tag der mündlichen Prüfung	:19.02.2020
Erscheinungsjahr	:2020

I. Acknowledgements

It is hard to find the adequate wording to thank all the people who supported, guided and accompanied me during the last years either scientifically or on a social level.

First of all I want to express my deep gratitude to my supervisor Prof. Bernd Diekkrüger, who was always available, on all channels – either personally or via Email to answer my questions or give feedback to my work. I truly appreciate your guidance, support and your friendly leadership! Secondly, I want to thank Prof. Mariele Evers for showing her trust in my work and for giving me the opportunity to continue my research in the Kilombero Catchment with a new perspective concerning human-water interactions. I value the opportunity to bring in my ideas and discuss them with you and the team. Thirdly, I want to thank Prof. Barbara Reichert and Prof. Thomas Heckelei for joining my doctoral committee, but also for interesting discussions either in Bonn or in Tanzania and Kenya, while visiting conferences and workshops.

I was and I am privileged to belong to two outstanding research groups that combine scientific expertise with a pleasant working atmosphere. In the Hydrology Research Group I want to give a special thanks to Dr. Constanze Leemhuis, who was a great tutor and an incredible support during the GlobE project. Another special thanks goes to Dr. Aymar Bossa, who introduced me to the SWAT model during my Diploma Thesis and helped me to crack some nuts with regard to some modeling issues. My Ugandan brother – Dr. Geofrey Gabiri – I will never forget our discussions in office and the time we spent outside academia. Tutaonana baadaye rafiki! A huge thanks also to Claudia Schepp – you were always there when help or assistance was needed despite your busy-schedule. My sincere thanks to all the other colleagues at the HRG namely Alexander Ahring, Dr. Thomas Cornelissen, Dr. Alexandre Danvi, Mouhamed Idrissou, Emmanuel Nkundimana, Dr. Felix Op de Hipt (master of ExtRemes!), Dr. Thomas Poméon, Dr. Inken Rabbel, Johannes Rosleff Sörensen, Gero Steup, Dr. Yacouba Yira, Fabian Weidt for enlightening discussions and several joyful activities and innumerable cups of coffee together. And of course a big thanks to all the guest researchers who broadened my horizon during many coffee break talks or in several presentations. My thanks goes to Dr. Djigbo Félicien Badou, Dr. Charlène Gaba, Dr. Jean Hounkpè, Dr. Djiby Sambou and Dr. Adama Touré. A special thanks goes to Dr. Britta Höllermann for your great support in the CRC and all the activities we planned and executed together. Without your help, this thesis still would have been work in progress. My sincere gratitude to all the other members of the Eco-Hydrology and Water Resources Management working group who gave me a warm welcome and whose company I enjoy every day. Thanks to Dr. Adrian Almoradie, Arne Claßen, Dr. Mariana Madruga de Brito, Rholan Houngue, Ivana and Milos Mirosavic, Joshua Ntajal, Dennis Schmiege, Nikola Schulte-Kellinghaus, Dörte Schultz, Dr. Linda Taft and Michelle Zülich.

I want to express my sincere gratitude to the whole GlobE Family. All of you made these last years to a unique and wonderful experience! However, I want to give a special thanks to Prof. Mathias Becker who guided the GlobE Team through all waters with a contagious enthusiasm and to Prof. Salome Misana who paved my way in Tanzania and guided me through all unknown administrative procedures.

For all the talks either about science or something completely different: Thanks a lot to Dr. Sonja Burghof, Kristina Grotelüschen, Susanne Hermes, Julius Kwesiga and Prof. Matthias Langensiepen. During my time at the GlobE project I had the pleasure to share my office with colleagues who became true friends – an extraordinary thanks to Dr. Miguel Alvarez, Kai Behn and Eike Kiene.

I owe many thanks to my research assistants and colleagues in Tanzania! Without your help and insights this work would be less valuable. I also want to thank my new colleagues at the CRC on Future Rural Africa – who constantly feed me with information from the ground and improve my understanding with regard to social science.

Furthermore, I want to thank the Co-Authors of my publications in this thesis from the Meteorology and Remote Sensing groups of the GlobE project Dr. Frank Thonfeld, Stefanie Steinbach, Dr. Roderick van der Linden and Larisa Seregina. I enjoyed, and still enjoy, the interdisciplinary work with you and I learned a lot during our joint work on several publications.

Last-but-one I want to thank my family and friends for their unconditional and tireless support. You are my foundation stone! Last but not least I want to express my deepest gratitude to my wife Christiane for your loving support through all the years. You were always there when I was in need for a companion outside of academia but also available for scientific discussions and to sharpen my wording. This piece of work is dedicated to you.

II. Abstract

Water is the key to sustainable development, especially in sub-Saharan Africa (SSA), where a large part of the population lives on subsistence farming. Reliable knowledge of available water resources therefore is an indispensable component of sustainable water resource management. An important tool for the management of water resources is hydrological modeling, which, depending on the model type, is capable to quantify water quantities spatially explicit and to predict water availability under changing conditions. The bottleneck for these simulations often is the lack of data availability, especially in sub-Saharan Africa. In recent decades, however, satellite data sources have been developed for hydrological modelling on different scales. The aim of this work is to develop a modeling framework for a meso-scale catchment area in Tanzania based on locally collected data and freely available satellite data sets. This model system should serve to better understand the hydrological processes in the catchment area with an emphasis on wetland-catchment interactions. At the same time the model should be able to estimate the availability of water resources under changing environmental conditions for the catchment area.

The Soil and Water Assessment Tool (SWAT) was applied to the Kilombero Catchment area in Tanzania, which, like many other East African catchments, is characterized by a general data shortage. Due to the lack of current discharge data, the model was calibrated for the period 1958-1965 (R^2 = 0.86, NSE = 0.85, KGE = 0.93) and validated from 1966-1970 (R^2 = 0.80, NSE = 0.80, KGE = 0.89) with the sequential uncertainty fitting algorithm (SUFI-2) at a daily resolution. The model results show the water-related dependency of the floodplain in the center of the catchment area on the base flow of the surrounding highland forests and savannas, especially in the dry season.

In addition, this study investigates the influence of climate change on water resources in the catchment area. To account for these changes, regional climate models of the Coordinated Regional Downscaling Experiment (CORDEX) Africa project were applied to investigate changes in climate patterns up to 2060 according to the RCP4.5 (representative concentration paths) and RCP8.5 scenarios. The SWAT model was used to investigate the impacts of climate change on water resources under different scenarios and model combinations. The climate models show a clear temperature increase, especially in the hot dry season, which further reinforces the pronounced differences between the dry and rainy seasons. This, together with changing precipitation patterns, leads to an intensification of hydrological extremes in the catchment area, e.g., more pronounced flooding in the rainy season and decreasing low flows in the dry season. Overall, the annual average values of water yield and surface runoff within the simulations increase by up to 61.6% and 67.8%, respectively, by 2060 compared to the historical simulations. The changes of the hydrological processes show a heterogeneous spatial-temporal pattern within the catchment area.

In many parts of sub-Saharan Africa and also in the study area, natural systems are being converted into agricultural land in order to feed the growing population. Therefore, this study additionally examines historical land use and land cover patterns as well as potential future land use and land cover patterns and their impacts on water resources in the catchment area. The Land Change Modeler (LCM) is used for the analysis and projection of land use patterns until 2030 and the SWAT model is then utilized to simulate the water balance under changing conditions. The results show that the low flow in the land use/land cover scenarios decreases by 6-8%, while the high flow in the combined land use/land cover scenarios increases by up to 84% considering also the climate scenarios. The impacts of climate change are therefore more pronounced than the impacts of changing land use/land cover patterns, but also

contain higher uncertainties and show different patterns in the climate model combinations applied in this study.

Within this study, a methodological approach was developed to quantify the impacts of land use/land cover patterns and climate change for data-scarce regions. The results and the methodology from this study thus contribute to the sustainable management of the investigated catchment area, as they show the effects of environmental changes on hydrological extremes (low flows and high flows) and additionally identify particularly sensitive subcatchments that are of essential importance for the preservation of the social-ecological system.

III. Zusammenfassung

Wasser ist der Schlüssel für eine nachhaltige Entwicklung. Das gilt insbesondere für Sub-Sahara Afrika (SSA), wo ein Großteil der Bevölkerung von der Subsistenzlandwirtschaft lebt. Verlässliche Kenntnisse zu verfügbaren Wasserressourcen sind daher unverzichtbarer Bestandteil eines nachhaltigen Wasserressourcenmanagements. Ein wichtiges Werkzeug zum Management von Wasserressourcen stellt die hydrologische Modellierung dar, welche, je nach Modelltyp, in der Lage ist, Wassermengen räumlich explizit zu quantifizieren und Prognosen für die Wasserverfügbarkeit unter sich verändernden Rahmenbedingungen zu stellen. Problematisch für die Modellierung ist jedoch die mangelhafte Verfügbarkeit von Daten, insbesondere in Sub-Sahara Afrika. In den letzten Jahrzenten sind jedoch vermehrt Datenquellen auf Satellitenbasis für die hydrologische Modellierung auf unterschiedlichen Skalen erschlossen worden. Ziel dieser Arbeit ist es, auf Basis von lokal erhobenen Daten und frei verfügbaren Datensätzen auf Satellitenbasis ein Modellsystem für ein mesoskaliges Einzugsgebiet in Tansania zu erstellen. Dieses Modellsystem soll dazu dienen, die hydrologischen Prozesse im Einzugsgebiet besser zu verstehen. Der Fokus liegt dabei insbesondere in der hydrologischen Interaktion der Überschwemmungsebene und dem umliegenden Hochland, die vom Großteil der Bevölkerung genutzt werden. Darüber hinaus soll die Verfügbarkeit von Wasserressourcen unter sich verändernden Umweltbedingungen für das Einzugsgebiet bewertet werden.

Hierzu wurde das „Soil and Water Assessment Tool“ (SWAT) auf das Kilombero-Einzugsgebiet in Tansania angewendet, das wie viele andere ostafrikanische Einzugsgebiete durch eine allgemeine Datenknappheit gekennzeichnet ist. Aufgrund des Fehlens aktueller Abflussdaten wurde das Modell für den Zeitraum von 1958-1965 (R^2 = 0,86, NSE = 0,85, KGE = 0,93) kalibriert und von 1966-1970 (R^2 = 0,80, NSE = 0,80, KGE = 0,89) mit dem „sequential uncertainty fitting algorithm“ (SUFI-2) in einer täglichen Auflösung validiert. Die Modellergebnisse zeigen die hydrologische Abhängigkeit der Überschwemmungsebene im Zentrum des Einzugsgebietes vom Basisabfluss der umliegenden Hochlandwälder und Savannen, insbesondere in der Trockenzeit.

Zusätzlich untersucht diese Studie den Einfluss des Klimawandels auf die Wasserressourcen im Einzugsgebiet. Um diesen Veränderungen Rechnung zu tragen, wurden regionale Klimamodelle des Coordinated Regional Downscaling Experiment (CORDEX) Africa Projekts angewandt, um Veränderungen der Klimamuster bis 2060 gemäß RCP4.5 (repräsentative Konzentrationswege) und RCP8.5 zu untersuchen. Das SWAT Modell wurde eingesetzt, um die Auswirkungen des Klimawandels auf die Wasserressourcen unter verschiedenen Szenarien und Klimamodellkombinationen zu untersuchen. Die Modellergebnisse zeigen einen klaren Temperaturanstieg, insbesondere in der heißen Trockenzeit, was die ausgeprägten Unterschiede der Trocken- und Regenzeit zusätzlich verstärkt. Dies führt, zusammen mit sich verändernden Niederschlagsmustern, zu einer Verschärfung hydrologischer Extreme im Einzugsgebiet, wie z.B. stärker ausgeprägten Überschwemmungen in der Regenzeit und abnehmenden Niedrigwassermengen in der Trockenzeit. Insgesamt erhöhen sich die jährlichen Durchschnittswerte des Gesamtabflusses und des Oberflächenabflusses innerhalb der Simulationen bis 2060 im Vergleich zu den historischen Simulationen um bis zu 61,6% bzw. 67,8%. Die Veränderungen der hydrologischen Prozesse zeigen insgesamt ein heterogenes räumlich-zeitliches Muster innerhalb des Einzugsgebietes auf.

Eine weitere wichtige Randbedingung für die Simulation von Wasserressourcen sind Landnutzungs-/Landbedeckungsmuster, die sich ebenfalls verändern. In vielen Teilen Sub-Sahara Afrikas und auch im Untersuchungsgebiet werden natürliche Systeme in landwirtschaftliche Flächen umgewandelt, um die

wachsende Bevölkerung zu ernähren. Diese Studie untersucht deshalb zusätzlich historische Landnutzungs-/Landbedeckungsmuster sowie potenzielle zukünftige Landnutzungs-/Landbedeckungsmuster und deren Auswirkungen auf die Wasserressourcen im Einzugsgebiet. Der Land Change Modeler (LCM) wird zur Analyse und Projektion von Landnutzungs-/Landbedeckungsmustern bis 2030 genutzt und das SWAT Modell anschließend zur Simulation des Wasserhaushalts unter den sich verändernden Bedingungen eingesetzt. Die Ergebnisse zeigen, dass die Niedrigabflüsse in den Landnutzungs-/Landbedeckungsmuster Szenarien um 6-8% zurückgehen, während die Hochwasserabflüsse in den kombinierten Landnutzungs-/Landbedeckungsmuster unter Einbezug der Klimaszenarien um bis zu 84% zunehmen. Die Auswirkungen des Klimawandels sind daher stärker ausgeprägt als die Auswirkungen von sich verändernden Landnutzungs-/Landbedeckungsmustern, enthalten aber auch höhere Unsicherheiten und zeigen, je nach Klimamodellkombination, auch unterschiedliche Muster bzgl. Niederschlag und resultierendem Abfluss.

Innerhalb dieser Studie wurde eine Methodik zur Quantifizierung der Auswirkungen von sich ändernden Landnutzungs-/Landbedeckungsmustern, sowie des Klimawandels für datenarme Regionen entwickelt. Die Ergebnisse und die entwickelte methodische Vorgehensweise tragen damit zum nachhaltigen Management des untersuchten Einzugsgebiets bei, da sie die Auswirkungen von Umweltveränderungen auf hydrologische Extreme (Niedrigwasser und Überschwemmungen) aufzeigen. Zusätzlich können besonders sensitive Teileinzugsgebiete identifiziert werden, die für die Erhaltung des sozio-ökologischen Systems von essentieller Bedeutung sind.

IV. Table of Contents

V. List of Figures

VI. List of Tables

VII. List of Abbreviations

ALPHA_BF	Base flow alpha factor (days)
BMBF	German Federal Ministry of Education and Research
CCCma	Canadian Centre for Climate Modelling and Analysis
CDF	Cumulative distribution function
CH_K1	Effective hydraulic conductivity in the tributary channel (mm/h)
CH_K2	Effective hydraulic conductivity in the main channel (mm/h)
CHIRPS	Climate Hazards Group Infrared Precipitation with Station data
CLMcom	Climate Limited-area Modelling Community
CMORPH	Climate Prediction Center Morphing Technique
CORDEX	Coordinated Regional Climate Downscaling Experiment
DEM	Digital Elevation Model
ENSO	El Niño–Southern Oscillation
EPCO	Plant uptake compensation factor
EPIC	Erosion-Productivity Impact Calculator
ESCO	Soil evaporation compensation factor
FAO	Food and Agricultural Organization
FDC	Flow Duration Curve
GCM	General Circulation Models
GDP	Gross domestic product
GEV	Generalized extreme value
GMLE	Generalized maximum likelihood estimation
GPCC	Global Precipitation and Climatology Center
GPDS	Global precipitation datasets
GRACE	Gravity Recovery and Climate Experiment
GRDC	Global Runoff Database
GW_DELAY	Groundwater delay time (days)
GW_REVAP	Groundwater “revap” coefficient
GWQMN	Threshold depth of water in the shallow aquifer for return flow to occur (mm)
HRU	Hydrologic Response Unit
HWSD	Harmonised World Soil Database
IOZM	Indian Ocean zonal mode
ITCZ	Intertropical Convergence Zone
IUCN	International Union for Conservation of Nature
IWRMDP	Integrated Water Resource Management Development Plan
KATRIN	Kilombero Agriculture Training and Research Institute
KGE	Kling-Gupta efficiency
LCM	Land Change Modeler
LULC	Land use and Land cover
LULCC	Land use and Land cover change
MERRA	Modern Era Retrospective-Analysis for Research and Applications
MLP	Multi-Layer Perceptron

MSS	Multispectral scanner
NDVI	Normalized Difference Vegetation Index
NDWI	Normalized Difference Water Index
NGO	Non-Governmental Organization
NSE	Nash-Sutcliffe efficiency
PBIAS	Percent bias
PCC	Post-classification comparison
PLAPS	Precipitation lapse rate (mm H2O/km)
PPP	Public-private partnership
Q10	Flow exceeded in 10% of the specified period
Q90	Flow exceeded in 90% of the specified period
R^2	Coefficient of determination
R_CN2	SCS runoff curve number for moisture condition II
R_OV_N	Manning's "n" value for overland flow
RCHRG_DP	Deep aquifer percolation fraction
REVAPMN	Threshold depth of water in the shallow aquifer for "revap" to occur (mm)
RBWB	Rufiji Basin Water Board
RCM	Regional Climate Model
RCP	Representative Concentration Pathways
RF	Random Forest
RSR	Standard deviation of measured data
SAGCOT	Southern Agricultural Growth Corridor
SCS	Soil Conservation Service
SDG	Sustainable Development Goals
SMHI	Swedish Meteorological and Hydrological Institute
SOL_AWC	Available water capacity of the soil layer (mm H_2O/mm soil)
SOL_K	Saturated hydraulic conductivity (mm/h)
SOL_Z	Depth from soil surface to bottom of layer (mm)
SRTM	Shuttle Radar Topography Mission
SSA	Sub-Saharan Africa
SUFI-2	Sequential Uncertainty Fitting
SURLAG	Surface runoff lag coefficient
SWAT	Soil and Water Assessment Tool
SWAT-CUP	Soil and Water Assessment Tool - Calibration and Uncertainty program
TAMSAT	Tropical Applications of Meteorology using Satellite data and ground-based observations
TAZARA	Tanzania-Zambia Railway
TLAPS	Temperature lapse rate (°C/km)
TMA	Tanzania Meteorological Agency
TPI	Topographic Position Index
TRI	Terrain Ruggedness Index
TRMM	Tropical Rainfall Measuring Mission

TWI	Topographic Wetness Index
UDSM	University of Dar es Salaam
WASIM	Water Balance Simulation Model
WDPA	World Database of Protected Areas
WRB	World Reference Base
WUA	Water User Association
95PPU	95% prediction uncertainty

1. General introduction

1.1. Problem statement

Water is a key resource to sustain life and ensure food security through agricultural production. However, water security is endangered, especially in less wealthy regions like Sub-Saharan Africa (SSA) (Vörösmarty et al., 2010) water scarcity is becoming increasingly important due to global change aspects like climate change, demographic growth accompanied by land use and land cover change (LULCC) and with agriculture as the largest water consumer accounting for 69% of the global annual water withdrawal (WWAP (UNESCO World Water Assessment Programme), 2019). Access to water is of utmost importance to people in SSA to sustain their livelihood and with increasing population pressure and the need for agricultural land, agricultural systems in East Africa are shifting from traditional upland cultivation into wetlands (Dixon and Wood, 2003). Wetlands are characterized by sufficient soil water availability and numerous ecosystem services throughout the year (Dixon and Wood, 2003; Heinkel, 2018; Rebelo et al., 2010).

The Ramsar secretariat (Ramsar Convention Secretariat, 2016) defines wetlands as *"areas of marsh, fen, peatland or water, whether natural or artificial, permanent or temporary, with water that is static or flowing, fresh, brackish or salt, including areas of marine water the depth of which at low tide does not exceed six metres"*. Beside the human-made wetlands, five major wetland types are generally recognized (Ramsar Convention Secretariat, 2016):

1. marine (coastal wetlands including coastal lagoons, rocky shores, seagrass beds and coral reefs);
2. estuarine (including deltas, tidal marshes and mudflats, and mangrove swamps);
3. lacustrine (wetlands associated with lakes);
4. riverine (wetlands along rivers and streams);
5. palustrine (meaning "marshy" – marshes, swamps and bogs).

Mitsch and Gosselink (Mitsch and Gosselink, 2007) argue that there are several definitions of wetlands, but depending on the subject of interest, the definitions differ. This lack of a general definition is also attributed to the fact that wetlands have been drained until the 19th century and defining wetlands was of no particular interest. In the mid of the 20th century the term "wetland" became more common and in the late 1970s wetlands were being recognized for their ecological functions and the need for a proper definition became apparent. For this study the definition of the U.S. Army Corps of Engineers Definition is being used that fits well for ecological studies (Mitsch and Gosselink, 2007):

"The term wetlands means those areas that are inundated or saturated by surface water or groundwater at a frequency and duration sufficient to support, and that under normal circumstances do support, a prevalence of vegetation typically adapted for life in saturated soil conditions. Wetlands generally include swamps, marshes, bogs, and similar areas."

East Africa inhibits a huge amount of wetland types and an area of about 18 Mio ha are defined as wetlands (Leemhuis et al., 2016). However, the definition, identification and delineation of wetlands is still part of current research (Amler et al., 2015; Muro, 2019; Yeo et al., 2019a). Nevertheless, remote sensing techniques and new satellites allow for more detailed and consistent analysis with regard to the

designation of wetland areas (Muro, 2019). However, the various types of wetlands and the manifold definitions still allow for debates concerning the extent and distribution of wetlands. One aspect highlighted by Mitsch and Gosselink (Mitsch and Gosselink, 2007) concerning wetlands, is the wetland´s interaction with its surrounding catchment on the one hand and the wetland´s influence on downstream riparians as sources, sinks and transfomers of nutrients on the other hand. Consequently, wetlands are in a particular position at the interface of terrestrial systems such as upland forests or grasslands and the subsequent aquatic systems such as deep lakes or oceans. Still, wetlands are different to both of these systems and at the same time highly depend on both (Mitsch and Gosselink, 2007). This transmitting function of wetlands in between headwater catchments and aquatic systems such as oceans at the very end of the cascading system is of high importance due to the several ecosystem services that wetlands provide. For example, upland agriculture might affect water quality adversely, while wetlands might act as a buffer zone and increase water quality for downstream riparians (McCartney et al., 2010; Ramsar Convention Secretariat, 2016). Several studies on the various ecosystem services of wetlands on adjacent ecosystems exist (Heinkel, 2018; McCartney et al., 2010; Rebelo et al., 2010) and therefore, the knowledge of lateral and longitudinal interactions of wetlands with their surrounding ecosystems or the entire catchment is of essential importance to preserve the functioning of the system (Lee et al., 2019; Reis et al., 2019; Yeo et al., 2019b). Wetland systems are as any other human or natural system, moving through cycles of steady states, destabilization phases, reorganization phases and new phases of stability. The ability of the wetland system to provide its services relies on its state or health (Beuel et al., 2016; Kotze et al., 2012) and this is depending on the vulnerability of the system and the susceptibility to external forces like climate change or anthropogenic interventions as e.g., LULCC (Elmqvist et al., 2003).

This study deals with the Kilombero Catchment in Tanzania that contains a floodplain wetland embedded in a mountainous catchment. The Kilombero River forms a floodplain wetland and is the most important tributary for the Rufiji River, which is the biggest river system in Tanzania (Wilson et al., 2017). The Kilombero Catchment contains on the one hand a unique ecosystem with a high biodiversity and several endemic species (Andrew et al., 2015, 2012; Dinesen, 2016; Ntongani et al., 2013) and on the other hand it is progressively being utilized for agricultural production and envisioned as part of the Southern Agricultural Growth Corridor of Tanzania (SAGCOT) (Environmental Resources Management, 2013). Hence, the reconciliation of environmental protection and food production is at the core for a sustainable development of the area, while *“water resource management is seen as integral to poverty reduction and food security”* for the Kilombero Catchment (Koutsouris et al., 2016). However, several interests are competing for natural resources such as water because the development of the catchment is highly dynamic and several internal and external factors are influencing the recent development of the local socio-ecological system. On the one hand migration into the valley, especially of pastoralists, in combination with investments of foreign investors as well as investors from the big cities of Tanzania e.g., Dar es Salaam and Morogoro push local farmers either into the wetland or towards the upland forest systems (Daconto et al., 2018; Nindi et al., 2014). Additionally, farming practices are changing with the introduction of new rice varieties (e.g. TXD 306) and the increasing utilization of herbicides, pesticides, and machinery like tractors. Furthermore, industrialization in the country is being pushed and several hydropower dams are planned in the catchment (WREM International Inc., 2015). On the other hand, several protected areas do exist in the catchment and national and international organizations

advocate to preserve these ecosystems either due to their intrinsic value, the ecosystem services they provide or for potential tourism developments (Daconto et al., 2018; Dinesen, 2016; Kolding et al., 2017).

Potential risks of mismanagement in reconciling the economic development and environmental integrity are visible in the neighboring catchment of the Great Ruaha River, where the Great Ruaha has been drying up since 1993 with severe impacts on wildlife, tourism, irrigation and electricity generation (Economic Research Bureau University of Dar es Salaam, 2006). One key aspect for a sustainable management of water resources is a reliable data source, but unfortunately *"some of the most valued natural and cultural landscapes on Earth lie in river basins that are poorly gauged and have incomplete historical climate and runoff records"* (Mango et al., 2011). This is also true for the Kilombero Catchment, but despite this lack of measured data, these regions are commonly the regions that are most in need of adequate scientific guidance for decision makers and stakeholders in water resource management (Mango et al., 2011). On a larger scale it was already shown by Poméon (Poméon, 2018) that a combination of freely available products works well to account for water resources. However, some products that were used by Poméon do not work properly on a mesoscale like the Kilombero Catchment and do not work on management relevant scales for the Kilombero Catchment (e.g., data from the Gravity Recovery and Climate Experiment (GRACE) (Wahr et al., 1998)). Yet, a sound modelling framework for water resources is needed to understand and maintain the water-related processes within the catchment and to adequately support water resource managers with quantitative data. Additionally, this framework should also allow to incorporate scenario planning with regard to important development processes in the catchment like LULCC or climate change to account for changing conditions.

1.2. Research questions

The problem statement above raises several research questions that are addressed in this thesis:

(i) How do the wetland and the catchment interact and what are the major hydrological processes?

The first question deals with the overall hydrological understanding of the catchment. Until this study, there was no distributed hydrological model of the catchment available, although the hydrology is of major concern to the development of the region, due to the agricultural suitability of the catchment and the governmental growth corridor plans for the Kilombero Valley. Data scarcity in the region, especially with regard to hydrological data, complicates the task to setup a physically-based hydrological model. Nevertheless, a model setup based on freely available geodata and historic discharge and precipitation data allowed to simulate the historical hydrological situation with good results and remote sensing methods enabled the establishment of a time series for LULCC from the 1970s until 2014. Chapter 4 provides a detailed overview on the hydrology of the catchment as well as the impact of historic LULCC.

(ii) What are potential impacts of climate change on the hydrology of the catchment?

The second question addresses the issue of climate change and its impact on the hydrology of the catchment. While temperatures are consistently increasing according to climate models for the region, the issue of rainfall variability is much more complex due to the manifold climatic driving forces and the topographical complexity of the region. Therefore, an ensemble of six bias-corrected RCM models forced by GCM models were used in combination with two RCP scenarios to account for the uncertainty with regard to climate change. Furthermore, changes in rainfall patterns do not linearly correlate with discharge, as the water interacts with the biosphere and pedosphere. Consequently, water can be (temporarily) stored within the catchment's soils, vegetation or aquifers and contribute either as surface runoff, lateral flow or baseflow to the discharge of the catchment. The SWAT model was utilized with all GCM-RCM models and the RCP scenarios to estimate changes in the hydrology driven by climate change. Additionally, extreme flow situations were analyzed to account for changes in hydrological risks like floods and droughts. Chapter 5 addresses these issues in detail.

(iii) What is the impact of LULCC on the hydrology of the catchment and what are potential future impacts and how do they interact with climate change?

The third question focusses on the issue of LULCC. Nowadays the focus is on climate change impacts, while many studies neglect the impact of LULCC. LULCC have significant impacts on water resources and beside that, several ecosystem services might be lost in trade-offs to food production. Historical LULCC were analyzed and their impact on water resources on several spatio-temporal scales was assessed in order to identify hot spots of change and allow local water managers to prioritize their available resources. Potential future LULCC until 2030 were modeled to assist a wise planning for water management. All these changes were modeled for classifications with no specific categorization of cropland and additionally for a classification with rice as subdivision in order to assess the impact of rice intensification, due to the importance of rice cultivation for the catchment. For these analyses the impact of climate change was also considered to estimate the combined impact of climate change and LULCC on the catchment as a whole, but also for specific areas on subcatchment level.

1.3. Objectives of the study

The overall objective of this study is to acquire a decent understanding of the hydrology of this highly dynamic catchment, which is target to agricultural intensification plans on the one hand and a hot spot of biodiversity on the other hand (Ntongani et al., 2013; Wilson et al., 2017) and additionally livelihood for many smallholder farmers. Furthermore, the study explores the impact of global change scenarios, namely LULCC and climate change, on the hydrology of the catchment in order to ensure a sustainable use of the natural resources, but also to contribute to food security of the region by investigating the impact of agricultural development on water resources. Specifically, the objectives of this study are:

(i) Set up a distributed hydrological model suitable to simulate impacts of LULCC and climate change on the catchment's hydrology;
(ii) Assess the possible climatic future of the Kilombero Catchment;
(iii) Estimate the impact of these climatic changes on hydrology by analyzing temporal and spatial changes in the water balance;
(iv) Analyze the impact of climate change on hydrological risks;
(v) Assess LULCC in the Kilombero Catchment since the 1970s;
(vi) Analyze the impacts of LULCC on water balance components in the catchment;
(vii) Develop LULC scenarios for the catchment;
(viii) Analyze the impact of the different LULC scenarios on water resources at various temporal and spatial scales and on low flows and high flows;
(ix) Assess the combined impact of LULCC and climate change on water resources.

1.4. Research framework

This study was conducted within the framework of the "GlobE – Wetlands in East Africa" (FKZ: 031A250A-H) project. The GlobE initiative was launched by the Federal Ministry of Education and Research of Germany (BMBF) and comprised several research initiatives with interdisciplinary approaches to tackle the central goal of the National Research Strategy BioEconomy 2030 (Federal Ministry of Education and Research (BMBF), 2011), which is to secure the global food supply. To achieve this goal, all GlobE initiatives did research on the African continent to investigate and support sustainable agricultural practices and economies with a consortium of African and German research partners.

The GlobE – Wetlands project focused on wetland systems in East Africa (Kenya, Rwanda, Tanzania, Uganda) and explored the possibilities to reconcile future food production with environmental protection. Therefore, the overall GlobE – Wetlands in East Africa project was organized in five clusters (Figure 1.1). These clusters focused on the understanding of the wetland system (Cluster A), the exploration of management options (Cluster B) and the integration of several disciplines and the development of scenarios (Cluster C). Additional clusters focused on the extrapolation of the findings on a broader, regional scale to formulate recommendations from the findings. One overarching goal was capacity building within the four researched countries in order to consolidate the gathered knowledge on-site. This study is located in Cluster A, as it is trying to understand the hydrological processes of the wetland and the interaction of the wetland with its surrounding catchment. However, scenarios with regard to (LULCC) and climate change are a fundamental part of this study as well.

Within the GlobE project this study is closely connected to the work of Dr. Sonja Burghof (Burghof, 2017) and Dr. Geofrey Gabiri (Gabiri, 2018), who were PhD students in the project and analyzed the hydrogeology and hydrology on the local scale near the town of Ifakara in Tanzania (Figure 2.1). Furthermore, the work of the remote sensing group and the meteorology group of the project were essential for the baseline data of the scenario development regarding LULCC and climate change and the interdisciplinary work with regard to scenario analysis.

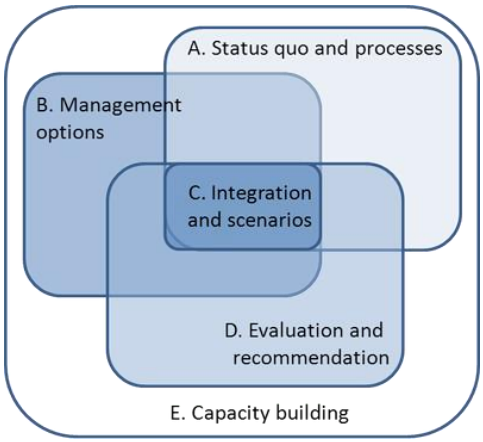

Figure 1.1 Conceptual overview on the five research clusters of the "GlobE – Wetlands in East Africa" project and their connections (GlobE Wetlands, 2013).

1.5. Structure of the thesis

This doctoral thesis is a cumulative dissertation and consists in total of 9 chapters. The first chapter is a general introduction to the thesis followed by a description of the study area focusing on the physical attributes and complemented by the socioeconomic background. The third chapter provides an overview on the model routines of the SWAT model and explains why it was chosen. The chapters 4 and 5 were both published in the journal "*Water*", while chapter 6 is published in "*Sustainability*". Table 1.1 provides a brief overview of the content of the three articles from chapter 4, 5 and 6. All articles were formatted to fit the style of this thesis. A general conclusion on the findings of the articles and this thesis is given in chapter 7, followed by references (chapter 8) and a publication list (chapter 9) of the author.

Table 1.1 Summary of the key points of the three articles within this thesis

Chapter	Publication	Key points	Main contribution
4	Näschen, K., Diekkrüger, B., Leemhuis, C., Steinbach, S., Seregina, L., Thonfeld, F., Linden, R. van der, 2018. Hydrological Modeling in Data-Scarce Catchments: The Kilombero Floodplain in Tanzania. Water 10, 599. doi:10.3390/W10050599	• Setup of a SWAT model • Assessment of LULCC from 1970s to 2014 • Analysis of the impact of historic LULCC on water resources • Scale dependency of water resources in the catchment was shown • Example how to utilize a mixture of local and freely available global data in a data scarce catchment in SSA	Improved understanding and (semi-) distributed quantification of the hydrological processes in the catchment
5	Näschen, K., Diekkrüger, B., Leemhuis, C., Seregina, L.S., Linden, R. van der, 2019. Impact of Climate Change on Water Resources in the Kilombero Catchment in Tanzania. Water 11, 859. doi:10.3390/W11040859	• Assessment of possible future climatic conditions emphasizing on precipitation and temperature • Estimation of the impact of a broad range of climate change models on water resources • Extreme value analysis with regard to low flows and high flows • Shift of the peak flow in the next decades • Flood events are likely to increase, while more severe droughts are less pronounced	Assessment of climate change effects on water resources in the catchment with regard to several climate models.
6	Näschen, K., Diekkrüger, B., Evers, M., Höllermann, B., Steinbach, S., Thonfeld, F., 2019. The Impact of Land Use/Land Cover Change (LULCC) on Water Resources in a Tropical Catchment in Tanzania under Different Climate Change Scenarios. Sustainability 2019, Vol. 11, 7083. doi:10.3390/SU11247083	• Development of potential LULCC distributions until 2030 • Impact assessment of LULCC with regard to water resources with an emphasis on rice production • Combined effect of LULCC and climate change on water resources and low and high flows aggravate seasonalities • The impact of climate change on water resources is more pronounced, but has also higher uncertainties.	Potential LULC distributions until 2030 and their effect on water resources under different climate change scenarios. Modelling framework for global change impacts on water resources established.

2. Study area

2.1. Location and Topography

The Kilombero Catchment is located in the Morogoro region in south central Tanzania. It covers an area of 40,240 km², spanning from 7.68 °S to 10.03 °S latitude and 34.56 °E to 37.30 °E longitude.

The Kilombero Catchment is part of the Rufiji River basin, which forms the largest river basin of Tanzania. For this study, the catchment was delineated with the outlet at the junction of Kilombero and Luwego River in the eastern part of the catchment. Downstream of this point, the river is called Rufiji and drains into the Indian Ocean south to Dar es Salaam. The catchment is encapsulated by the Udzungwa mountains in the northwest with altitudes ranging up to 2500 m and the Mbarika Mountains and Mahenge Highlands in the southwestern parts (Koutsouris, 2017). A broad seasonal floodplain with a size of 7,967 km² is in the center of the catchment, forming the biggest freshwater wetland in East Africa below 300 m (Mombo et al., 2011). An overview of the catchment is given in Figure 2.1.

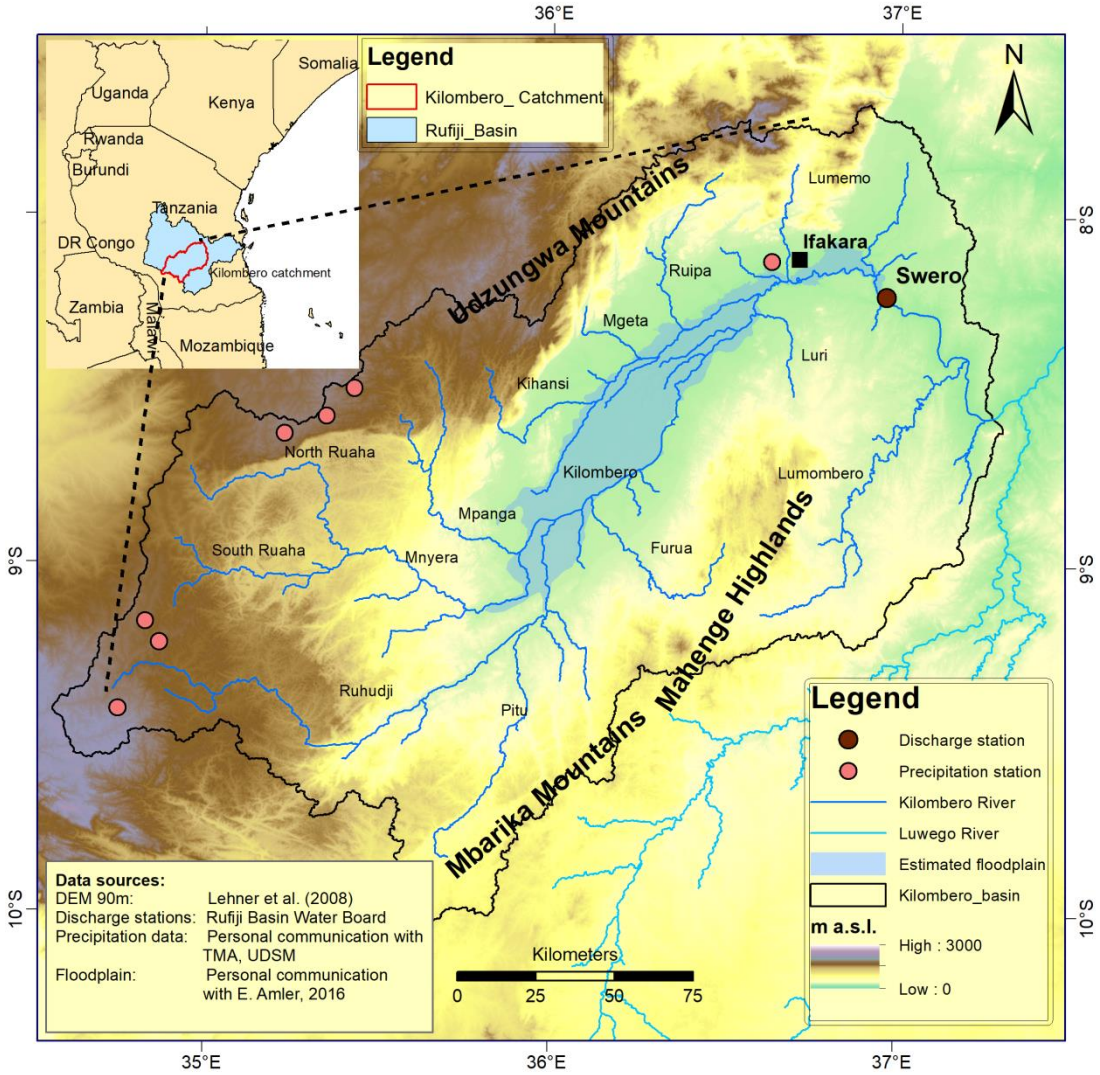

Figure 2.1 Overview map of the Kilombero Catchment, including locations of available precipitation stations and the utilized discharge station (Swero). The estimated floodplain area is based on visual interpretation of Landsat images by E. Amler (modified after (Näschen et al., 2019)).

2.2. Geology

The catchment is situated at the foot of the Great Escarpment of East Africa and is a southern extension of the East African Rift System (Jätzold and Baum, 1968). The Kilombero Valley is described as a SW-NE trough-like depression between the Udzungwa Mountains in the north and the Mahenge Highlands in the south (Beck, 1964; Burghof, 2017). The Udzungwa Mountains are part of the Neoproterozoic Mozambique Belt and were formed during the collision of East and West Gondwana (Burghof, 2017; Reddy et al., 2003). The Udzungwa Mountains consist of metamorphic rocks, mainly gneisses with greenschist at the northwestern flank facing the Kilombero Valley (Burghof, 2017; Tenczer et al., 2007). The Mahenge Mountain Block in the south and the Mbarika Mountains belong to the Eastern Granulite Cabo Degado nappe of the Mozambique Belt and consist of complex igneous, metamorphic and sedimentary rocks of neoproterozoic age (Sommer et al., 2017).

The valley itself is filled with sediments, however only little information about the thickness and composition of the sediments is available. In the area north of the Kilombero Valley 4,000 to 5,000 m thick formations of sandstones and conglomerates are deposited and it is assumed to be similar in large parts to the Kilombero Valley as well (Burghof, 2017). Beck (Beck, 1964) describes the valley as being covered with Pliocene, Pleistocene and alluvial deposits. Typical structures are alluvial fans, located at the fringes of the floodplain in the southern and northern parts, where tributaries of the Kilombero River enter the floodplain. The biggest settlement in the catchment, the city of Ifakara, is built on the alluvial fan of the Lumemo River.

2.3. Climate

The climate of the catchment can be described as a sub-humid tropical climate (Koutsouris et al., 2016) and according to the updated Köppen-Geiger climate classification it is classified as a tropical savanna (Aw) climate (Peel et al., 2007) (s. Figure 2.2). The annual mean temperature in the lowlands is about 24 °C while the uplands mean annual temperature is about 17 °C. The annual areal precipitation within the catchment is about 1300 mm with a huge spatio-temporal variation of rainfall. The Udzungwa Mountains, as well as the Mahenge Highlands, act as water towers to the catchment with annual rainfall amounts exceeding 2000 mm, while some lowlands receive 1000 mm less rainfall within a year (Wilson et al., 2017). The intra- and interannual rainfall variability is markedly pronounced with a distinct dry and rainy season. The rainy season is divided into the Short Rains (locally called “Vuli”) from November to January and the Long Rains (“Masika”) from March to May (Camberlin and Philippon, 2002; Koutsouris et al., 2016; Wilson et al., 2017). However, this separation of the rainy season with a distinct bimodal distribution is more common for northern parts of Tanzania, inter alia due to the movement of the ITCZ (Intertropical Convergence Zone) (Camberlin and Philippon, 2002). Yet, Nicholson (Nicholson, 2017) showed that a monocausal argumentation for the northern parts of East Africa is inadequate to the complex system. The southern parts, like the Kilombero Catchment, typically show a unimodal rainfall distribution (Seregina et al., 2018). Nevertheless, the climate in East Africa is highly complex due to several teleconnections in combination with a complex topography and influences of the lakes on the local and regional climate (Nicholson, 2017). Therefore, it appears that many years still show a bimodal distribution of rainfall for the Kilombero Catchment with a short dry spell in February. Several studies

underlined the correlation of the Short Rains with El Niño–Southern Oscillation (ENSO) and the Indian Ocean zonal mode (IOZM) (Goddard and Graham, 1999; Hastenrath et al., 1993; Nicholson, 2017), while variations for the Long Rains are more complex to understand and show only weak correlations to ENSO, IOZM, ITCZ, the easterly wind anomalies over equatorial Africa and the energy gradient from the highlands of East Africa (Camberlin and Philippon, 2002; Koutsouris et al., 2016). Recent research recommends to consider each month of the Long Rains separately to better account for the various climatic influences, instead of analyzing the whole season as one (Nicholson, 2017; Seregina et al., 2018).

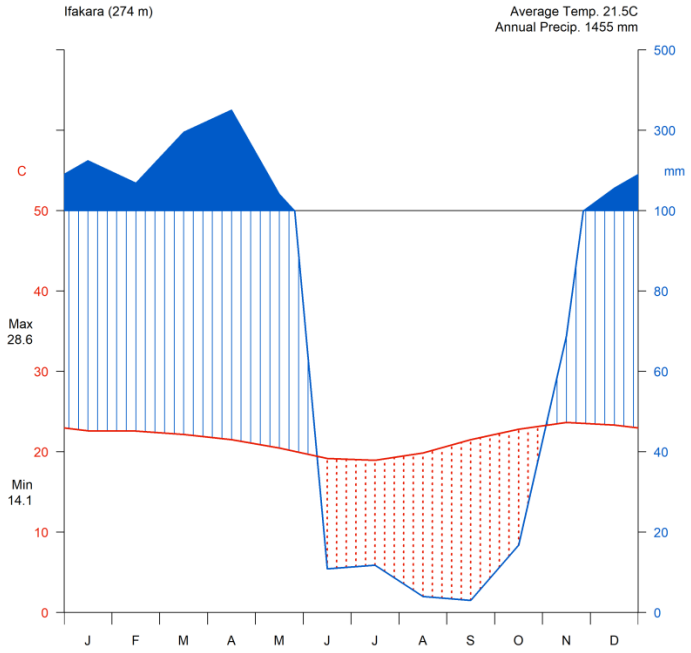

Figure 2.2 Walter-Lieth climate diagram showing the precipitation and temperature conditions in the Kilombero Valley (based on precipitation data from the Kilombero Agriculture Training and Research Institute (KATRIN) from 1974 to 2005; Bias-corrected temperature data from the Coordinated Regional Downscaling Experiment (CORDEX) Africa project from 1979 to 2005 (Gutowski et al., 2016; Näschen et al., 2019)).

2.4. Soils

Up to today there was no detailed soil exploration of the whole Kilombero Catchment. Nevertheless, several continental and global mapping approaches exist and are combined in the Harmonized World Soil Database (HWSD), which gives an overview on the distribution of soils (Figure 2.3).

The steep and forested uplands of the Udzungwa Mountains are characterized by humic Nitisols. These soils are typical for tropical uplands and have > 1 % humus in the upper 18 cm due to the relatively cold and humid climate in higher altitudes. They are marked by a profound rootability and a high usable field capacity combined with a medium amount of available nutrients, which allows for the cultivation of demanding tropical plants like tea (Scheffer and Schachtschabel, 2010) e.g., in the northwestern parts of their distribution in the catchment. The western part of the catchment is dominated by Lixisols. These are heavily weathered soils with high shares of kaolinite, but rich in bases with a saturation > 50 %. Lixisols can be used for agricultural purposes e.g., cultivation of cassava, but they do need fertilization

due to their low nutrient pool (Scheffer and Schachtschabel, 2010). The distribution of Lixisols coincides well with the agricultural activities on the western parts of the catchment. The floodplain itself is typically characterized by Fluvisols. These are relatively young soils that receive fresh sediments and nutrients in regular flood events. Fluvisols are often used for annual crops and grazing (FAO, 2001).

A study by Daniel et al. (Daniel et al., 2017) shows the heterogeneity in physical and chemical soil attributes along a transect near the city of Ifakara at the bottleneck of the floodplain. At the fringe of the floodplain patches of Arenosols can be found as well, which are less favorable for cultivation compared to the adjacent Fluvisols. The southern part of the floodplain is enclosed by a V-shaped distribution of ferric, haplic and humic Acrisols, which are similar to Lixisols in their characteristics, although they are less productive and furthermore susceptible for water erosion if utilized for agricultural cultivation (Scheffer and Schachtschabel, 2010). The vulnerability to water erosion is enhanced by the carved landscape and the steep slopes in the range of the Acrisols.

The eastern part of the catchment, which mainly belongs to the Selous Game Reserve, is dominated by ferralic Cambisols, which are relatively poor in nutrients. However, they are still richer in nutrients than associated Acrisols and are characterized by a greater cation exchange capacity (FAO, 2001).

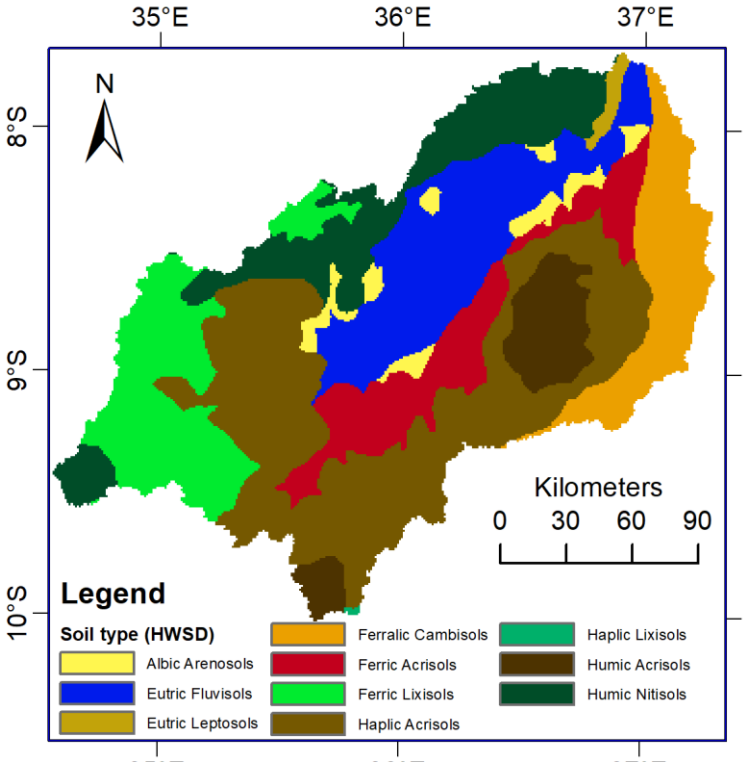

Figure 2.3 Dominant soil types in the Kilombero Catchment according to the Harmonised World Soil Database (HWSD) (Dewitte et al., 2013) based on the World Reference Base (WRB) for Soil Resources classification system (modified after Näschen et al. (Näschen et al., 2019)).

2.5. Hydrology

The catchment area till the junction of Kilombero River and Luwego River comprises 40,240 km². The river is called Kilombero River from the junction of Ruhudji, Pitu and Mnyera River onwards. These tributaries origin are the steep uplands of the Mbarika and Udzungwa Mountains in the southwestern part of the catchment (Figure 1.1). The river bifurcates and meanders as soon as it enters the flat valley bottom with a slope of 0,25‰ (Jätzold and Baum, 1968). Perennial (Figure 1.1) and seasonal tributaries from the northern and southern mountainous areas contribute to the SW-NE flowing Kilombero River. A bottleneck structure exists in the northeastern part near the city of Ifakara, from where the river turns and flows to a NW-SE direction into the Selous Game Reserve to enter the Rufiji River. The most important discharge gauging station to this study called Swero (Figure 1.1 and Figure 2.4) is also near the border of the Selous Game Reserve. The data at this station has a huge gap since the 1970s due to limited accessibility and lack of funds for the local authorities, but it was recently reconstructed by the Rufiji Basin Water Board (RBWB) and a new rating curve is being established. The Swero station comprises 34,000 km² of the catchment and therefore records crucial data indicating the hydrological processes within the catchment.

Figure 2.4 Gauging station Swero and the Kilombero River at the end of the dry season in 2015 (pictures taken by the author).

The average discharge at the Swero station is at 520 m³/s (Yawson et al., 2005) and the Kilombero River contributes 62% of the annual discharge amount of the Rufiji River, although it covers only 23% of the overall drainage area (Wilson et al., 2017). Main water source of the river is a year-round groundwater supply (Näschen et al., 2018) complemented by the tributaries inflow. This groundwater also is the major source of drinking water for the communities near the city of Ifakara and for many villages (Figure 2.5) (Burghof, 2017). Nevertheless, the use of surface water from rivers or open wells as drinking water is still common, especially for farmers in their agricultural fields (“shambas”) (Figure 2.5, right picture). Water management at the grassroot community level is done by Water User Associations (WUA). These associations manage, distribute and conserve water sources jointly with other members of the association. They are responsible for the acquisition and management of water use permits, solving conflicts among water users and to advocate for water related public purposes like the protection of water sources (WREM International Inc., 2015).

Figure 2.5 A modern and sealed pumping well in the city of Ifakara, which gathers groundwater at about 30 m depth in the left picture. The right picture shows an open well in the surroundings of Ifakara that is prone to contamination from the surface. Both wells are typical examples for water sources in the city and its surroundings (pictures taken by the author).

The rainy season is accompanied by heavy rains and a marked flooding in April or May with water level rising at the bottleneck in Ifakara by up to 4.5 m (Daconto et al., 2018) over the riverbanks. Although the annual flooding is important to the recession agriculture in the valley, it might also cause serious damages. A serious flooding event on April 1st 2011 in the Kilombero District affected 6,643 people in total and destroyed 2,731.5 ha of farms, 6 bridges, 677 houses and several roads (National Bureau of Statistics. United Republic of Tanzania, 2017). Dams might buffer these impacts of floods, but they are attended by other environmental and social impacts (Duvail and Hamerlynck, 2007). Up to today only the Kihansi dam (180 MW) is established at the Kilombero River. However, the Integrated Water Resource Management Development Plan (IWRMDP) identified potential for further dams at Ruhudji (358 MW), Mpanga (144 MW) and the upper Kihansi (248 MW) (WREM International Inc., 2015) in the catchment.

2.6. Vegetation, land use and land cover

The Vegetation changes gradually from the lowlands, adjacent to the floodplain, up to the mountains. The floodplain is widely used for maize, rice and sugarcane cultivation and non-cultivated areas are covered by edaphic grasses such as *Hyparrhenia* spp., *Panicum fluviicola* Steud., *Panicum maximum, Penisetum purpureum*, *Phragmites mauritianus* Kunth. and some single trees of *Ficus* spp. and *Kigelia africana* (Behn et al., 2018; Dinesen, 2016; Kato, 2007; Msofe et al., 2019; Nindi et al., 2014). Annual fires occur between the months of August and October in these grasslands (Andrew et al., 2012). Another source of disturbance is grazing of about 300,000 cattle and goats and additional 43,000 sheep, which is accompanied by trampling, gap openings and nutrient inputs consequently leading to the destruction of critical habitats and the spreading of invasive species (Andrew et al., 2012).

The valley is framed by a *miombo* woodland belt dominated by *Brachystegia* spp., whereas the uplands are covered by a mixture of broadleaved and evergreen forests, bush- and wooded grasslands

with patches of agricultural fields especially in the western part of the catchment (Zemandin et al., 2011).

An example of a typical transect profile taken near the city of Ifakara is shown in Figure 2.6.

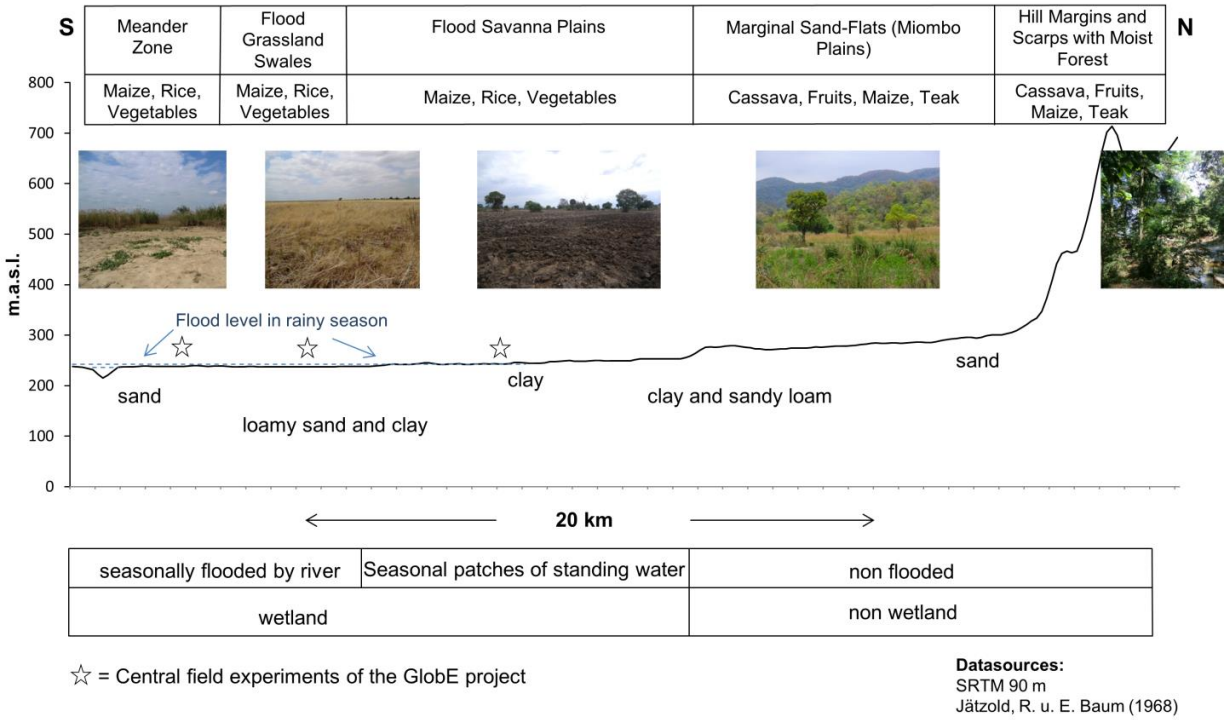

Figure 2.6 Transect starting at the Kilombero River, near the town of Ifakara, towards the Udzungwa Mountains at the northern border of the catchment. Pictures illustrate the typical vegetation along the transect and were taken during the dry season. The picture to the very right was taken at the Udzungwa Mountains National Park, further northeast of the transect. The visualization at the bottom displays the different hydrological zones along the floodplain (see also (Gabiri et al., 2018)). Nevertheless, the flooding level and therefore the river extension varies greatly among the years and the longitudinal river profile positions from its source to its junction with the Luwego River.

The floodplain of the Kilombero Valley was declared as a Ramsar site in 2002 to underline its importance in terms of ecology and biodiversity. It is seen as a source of water and nutrients for downstream riparians as well as for residents of the catchment. Additionally, the surrounding Miombo and evergreen forests are highlighted as integral parts of the designated Ramsar site (Ramsar, 2002). Without counting the overlapping areas, 22,343 km² of the 40,240 km² catchment area is listed in the World Database of Protected Areas (WDPA) (IUCN and UNEP-WCMC, 2019) under different categories from a national park (Udzungwa Mountains), to a Ramsar site (Kilombero), a game reserve (Selous), a game controlled area (Kilombero), a wildlife management area (Mbanrang'andu) and several forest reserves and open areas (Figure 2.7, Thonfeld et al., unpublished). These habitats comprise several threatened species that are also listed in the red list of the International Union for Conservation of Nature (IUCN) like the blue duiker, cheetah, lion and birds like Kilombero Weaver (Ploceus burnieri), Stierling's woodpecker (Dendropicos stierlingi) and Southern-banded snake eagle (Circaetus fasciolatus) among others (Ntongani et al., 2014).

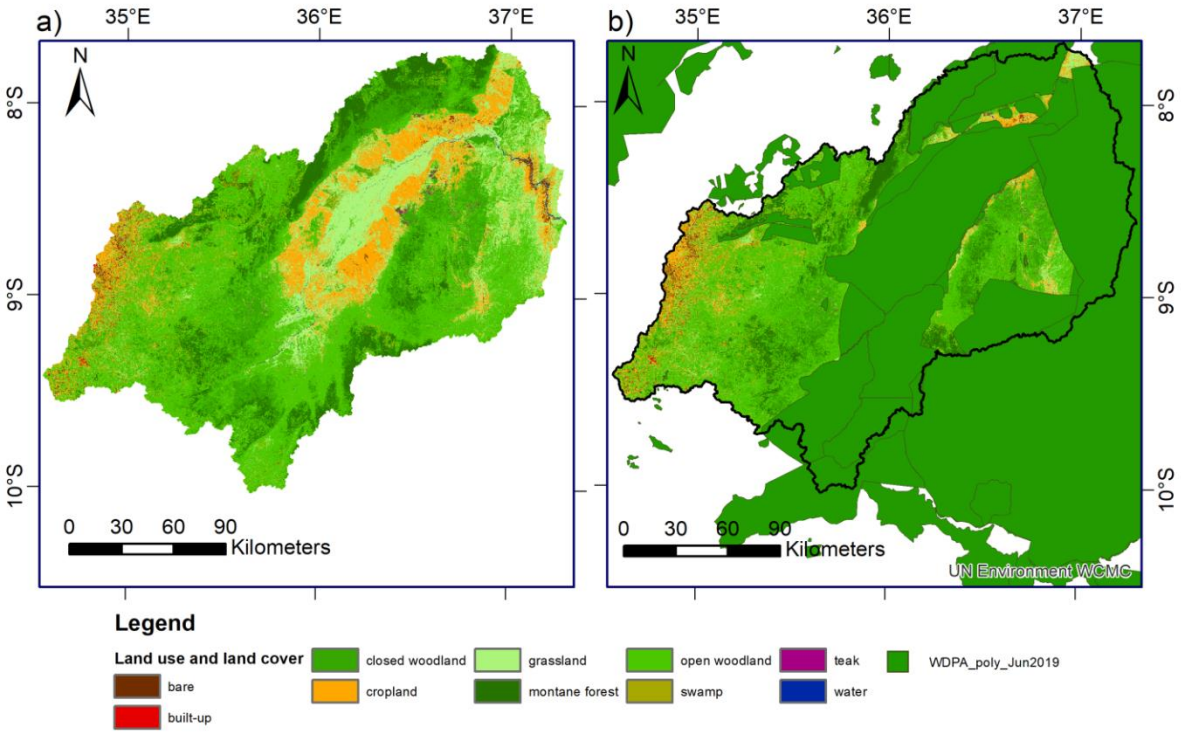

Figure 2.7 The map (a) shows the Kilombero Catchment with its land use and land cover distribution according to the year 2014 (Näschen et al., 2018). (b) shows the same map overlaid by the areas under different protection categories according to WDPA in June 2019 (IUCN and UNEP-WCMC, 2019).

2.7. Socioeconomic background

The National census from 2012 counted more than 670,000 people living in the administrative districts of Kilombero and Ulanga (Figure 2.8), which lie within the hydrologically delineated catchment (Leemhuis et al., 2017; National Bureau of Statistics. United Republic of Tanzania, 2012). Since 2000 the population in the valley has doubled and calculations estimate to reach 1.2 million inhabitants in the Kilombero Valley in the next 20 years due to natural growth and immigration (Daconto et al., 2018). The high pace of development in the last decades led to the establishment of hundreds of new villages and the administration struggles to keep pace. This resulted in an unregulated development of the valley in many areas, which is also a source of conflicts, especially among local farmers and pastoralists (Daconto et al., 2018; Nindi et al., 2014). Indigenous people of the Kilombero Valley descent mainly from Bantu origin. The most important ethnic groups are Ndamba, Mbunga and Ngindo, while Pogoro, Hehe and Bena are less represented. Pastoralists and agro-pastoralists migrating into the valley are mainly Maasai, Sukuma and Barbaigs. However, also business people from the whole country are moving into the Kilombero Valley (Nindi et al., 2014).

The construction of the Tanzania-Zambia Railway (TAZARA) in the 1970s and their associated resettlement schemes (Daconto et al., 2018) as well as the “Ujamaa” plan of the first president Julius Nyerere were important milestones for the socioeconomic development of the area. They supported agricultural projects and acted as pull factor for the migration into the valley (Daconto et al., 2018; Kato,

2007; Sheikheldin, 2015). Recent initiatives like SAGCOT or “Big Results Now” still influence the socioeconomic setting. Infrastructure like the “Magufuli Bridge” near Ifakara and a tamarc road from Morogoro/ Mikumi to Ifakara is being developed to foster the trade into and out of the valley, but also to regulate the uncontrolled expansion (Daconto et al., 2018; Environmental Resources Management, 2013). The contribution of agriculture to the gross domestic product (GDP) is about 29 % of Tanzania and employs 75 % of the total labor force underlining its importance for the whole country (National Bureau of Statistics. United Republic of Tanzania, 2017).

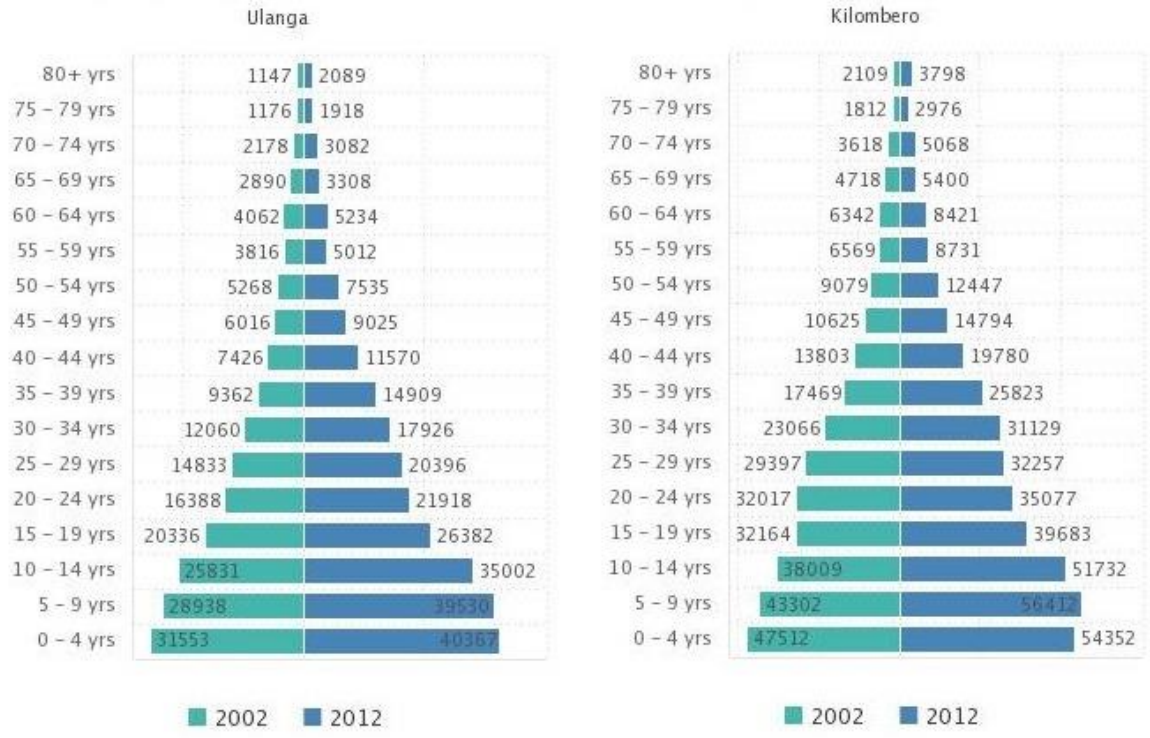

Figure 2.8 Population size by age groups for the Ulanga and the Kilombero district. Total numbers increased for Ulanga district from 193,280 to 265,203 and for the Kilombero district from 321,611 to 407,880 (National Bureau of Statistics. United Republic of Tanzania, 2012).

3. Modeling approach

3.1. Model choice

The purpose of this study was to evaluate the effects of climate change and LULCC on several spatio-temporal scales in a data sparse catchment. These requirements were all fulfilled by the Soil and Water Assessment Tool (SWAT) (Arnold et al., 1998; Neitsch et al., 2011), which was already successfully applied in the region (Natkhin et al., 2015; Notter et al., 2012; Wambura et al., 2018). The SWAT model is able to continuously simulate the impact of climate on a daily time resolution and is therefore also able to analyze variations in the onset or offset of the dry or wet season. The semi-distributed hydrologic response unit (HRU) approach of the SWAT model balances well between the data demand of distributed and the limited spatial information of lumped models and allows to identify hot spots of change without the need for high resolution gridded data, which are rarely available in SSA (Mango et al., 2011). The HRU approach in combination with the dynamic vegetation growth module implemented in SWAT allows simulating the impact of LULCC on the hydrology of a catchment. Furthermore, the influence of management practices as well as sediment and nutrient dynamics can be simulated by SWAT. However, this study did not account for sediment and nutrient dynamics due to the lack of measured data to calibrate and validate the model. Finally, the HRU approach of the SWAT model is computationally efficient and allows for long term modelling of this complex and large catchment (40,240 km²) in a reasonable computation time. This was particularly important for the climate change impact study that simulated several climate models for a period from the 1950s up to 2060 on a daily time resolution (Chapter 5).

3.2. The SWAT model

This chapter provides an overview on the general structure and the main processes of the SWAT model (s. Figure 3.1) based on the theoretical manual of the model (Neitsch et al., 2011). Further information on the basic model setup, it´s calibration and validation (Chapter 4) as well as the scenarios concerning climate change and LULCC are given in the respective chapters on climate change (Chapter 5) and LULCC impacts (Chapter 6).

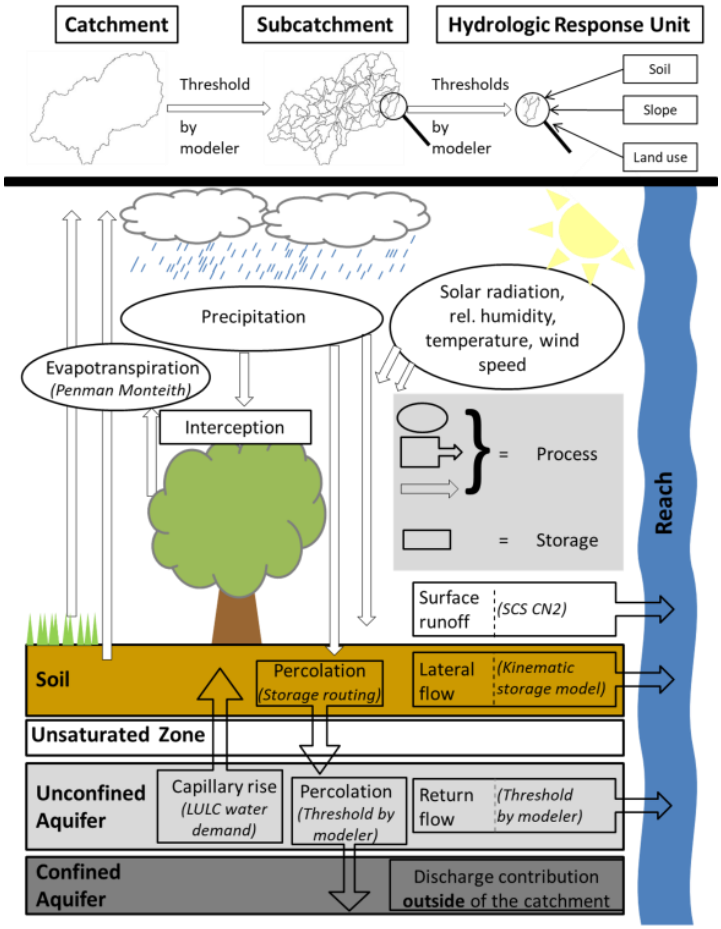

Figure 3.1 Catchment discretization and schematic overview of processes and storages simulated by the SWAT model. Applied methods to simulate evapotranspiration and water fluxes are shown in parentheses (taken from (Näschen et al., 2019) and modified after (Neitsch et al., 2011)).

The SWAT model divides the hydrological cycle in two phases, that are the land phase and the routing phase. The land phase is partitioned into several storages and processes that are based on the water balance equation (equation 3.1):

$$SW_t = SW_0 + \sum_{i=1}^{t}\left(R_i - Q_i - ET_{a,i} - W_{seep,i} - Q_{gw,i}\right) \quad \text{(Equation 3.1)}$$

where SW_t is the final soil water content [mm], SW_0 is the initial soil water content on day i [mm], t is the time [days], R_i is the net precipitation on day i [mm], Q_i is the amount of surface runoff on day i [mm], $ET_{a,i}$ is the amount of actual evapotranspiration on day i [mm], $W_{seep,}$i is the amount of water entering the vadose zone from the soil profile on day i [mm], and $Q_{gw,i}$ is the amount of return flow on day i [mm].

The first steps in the simulation process are the atmospheric processes. Daily values for the climate parameters are either provided by the modeler or simulated by the built-in WXGEN weather Generator (Sharpley and Williams, 1990),while evapotranspiration is calculated based on the formula of Penman-Monteith (Penman, 1956), Hargreaves (Hargreaves et al., 1985) or Priestley-Taylor (Priestley and Taylor, 1972). This study calculated evapotranspiration based on Penman-Monteith.

Once precipitation occurs it reaches the ground and generates surface runoff or infiltrates the soil. Surface runoff is simulated based on a modified version of the Soil Conservation Service Curve Number (SCS CN) method (Mockus, 1972), developed within the United States Department of Agriculture (USDA) (equation 3.2). This method includes physical factors like the vegetation attributes, the hydrologic soil group, slope and soil moisture conditions. Additionally a retention parameter is given (equation 3.3.) that might vary with changing soil moisture conditions. If the Green and Ampt method (Green and Ampt, 1911) is chosen over the SCS CN method, several processes are simulated differently e.g., the canopy storage has to be simulated separately. However, this is explained more in detail in (Neitsch et al., 2011), while this study here used the SCS CN method because rainfall data as required in a high temporal resolution for the Green and Ampt method is not available.

$$Q = \frac{(\mathrm{R}_{day} - 0.2s)^2}{(R_{day} + 0.8s)} \text{ for R} > 0.2\text{s}$$

$$Q = 0 \text{ for R} \leq 0.2\text{s} \qquad \text{(Equation 3.2)}$$

$$s = 25.4\left(\frac{1000}{CN} - 10\right) \qquad \text{(Equation 3.3)}$$

where Q is the daily surface runoff [mm], R is the daily rainfall [mm], and s is a retention parameter

Percolation of water in SWAT is calculated for each soil layer individually and in total for up to ten soil layers using a storage routing technique (Equation 3.4). Once a soil layer reaches field capacity, water moves to the underlying soil layer based on equation 3.4 and controlled by the saturated conductivity. If all layers are saturated, the water will enter the vadose zone, from where it may move back to the surface as capillary rise or enter the shallow groundwater aquifer. To account for the amount of water that percolates to the next subsequent layer the following equation is used:

$$\mathrm{SW}_{perc,ly} = \mathrm{SW}_{ly,excess} \cdot \left(1 - \exp\left\lfloor\frac{-\Delta t}{TT_{perc}}\right\rfloor\right) \qquad \text{(Equation 3.4)}$$

where $SW_{perc,ly}$ is the amount of water percolating to the underlying soil layer on a given day [mm], $SW_{ly,excess}$ is the drainable volume of water in the soil layer on a given day [mm], Δt is the length of the time step [h], and TT_{perc} is the travel time for percolation [h]

Groundwater is separated into two aquifers in SWAT, a shallow and a deep aquifer. Water percolating from the vadose zone enters the shallow aquifer from where it may rise back into the unsaturated zone depending on the evaporative demand of the vegetation. Otherwise water can contribute to the base flow using a linear storage approach and a recession coefficient or percolate into the deep aquifer. The deep aquifer water was originally treated in SWAT as lost for the water balance and assumed to contribute to other catchments outside the watershed. However, since revision 538 a new parameter

alpha_bf_d was introduced, that allows water from the deep aquifer to reenter the system and contribute e.g., as base flow. The water balance of the shallow aquifer is shown in equation 3.5 and equation 3.6 shows the water balance for the deep aquifer:

$$\mathrm{aq}_{sh,i} = aq_{sh,i-1} + \mathrm{W}_{rchrg,sh} - Q_{gw} - W_{revap} - W_{pump,sh} \quad \text{(Equation 3.5)}$$

where $\mathrm{aq}_{sh,i}$ the amount of water is stored in the shallow aquifer on day i [mm], $aq_{sh,i-1}$ is the amount of water stored in the shallow aquifer on day i-1 [mm], $\mathrm{W}_{rchrg,sh}$ is the amount of recharge entering the shallow aquifer on day i [mm], Q_{gw} is the groundwater flow, or base flow, into the main channel on day i [mm] , W_{revap} is the amount of water moving into the soil zone in response to water deficiencies on day i [mm] and $W_{pump,sh}$ is the amount of water removed from the shallow aquifer by pumping on day i [mm].

$$\mathrm{aq}_{dp,i} = aq_{dp,i-1} + \mathrm{W}_{deep} - W_{pump,dp} \quad \text{(Equation 3.6)}$$

where $\mathrm{aq}_{dp,i}$ the amount of water is stored in the deep aquifer on day i [mm], $aq_{dp,i-1}$ is the amount of water stored in the deep aquifer on day i-1 [mm], W_{deep} is the amount of water percolating from the shallow aquifer into the deep aquifer on day i [mm], $W_{pump,dp}$ is the amount of water removed from the deep aquifer by pumping on day i [mm].

Lateral movements of water (equation 3.7) are also simulated by the SWAT model, besides these vertical movements explained before. Lateral flow occurs when an impermeable layer exists, parameterized by several factors like the hydraulic conductivity of the soil layers, the slope and it´s length. Lateral movement is simulated using a kinematic storage module by Sloan and Moore (Sloan and Moore, 1984).

$$\mathrm{Q}_{lat} = 0.024 \,.\left(\frac{2.SW_{ly,excess} \,.\, K_{sat} \,.\, slp}{\emptyset_d \,.L_{hill}}\right) \quad \text{(Equation 3.7)}$$

where Q_{lat} is the water discharged from the hillslope (mm H_2O/day), $SW_{ly,excess}$ is the drainable volume of water in the saturated zone of the hillslope per unit area [mm], K_{sat} is the saturated hydraulic conductivity [mmh^{-1}], slp is the slope as the increase in elevation per unit distance, $\emptyset_d$ is the drainable porosity of the soil layer [mm/mm], L_{hill} is the hillslope length [mm], and 0.024 is a conversion factor from meters to millimeter and hours to days

Once SWAT has calculated the land phase, water, as well as sediments, nutrients and pesticides enter the routing phase. They are routed through the stream network of the catchment using a structure similar to HYMO (Williams and Hann, 1972), while additionally simulating transformation of chemicals in the stream and streambed. However, sediment processes, nutrient cycling and transportation as well as processes related to bacteria and pesticides are simulated by SWAT, but these processes are not the main interest of this study and are described in more detail in (Neitsch et al., 2011)

4. Hydrological Modeling in Data-Scarce Catchments - The Kilombero Floodplain in Tanzania

This chapter has been published as: Näschen, K., Diekkrüger, B., Leemhuis, C., Steinbach, S., Seregina, L., Thonfeld, F. & R. van der Linden (2018): Hydrological Modeling in Data-Scarce Catchments - The Kilombero Floodplain in Tanzania. Water 2018, Vol. 10, Page 599 10, 599. doi:10.3390/W10050599.
https://www.mdpi.com/2073-4441/10/5/599

Abstract: Deterioration of upland soils, demographic growth, and climate change all lead to an increased utilization of wetlands in East Africa. This considerable pressure on wetland resources results in trade-offs between those resources and their related ecosystem services. Furthermore, relationships between catchment attributes and available wetland water resources are one of the key drivers that might lead to wetland degradation. To investigate the impacts of these developments on catchment-wetland water resources, the Soil and Water Assessment Tool (SWAT) was applied to the Kilombero Catchment in Tanzania, which is like many other East African catchments, as it is characterized by overall data scarcity. Due to the lack of recent discharge data, the model was calibrated for the period from 1958–1965 (R^2 = 0.86, *NSE* = 0.85, *KGE* = 0.93) and validated from 1966–1970 (R^2 = 0.80, *NSE* = 0.80, *KGE* = 0.89) with the sequential uncertainty fitting algorithm (SUFI-2) on a daily resolution. Results show the dependency of the wetland on baseflow contribution from the enclosing catchment, especially in dry season. Main contributions with regard to overall water yield arise from the northern mountains and the southeastern highlands, which are characterized by steep slopes and a high share of forest and savanna vegetation, respectively. Simulations of land use change effects, generated with Landsat images from the 1970s up to 2014, show severe shifts in the water balance components on the subcatchment scale due to anthropogenic activities. Sustainable management of the investigated catchment should therefore account for the catchment–wetland interaction concerning water resources, with a special emphasis on groundwater fluxes to ensure future food production as well as the preservation of the wetland ecosystem.

Keywords: SWAT model; hydrological modeling; East Africa; land use changes; water balance; wetlands

4.1. Introduction

Recent developments show an increasing trend to utilize wetlands in East Africa (Jew and Bonnington, 2011; Leemhuis et al., 2016; Sakané et al., 2011; Ulrich, 2014). This development is triggered by several issues, such as increasing food demand caused by demographic growth, climate change, and degradation of upland soils. Unlike the uplands, wetlands hold potential for year-round harvest, due to their fertile soils with a balanced soil water availability throughout the year (Gabiri et al., 2017).

In Tanzania the “Kilimo Kwanza” (Agriculture First) policy of the government prioritizes agricultural development and leads to agricultural intensification and expansion (Munishi-Kongo, 2013). This increased utilization results in an intensive use of wetland resources, and may lead to a degradation of the wetland system (Beuel et al., 2016; McCartney et al., 2010). The understanding of the functioning of

a wetland lies in the water budget, hence, information on water resources is essential to establish a sustainable land management system within a wetland. Without sufficient water, agricultural production deteriorates and food security is endangered (Godfray et al., 2010). For a holistic view on water resources and their fluxes, it is not sufficient to consider only processes within the wetland—one also has to consider the hydrological processes occurring within the entire catchment.

A typical approach to adequately calculate and represent hydrological processes within a catchment is the application of a hydrological model. Process-based models like the water balance simulation model (WaSiM) (Schulla, 2017), SWAT (Arnold et al., 1998), or MIKE SHE (Refsgaard and Storm, 1995) are capable of simulating water resources under changing environmental conditions, such as climate change or land use and land cover changes (LULCC). A drawback of these models is the intensive data demand due to their physically-based approach. Unfortunately, data scarcity is an obstacle with regard to hydrological modeling in East Africa. Local water authorities face numerous challenges, like accessibility of discharge stations (especially in the rainy season), limited staff, and insufficient equipment due to restricted funds (Munishi-Kongo, 2013). This implies heterogeneous datasets, with a low quantity and quality of the available data with regard to spatial and temporal coverage. Besides the hydrological data, other geodata, like topography, land use/land cover (LULC), soil, or climate data is needed to simulate biophysical processes. Local biophysical data (e.g., vegetation, soil, climate) is rarely available, but these gaps can be closed by applying remote sensing data, when operating on meso- to macroscale catchments (Montzka et al., 2008; Poméon et al., 2017).

Nevertheless, scientific guidance is particularly needed in data-scarce regions of East Africa, to assist with water resource management on the catchment scale (Mango et al., 2011). In particular, the increased pressure on wetlands and their surroundings might alter the distribution and amount of water resources through LULCC. Hence, a spatially-distributed hydrological model is needed, to simulate the water balance. The capability of SWAT to simulate the water balance in data-scarce tropical regions of different scales has been proven in various studies (Baker and Miller, 2013; Bossa et al., 2014; Cornelissen et al., 2013; Wagner et al., 2013), but only a few within East Africa (Alemayehu et al., 2017; Mango et al., 2011; Mashingia et al., 2014; Notter et al., 2013; Wambura et al., 2015).

This study was undertaken in the Kilombero Catchment in Tanzania. Although there is an urgent need to gather a detailed understanding of the water resources in the Kilombero Catchment, only a few attempts have been made to understand the hydrological system. Yawson et al. (Yawson et al., 2005) applied lumped models and linear transfer approaches, while Lyon et al. (Lyon et al., 2015) investigated spatio-temporal drainage patterns. Subcatchments of the Kilombero Catchment were analyzed by Burghof et al. (Burghof et al., 2017), Koutsouris et al. (Koutsouris, 2017), and Daniel et al. (Daniel et al., 2017), by developing a conceptual model, setting up an HBV (Hydrologiska Byråns Vattenavdelning) light model (Seibert and Vis, 2012) for two subcatchments and by analyzing soil hydrological properties in a floodplain transect. These studies investigated water-related relationships within the Kilombero Catchment, giving either a detailed insight into specific subcatchments without considering the entire catchment (Burghof et al., 2017; Koutsouris, 2017; Lyon et al., 2015)—or the entire catchment was analyzed, but without considering the spatial heterogeneity (Yawson et al., 2005). This spatial heterogeneity needs to be considered, according to Lyon et al. (Lyon et al., 2015), who demonstrated the importance of the spatio-temporal variations in hydrological processes within the catchment. Nevertheless, Lyon et al. (Lyon et al., 2015) applied recession analysis only as a kick-off for more detailed

hydrological modeling. Altogether these studies did very good preparatory work, but there is still a research gap concerning the understanding of the distributed hydrological processes in the entire Kilombero Catchment. This research tries to bridge this gap by establishing the semi-distributed SWAT model, to gather a better spatial understanding of the hydrological processes in the Kilombero Catchment.

The main objective of this study is therefore to enhance the knowledge about the hydrological system of the Kilombero Catchment, in order to support water management in this changing environment (Leemhuis et al., 2017; Muro et al., 2016). Accordingly, three specific objectives were formulated:

(i) Assessing LULCC in the Kilombero Catchment since the 1970s;
(ii) Setting up a distributed hydrological model suitable to simulate impacts of LULCC;
(iii) Analyzing the impacts of LULCC on water balance components in the catchment.

These objectives are achieved by combining available local data with freely available global geodata, in order to adequately represent the hydrological system with the SWAT model. To obtain a better spatio-temporal understanding of the water balance components, the SWAT model is calibrated and validated against measured historical discharge data, and a spatio-temporally detailed water balance analysis on the catchment and subcatchment scale is presented. The observed impacts of LULCC from 1970 to 2014 were analyzed by deriving land use maps from Landsat images and implementing them into the calibrated model (Leemhuis et al., 2017).

4.2. Materials and Methods

4.2.1.Study Site

The Kilombero Catchment is located in south-central Tanzania (Figure 4.1). The catchment is characterized by high relief energy, with altitudes ranging from 200 m to 2500 m above sea level, and is surrounded by the Udzungwa Mountains in the north, as well as the Mbarika Mountains and the Mahenge Highlands in the southeast (Figure 4.1). In total, the catchment comprises 40,240 km2 up to the confluence of Kilombero and Rufiji River. Although the Kilombero Catchment only covers 23% of the drainage area of the Rufiji Basin, it contributes 62% of the annual runoff volume (Wilson et al., 2017). The floodplain system covers an area of 7967 km^2 (Mombo et al., 2011), and contains the largest freshwater wetland within East Africa below a threshold of 300 m above mean sea level (Kangalawe and Liwenga, 2005). A big share of the floodplain is designated as a Ramsar site, which underlines the wetland's international environmental importance (Ramsar, 2002; Wilson et al., 2017).

The Kilombero River is the main tributary of the Rufiji River, representing the largest river basin in Tanzania. Water resources monitoring is scarce in the Kilombero Catchment, although it is prone to environmental changes with implications on water availability. Recent developments show an increase in population and agricultural land, and a decrease of natural landscapes, especially in the lower floodplain wetland of the catchment, while the upper catchment area is undergoing deforestation activities (Leemhuis et al., 2017; Wilson et al., 2017). Up to today, 9% of the national rice yield is produced in the Kilombero wetland, and the wetland area is characterized by patches of several land use activities, from small- and large-scale farmers to pastoralists and urban populations near the town of Ifakara at the

northeastern bottleneck of the wetland (Gabiri et al., 2018). All these anthropogenic activities, in combination with ongoing climate change, alter the hydrological regime of the Kilombero River. Future activities foresee the establishment of an agricultural growth corridor in the Kilombero Catchment (Environmental Resources Management, 2013), which will foster the pressure on water resources in terms of quantity and quality in the research area and for downstream riparians.

The regional climate is defined as sub-humid tropical climate (Koutsouris et al., 2016), with distinct dry and rainy (November–May) seasons with a predominantly unimodal rainfall pattern (Kangalawe and Liwenga, 2005; Koutsouris et al., 2016). Nevertheless, many teleconnections influence the regional climate, resulting in shifts between unimodal and bimodal rainfall patterns among the years. Years with a unimodal distribution of rainfall lack the short rains (November–January), whereas the bimodal rainy seasons are characterized by short (November–January) and long rains (March–May) (Wilson et al., 2017), which correspond mainly to the movement of the Intertropical Convergence Zone (ITCZ) (Camberlin and Philippon, 2002). The average annual precipitation is between 1200 and 1400 mm (Koutsouris et al., 2016), with strong interannual variability (Nicholson, 2000) and spatial variability between the mountainous area and the lowlands, with precipitation up to 2100 mm and 1100 mm, respectively (Wilson et al., 2017). The temperature mirrors this pattern inversely, with annual mean temperatures of 24°C in the valley and 17 °C in the uplands (Wilson et al., 2017).

According to the Harmonized World Soil Database (HWSD) (Dewitte et al., 2013), the catchment is predominantly characterized by Fluvisols in the valley bottom, whereas the upland regions are dominated by Acrisols and Nitisols. The western upland soils are mainly described by Lixisols, and in the lower eastern part Cambisol is the dominant soil type (Figure 4.2).

The land cover of the upper catchment embraces a mixture of natural vegetation like tropical rainforests, bush lands, and wooded grasslands, with some patches of agricultural fields (Zemandin et al., 2011). The valley is surrounded by a Miombo woodland belt, whereas the floodplain itself is dominated by agricultural use and grassland (Kato, 2007; Nindi et al., 2014).

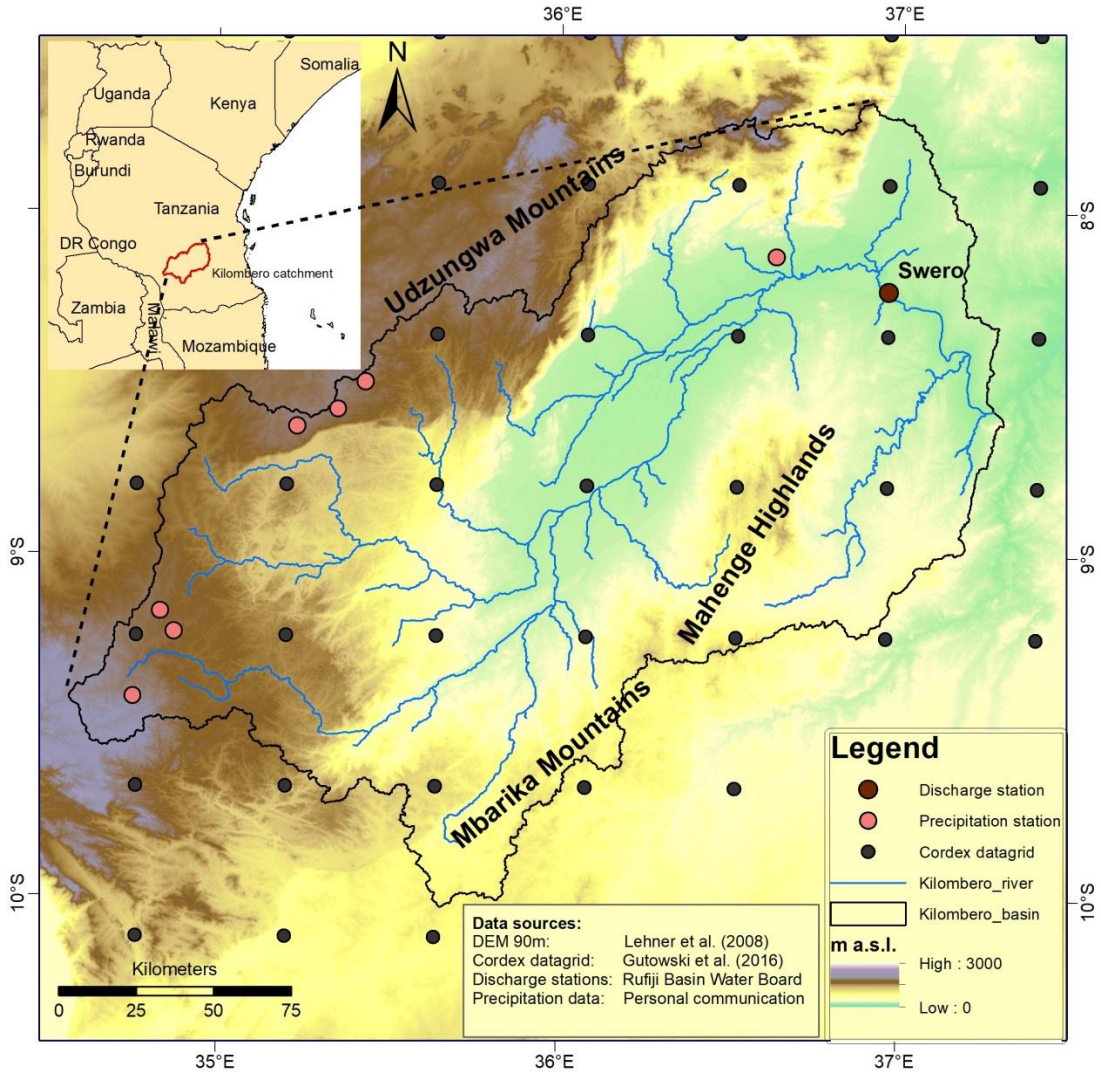

Figure 4.1 Overview map of the study area, including available precipitation and discharge stations as well as the 0.44° Coordinated Regional Downscaling Experiment (CORDEX) Africa grid.

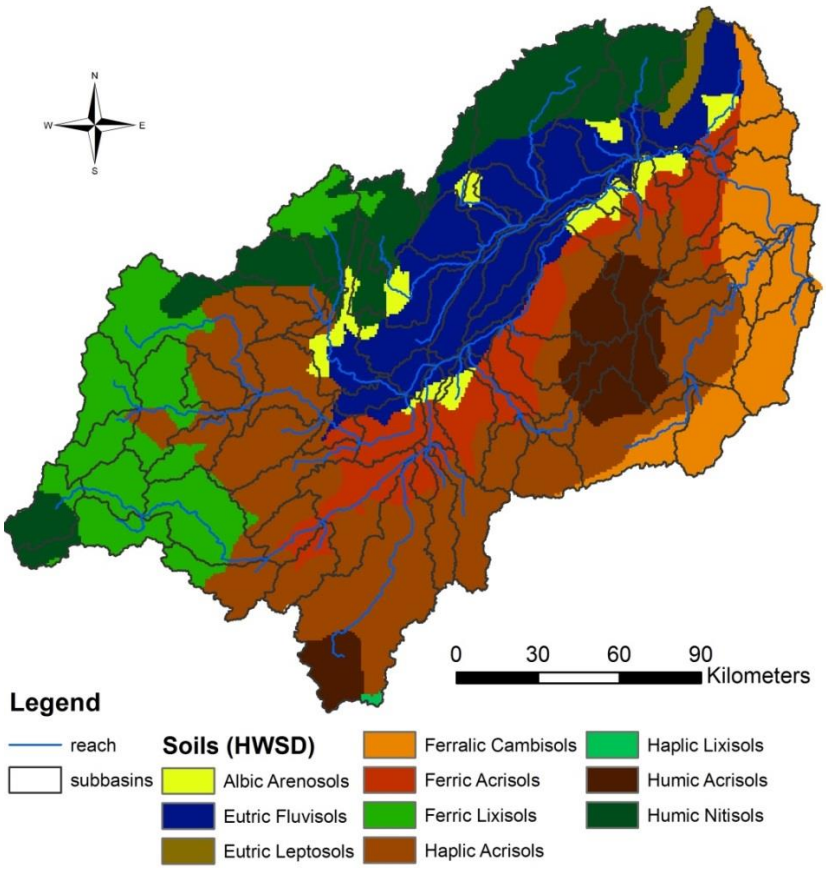

Figure 4.2 Distribution of soils for the Kilombero Catchment, according to the Harmonized World Soil Database (Dewitte et al., 2013).

4.2.2.Input Data

Data scarcity is a major problem in East Africa, and therefore a mixture of freely available global geo datasets and local measurements were combined and processed to run the hydrological model, following the approach of Leemhuis et al. (Leemhuis et al., 2016). Model calibration and validation is difficult because of low data availability, caused by the challenges of installing and maintaining the hydrometeorological network (Munishi-Kongo, 2013) for the Rufiji Basin Water Board (RBWB). The longest period with good quality discharge data was monitored from 1958–1970. The station utilized in this study is named Swero (Figure 4.1) and comprises 34,000 km^2, representing roughly 84% of the entire catchment area. The discharge time series of the Swero station ends in 1970, and therefore excludes the application of precipitation estimates from satellites. Hence, available station data from that period was included in the model, although the spatial distribution of precipitation stations is limited (Figure 4.1). Nevertheless, the temporal availability of the precipitation data for this study was good, with only 5.15% missing data for all stations and the entire simulation period. The other climate variables (Table 4.1) were taken from the CORDEX (Coordinated Regional Downscaling Experiment) Africa (Gutowski et al., 2016) regional climate models, with a spatial resolution of 0.44°.

Temperature data was bias-corrected with the ERA-Interim reanalysis (Dee et al., 2011), by using the differences of the mean annual cycle of the 11-day running mean between each CORDEX model and the

reanalysis. To account for the different topography, due to the different horizontal resolutions of the ERA-Interim and CORDEX models (namely 0.75° versus 0.44°), the correction was based on potential temperatures on the 700-hPa level. All climate variables, except precipitation, were taken as an ensemble mean of six historic regional climate model runs (Table 4.2). These six models represent a broad range of precipitation signals, with increasing, decreasing, and constant precipitation patterns when comparing the periods from 1986 to 2005 with 2040 to 2059.

Due to the lack of suitable Landsat images for one single year in the 1970s, a mosaic of eight Landsat pre-collection Level 1 images from the 1970s, downloaded from EarthExplorer (United States Geological Survey (USGS), n.d.), was classified using the supervised Random Forest classification (Breiman, 2001) to adequately represent the land cover characteristics for the simulation. The 1994, 2004, and 2014 LULC maps are based on Landsat TM, ETM+, and OLI Surface Reflectance Level 2 Science Product imagery (USGS Department of the Interior, n.d., n.d.). Due to recurrent extensive cloud cover, a year before and a year after the year in question were considered in addition. All scenes with <80% cloud coverage were cloud masked and additionally orthorectified where necessary, and the tasseled cap components wetness, greenness, and brightness (Crist, 1985; Crist and Cicone, 1984; Yamamoto and Finn, 2012), and the Normalized Difference Water Index (NDWI) (McFeeters, 1996) and Normalized Difference Vegetation Index (NDVI) (Tucker, 1979) were calculated to account for seasonal dynamics of specific land cover classes. Based on the 30 m resolution Shuttle Radar Topography Mission (SRTM) Digital Elevation Model (DEM) (Lehner et al., 2008), we calculated slope and four morphometric indices (the terrain ruggedness index (TRI) (Riley et al., 1999), slope variability (SV) (Ruszkiczay-Rüdiger et al., 2009), topographic position index (TPI) (Gallant and Wilson, 2000; Jenness, 2006), and the topographic wetness index (TWI) (Beven and Kirkby, 1979). The spectral multi-temporal metrics in combination with the DEM, slope, and topographic indices were classified using a random forest approach (Breiman, 2001). For the supervised classification, as well as for map validation, different reference datasets gathered on the ground in combination with high-resolution remotely-sensed data were used according to their availability. In order to complete the dataset, freely available data with varying spatial resolution were applied (Table 4.2). The changes in land cover from 1970 to 2014 are shown in Figure 4.3.

Table 4.1 Applied datasets, their resolution, sources, and the required parameters in this study.

Data set	Resolution/Scale	Source	Required Parameters
DEM	90 m	SRTM (Lehner et al., 2008)	Topographical data
Soil map	1 km	FAO (Dewitte et al., 2013)	Soil classes and physical properties
Land use maps	60 m (1970s) 30 m (1994, 2004, 2014)	Landsat pre-Collection Level-1 (United States Geological Survey (USGS), n.d.), Landsat TM, ETM+, OLI Surface Reflectance Level-2 Science Products (USGS Department of the Interior, n.d., n.d.), SRTM (Lehner et al., 2008)	Land cover and use classes
Precipitation	Daily	Personal communication: RBWB, University of Dar es Salaam (UDSM), Tanzania Meteorological Agency (TMA)	Rainfall
Climate	Daily/0.44°	CORDEX Africa (Gutowski et al., 2016)	Temperature, humidity, solar radiation, wind speed
Discharge	Daily (1958–1970)	RBWB (RBWB, 2014)	Discharge

Table 4.2 Overview of the applied Regional Climate Models (RCMs) and their driving Global Climate Models (GCMs).

GCM	RCM	Institution	URL
CanESM2	CanRCM4_r2	Canadian Centre for Climate Modelling and Analysis (CCCma)	http://climate-modelling.canada.ca/
CanESM2	RCA4_v1	Rossby Centre, Swedish Meteorological and Hydrological Institute (SMHI)	https://esg-dn1.nsc.liu.se/
CNRM-CM5	CCLM4-8-17_v1	Climate Limited-area Modelling Community (CLMcom)	https://esg-dn1.nsc.liu.se/
EC-EARTH	CCLM4-817_v1	Climate Limited-area Modelling Community (CLMcom)	https://esg-dn1.nsc.liu.se/
EC-EARTH	RCA4_v1	Rossby Centre, Swedish Meteorological and Hydrological Institute (SMHI)	https://esg-dn1.nsc.liu.se/
MIROC5	RCA4_v1	Rossby Centre, Swedish Meteorological and Hydrological Institute (SMHI)	https://esg-dn1.nsc.liu.se/

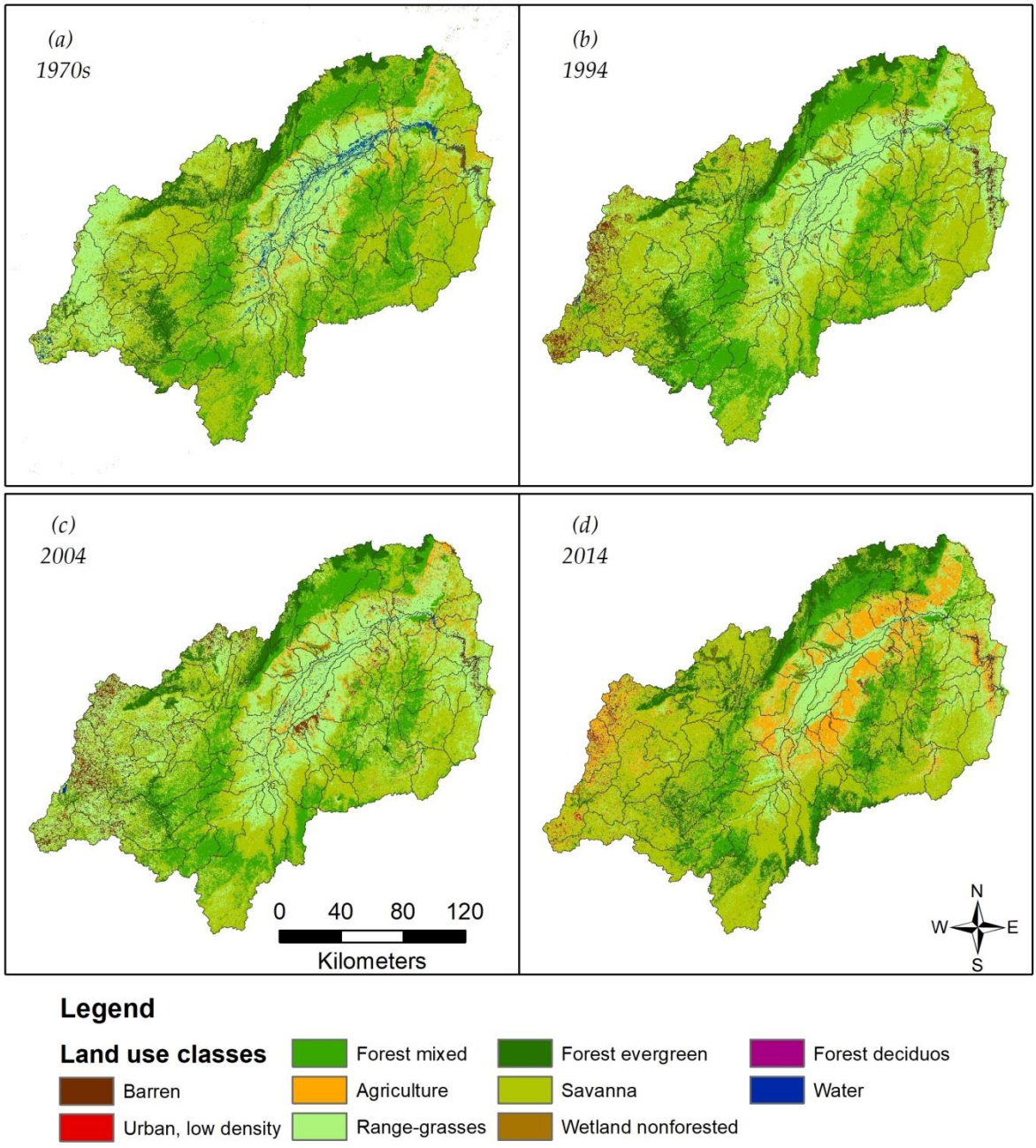

Figure 4.3 Land use and land cover classifications for four time steps ranging from (a) 1970s, (b) 1994 and (c) 2004 to (d) 2014 (modified after (Leemhuis et al., 2017)).

4.2.3.Model Description

In this study, the SWAT model (Arnold et al., 1998) was applied to simulate the water balance for the chosen time period and under changing LULC conditions. SWAT is a semi-distributed and physically-based catchment model for continuous simulations of discharge, sediments, nutrients, and pesticides on a daily basis. The model divides the catchment into subcatchments, which are generated from drainage patterns derived from the DEM, and by setting a threshold that defines the minimum drainage area to

form a stream. These subcatchments are further discretized into hydrologic response units (HRU) with unique combinations of LULC classes, soil types, and slope classes. LULC classes, soil types, and slope classes covering less than 10% of the area within the single subcatchments were neglected within the HRU generation. The model is divided into land phase and channel processes. Most of the processes within the land phase are simulated on the HRU level and summed up for each subcatchment, to calculate the overall water balance with the integration of climate station data and the channel processes (Neitsch et al., 2011). The most important processes simulated by the model are surface runoff, infiltration, lateral flow, baseflow, evapotranspiration, and groundwater recharge. Precipitation can either be intercepted by plants or hit the ground, where it may flow as surface runoff to the reach (Mockus, 1972), infiltrate into the soil, or evaporate from the ground (Monteith and Moss, 1977). If the water infiltrates into the soil, it is stored as soil moisture or percolates with a storage routing technique, which is based on the saturated hydraulic conductivity and the field capacity of the soil profile. Lateral flows are simulated with a kinematic storage model (Sloan and Moore, 1984). Once water percolates below the unsaturated zone, it reaches the shallow aquifer, which is treated as an unconfined aquifer. Once a certain threshold defined by the modeler is exceeded, baseflow contributes to the reach. Water may also move into a deeper confined aquifer, where the water is assumed to contribute to the discharge outside of the catchment and is treated as lost for the processes inside the catchment. Furthermore, the water can move from the shallow aquifer into the unsaturated zone, where it can be lost by evapotranspiration. This capillary rise and evapotranspiration are controlled by the water demand of the LULC and several parameters specified by the modeler. A detailed description of the model is given by Arnold et al. (Arnold et al., 1998) and Neitsch et al. (Neitsch et al., 2011)., and further information on the model parameters can be found in Arnold et al. (Arnold et al., 2012a).

4.2.4.Model Setup and Evaluation

In total the catchment was divided into 95 subcatchments and 1087 HRUs. Eight different soil types, seven LULC classes, and five slope classes were considered (Table 4.3). Due to the complex topography and the high relief energy, five elevation bands (Neitsch et al., 2011) were integrated to account for orographic precipitation patterns, as well as altitudinal temperature changes. These elevation bands divide each subcatchment into five elevation zones. Within these zones, precipitation and temperature are modified according to the altitudinal difference among the elevation of the nearest rainfall, respective climate station, and the average elevation of the elevation band. The exact modification is calculated with a certain factor called PLAPS or TLAPS, respectively (Table 4.4). Evapotranspiration was calculated after Penman–Monteith (Monteith and Moss, 1977), using historical runs of an ensemble mean of CORDEX Africa (Gutowski et al., 2016) data from six different models (Table 4.2), with a spatial resolution of 0.44° and 21 stations (Figure 4.1). Surface runoff and infiltration were calculated using the Soil Conservation Service (SCS) curve number method (Mockus, 1972). After setting up the model within ArcSWAT 2012 (revision664), the model was calibrated and validated using the SUFI-2 algorithm in SWAT-CUP (version 5.1.6.2)(Abbaspour, 2013), basically following the guidelines of Arnold et al. (Arnold et al., 2012b) and Abbaspour et al. (Abbaspour et al., 2015). As the SUFI-2 program within the SWAT-CUP software was utilized for parameter optimization, the Latin Hypercube sampling iteratively discarded the worst simulations by rejecting the 2.5th and 97.5th percentile of the cumulative distribution. Therefore,

the best 95% of simulations generated a parameter range (95% prediction uncertainty, 95PPU) instead of a single final parametrization. This uncertainty band represented by the 95PPU was used to account for the modeling uncertainty (Abbaspour, 2013), and is quantified as the P-factor, which measures the ability of the model to bracket the observed hydrograph with the 95PPU. Finally, the P-factor is simply the fraction enveloped by the 95PPU. Hence, the P-factor can be between 0 and 1, where 1 means a 100% bracketing of the measured data. The width of the 95PPU is calculated by the *R-factor* (Equation 4.1)). The *R-factor* divides the average distance between the lower and upper percentile with the standard deviation of the measured data (Abbaspour, 2013). The *R-factor* ranges from 0 to infinity, and should be below 1, implying a small uncertainty band (Abbaspour, 2013). The final parameter ranges are illustrated in Table 4.4, and a detailed description of the single parameters is given in Arnold et al. (Arnold et al., 2012a). The Kling–Gupta efficiency (*KGE*) (Equation 4.2)) (Gupta et al., 2009) was chosen as objective function. Ancillary criteria to assess the quality of the model were the Nash–Sutcliffe Efficiency (*NSE*) (Equation 4.3)) (Nash and Sutcliffe, 1970), coefficient of determination (R^2) (Equation 4.4)), percent bias (*PBIAS*) (Equation 4.5)) (Gupta et al., 1999), standard deviation of measured data (*RSR*) (Equation 4.6)), and the abovementioned P-factor and *R-factor*. Additionally, precipitation distribution was assessed with remote sensing products (Huffman et al., 2007; Koutsouris et al., 2016), a baseflow filter technique (Arnold et al., 1995) was utilized to estimate the share of surface runoff and baseflow, and literature research was performed (Burghof et al., 2017; Gabiri et al., 2018; Koutsouris, 2017; Lyon et al., 2015; Nicholson, 2000, 1996; Nyenzi et al., 1981; Yawson et al., 2005) to evaluate the gathered water balance component values for plausibility. After calibration and validation, different land use maps (Figure 4.3) were utilized to simulate the impact of LULCC. In order to attribute all alterations to the LULCC, nothing was modified except for the land use maps.

Table 4.3 Final spatial coverage with the different soil types, LULC classes, and slope classes of the study area after defining the HRUs.

Soil Type	Proportional Area (%)	LULC Class (1970s Land Use)	Proportional Area (%)	Slope Classes	Proportional Area (%)
Haplic Acrisol	30.82%	Savanna	45.30%	0–2%	22.45%
Eutric Fluvisol	14.77%	Range-Grasses	23.49%	2%–5%	12.09%
Humic Nitisol	13.14%	Forest-Mixed	22.05%	5%–8%	11.66%
Ferric Lixisol	13.05%	Forest-Evergreen	6.81%	8%–12%	13.96%
Ferric Acrisol	9.08%	Agricultural Land	1.20%	>12%	39.85%
Humic Acrisol	5.73%	Water	0.95%		
Albic Arenosol	2.75%	Barren	0.20%		
Eutric Leptosol	0.59%				

Table 4.4 Ranking of the calibrated parameters, according to their sensitivity and significance. A "v" in Method implies a replacement of the initial parameter value with the given value in the final range, whereas an "r" indicates a relative change to the initial parameter value.

Rank	Parameter	Description	Final Range	Method
1	GWQMN.gw	Threshold depth of water in the shallow aquifer for return flow to occur (mm).	1400–2200	v
2	ALPHA_BF.gw	Base flow alpha factor (days).	0.15–0.26	v
3	GW_REVAP.gw	Groundwater "revap" coefficient.	0.15–0.2	v
4	SURLAG.bsn	Surface runoff lag coefficient.	2.8–5.3	v
5	GW_DELAY.gw	Groundwater delay time (days).	4–30	v
6	SOL_K().sol	Saturated hydraulic conductivity (mm/h).	0.4–0.7	r
7	RCHRG_DP.gw	Deep aquifer percolation fraction.	0.31–0.37	v
8	SOL_Z().sol	Depth from soil surface to bottom of layer (mm).	0.35–0.5	r
9	SOL_AWC().sol	Available water capacity of the soil layer (mm H_2O/mm soil).	−0.1–0.13	r
10	R__OV_N.hru	Manning's "n" value for overland flow.	0.1–0.2	r
11	R__CN2.mgt	SCS runoff curve number for moisture condition II.	−0.5–(−0.35)	r
12	CH_K1.sub	Effective hydraulic conductivity in the tributary channel (mm/h).	65–80	v
13	ESCO.hru	Soil evaporation compensation factor.	0–0.1	v
14	CH_K2.rte	Effective hydraulic conductivity in the main channel (mm/h)	100–130	v
15	REVAPMN.gw	Threshold depth of water in the shallow aquifer for "revap" to occur (mm).	13–30	v
16	EPCO.hru	Plant uptake compensation factor.	0.9–1	v
17	PLAPS	Precipitation lapse rate (mm H_2O/km).	130	v
18	TLAPS	Temperature lapse rate (°C/km).	−6	v

$$R - factor = \frac{1}{n\sigma_O}\sum_{n=1}^{n}(S_U - S_L) \quad \text{(Equation 4.1)}$$

$$KGE = 1 - \sqrt{(r-1)^2 + (\alpha-1)^2 + (\beta-1)^2} \quad \text{(Equation 4.2)}$$

$$NSE = 1 - \frac{\sum_{i=1}^{n}(O_i - S_i)^2}{\sum_{i=1}^{N}(O_i - \bar{O})^2} \quad \text{(Equation 4.3)}$$

$$R^2 = \frac{[\sum_{i=1}^{n}(O_i - \bar{O})(S_i - \bar{S})]^2}{\sum_{i=1}^{n}(O_i - \bar{O})^2 \sum_{i=1}^{n}(S_i - \bar{S})^2} \quad \text{(Equation 4.4)}$$

$$PBIAS = 100 \times \frac{\sum_{i=1}^{n}(O - S)_i}{\sum_{i=1}^{n} O_i} \quad \text{(Equation 4.5)}$$

$$RSR = \frac{\sqrt{\sum_{i=1}^{n}(O-S)_i^2}}{\sqrt{\sum_{i=1}^{n}(O_i-\bar{S})^2}} \quad \text{(Equation 4.6)}$$

where *n* is the number of observations, σ_O is the standard deviation of the observed discharge, with S_U and S_L representing the upper 97.5th and lower 2.5th percentiles of the simulated 95PPU, respectively; *r* is the linear regression coefficient between observed and simulated data; α is the ratio of the standard deviation of simulated and observed data; β is the ratio of the means of simulated and observed data; O_i and S_i are the observed and simulated discharge values, respectively; and $\bar{O}$ and $\bar{S}$ are the mean of observed and simulated discharge values.

4.3. Results

4.3.1.Model Calibration and Validation

Figure 4.4 illustrates the results of the calibration and validation for the modeled discharge, using the SUFI-2 calibration technique. The hydrograph generally indicates a good fit of the daily discharge dynamics by the SWAT model. This is also emphasized by the statistical quality of the model shown in Table 4.5. According to Moriasi et al. (Moriasi et al., 2015), *PBIAS*, *NSE*, and R^2 perform very well for both the calibration and the validation period. Nevertheless, in some years (e.g., 1959, 1961) the model overestimates discharge, whereas in contrast, slight underestimations can be observed at the transitions from the dry to the rainy seasons (e.g., 1963/1964, 1964/1965, 1965/1966, 1966/1967, 1969/1970) (Figure 4.4). However, the general model performance shows a good agreement between simulated and observed discharge, which is also highlighted by the flow duration curve (FDC) (Figure 4.5). The FDC nearly indicates a perfect fit, with slight underestimations of the low flows and the upper 2%–3% of the exceedance probabilities by the model. These extreme flows account in total for about 11%–15% of the annual water yield. The uncertainty of the simulations represented by the 95PPU band are quite low for the low flows, whereas the uncertainty is highest for flows between 1000–2300 m^3/s. This can be attributed to some overestimated peaks (1959, 1961) and also the model´s difficulties in simulating a small peak just before the main peak (e.g., 1963, 1964). The water balance values (Table 4.6) are consistent with other publications in this area with regard to the groundwater recharge (Gabiri et al., 2018; MacDonald and Bonsor, 2010), precipitation (Koutsouris, 2017; Koutsouris et al., 2016; Yawson et al., 2005), evapotranspiration (Nyenzi et al., 1981), and potential evapotranspiration (Dagg et al., 1970). The ratio of surface runoff and baseflow coincides with the baseflow filter technique of Arnold et al. (Arnold et al., 1995). Precipitation data is the key driver of rainfall runoff models, but is also a source of uncertainty, especially in data-scarce regions (Beven, 2012). Due to the low number of precipitation stations and their distribution within the catchment in either low altitudes in the eastern part or high altitudes in the western part of the catchment, elevation bands (Neitsch et al., 2011) were implemented. The effect on the average precipitation among the subcatchments is shown in Figure 4.6. The figure clearly illustrates the variation of precipitation within the single subcatchments. This is particularly true in the eastern part, where the mountainous region of the Udzungwa Mountains in the north and the Mahenge Highlands in the south receive more than 50 mm of additional precipitation as measured in the

valley. In the western part of the catchment, a reverse effect is visible, with decreased precipitation in the low altitude subcatchments due to the high altitude of the precipitation stations. All these changes are attributed to the implementation of the elevation bands, as all parameters of the final parameter solution are unchanged except for the elevation bands. Due to the numerous solutions within the uncertainty band, this is only one representative example of the importance of orographic precipitation patterns in the Kilombero Catchment.

Table 4.5 Summary of the quantitative model performance analysis for the calibration and validation period. P-factor is the percentage of measured data covered by the 95PPU uncertainty band, *R-factor* is the relative width of the 95PPU uncertainty band, R^2 is the coefficient of determination, *NSE* is the Nash–Sutcliffe efficiency, *PBIAS* is the percent bias, *KGE* is the Kling–Gupta efficiency, and *RSR* the standard deviation of measured data.

Simulation Period (Daily)	**P-Factor**	***R-Factor***	***R^2***	***NSE***	***PBIAS***	***KGE***	***RSR***
Calibration (1958–1965)	0.62	0.45	0.86	0.85	0.3	0.93	0.38
Validation (1966–1970)	0.67	0.56	0.80	0.80	2.5	0.89	0.45

Table 4.6 Water balance components for the entire simulation period (1958–1970).

Water Balance Components	**in (mm)**
Precipitation	1344
Actual evapotranspiration	788
Potential evapotranspiration	1380
Surface runoff	43
Lateral flow	58
Base flow	209
Recharge to the deep aquifer	242

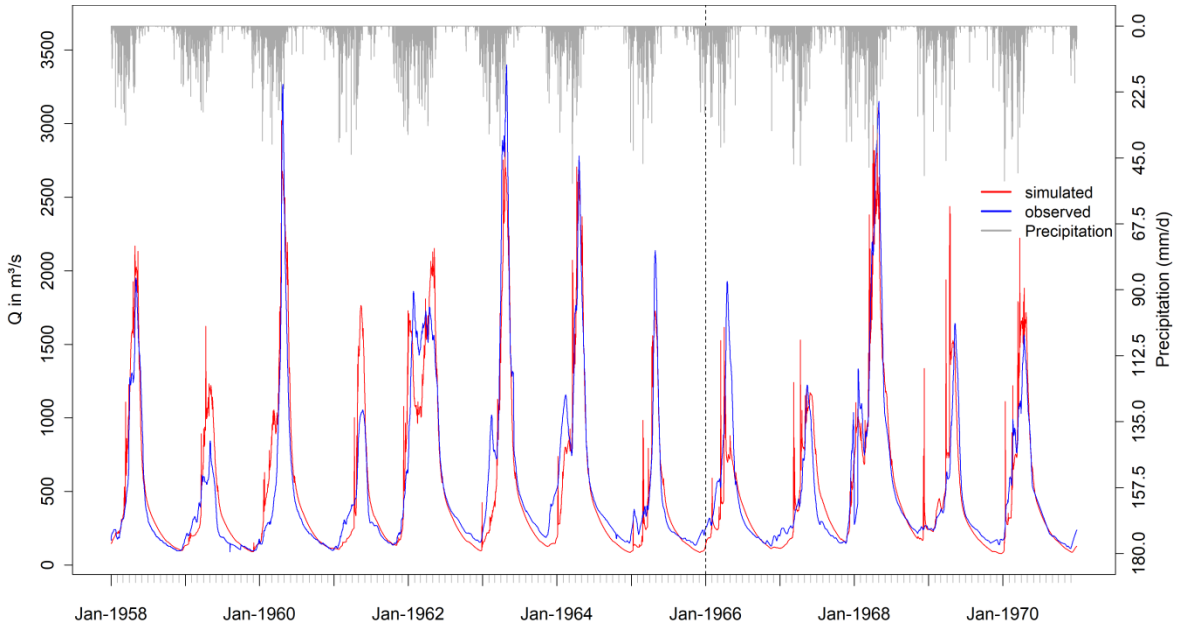

Figure 4.4 Hydrograph showing the observed and the simulated discharge for the calibration (1958–1965) and the validation period (1966–1970), separated by the vertical dashed line. Statistical measures are shown in Table 4.5.

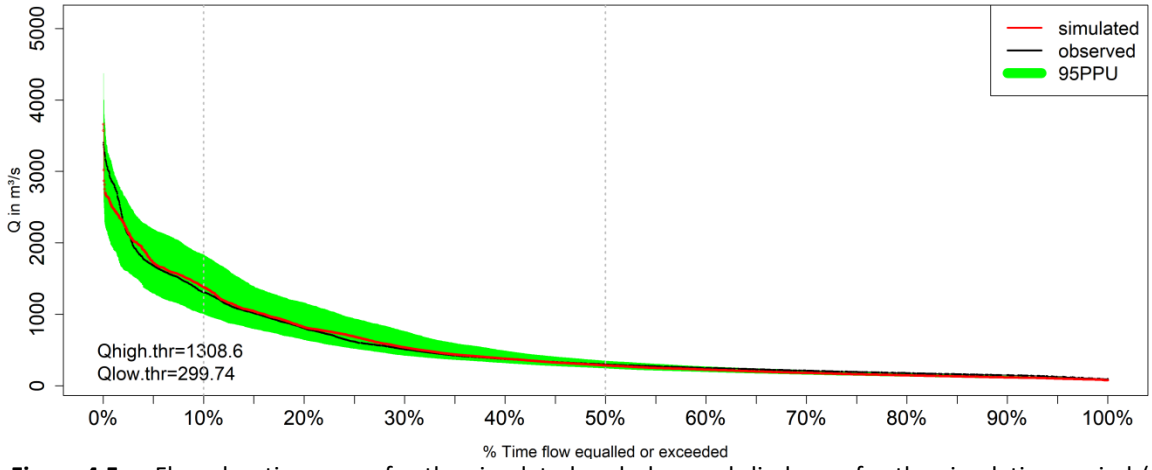

Figure 4.5 Flow duration curve for the simulated and observed discharge for the simulation period (1958–1970). Additionally, the 95PPU is illustrated, which represents the modeling uncertainty by showing the cumulative distribution of flow between the 2.5th and 97.5th percentiles of all the simulation solutions. Statistical measures for the ranked simulated and observed values are 0.99 for R^2 and *NSE*, respectively.

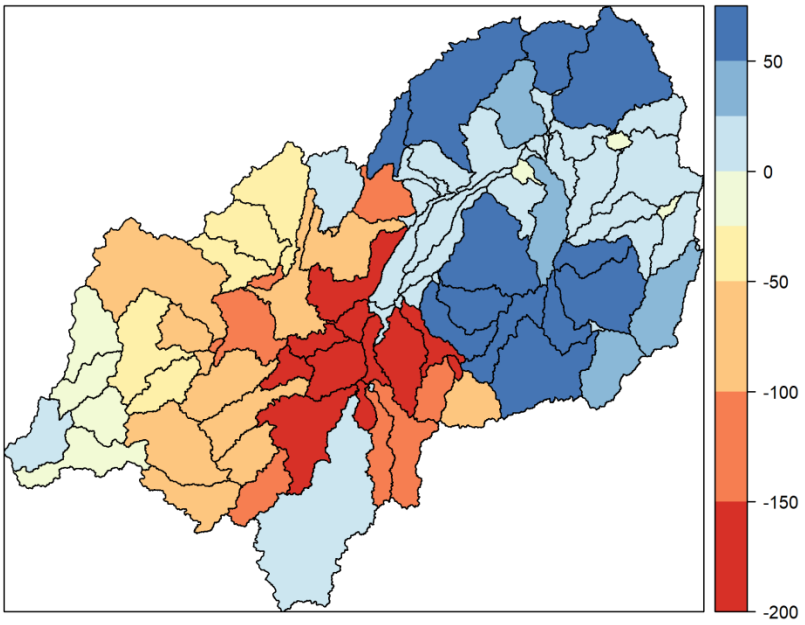

Figure 4.6 Spatial variations in average precipitation (mm) between 1958–1970, due to the implementation of elevation bands. Positive values correspond to increased precipitation due to the implementation of elevation bands, and vice versa.

4.3.2.Spatio-Temporal Analysis

Precipitation is the main driver for hydrological processes (Tang et al., 2009), hence an overview of the temporal precipitation pattern (Figure 4.7) is crucial for the interpretation of the hydrological processes occurring in the catchment. Figure 4.7 underlines the distinction of wet and dry seasons by showing the monthly precipitation patterns for the entire catchment. The rainy season starts in November/December and lasts until April—and in some years up to May (1961, 1967, and 1968). Alterations with bimodal and unimodal patterns are also visible, whereas some years show pronounced monthly precipitation peaks in December or January, representing the irregular occurrence of the small rainy season (1961, 1967, and 1970) (Koutsouris et al., 2016). In March 1963, which was an exceptionally wet period over all East Africa (Nicholson, 1996), precipitation exceeded 400 mm.

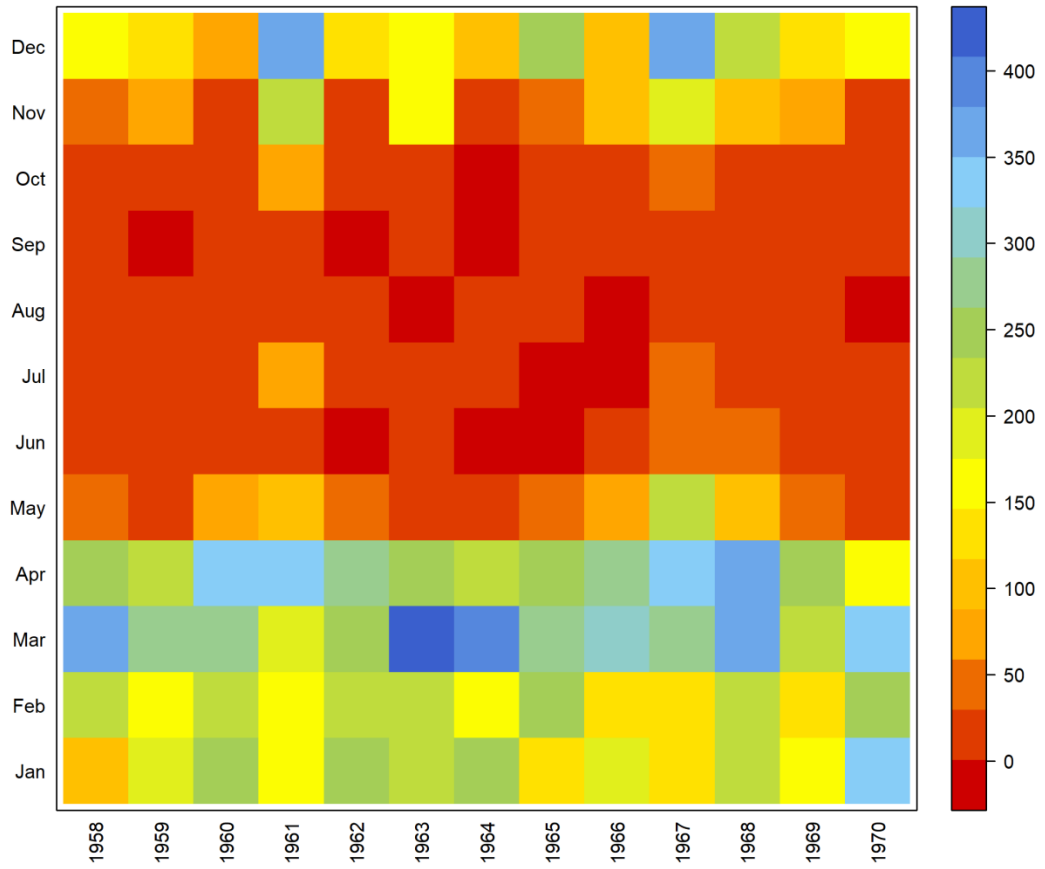

Figure 4.7 Matrix illustrating the mean monthly areal precipitation (mm) patterns within the simulation period (1958–1970) for the Kilombero Catchment.

The boxplots in Figure 4.8 illustrate the high (a) interannual and (b) intraannual variability of discharge. The clear distinction between the wet and dry seasons is obvious from the boxplots in Figure 4.8b. The seasonal distinction of the overall discharge is deconstructed into the single water balance components on a monthly timescale in Figure 4.9. Lateral and surface runoff only occur in the rainy season, with peaks in March and April, whereas the more pronounced baseflow peaks in April and May result in the highest water yield in April. Evapotranspiration and potential evapotranspiration are almost identical from February to May, but differ by more than 150 mm in September and October, indicating a water deficit in the dry season. The potential evapotranspiration more or less follows an antithetical pattern compared to the precipitation pattern (Figure 4.9).

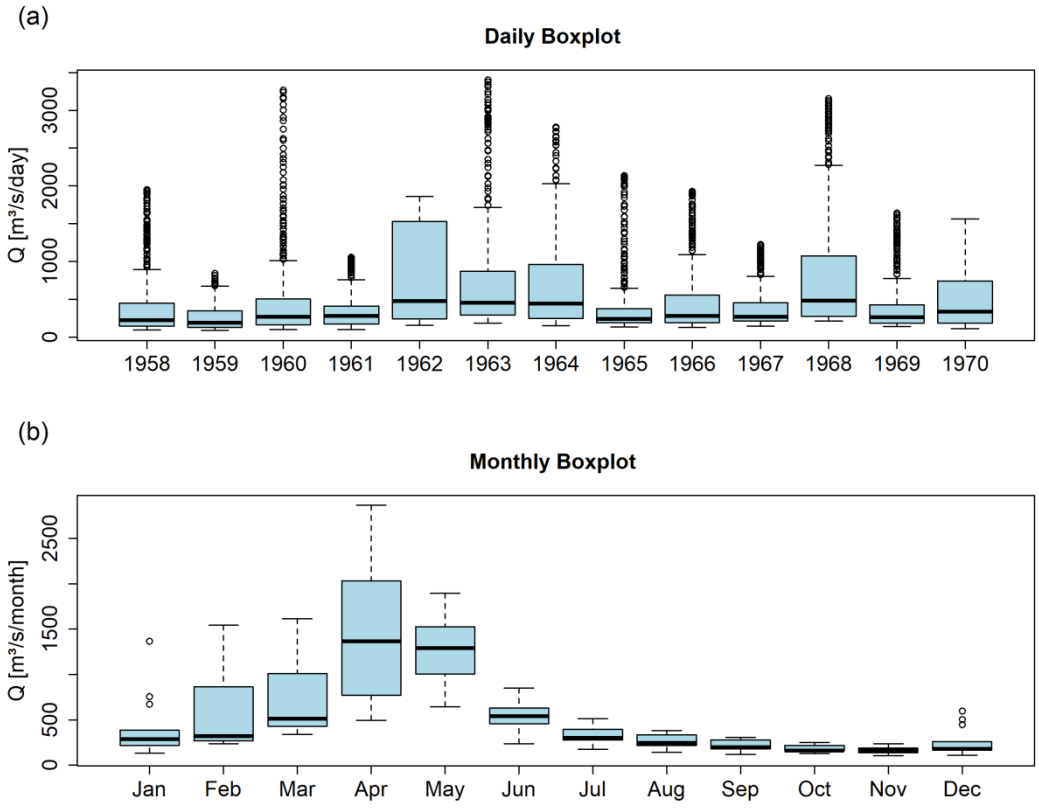

Figure 4.8 Boxplots for discharge on (a) daily and (b) monthly resolution, emphasizing the variation of discharge on different timescales and the distinction of wet and dry season.

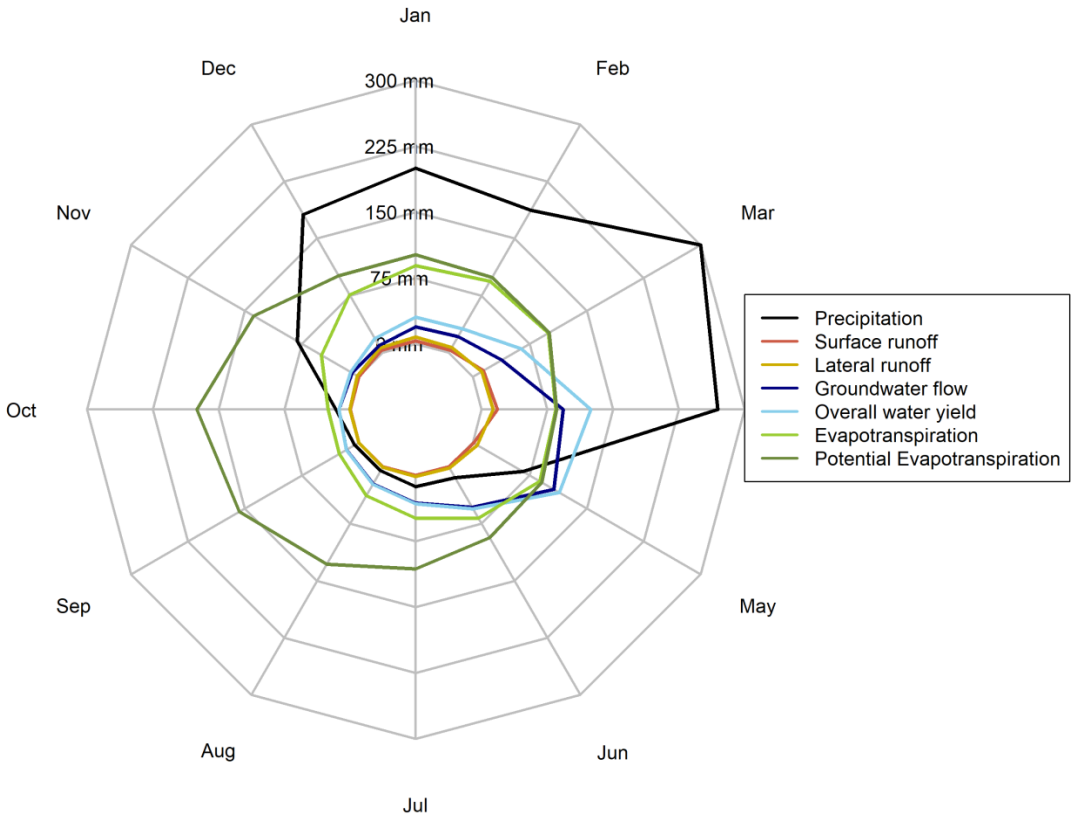

Figure 4.9 Monthly averages of the water balance components for the Kilombero Catchment within the simulation period (1958–1970).

Figure 4.10 illustrates the influence of single water balance components on the subcatchment scale. The spatial pattern of the water yield fluxes (Figure 4.10 a–d) mirrors the general picture of the precipitation, by showing a high contribution from the mountainous subcatchments compared to the contribution of water from the valley. The patterns of surface (Figure 4.10a), lateral (Figure 4.10b), and groundwater (Figure 4.10c) contribution also show contradictory patterns in several subcatchments. Surface runoff and lateral flow show some discharge hotspots, which mainly occur in steep areas with clayey (surface runoff) or sandy (lateral flow) topsoils. Figure 4.10d shows the overall water yield, underlining the contribution of water from the mountains to the valley, especially from the northern Udzungwa Mountains and the Mahenge Highlands. Vice versa, the evapotranspiration and potential evapotranspiration patterns exhibit high values in the valley compared to the mountainous parts of the catchment (Figure 4.10e, f).

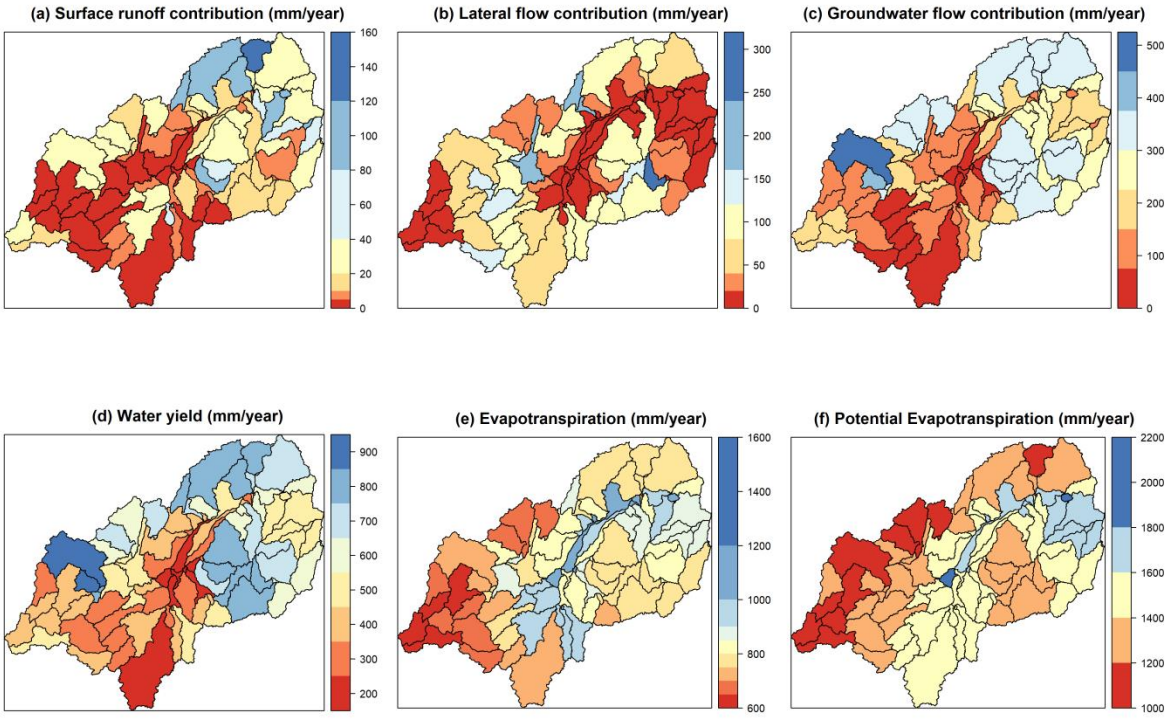

Figure 4.10 Spatial mapping of mean annual values of (a) surface runoff contribution, (b) lateral flow contribution, (c) groundwater contribution, (d) the overall water yield, (e) actual evapotranspiration, and (f) the potential evapotranspiration for the subcatchments.

4.3.3.Land Use and Land Cover Changes and their Impact on Water Resources

Figure 4.11 shows the percentage shifts among the LULC classes from the 1970s up to 2014, as opposed to the classes' spatial representation shown in Figure 4.3. In this case study, most parts of the wetland are classified as grassland and cropland, as it is a seasonally flooded grassland prone to conversions into cropland (Figure 4.3a–d). Noteworthy is the high share of savanna and grassland, as well as the shift among savanna, grassland, and agriculture, besides forest-mixed and forest-evergreen, which is mainly attributed to problems in the classification of the Landsat images. These misclassifications are mainly caused by spectral class similarity and lack of suitable data, especially in early dates. Nevertheless, the share of agricultural land increased significantly from 2004 to 2014, which is also reported by other studies (Leemhuis et al., 2017; Mombo et al., 2011). The fringe of the wetland and the western part of the catchment (Figure 4.3) are most strongly affected by an increase in agricultural land.

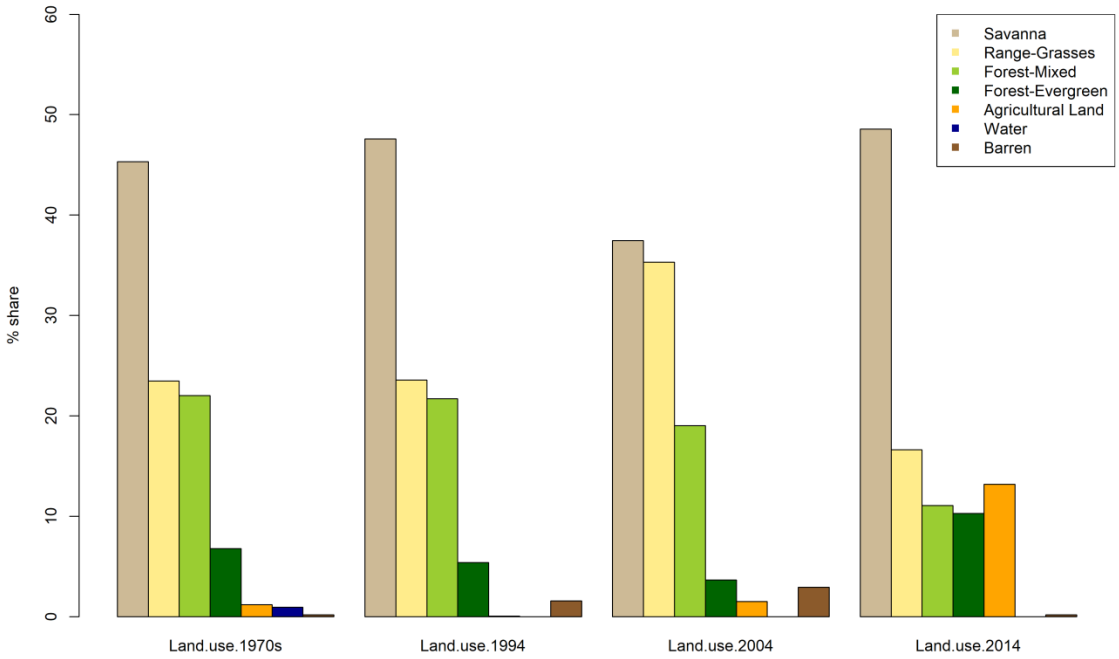

Figure 4.11 Percentage share of the land use/land cover (LULC) classes within the Kilombero Catchment from the 1970s up to 2014.

Figure 4.12 shows the variations of surface runoff (Figure 4.12a), groundwater contribution (Figure 4.12b), evapotranspiration (Figure 4.12c), and the overall water yield (Figure 4.12d) on subcatchment scale between the LULC setup from the 1970s to 2014. Evapotranspiration and groundwater contribution show decreasing trends in the floodplain, where grassland is turned into cropland and the share of water on the total land cover is reduced (Figure 4.3 and Figure 4.11). One subcatchment in the western part, where grassland was converted into either agricultural land or barren, indicates a strong decrease in groundwater contribution (Figure 4.3 and Figure 4.12b). This decrease in groundwater contribution coincides with higher evapotranspiration (agricultural land) and higher surface runoff (barren). However, many subcatchments in the mountainous parts show increasing groundwater contributions and water losses due to evapotranspiration. These higher values are mainly occurring in subcatchments with a rising share of evergreen forests or savanna in 2014. Between 1970 and 2014, in areas where savanna was converted into grassland or agricultural land, the development of surface runoff showed an inverted development, with increasing surface runoff amounts. This happened mainly in the eastern parts of the catchment and on the fringe of the floodplain (Figure 4.12a). The general picture indicates a decrease of water yield (Figure 4.12d) in the Kilombero Valley related to the lower evapotranspiration values, whereas some subcatchments in the Udzungwa Mountains and the Mahenge Highlands show increasing water contribution, which corresponds to the spatial pattern of the increased groundwater contribution (Figure 4.12b).

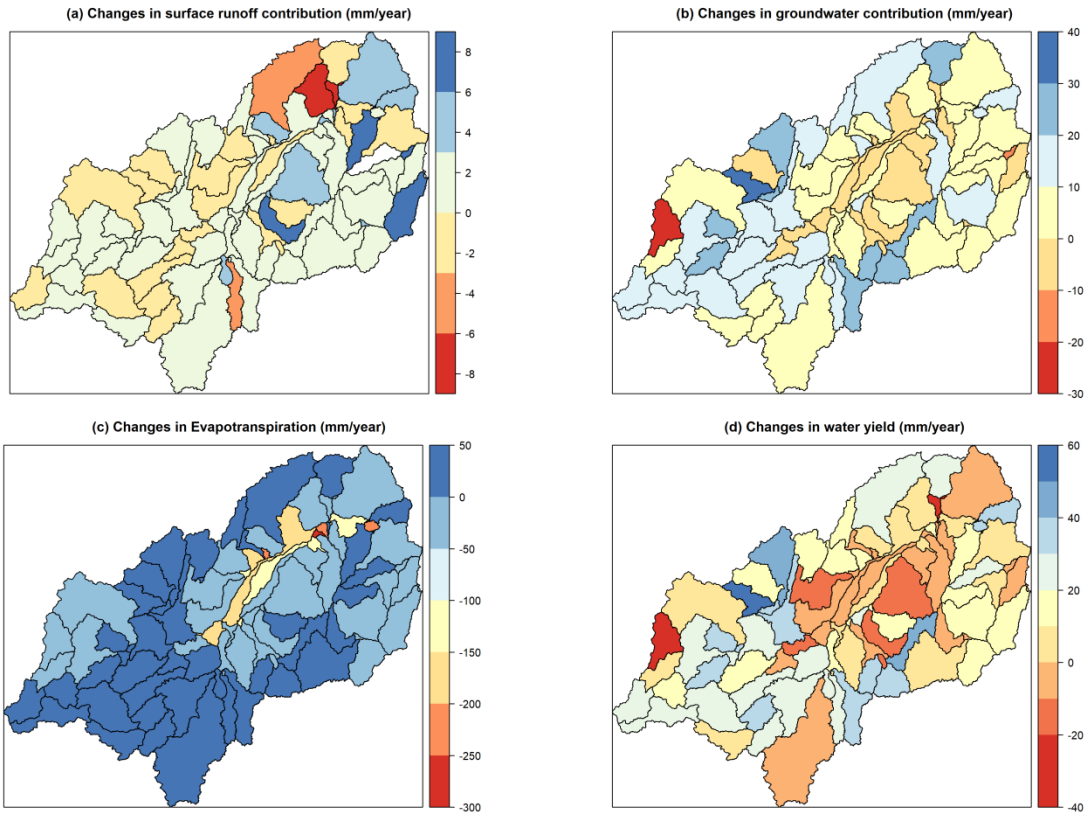

Figure 4.12 Average shifts in water balance components (in mm) for the simulation period, comparing changes from the 1970s land use map with the 2014 land use map. (a) Deviations in surface runoff, (b) groundwater contribution, (c) evapotranspiration, and (d) the overall water yield are displayed.

Figure 4.13 shows the average hydrological impacts within the simulation period for the Kilombero Catchment, considering another temporal scale that shows the monthly changes for the single water balance components. Except for increasing groundwater flow and changes in evapotranspiration (Figure 4.13b), the monthly changes within the entire catchment are rather small. The shift from 2004 to 2014 (Figure 4.13d) seems to be negligible. However, Figure 4.14 shows more pronounced the effects of the LULCC from 2004 to 2014 on the subcatchment scale. Surface runoff contribution is increasing in almost the entire valley and in the eastern Udzungwa Mountains by up to 10 mm (Figure 4.14a), which is 23% higher surface runoff compared to the average catchment surface runoff (Table 4.6). This is due to accelerated conversion into agricultural land. In contrast, the groundwater contribution is decreasing by up to 20 mm within this area, reinforcing changes in the system's hydrology (Figure 4.14b). The overall water yield patterns (Figure 4.14d) are more complex, with decreasing water fluxes in subcatchments prone to anthropogenic activities in the fringe of the wetland, due to the lower groundwater contribution. Hence, water yield in the upper western part of the catchment is increasing, because of the increasing surface runoff and the conversions into barren and cropland. Evapotranspiration (Figure 4.14c) is slightly increasing within the wetland and in most of the mountainous subcatchments, resulting in a loss of water for the catchment. Only the fringe of the wetland shows coherent lower evapotranspiration values. The changes from 2004 to 2014 were exemplarily chosen to be shown here,

as their pattern of change with the distinct conversion into cropland (Figure 4.11) is the most probable future land use pattern for the Kilombero Catchment.

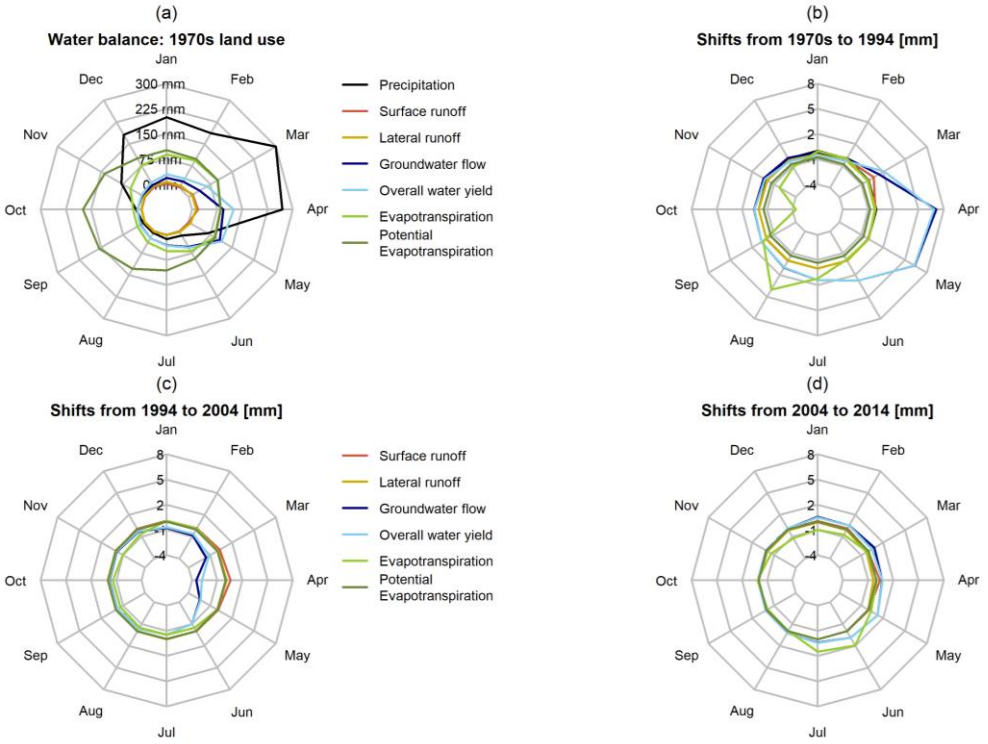

Figure 4.13 Shifts in water balance components (in mm) for the entire catchment on a monthly time scale running the model with four different land use maps. (a) Shows the water balance of the 1970s land use map run, (b) displays a comparison of the 1970s map with the land use of 1994, (c) the changes from 1994 to 2004, and (d) illustrates the shifts from 2004 to 2014. All inputs except for land use maps are not modified.

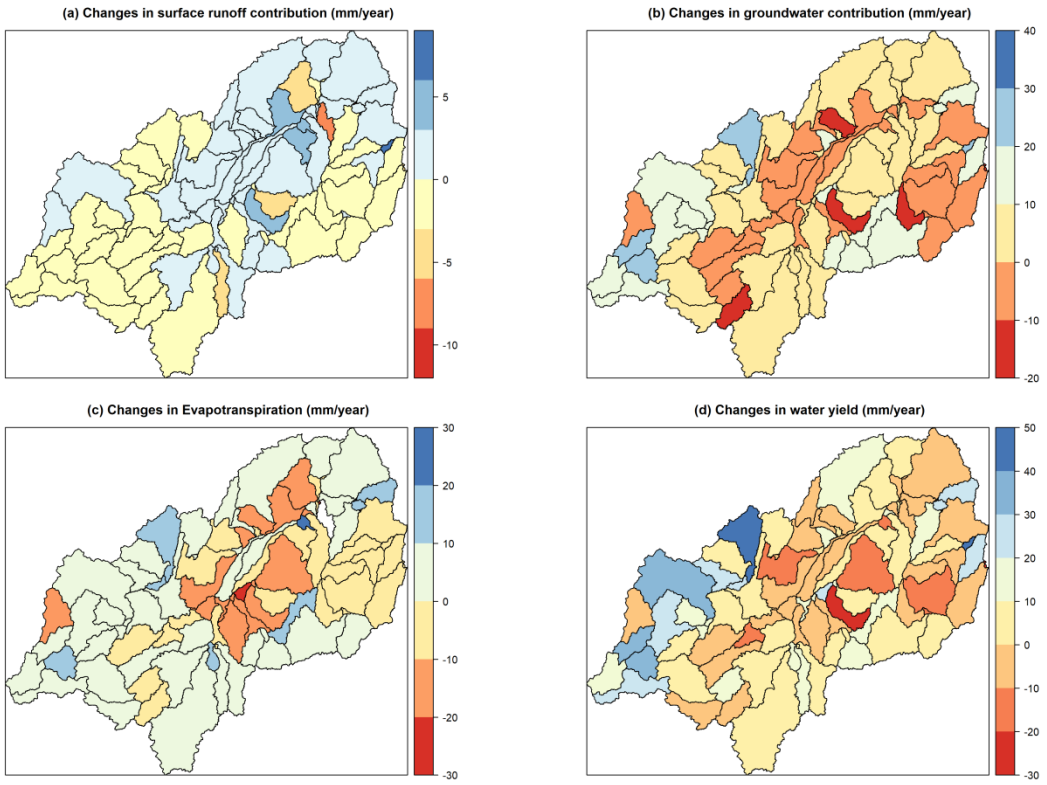

Figure 4.14 Average shifts in water balance components (in mm) for the simulation period, while comparing changes from the 2004 land use map with the 2014 land use map. (a) Changes in surface runoff, (b) groundwater contribution, (c) evapotranspiration, and (d) the overall water yield.

4.4. Discussion

4.4.1.Model Evaluation and Spatio-Temporal Analysis

Despite the low number of precipitation stations, the spatio-temporal precipitation pattern of the catchment is represented quite well with the implementation of elevation bands, which was crucial due to the high altitude of the precipitation stations in the western part and the low altitude of the stations in the eastern part of the catchment (Figure 4.6). A comparison of global precipitation datasets (GPDS) has already been published by Koutsouris et al. (Koutsouris et al., 2016), visualising the average spatial precipitation distribution for the Kilombero Catchment among frequently-utilized GPDS. As a result of their study, Koutsouris et al. (Koutsouris et al., 2016) showed large differences in the spatial precipitation patterns of eight different products in some areas within the catchment. What all GPDS have in common is the relatively high rainfall in the Udzungwa Mountains and Mahenge Highlands, which was also the case for the precipitation stations utilized in this study, due to the orographic correction factor implemented with the elevation bands (Figure 4.6). It should not be ignored that most of the GPDS estimated relatively high precipitation amounts for the southwestern part of the catchment, which contradicts with station data available within this study. However, it should be noted that the study of Koutsouris et al. (Koutsouris et al., 2016) applied satellite precipitation estimates that were not operational during our period of investigation, whereas our utilized precipitation stations stopped being

functional before the onset of the satellite products. This temporal mismatch aggravated further comparisons among the GPDS and station data, and we concentrated on the general spatial patterns of precipitation. Moreover, the GPDS pattern for the southwestern region can just be altered by ignoring all three available precipitation stations in this area. This is also not a suitable option, keeping in mind the generally high uncertainty with regard to precipitation patterns in that region, according to the GPDS, which has already been proven by Koutsouris et al. (Koutsouris et al., 2016). For example, the difference between the station data and the patterns of the GPDS in the southwestern catchment area is still smaller than the differences between certain GPDS, like the Global Precipitation and Climatology Center v6 data set (GPCC) (Becker et al., 2013) and the Modern Era Retrospective-Analysis for Research and Applications (MERRA) (Rienecker et al., 2011). These both show opposing results when comparing precipitation patterns from the Mahenge Highlands and the Udzungwa Mountains (Koutsouris et al., 2016), and therefore much larger differences than the station data and the general picture of the GPDS in the southwestern Kilombero Catchment. Thus, in mountainous tropical regions, with persistent cloud coverage, an understanding of the strengths and limitations of remote sensing products are a prerequisite for an adequate application (Munishi-Kongo, 2013). In spite of these uncertainties, large-scale precipitation patterns are captured quite well with remote sensing products (Adjei et al., 2014; Mashingia et al., 2014).

The hydrograph (Figure 4.4), the flow duration curve (Figure 4.5), and the statistical model performance (Table 4.5) all indicate a good to very good performance of the SWAT model for the simulation period (Moriasi et al., 2015). However, some peaks are not captured well, and for some years the discharge is overestimated (1959, 1961 in Figure 4.4), which leads to the slightly lower *NSE* (Table 4.5) compared to the other evaluation criteria, because of the high sensitivity of the *NSE* to peaks (Legates and McCabe Jr., 1999). For the model setup, this study followed the procedure and calibration techniques given by Arnold et al. (Arnold et al., 2012b) and Abbaspour et al. (Abbaspour et al., 2015), by keeping the model parametrization within the requirements of parsimony and robustness (Troch et al., 2013). Although the number of parameters is quite large compared to other model applications in the tropics (Yira et al., 2016), it is still in the range of similar applications of the SWAT model under tropical conditions (Bossa et al., 2012; Mango et al., 2011; Ndomba et al., 2008; Strauch and Volk, 2013). Five out of the seven most sensitive parameters are related to groundwater (Table 4.4), which underlines the importance of baseflow for the catchments water yield. These parameters are typical parameters used in SWAT to calibrate baseflow, which was also demonstrated in a meta study by Arnold et al. (Arnold et al., 2012b). In conclusion, these parameters mainly control the occurrence (GWQMN), recession (ALPHA_BF, GW_DELAY), and the vertical movement of groundwater (GW_REVAP, RCHRG_DP), and were calibrated within the default ranges given by SWAT-CUP. The relevance of baseflow in the Kilombero Catchment was already highlighted by Burghof et al. (Burghof et al., 2017). Figure 4.9 illustrates that baseflow contributes nearly 100% of the water yield from June to November on the catchment scale. Furthermore, Gabiri et al. (Gabiri et al., 2018) and Burghof et al. (Burghof, 2017) showed that the depth to the groundwater table is closer to the surface at the fringe of the floodplain compared to the riparian zone, due to the high influence of baseflow contribution from the mountains, especially in the dry season. This shallow groundwater affects plant growth patterns and agricultural activities within the valley, and transects from the river to the fringe with year-round water availability for deeply rooted plants (1–2 m) in the fringe of the floodplain (Gabiri et al., 2018). With regard to water management and

agricultural utilization of the floodplain (Environmental Resources Management, 2013), the findings of this research combined with the aforementioned information on groundwater contribution (Burghof et al., 2017; Gabiri et al., 2018) might raise awareness for the importance of the upland catchment, which is closely linked to the wetland system. This linkage is represented by the already highlighted influence of year-round groundwater contribution from the higher elevations into the valley bottom. Model results show that groundwater contribution is virtually the only water source from June to November (Figure 4.9), and this groundwater is generated in the upper catchment (Figure 4.10d), whereas the wetland itself is prone to high evapotranspiration (Figure 4.10e) and contributes much less water to the stream (Figure 4.10d).

4.4.2.Impact of Land Use and Land Cover Change

Despite different technologies, there is high congruence between the Landsat 5, 7, and 8 sensors, which have the same spatial resolution of 30 m. Their band definitions differ only slightly for most bands, and the effect has been found to be negligible (Vogelmann et al., 2016). A stronger technical and methodological difference exists between the 1970s time step, using the Landsat pre-collection Level 1 at 60 m spatial resolution, and using a conventional mosaicking method due to the lack of a sufficient number of images. The post-classification comparison (PCC) method was used for detecting change, as methodological and technological inter-classification differences are less important. More crucial is the respective classification accuracy, as with PCC errors are propagated (Hecheltjen et al., 2014). For the Kilombero Catchment, classes more prone to error were the natural classes: savanna, range grasses, wetland, and forest-mixed. Some confusion also exists among savanna, range grasses, and agriculture; however, our PCC results are mostly logically consistent and conform to historical maps. The conversion of natural classes to agriculture results in rather strong spectral changes, whereas the modification of forests by single tree extraction cannot be adequately resolved, neither with PCC nor with methods based on spectral bands.

Due to the aforementioned circumstances, the conversion of forested areas and savanna in the upper catchment might significantly influence water quantity and the year-round water contribution to the stream. Deforestation activities in the entire catchment are already occurring (Leemhuis et al., 2017; Wilson et al., 2017), and may lead to a shift from slow groundwater contribution to fast surface water contribution from the uplands (Lal, 1997). The increased share of cropland, which results in a reduced retention capacity, will influence the flow regime, with declining low flows and aggravated flooding. This is especially important, as vulnerability to floods and droughts is already highlighted as a challenge for the floodplain area in the Integrated Water Resources Management and Development Plan (IWRMDP) (WREM International Inc., 2013). The conversion of forests and savanna into crop- and grassland and its subsequent hydrological impacts will aggravate this vulnerability. These relationships are visualized in Figure 4.13 and Figure 4.14. While interpreting Figure 4.13, one has to keep in mind that complex large river basins like the Kilombero could conceal small-scale effects (Wilk and Hughes, 2002), as already shown by Wagner et al. (Wagner, 2013). Furthermore, this figure illustrates monthly averages of a 13-year simulation period, implying additional concealing effects and a too-broad time scale to account for daily events. Following the approach of Wagner et al. (Wagner, 2013), Figure 4.14 shows the impacts on subcatchment scale, with increasing surface runoff due to anthropogenic activities. The decreasing

evapotranspiration at the fringe of the floodplain (Figure 4.14c) can be attributed to the lower evapotranspiration of the agricultural land. For the envisioned large-scale rice schemes of the SAGCOT plans, the floodplain could be modified into rice instead of agricultural land use, which will influence evapotranspiration significantly. Figure 4.14generally shows a complex picture with regard to changes in water balance components (see section 3.3). This complex picture fosters the concealing effects of the large catchment. Furthermore, the different results from Figure 4.13 and Figure 4.14, as well as the temporal changes in water balance components (Figure 4.9) underline the scale dependency of the hydrological processes in both space and time within the Kilombero Catchment, and therefore the need to consider various spatio-temporal scales for water management plans.

Apart from these scale effects, LULCC within the valley itself in relation to the implementation of a growth corridor are far from being negligible concerning water quantity. The especially high contribution of groundwater fluxes from the upper catchment throughout the whole year is important for the wetland, its vegetation, and also for the agricultural activities and the attached food security. The implicated conversion from grassland to cropland in the growth corridor (Leemhuis et al., 2017) additionally affects water quality negatively, which is another important aspect when investigating wetlands. Regarding the transport of sediments, nutrients, pesticides, and bacteria, data availability is insufficient. Nevertheless, this topic could be interesting for future investigations, especially with regard to the planned intensification of agricultural activities (Environmental Resources Management, 2013). These increased agricultural activities potentially result in economic benefits, consequently followed by increasing population through demographic growths and migration. This increasing population might lead to further encroachment of the uplands, and therefore increased pressure on savanna as well as upland forests, which will foster the aforementioned changes with regard to water resources. Considering these circumstances, the long-term effects might therefore imply increasing surface runoff contributions due to upland deforestation, and consequently lower retention potentials for flood mitigation in the rainy season, as well as decreased low flow supply in the dry season. Another aspect that needs more investigation from social science perspective, with regard to the planned large-scale utilization of the valley, are rising land use conflicts among farmers and pastoralists, which are often caused by a lack of sufficient pasture or water supplies (Benjaminsen et al., 2009).

According to the IWRMDP, significant groundwater resources exist within the northeastern part of the Ramsar site (Kibasila Wetland). These groundwater resources are seen as a potential source for irrigation, although the overall potential of this aquifer is not yet explored and the implications on surface-groundwater interactions are uncertain (WREM International Inc., 2013). However, for some areas, a moderately low hydraulic conductivity towards the riparian zone has already been investigated (Bonarius, 1975; Gabiri et al., 2018). For a sustainable use of water resources in the Kilombero Catchment, future research should focus on the ongoing responses to anthropogenic impacts like land cover conversion and the impact of climate change, as well as management impacts, such as the construction of dams or the intensified utilization of nutrients and pesticides.

4.5. Conclusions

A combination of local discharge and precipitation data, combined with multi-temporal Landsat images and freely available geo datasets, allowed a detailed and distributed analysis of the hydrological system of a topographical complex East African catchment. This is the first study with distributed information on the water balance in Kilombero Catchment, which is strongly affected by LULCC and will be further affected by climate change and more pronounced LULCC in the near future. As it also comprises a Ramsar site, many interests collide within the catchment. They need to be harmonized by sustainable water management, and therefore, well-informed decisions are needed. This study showed the scale dependency of water resources in the Kilombero Catchment and the need for distributed modeling. It was demonstrated that the wetland is severely dependent on mountainous water resources and year-round groundwater contribution. Therefore, we emphasize the necessity of protecting upland forests as one important factor to ensure a perennial water supply for the valley bottom, its embedded wetland, and the inherent ecosystem services provided by both the wetland and the upland forests. So far, LULCC occur predominantly within the Kilombero Valley, and has had rather local effects on the water balance components over the past years. At the same time, the mountainous areas that are the most important source of groundwater experienced much less LULCC. For future management of the Kilombero Catchment, it will be important to prevent these upland areas from extensive LULCC, in order to sustain water availability in the wetland. Apart from this case study, this article might serve as an example of how to utilize the available historic precipitation (Funk et al., 2015a) and discharge data (Tang and Oki, 2016), and how to combine them with historic climate model runs, global soil data, and LULC data gathered from earth observation images for meso- to large-scale applications, especially in data-sparse regions like Sub-Saharan Africa.

Author Contributions: K.N., B.D. and C.L. conceived and designed the experiments; K.N. performed the experiments; K.N., B.D. and C.L. analyzed the data; S.S. and F.T. produced the land use maps; R.v.d.L. and L.S.S. processed the climate data. K.N. wrote the article. All authors made revisions and improvements to the final version.

Funding: This study was supported through funding from the German Federal Ministry of Education and Research (FKZ: 031A250A-H); German Federal Ministry for Economic Cooperation and Development under the “GlobE: Wetlands in East Africa” project.

Acknowledgments: The authors would like to thank the Rufiji Basin Water Board for data sharing and assistance in the field and Salome Misana for her administrative guidance and logistic assistance.

Conflicts of Interest: The authors declare no conflict of interest. The founding sponsors had no role in the design of the study; in the collection, analyses, or interpretation of data; in the writing of the manuscript; or in the decision to publish the results.

5. Impact of Climate Change on Water Resources in the Kilombero Catchment in Tanzania

This chapter has been published as: Näschen, K., Diekkrüger, B., Leemhuis, C., Seregina, L.S. und R. van der Linden (2019): Impact of Climate Change on Water Resources in the Kilombero Catchment in Tanzania. Water 11, 859. doi:10.3390/W11040859.
https://www.mdpi.com/2073-4441/11/4/859

Abstract: This article illustrates the impact of potential future climate scenarios on water quantity in time and space for an East African floodplain catchment surrounded by mountainous areas. In East Africa, agricultural intensification is shifting from upland cultivation into the wetlands due to year-round water availability and fertile soils. These advantageous agricultural conditions might be hampered through climate change impacts. Additionally, water-related risks, like droughts and flooding events, are likely to increase. Hence, this study investigates future climate patterns and their impact on water resources in one production cluster in Tanzania. To account for these changes, a regional climate model ensemble of the Coordinated Regional Downscaling Experiment (CORDEX) Africa project was analyzed to investigate changes in climatic patterns until 2060, according to the RCP4.5 (representative concentration pathways) and RCP8.5 scenarios. The semi-distributed Soil and Water Assessment Tool (SWAT) was utilized to analyze the impacts on water resources according to all scenarios. Modeling results indicate increasing temperatures, especially in the hot dry season, intensifying the distinctive features of the dry and rainy season. This consequently aggravates hydrological extremes, such as more-pronounced flooding and decreasing low flows. Overall, annual averages of water yield and surface runoff increase up to 61.6% and 67.8%, respectively, within the bias-corrected scenario simulations, compared to the historical simulations. However, changes in precipitation among the analyzed scenarios vary between −8.3% and +22.5% of the annual averages. Hydrological modeling results also show heterogeneous spatial patterns inside the catchment. These spatio-temporal patterns indicate the possibility of an aggravation for severe floods in wet seasons, as well as an increasing drought risk in dry seasons across the scenario simulations. Apart from that, the discharge peak, which is crucial for the flood recession agriculture in the floodplain, is likely to shift from April to May from the 2020s onwards.

Keywords: SWAT model; climate change; scenario analysis; hydrology; return probabilities; hydrological extremes

5.1. Introduction

Wetlands in East Africa cover an area of approximately 180,000 km^2 (Leemhuis et al., 2016; Stevenson and Frazier, 1999) and a share of about 10% of the land surface in Tanzania, although numbers vary regarding this (Amler et al., 2015). Nevertheless, the importance of wetlands in East Africa for the provision of numerous ecosystem services, ranging from the improvement of mental well-being (Heinkel, 2018) to water and climate regulation (Maltby and Acreman, 2011), is well proven. Yet, East African wetlands are endangered due to anthropogenic activities (Gardner and Finlayson, 2018). This pressure is driven by several push factors, such as population growth, degradation of upland soils, and

increasing rainfall variability due to climate change. In contrast, wetlands have relatively fertile soils in combination with year-round water availability as pull factors for the conversion of wetlands into cropland (Behn et al., 2018; Beuel et al., 2016; Gabiri et al., 2017; Kirimi et al., 2018). This conversion in favor of food production consequently has negative trade-off effects on other ecosystem services.

Policies attempting to protect wetlands have often been weakly enforced (Mombo et al., 2011). Furthermore, the government of Tanzania introduced the "Kilimo Kwanza" (agriculture first), prioritizing agricultural development (Munishi-Kongo, 2013), especially in designated growth corridors. In Tanzania, the SAGCOT (Southern Agricultural Growth Corridor of Tanzania) growth corridor plays a key role. It is composed of several clusters, including the Kilombero cluster, which contains an endangered Ramsar site with considerable biodiversity resources under a condition of high stress (Wilson et al., 2017). The most important cash crop is, and will be, according to the plans of SAGCOT, rice (Environmental Resources Management, 2013). Apart from potential ecological trade-offs due to large-scale rice production and outgrower schemes in the Kilombero area (Wilson et al., 2017), analysis of the availability of water resources is inevitable to sustainably manage the highly water-dependent rice schemes. Although some research was done on water resources (Burghof, 2017; Daniel et al., 2017; Gabiri et al., 2018; Koutsouris et al., 2016; Leemhuis et al., 2017; Lyon et al., 2015; Näschen et al., 2018; Yawson et al., 2005), the plans of SAGCOT outline future scenarios and demand wise planning, especially with regard to a changing and highly variable climate (Koutsouris, 2017; Seregina et al., 2018).

This work tries to bridge this research gap by simulating possible future climate scenarios with regard to water availability according to the current knowledge (regional) of climate change and hydrological modeling. Hydrological modeling in combination with climate change scenarios allows assessment of potential impacts of climate change on water resources to enable wise planning in agricultural development, as in the SAGCOT corridor, as well as for long term infrastructure projects, such as the planned dam at Stiegler's Gorge (Duvail et al., 2014), which relies to 62% on water from the Kilombero Catchment (Wilson et al., 2017).

There are numerous studies worldwide on the effects of climate change on hydrology. For example, Schneider et al. (Schneider et al., 2013) analyzed large scale impacts of climate change on flow regimes in Europe and found considerable changes in specific regions. The Mediterranean region will become drier due to less precipitation, while the boreal zone of northern Europe will become drier due to rising temperatures and reduced snowmelt. Nevertheless, flood peaks might be aggravated in some northern European regions due to seasonal precipitation and temperature changes. An aggravation of seasonality in streamflow was also observed for two (out of eleven) large river basins in Europe and Australia by Eisner et al. (Eisner et al., 2017). Changes in hydrology are also reported for the western United States due to changing precipitation patterns and anthropogenically-induced impacts, leading to water shortages and aggravated seasonality (Barnett et al., 2008, 2005). Yira et al. (Yira et al., 2017) showed that opposing discharge trends might result from the impact analysis from six climate models in a catchment in West Africa. The findings of these exemplary studies demonstrate the potential impact of climate change on hydrology through the alteration of streamflow amount and seasonality in a global context and emphasizes the nonlinear rainfall-runoff behavior, although the example's concrete results are site specific (Feng et al., 2019). Moreover, uncertainty and variability in climate projections, and therefore the impacts on hydrology, rise with the time horizon (Gelfan et al., 2017).

Several studies have also analyzed climate change in East Africa and specifically in Tanzania (Lalika et al., 2015; Natkhin et al., 2015; Seregina et al., 2018), but the implications for water resources due to climate change on a quantitative level are less well explored, particularly for the Kilombero Catchment and its surroundings. We hypothesize that the outcome of the study is helpful for water and agricultural management in the Kilombero Valley and the projections of the inflow to the planned Stiegler`s Gorge hydropower dam project.

The main objectives arising from this contextual background are the following:

(i) Assess the possible climatic future of the Kilombero Catchment with an emphasis on precipitation patterns and temperature variations;

(ii) Estimate the impact of these climatic changes on hydrology by analyzing temporal and spatial changes in the water balance;

(iii) Analyze the impact of climate change on hydrological risks, such as floods and droughts, through analyzing extreme flow situations.

These objectives are achieved by applying the well-proven hydrological model SWAT (Soil and Water Assessment Tool) in combination with an ensemble of six regional climate model simulations from the Coordinated Regional Downscaling Experiment (CORDEX) Africa project (Gutowski et al., 2016). These model simulations, and furthermore different representative concentration pathways (RCPs), were utilized in the hydrological SWAT model to account for uncertainty with regard to future developments (Moss et al., 2010). The six regional climate models were bias-corrected using local measurements to adequately represent the conditions within the catchment. The results from the SWAT model runs were analyzed with regard to general hydroclimatic patterns and extreme values, concerning peak discharge as well as low flows.

5.2. Materials and Methods

5.2.1.Study Site

The Kilombero Catchment is part of the Rufiji basin, which forms the largest river basin in Tanzania (Figure 5.1). The catchment is situated in the Morogoro region in southern Tanzania and comprises 40,240 km^2 until its confluence with the Rufiji River. The Udzungwa Mountains in the north, with elevation ranging up to 2500 m, as well as the Mbarika Mountains and the Mahenge Highlands in the south, demarcate the border of the catchment. The Kilombero River itself receives perennial inflow mainly from the Udzungwa Mountains forming a seasonal floodplain at around 200 m above sea level (Figure 5.1). The floodplain itself covers an area of 7967 km^2 (Mombo et al., 2011), representing the biggest freshwater wetland in East Africa below 300 m above sea level (Mombo et al., 2011), and is listed as an endangered Ramsar site (Wilson et al., 2017). Intensive mountainous rainfall in combination with year-round groundwater supply (Näschen et al., 2018) ensure a contribution of 62% of the annual runoff volume of the Rufiji River, although the Kilombero Catchment covers only 23% of the drainage area (Wilson et al., 2017).

The climate is sub-humid tropical (Wilson et al., 2017) with annual mean temperatures between 24 °C in the valley and about 17 °C in the higher altitudes (Wilson et al., 2017). The areal annual precipitation amounts are between 1200 and 1400 mm (Koutsouris et al., 2016), with a high spatio-

temporal variability. The mountainous area receives up to 2100 mm precipitation, and therefore up to 1000 mm more precipitation compared to the valley (Näschen et al., 2018; Wilson et al., 2017). The temporal distribution of the annual precipitation is divided into a dry season from June to November and a rainy season from November to May. Additionally, the rainy season can be split into Short Rains from November to January and Long Rains from March to May (Wilson et al., 2017). However, the interannual variability is high (Nicholson, 2000) and the reliability of the Short Rains is not as pronounced as for the Long Rains (Näschen et al., 2018). Given that some parts of the catchment lack the Short Rains, the whole catchment can be characterized by a unimodal to bimodal rainfall distribution, depending on the year and the specific area (Kangalawe and Liwenga, 2005; Koutsouris et al., 2016). The main drivers of these rainfall patterns are the Intertropical Convergence Zone (ITCZ) (Camberlin and Philippon, 2002) and remote forcings, such as the Walker circulation and the Indian Ocean zonal mode (Nicholson, 2017). However, local and regional factors, such as topography and lakes, additionally influence the seasonal rainfall cycle (Seregina et al., 2018). When assessing the possible climatic future of the Kilombero Catchment, it should be noted that rainfall patterns all over East Africa are already changing at present. The long rains, which are influenced by multiple factors, such as local geographic factors, remote forcings, and regional circulations, have been declining in recent decades in eastern Africa, whereas droughts are becoming longer and increasingly stretch into the rainy seasons. Nevertheless, interannual climate variability overall for East Africa has increased in the last decades, resulting in drought periods but also unusual heavy flood events (Nicholson, 2017).

The Harmonized World Soil Database (HWSD) (Dewitte et al., 2013) describes the dominating soils in the valley as Fluvisols and the uplands are predominantly covered by Acrisols and Nitisols (Figure 5.2). In the high altitudes of the western parts of the catchment Lixisols dominate, whereas in the lower altitudes of the eastern catchment mainly Cambisols are found, according to the HWSD.

The upper catchment is dominated mainly by natural vegetation, such as tropical rainforests, bushlands, and wooded grasslands, with some patches of agricultural fields (Zemandin et al., 2011). The valley contains the seasonal floodplain (Figure 5.1), which is characterized by rainfed lowland rice cultivation during the rainy season, whereas agriculturally undisturbed areas are dominated by grassland, such as *Hyparrhenia* spp.*, Panicum fluviicola* Steud., and *Phragmites mauritianus* Kunth (Behn et al., 2018). The fringes of the floodplain successively change from grassland to Miombo woodland towards the upper catchment.

Recent developments demonstrate a strong increase in population, and therefore agricultural land in the area, whereas grassland, savanna, and forested land use are declining, especially at the fringe of the wetland (Leemhuis et al., 2017; Näschen et al., 2018; Wilson et al., 2017). These anthropogenically triggered land use changes in combination with ongoing climate change might alter the hydrological system of the catchment and also affect downstream riparians. Accordingly, small-scale farmers' food production envisioned in the planned large-scale and outgrower rice schemes of the SAGCOT growth corridor (Environmental Resources Management, 2013), as well as the planned dam at Stiegler's Gorge (Duvail et al., 2014), might presumably be influenced by changing water quantity and quality.

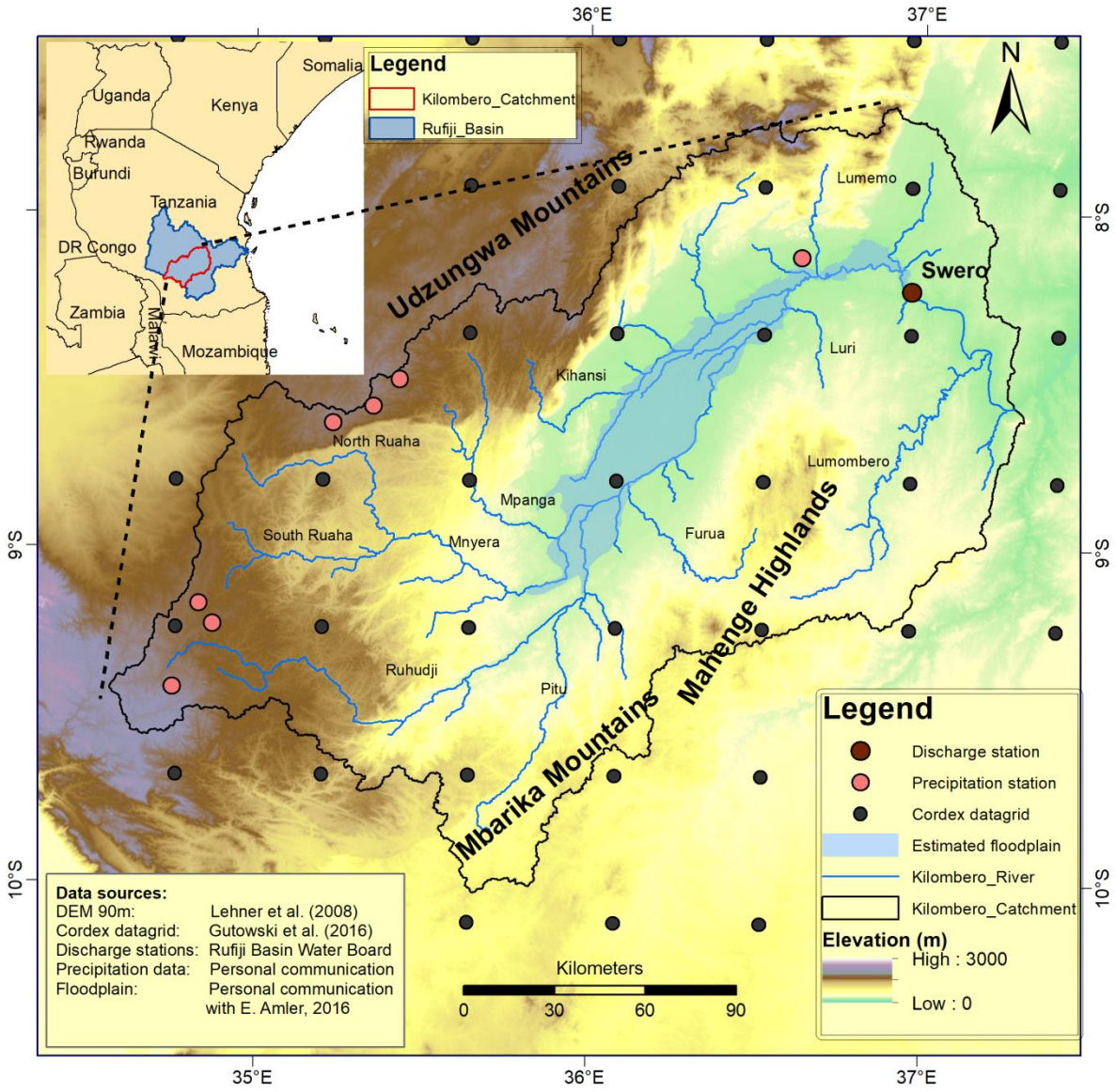

Figure 5.1 Overview map of the study area, including locations of available precipitation and discharge stations (Swero), as well as the 0.44° Coordinated Regional Downscaling Experiment (CORDEX) Africa grid. The estimated floodplain area is based on visual interpretation of Landsat images (modified after (Näschen et al., 2018)).

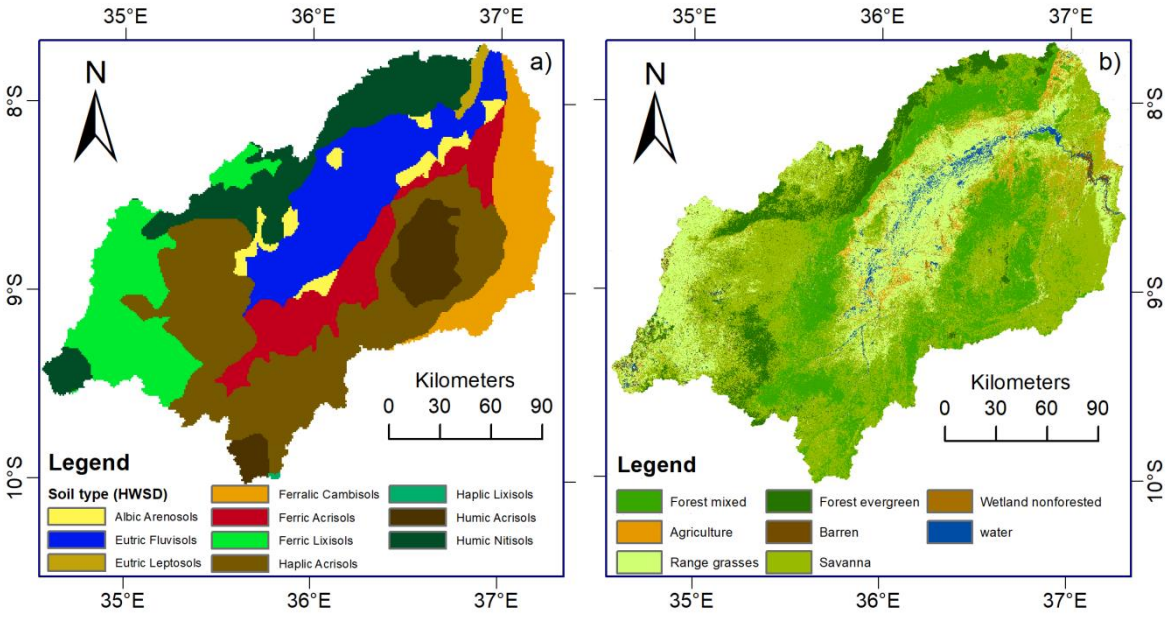

Figure 5.2 Soil map (a) and land use and land cover (LULC) map (b) of the study area. The distribution of soils is derived from the Harmonized World Soil Database (HWSD) (Dewitte et al., 2013) and the LULC map shows the LULC distribution derived from Landsat Level 1 images from 1970 (modified (Näschen et al., 2018) and Leemhuis et al. (Leemhuis et al., 2017)).

5.2.2.Input Data

This study is based on the study by Näschen et al. (Näschen et al., 2018) and follows the same approach as Leemhuis et al. (Leemhuis et al., 2017) to overcome data scarcity in the region through the application of freely available geo datasets in combination with data from local partners in Tanzania to run the hydrological model. The bottleneck to calibrate and validate the hydrological model is the discharge data for the Kilombero Catchment. Adequate discharge time series at the Swero station close to the main outlet of the catchment (Figure 5.1) are only available for the period of 1958–1970 (Table 5.1), due to the logistic challenges of the local authority Rufiji Basin Water Board (RBWB) to maintain the hydrometeorological monitoring network (Munishi-Kongo, 2013).

To gather a realistic representation of the LULC for this period, a mosaic of Landsat Level 1 images from the 1970s was classified with a supervised Random Forest classification (Breiman, 2001; Näschen et al., 2018). Images from the whole decade were utilized due to a lack of suitable images within one single year.

Satellite rainfall estimates could not be applied in this study, due to the temporal mismatch of available discharge data (up to 1970) and satellite estimates. However, a combination of precipitation stations (Figure 5.1, Table 5.1) and modelled climate parameters from the CORDEX Africa project (Figure 5.1, Table 5.1) with a spatial resolution of 0.44° were utilized for calibration and validation of the model.

For the future climate scenarios, Regional Climate Models (RCMs) that were forced with different Global Climate Models (GCMs; Table 5.2) were additionally bias-corrected for precipitation and temperature to adequately represent potential changes in future climate patterns based on available

data (further information in chapter 2.5). To complete the dataset for running the hydrological model, freely available datasets for the Digital Elevation Model (DEM) and the soil map (Table 5.1) were applied.

Table 5.1 Overview of the applied datasets, their resolution, sources, and the required parameters in this study.

Data Set	Resolution/Scale	Source	Required Parameters
Digital Elevation Model DEM	90 m	Shuttle Radar Topography Mission (SRTM) (Lehner et al., 2008)	Topographical data
Soil map	1 km	Food and Agriculture Organization of the United Nations (FAO) (Dewitte et al., 2013)	Soil classes and physical properties
Land use map	60 m (1970s)	Landsat pre-Collection Level-1 (United States Geological Survey (USGS), n.d.)	Land cover and use classes
Precipitation	Daily (1958–1970)	Personal communication: RBWB, University of Dar es Salaam (UDSM), Tanzania Meteorological Agency (TMA)	Measured precipitation
Climate	Daily/0.44° (1951–2060)	Coordinated Regional Downscaling Experiment (CORDEX) Africa (Gutowski et al., 2016)	Temperature, humidity, solar radiation, wind speed, precipitation
Discharge	Daily (1958–1970)	RBWB (RBWB, 2014)	Discharge

Table 5.2 Overview of the Regional Climate Models (RCMs), their driving Global Climate Models (GCMs), and the assigned naming for the model combination within this study.

GCM	RCM	Institution	URL	In this study referred to as
CanESM2	CanRCM4_r2	Canadian Centre for Climate Modelling and Analysis (CCCma)	http://climate-modelling.canada.ca/	Model 1
CanESM2	RCA4_v1	Rossby Centre, Swedish Meteorological and Hydrological Institute (SMHI)	https://esg-dn1.nsc.liu.se/	Model 2
CNRM-CM5	CCLM4-8-17_v1	Climate Limited-area Modelling Community (CLMcom)	https://esg-dn1.nsc.liu.se/	Model 3
EC-EARTH	CCLM4-8-17_v1	Climate Limited-area Modelling Community (CLMcom)	https://esg-dn1.nsc.liu.se/	Model 4
EC-EARTH	RCA4_v1	Rossby Centre, Swedish Meteorological and Hydrological Institute (SMHI)	https://esg-dn1.nsc.liu.se/	Model 5
MIROC5	RCA4_v1	Rossby Centre, Swedish Meteorological and Hydrological Institute (SMHI)	https://esg-dn1.nsc.liu.se/	Model 6

5.2.3.Model Description (SWAT Model)

The SWAT model (Arnold et al., 1998) was selected in this study due to the fact that it is able to simulate hydrological processes continuously- and physically-based. These features are necessary to simulate impacts of climate change on water resources. Additionally, SWAT was already successfully calibrated and validated for the study area (Näschen et al., 2018). The model follows a semi-distributed approach by dividing the catchment into subcatchments (Figure 5.3) based on a threshold defined by the modeler. This threshold defines the minimum drainage area needed to generate a stream. In combination with the drainage patterns calculated from the DEM, the stream network is calculated and a subcatchment is assigned to each stream, or whenever two streams merge. In the next step, Hydrologic Response Units (HRU) divide the subcatchments into unique combinations of soil types, slope, and land use. Again the modeler has to set a minimum threshold on the absolute or relative area covered by the HRU to be included. In this study each soil type, slope class, or land use unit covering less than 10% of the area within the single subcatchments was neglected, while discretizing the subcatchments into HRUs. The model is divided into two parts. Firstly, a land phase considering all the processes from the arrival of a raindrop on the land surface until it enters the reach. From here the second phase starts, considering the routing and in-stream processes of water, sediments, nutrients, and organic chemicals. Hence, most of the hydrological processes in SWAT are calculated at the HRU level and the spatial locations of the HRUs within the subcatchments are not considered any more, but are calculated as a lumped sum of all single HRU calculations to efficiently account computationally the processes within a subcatchment.

In general, the SWAT model solves the water balance equation for each HRU and sums up the HRU calculations for each subcatchment, while integrating climate station data at the subcatchment level. The single subcatchments are linked through channel processes, which calculate the movement of water from the spatial units. Figure 5.3 illustrates the most important processes calculated by SWAT. For some processes such as evapotranspiration or surface runoff, SWAT has several calculation options, but here only the applied methods to calculate the water balance are described. Precipitation is taken from single precipitation stations and is either intercepted by plants or hits the ground where it is divided into surface runoff or infiltration water by utilizing the SCS (Soil Conservation Service) curve number (Soil Conservation Service (ed.), 1972). As long as water is near or on the surface it might evaporate according to the atmospheric conditions (Monteith and Moss, 1977). Once water enters the soil it might move vertically following a storage routing technique based on physical soil parameters, or laterally by using a kinematic storage model (Sloan and Moore, 1984). If water percolates, it passes by the unsaturated zone and enters an unconfined aquifer, from where it either leaves as capillary rise due to water demand of the surface plants, or it moves laterally as return flow into the reach. A third option is to percolate further into the confined aquifer from where the water is treated as a discharge contributor to other catchments. A more detailed description on the theoretical background is given by Neitsch et al. (Neitsch et al., 2011) and all the relevant model parameters are described in detail by Arnold et al. (Arnold et al., 2012a).

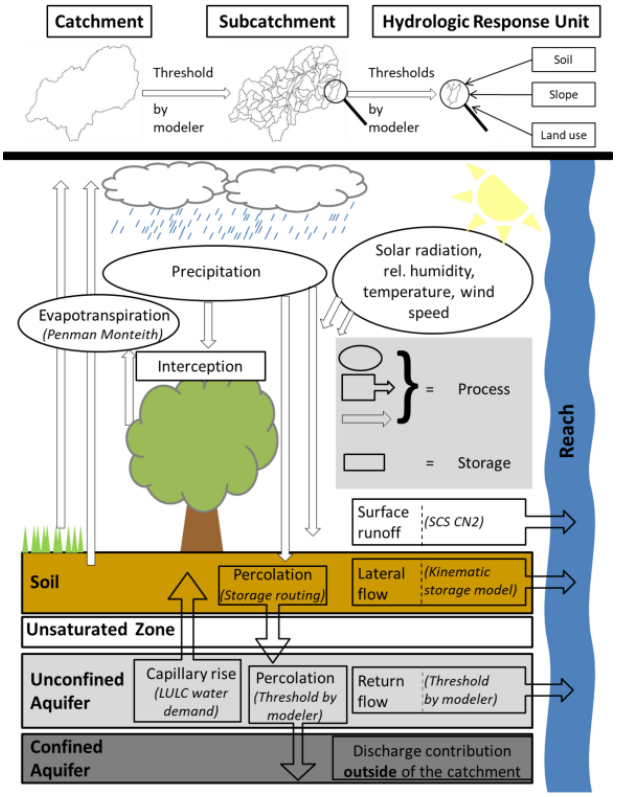

Figure 5.3 Catchment discretization and schematic overview of processes and storages simulated by the SWAT model. Applied methods to simulate evapotranspiration and water fluxes are shown in parentheses (modified after (Neitsch et al., 2011)).

5.2.4.Model Setup and Evaluation (SWAT Model)

The model was setup with ArcSWAT 2012 (revision 664). Basically, the catchment was divided into 95 subcatchments consisting of 1086 HRUs. Five elevation bands (Näschen et al., 2018; Neitsch et al., 2011) were integrated into the model due to the complex topography in combination with the sparse distribution of precipitation stations (Figure 5.1).

The model was calibrated and validated using SWAT-CUP (version 5.1.6.2) and the SUFI-2 algorithm (Abbaspour, 2013). Evaluation criteria were the coefficient of determination (R^2; Equation 5.1)), the Nash-Sutcliffe efficiency (NSE; Equation 5.2)) and the Kling-Gupta efficiency (KGE; Equation 5.3)). R^2 ranged between 0 and 1 (perfect fit) and both NSE and KGE ranged from $-\infty$ to 1 (perfect fit). In this study we focus on these three criteria, as they are well-known and provide a good assessment of the model. A full description of the model setup and evaluation procedure is given by Näschen et al., 2018 (Näschen et al., 2018).

$$R^2 = \frac{[\sum_{i=1}^{n}(O_i - \bar{O})(S_i - \bar{S})]^2}{\sum_{i=1}^{n}(O_i - \bar{O})^2 \sum_{i=1}^{n}(S_i - \bar{S})^2} \quad \text{(Equation 5.1)}$$

$$NSE = 1 - \frac{\sum_{i=1}^{n}(O_i - S_i)^2}{\sum_{i=1}^{N}(O_i - \bar{O})^2} \quad \text{(Equation 5.2)}$$

$$\mathrm{KGE} = 1 - \sqrt{(r-1)^2 + (\alpha-1)^2 + (\beta-1)^2} \qquad \text{(Equation 5.3)}$$

Here n is the number of observations, O_i and S_i are the observed and simulated discharge values, respectively, and $\bar{O}$ and $\bar{S}$ are the mean of observed and simulated discharge values; r is the linear regression coefficient between observed and simulated data; α is the ratio of the standard deviation of simulated and observed data; β is the ratio of the means of simulated and observed data.

5.2.5.Climate Change Scenarios and Bias-correction

The simulations from six CORDEX Africa RCMs were used to quantify the influence of future changes in the regional climate on the hydrology in the Kilombero Catchment. The RCMs were selected to represent the range of possible changes in seasonal rainfall amounts. Additionally, for all models two different scenarios of the Representative Concentration Pathways (RCPs) were considered. RCP4.5 and RCP8.5 assume a radiative forcing of 4.5 and 8.5 W m^{-2} at the end of the twenty-first century in comparison to the preindustrial level in the middle of the 19th century, respectively. The radiative forcings result from different assumptions of changes in greenhouse gas concentrations.

Systematic errors in RCM output require a comprehensive bias correction, which is based on an adjustment with respect to long-term observations. Constrained by the availability of adequate observation-based data, the bias correction could only be applied to minimum and maximum temperatures and rainfall. Due to different statistical properties and data availability, two different approaches were used for the bias correction of temperatures and rainfall.

a. For the bias correction of minimum and maximum temperatures, the simple approach that was already used in a previous study (Näschen et al., 2018) was adopted. In this approach, temperatures from the ERA-Interim reanalysis (Dee et al., 2011) were used as reference. Using the differences in the mean annual cycles, which were calculated from the 11-day running means of individual years between observations and model data in the period 1979–2005, model data was corrected towards observations. Due to the different representation of orography that results from the different horizontal resolutions of both datasets, i.e., 0.75° for ERA-Interim and 0.44° for CORDEX Africa RCMs, the correction was carried out for 700-hPa potential temperatures. After the correction, the RCM temperatures were transformed back to the initial level.
b. Due to the non-linear statistical behavior of precipitation, a more comprehensive approach was needed for the bias correction of daily rainfall sums. All available data from seven stations in the Kilombero Catchment (Figure 5.1) in the historical period 1951–2005 were used as reference for an empirical quantile mapping approach. In this approach the cumulative distribution function (CDF) based on simulated precipitation is adjusted towards the observation-based CDF (Piani et al., 2010). The nearest CORDEX datagrid to the respective station was thereby utilized for the bias-correction. The usefulness of the distribution-independent quantile mapping method was demonstrated by various previous studies (Lafon et al., 2013; Themeßl et al., 2012; Yira et al., 2017).

Assuming that the detected bias between the times series of models and observations stays spatio-temporally constant, the transfer functions found in a and b for the historical periods were applied to historical model data (1951–2005) and RCM projections (2006–2100).

5.2.6.Flood Frequency and Low Flow Analysis

A hydrological extreme value analysis was conducted for discharge simulated using bias-corrected RCM input to determine shifts in flood frequency and in low flows due to climatic changes. Therefore, the hydrological model was run with the historical bias-corrected RCM data for all six CORDEX Africa models (Table 5.2) from 1951 to 2005, as well as for the climatic projections based on the RCP 4.5 and RCP8.5 scenarios from 2010 to 2060.

Subsequently, after the model simulations, the annual maximum discharge values of the simulation periods for the six historical simulations and the RCP scenarios were extracted for further statistical analysis with regard to flood frequencies, using the extRemes 2.0 package (Gilleland and Katz, 2016) in the statistical software R. The generalized extreme value (GEV, Equations 5.4 and 5.5) model covering Weibull, Fréchet, and Gumbel distributions was used in combination with the generalized maximum likelihood estimation (GMLE) method to estimate the return levels of flood events from 2-year return levels up to 100-year return levels. The return levels are utilized as a proxy for deviations in discharge due to climatic changes among the historical and the RCP scenarios later on.

$$F(x) = exp\left[-\left\{1+\gamma\left(\frac{x-\mu}{\alpha}\right)\right\}^{-1/\gamma}\right] \quad \text{(Equation 5.4)}$$

where γ is the shape parameter, μ the location parameter, and α the scale parameter of the probability distribution function with $\alpha > 0$ and $(1+\gamma(x-\mu)/\alpha) > 0$. If $\gamma \to 0$, the function belongs to the Gumbel family and is as follows:

$$F(x) = \exp\left[-\exp\left\{-\left(\frac{x-\mu}{\alpha}\right)\right\}\right] \quad \text{(Equation 5.5)}$$

For the low flow analysis, the Q90, being a widely-used index (Smakhtin, 2001; van Vliet et al., 2013), was used to estimate changes among the six models and the different RCP scenarios. The Q90 index is defined here as a daily discharge value, which is exceeded in 90% of the daily simulations. These simulations were performed on decadal timescales to account for the inherent uncertainties of the scenario simulations and to identify possible decadal trends.

Additionally, the Q10 index was also calculated, which is defined here as a daily discharge value that is exceeded in 10% of the daily simulations to investigate the general flooding trend, additional to the annual maximum flooding approach based on the GEV model estimates described above. Q10 and Q90 were calculated using the hydrostats package in R (Bond, 2018). The Q10 value was added to the flood frequency analysis because it is less sensitive to outliers, in contrast to the annual maximum value utilized in the GEV analysis (van Vliet et al., 2013).

5.3. Results

5.3.1.Model Performance

A detailed overview on the model performance is given by Näschen et al. (2018) (Näschen et al., 2018). Nevertheless, the hydrograph for the calibration and validation period is shown in Figure 5.4 as an important indicator for the model performance. Furthermore, common hydrological statistical measures, such as R^2, NSE and KGE, are provided for both periods (Equations 5.1–5.3, Figure 5.4).

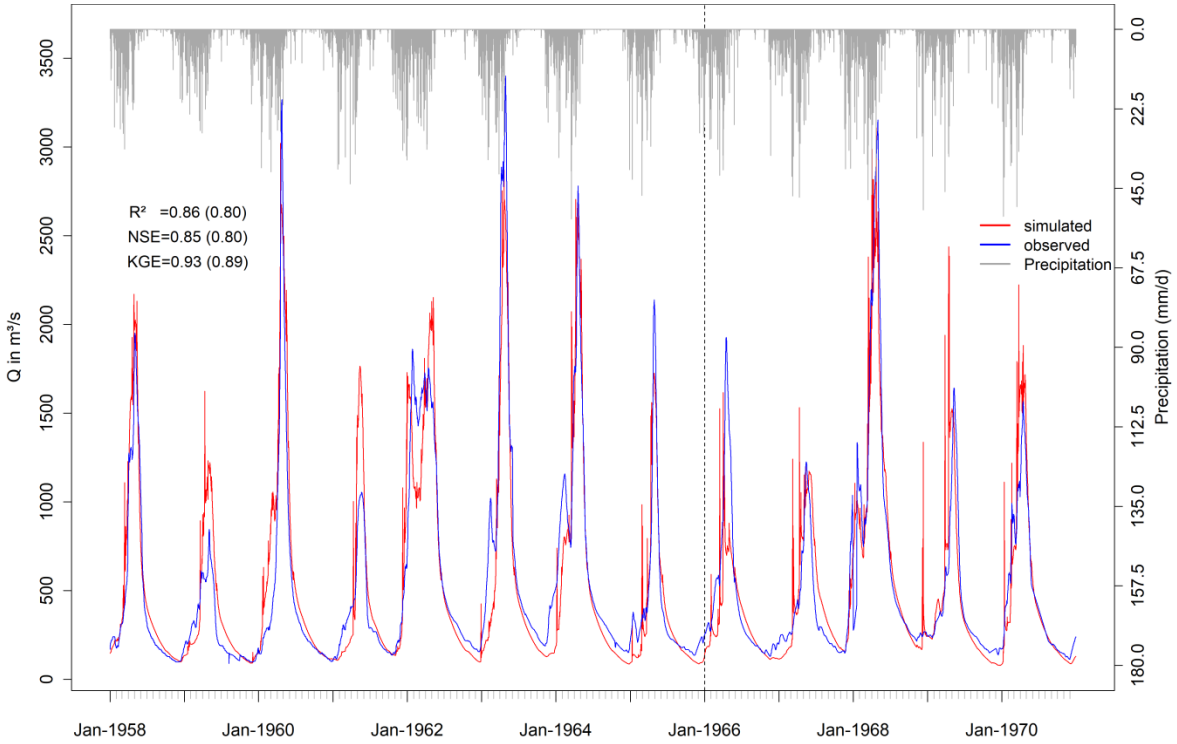

Figure 5.4 Hydrograph showing the observed and the simulated discharge for the calibration (1958–1965) and the validation period (1966–1970), separated by the dashed vertical line. Statistical measures are shown within the graph and refer to the coefficient of determination (R^2, Equation 5.1), the Nash-Sutcliffe efficiency (NSE, Equation 5.2) and the Kling-Gupta efficiency (KGE, Equation 5.3). The values in the parentheses refer to the validation period (modified Figure after (Näschen et al., 2018)).

5.3.2.Bias-correction

The bias-correction for all seven precipitation stations and the historic model runs for the six utilized regional climate models (Table 5.2) show very good results. Figure 5.5 shows the mean monthly precipitation for all stations and models within the period 1951–2005, with and without bias-correction. The deviation among non-bias-corrected data and the observed monthly precipitation is obvious, especially in the peak of the rainy season (March and April). Some stations indicate a shifting peak of the rainy season from April to March for all six RCMs (Figure 5.5c,d), in addition to these absolute deviations. Days with missing data were neglected in this analysis. In contrast to these strong deviations, Figure 5.5h–n shows virtually no deviations at all for the mean monthly precipitation after bias-correction.

Furthermore, the exceedance probabilities for all stations and models were analyzed (Figure 5.6), demonstrating a good performance of the bias-correction with regard to the cumulative distribution of rainfall events. The ensemble mean of the six models is also shown here with a completely different distribution of the ranked rainfall events, revealing a high amount of rainfall events below 10 mm, but much less events with 10 mm or more rainfall, compared to all the single model results. However, the temporal distribution of the daily rainfall patterns still varies among the observed precipitation and each single CORDEX model, apart from this ranked illustration.

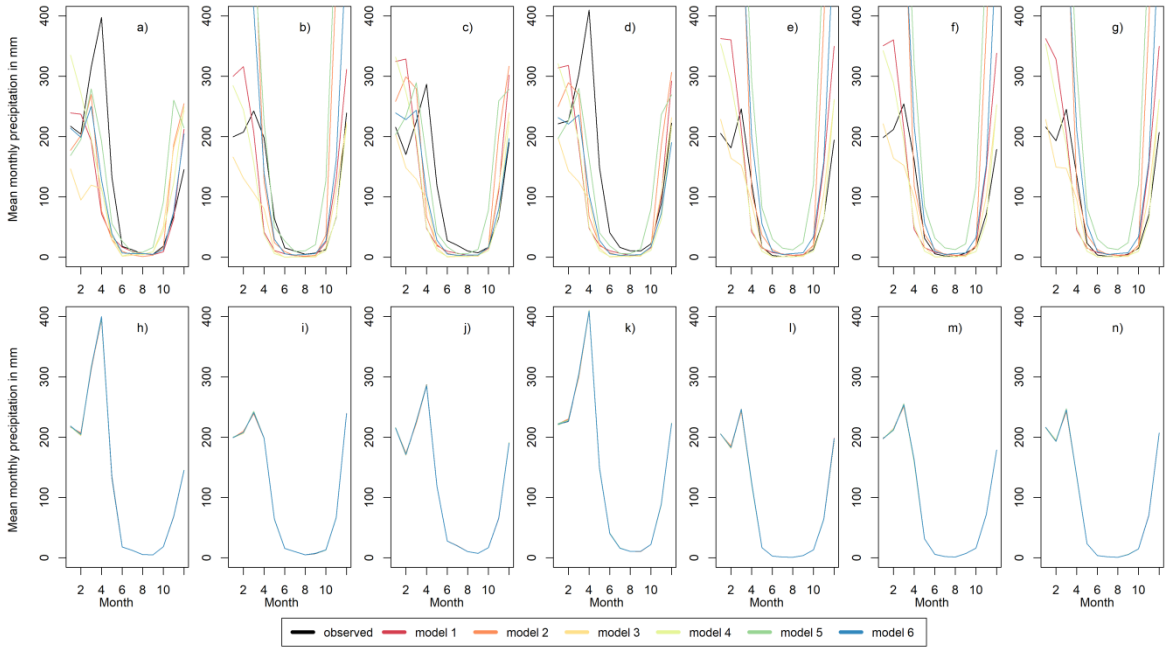

Figure 5.5 Average monthly precipitation from 1951–2005 for the seven datagrids of CORDEX Africa before bias-correction in (a–g) and for the same stations after bias correction in (h–n). The lines representing the precipitation for the observed precipitation, as well as for models 1 to 5, are superimposed by the lines for model 6 due to their similar precipitation after bias correction (h–n). Each graph shows the average monthly precipitation for all six models introduced in Table 5.2.

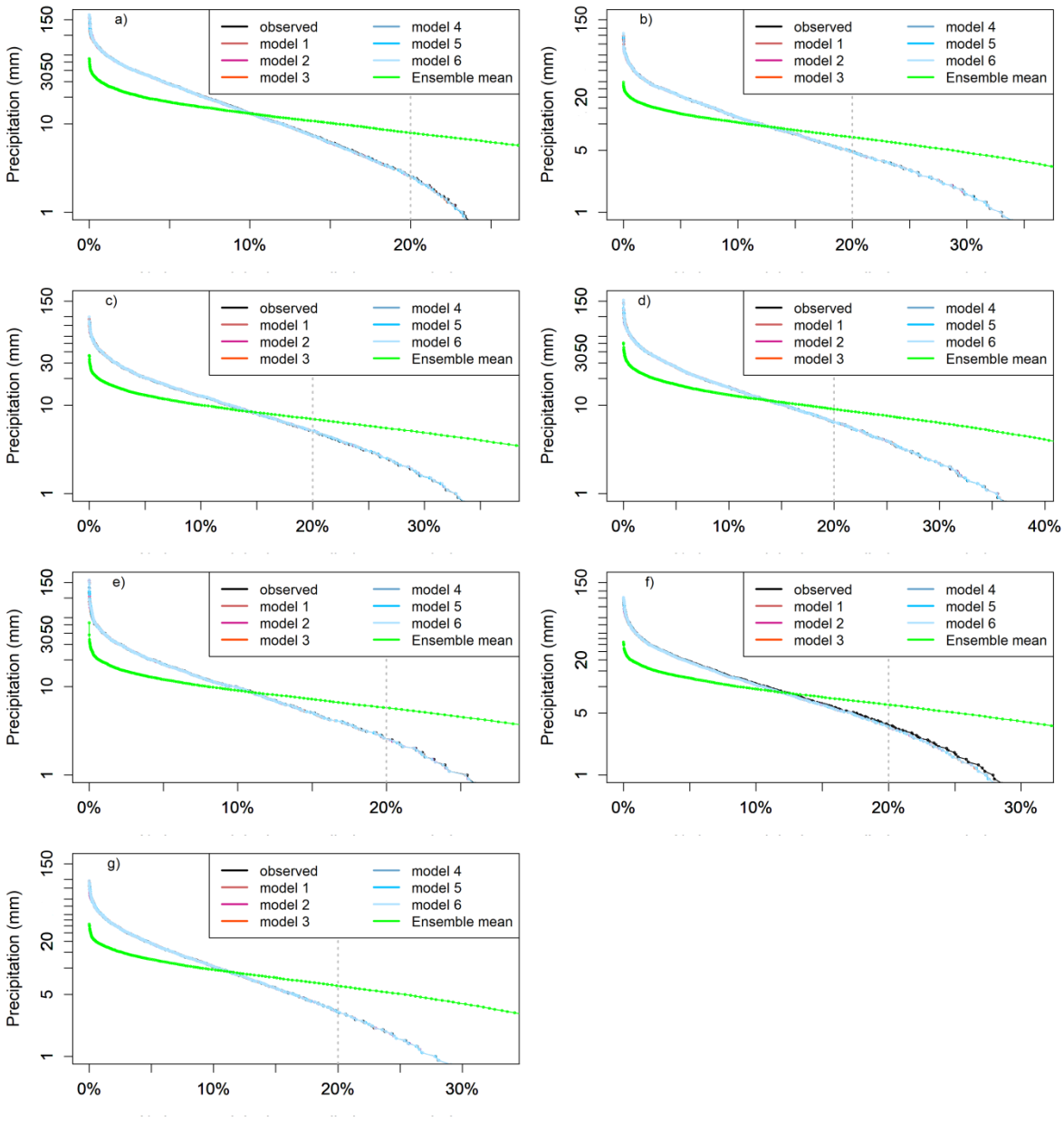

Figure 5.6 Exceedance probabilities for the seven utilized CORDEX Africa datagrids after bias-correction. Each graph shows the ranked precipitation for all six RCMs, their ensemble mean, and the observed precipitation at the corresponding datagrid (1951–2005). Missing values were neglected in this visualization. The lines representing the exceedance probabilities for the observed precipitation, as well as for models 1 to 5, are superimposed by the distribution of model 6 due to their similar exceedance probabilities after bias correction.

A similar picture can be observed for the temperature before and after (Figure 5.7) bias-correction. The figure shows the mean monthly temperature for two of the 21 CORDEX datagrids (also see CORDEX datagrids in Figure 5.1 and 5.A1, 5.A2) and each graph illustrates the minimum (Tmin) and maximum (Tmax) temperature of the six regional climate models. Discrepancies among all models and stations for Tmin and Tmax are obvious in Figure 5.7a,b, while Figure 5.7c,d clearly show the strong impact of the

bias-correction on the mean monthly Tmin and Tmax. Only minor deviations occur in the months of April to June, which are negligible for the purpose of this study. The bias-corrected temperature data shows in general a drop in Tmin, starting with the Long Rains in March and April until the end of the rainy season in June and July. The average decrease during that time frame is about 5 °C (Table 5.3). From July onwards, Tmin constantly rises from about 14 °C up to 19 °C in November, and is stable henceforward until March and April again. In the dry season, Tmax increases by about 5 °C from July (23.8 °C) until November (29.3 °C) and the beginning of the Short Rains (Table 5.3). By then, Tmax drops again to about 25°C on average until January and stays relatively constant between 24 and 25 °C until July (Table 5.3).

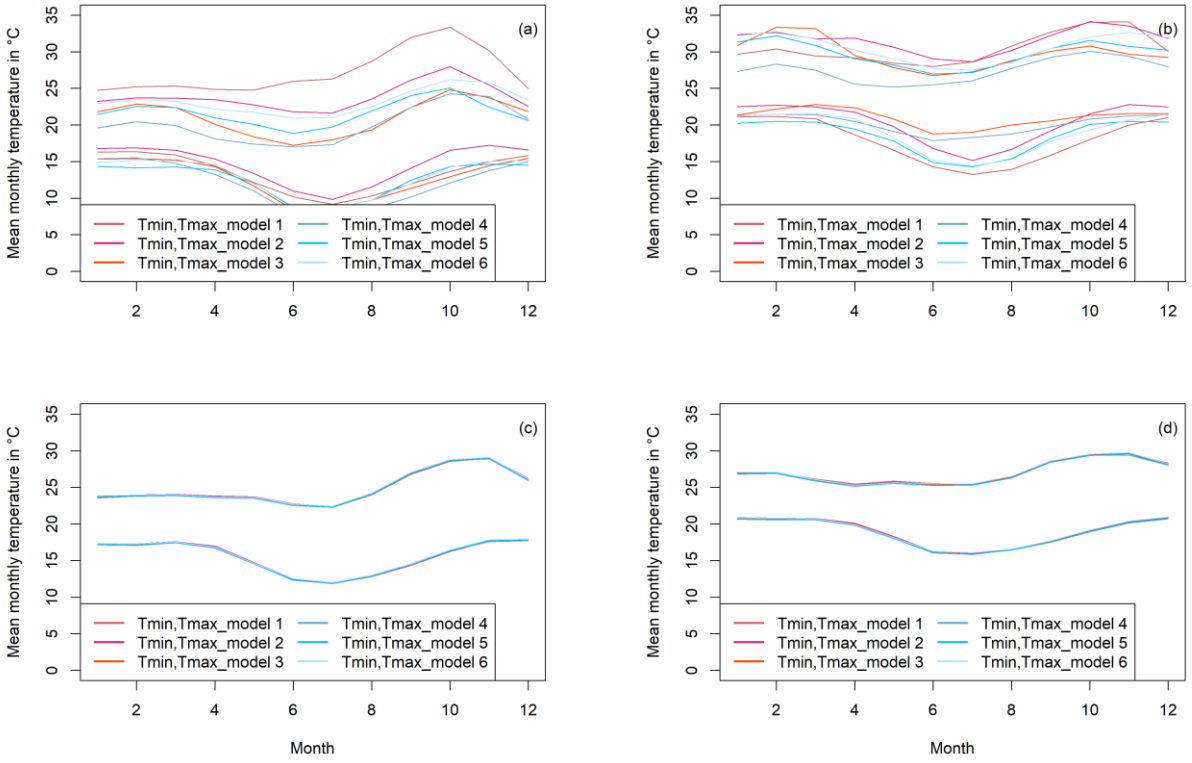

Figure 5.7 Mean monthly minimum and maximum temperatures from 1979 to 2005 for two exemplary stations out of the 21 utilized CORDEX Africa datagrids before and after bias-correction. (a,b) Temperatures before bias correction. (c,d) The same stations after bias-correction. Each graph shows the average Tmin and Tmax monthly temperature for all six models introduced in Table 5.2. (c,d) The last plotted lines from model 6 superimposed over the other models' lines due to their similarity after bias correction. All 21 stations can be found in the appendix before (Figure 5.A1) and after bias-correction (Figure 5.A2).

Table 5.3 Historical monthly average minimum (Tmin) and maximum temperature (Tmax) according to the bias-corrected RCM simulations (1979–2005). The given values represent the average of the monthly average Tmin and Tmax of all 21 utilized CORDEX Africa grids, respectively.

	Jan	Feb	Mar	Apr	May	Jun	Jul	Aug	Sep	Oct	Nov	Dec
Tmin	19.2	19.1	19.2	18.5	16.4	14.3	14.0	14.6	15.9	17.7	19.0	19.5
Tmax	25.4	25.4	24.8	24.3	24.5	23.9	23.8	25.2	27.6	29.0	29.3	27.2

5.3.3.Climate Change Signal

Two of the most important and commonly utilized climate parameters with regard to hydrological modeling of climate change impacts are precipitation and temperature. Figure 5.8 displays the climate change signal of both parameters for all six RCMs by comparing the bias-corrected historical model runs with the bias-corrected projections based on the RCP scenarios in a monthly time resolution. The temperature signal (Figure 5.8a) generally shows a clear trend of rising temperatures between 0.5 and 2.5 °C, with the highest increase in August and September. Furthermore, the chart indicates a higher increase in the results based on the RCP8.5 projections, although model 1 and model 2, based on RCP4.5, simulate higher temperatures compared to several RCP8.5 based modeling results. Nevertheless, all model projections. except for model 6 in RCP8.5, show a constant increase of temperature throughout the year, whereas model 6 in RCP8.5 reveals an increase of less than 1 °C in January and the highest increase of about 2.5 °C in August and September, indicating the strong impact of the RCP scenarios on temperature in the dry season.

Precipitation (Figure 5.8b) is projected to increase according to the mean change of precipitation of all models in the two RCP scenarios. The intra-annual precipitation pattern is unaffected in the dry season. The highest increase occurs in February with 157 mm (model 6, RCP8.5), whereas the highest decrease is −47 mm in April (model 2, RCP8.5). Although the precipitation changes within the rainy season appear more complex compared to the temperature signal, some patterns are clearly visible. The months of February and March receive additional rainfall in virtually all simulations except for model 2 and 5 in RCP4.5, while the signal is much more diverse in January and April, where several models simulate decreasing rainfall. The months of May, November, and December can be seen as transition months with fewer changes in precipitation compared to the months of January to April.

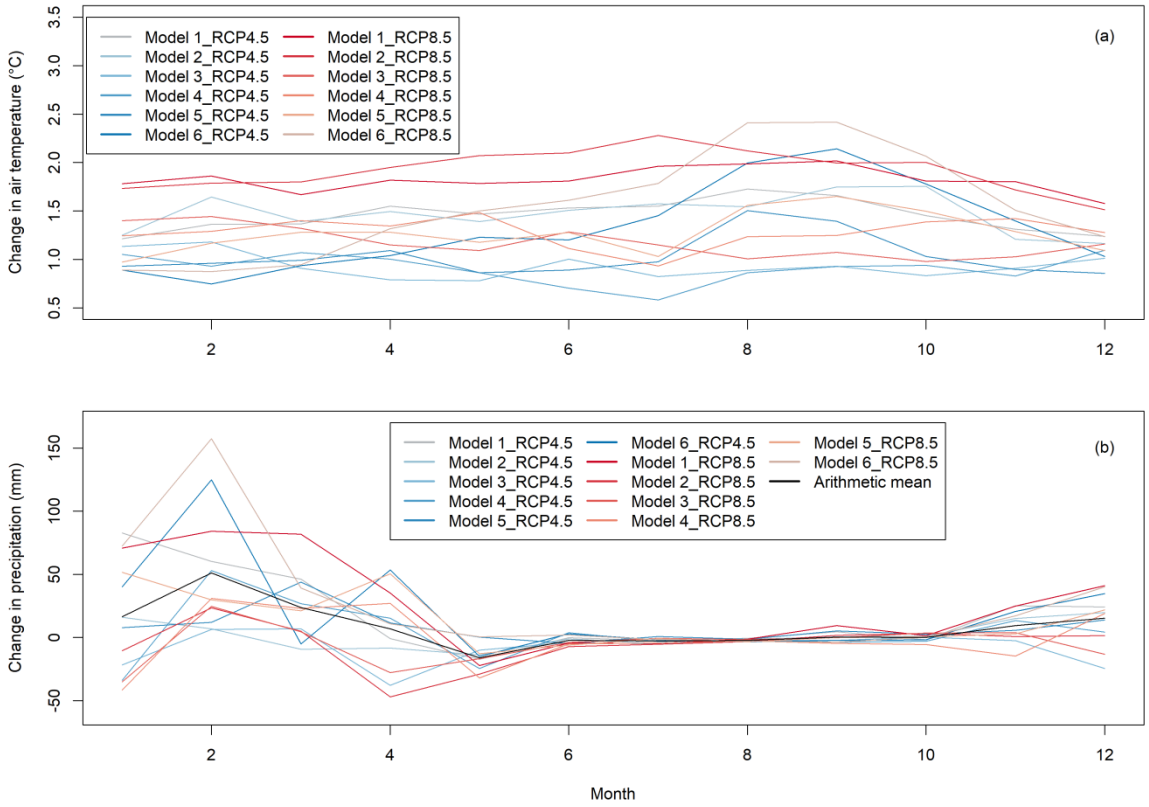

Figure 5.8 Climate change signal among the bias-corrected historical model runs for (a) mean temperature (1979–2005) and the bias-corrected scenarios RCP4.5 and RCP8.5 (2010–2060), and (b) precipitation changes among the bias-corrected historical model runs (1951–2005) and the bias-corrected scenarios RCP4.5 and RCP8.5 (2010–2060). All values represent the monthly spatial averaged temperature and precipitation for the given periods, respectively.

5.3.4.Impacts of Climate Change on Water Resources

5.3.4.1. General Trend Analysis

The impact of the RCMs and the applied RCP scenarios on selected water balance components is shown in Table 5.4. The changes in precipitation indicate a dryer future according to models 2, 3, and 4, although there is a high variation with regard to these three RCMs and the two RCP scenarios, with deviations in precipitation from +22 to −109 mm per year. The projected wetter future is more consistent and pronounced with regard to models 1, 5, and 6, especially in the RCP8.5 scenario, with an annual average increase of up to 302 mm in model 6. Also, the ensemble mean scenario projects 68 mm (RCP4.5) or 88 mm additional rainfall in both RCP scenarios. The actual evapotranspiration ET0 and the water yield are also closely linked to the precipitation trends, including the surface runoff (Table 5.4). Hence, the trends are similar; nevertheless, the magnitude differs and is in generally more pronounced for changes in water yield in contrast to changes in ET0. The potential evapotranspiration ETp is increasing in all RCMs by 43 mm up to 136 mm.

Table 5.4 Historical annual average precipitation according to the bias-corrected RCM simulations (1951–2005) and the absolute and relative changes of precipitation, and related impacts on selected water balance components in SWAT simulations (2010–2060) according to the projections based on RCP4.5 and RCP8.5 scenarios. Numbers in parentheses represent the changes in percentage. For each parameter (except for the historical precipitation) and RCP scenario, the lowest and highest values according to the absolute changes are highlighted in red and blue, respectively. EM represents the ensemble mean, ET0 the actual evapotranspiration, ETp the potential evapotranspiration, SQ the surface runoff, and WYLD the overall water yield.

Climate Model	Historical Precipitation (After bias correction)	RCP Precipitation Changes in mm (%)	RCP ET0 Changes in mm (%)	RCP ETp Changes in mm (%)	RCP SQ Changes in mm (%)	RCP WYLD changes in mm (%)
Model 1 (RCP4.5)	1338	195 (14.5)	39 (4.4)	73 (4.7)	23 (40.2)	124 (28.7)
Model 2 (RCP4.5)	1334	3 (0.2)	−4 (−0.4)	94 (5.3)	7 (12.0)	−20 (−4.9)
Model 3 (RCP4.5)	1311	−109 (−8.3)	−10 (−1.4)	66 (5.1)	−12 (−18.3)	−103 (−19.8)
Model 4 (RCP4.5)	1334	22 (1.7)	−9 (−1.3)	43 (3.8)	7 (10.8)	23 (3.6)
Model 5 (RCP4.5)	1355	75 (5.5)	11 (1.2)	54 (3.3)	11 (19.7)	52 (12.4)
Model 6 (RCP4.5)	1345	218 (16.2)	14 (1.5)	81 (4.5)	25 (42.1)	163 (42.1)
EM (RCP4.5)	1335	68 (5.1)	0 (0.0)	70 (5.0)	2 (25.4)	46 (8.5)
Model 1 (RCP8.5)	1338	288 (21.5)	39 (4.4)	96 (6.2)	39 (67.8)	216 (50.1)
Model 2 (RCP8.5)	1334	−83 (−6.2)	−16 (−1.8)	136 (7.8)	−5 (−9.7)	−91 (−22.5)
Model 3 (RCP8.5)	1311	−76 (−5.8)	11 (1.5)	76 (5.9)	−6 (−8.9)	−85 (−16.3)
Model 4 (RCP8.5)	1334	−33 (−2.4)	−28 (−4.2)	91 (8.1)	12 (18.6)	−28 (−4.4)
Model 5 (RCP8.5)	1355	130 (9.6)	1 (0.1)	75 (4.6)	18 (31.6)	102 (24.2)
Model 6 (RCP8.5)	1345	302 (22.5)	25 (2.7)	81 (4.5)	38 (63.4)	239 (61.6)
EM (RCP8.5)	1335	88 (6.6)	−2 (−0.2)	101 (7.2)	3 (34.6)	60 (10.9)

A more detailed overview of discharge behavior in the single models and RCP scenarios is given in Figure 5.9 by displaying the average intra-annual discharge for the single decades from 2010 to 2060. A comparison of the single decades across the six models and two RCP scenarios displays various decades as either dry or wet. Hence, a clear signal for the discharge pattern over time is not obtained. Nevertheless, Figure 5.9 shows a shift of the discharge peak from April to May for all the models, except for model 3, with a shift of the peak to June, from 2020 onwards.

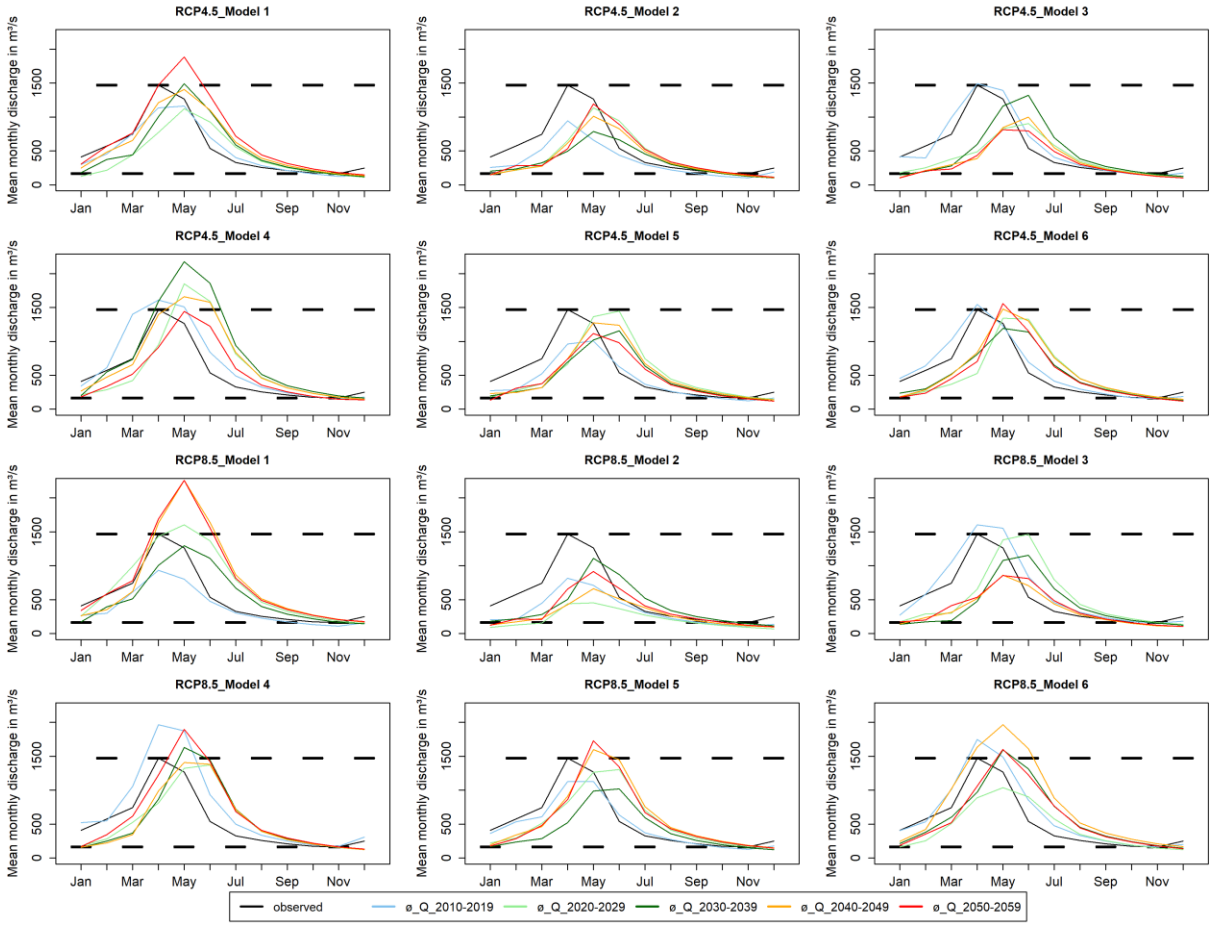

Figure 5.9 Changes in mean monthly discharge for the RCP4.5 and RCP8.5 scenarios for all utilized regional climate models introduced in Table 5.2. For each model and RCP scenario the average monthly discharge is visualized on a decadal resolution ranging from 2010 to 2059. Additionally, the mean monthly discharge of the observed discharge from 1958 to 1970 is shown. The dashed lines highlight the minimum and maximum values of the observed discharge for the period 1958–1970.

5.3.4.2. Flood Frequency and Low Flow Analysis

Figure 5.10 shows the return levels of flood events for all six models (Table 5.2) across all simulations (historical model run, RCP4.5, and RCP8.5), according to the bias-corrected CORDEX Africa data. The high variance across the six models is obvious, especially for the RCP8.5 scenarios, where the 100 year return level varies between 7782 $m^3 s^{-1}$ (model 5) and 20,707 $m^3 s^{-1}$ (model 1). Nevertheless, an increasing trend of return level values in the RCP8.5 scenario is apparent, particularly for the rare events (25 years up to 100 years), according to the simulation results. Model 5 is an exception for this finding, with rather constant return levels for a 100 year event among the scenarios.

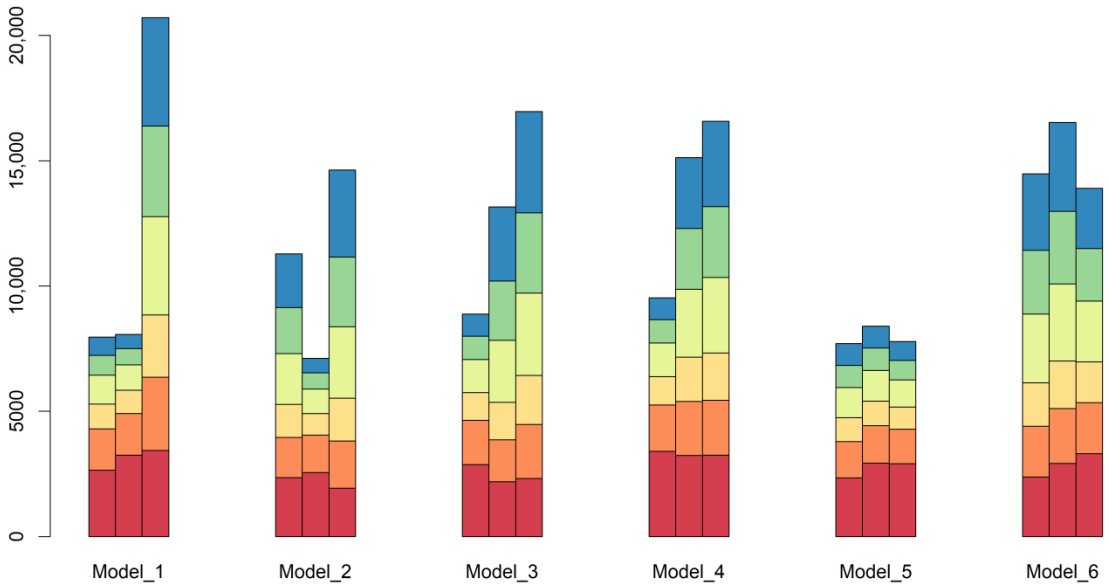

Figure 5.10 Return levels of flood events for all six models (Table 5.2) and all three scenarios. For each model there are three columns representing the historical (left), the RCP4.5 (middle), and the RCP8.5 scenario values. The discharge at the outlet for a 2-year, 5-year, 10-year, 25-year, 50-year, and 100-year event are indicated according to the generalized extreme value (GEV) model and the generalized maximum likelihood estimation (GMLE) method.

The aforementioned results are supported by Figure 5.11, which displays the arithmetic mean of all scenarios for each model (Figure 5.11a) and the arithmetic mean of all models for the specific scenarios (Figure 5.11b). According to these results, model 4 and model 5 incorporate the highest and lowest return levels, respectively, with regard to 25-year return levels or higher. Figure 5.11b indicates a rising intensity of flooding events for the RCP4.5 and RCP8.5 scenarios.

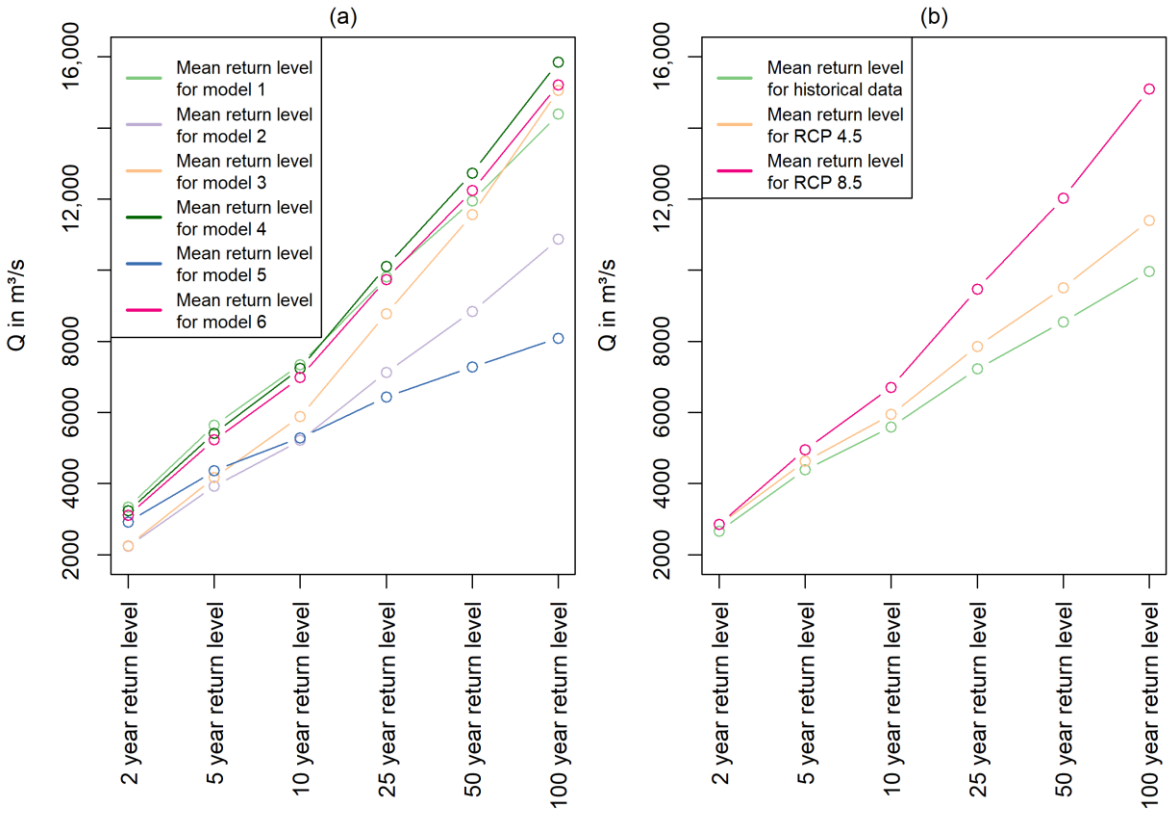

Figure 5.11 Arithmetic mean for each model across the two RCP scenarios for the return levels of discharge at the outlet (a) and arithmetic mean for each scenario across all six models for the return levels of discharge at the outlet (b).

Table 5.5 confirms the finding that the impact of RCP scenarios regarding a rise of flood magnitudes increases with increasing return periods. The relative change of all models and RCP scenario runs in comparison to their respective historical simulations is shown for the single return periods. The arithmetic mean of the percentage increase of the return levels rises constantly, while the standard deviation rises from the 5 year return level upwards, even though relative changes with increasing discharge values are considered as a baseline in these calculations.

Table 5.5 Arithmetic mean and standard deviation for the relative changes of the return levels across all six models and for the two RCP scenarios in comparison with the respective historical model runs. All values represent changes in %.

Statistic Measure	2-Year	5-Year	10-Year	25-Year	50-Year	100-Year
Arithmetic mean	8.60	9.58	13.19	20.47	27.89	37.19
Standard deviation	21.79	16.31	18.64	28.72	39.75	53.21

Figure 5.12 shows Q10 and Q90, representing the high flow and low flow conditions for the historic model runs and the future scenarios for each model. The historic model runs are only represented by one value (dashed lines) for the entire simulation period of each model, whereas the RCP scenario simulations contribute decadal values from 2010 to 2060 for both RCP scenarios, to concentrate on

future climate developments. The difference among the six models for Q10 and Q90 is obvious. Models 2 and 3 have comparably low Q10 and Q90 values, while models 1, 4, and 6 have comparably high Q10 values. Q90 values for models 1, 4, 5 and 6 are similar, and all simulated Q90 values are below the measured historical Q90. A more detailed analysis is given in Figure 5.13, which accounts for the decadal shifts of Q10 and Q90 in a Cartesian coordinate system. The changes in $m^3 s^{-1}$ for both RCP scenario simulations of the RCMs on a decadal basis are given in comparison to the historic Q10 and Q90 values of the respective model. For example, a red "2" in the bottom left quadrant refers to a RCP8.5 (red color) scenario simulation from 2020 to 2029 and represents decreasing Q90 (below zero line) and decreasing Q10 amounts (left to the zero line). A blue "5" in the top right quadrant refers to a RCP4.5 (blue color) scenario simulation from 2050 to 2059 and represents increasing Q90 (above zero line) and increasing Q10 amounts (right to the zero line).

After integrating all results a linear trend is obvious, with coinciding trends of decreasing Q10 and Q90 or increasing Q10 and Q90. Nevertheless, a few examples are located in the top left quadrant of the coordinate system, representing slightly increasing Q90, whereas Q10 is decreasing. Both RCP scenarios and simulations from the 2020s, 2030s, and 2050s show this pattern (Figure 5.13; blue and red "2", "3", and "5" in top left quadrant). The most extreme simulations with the highest changes for Q10 and for Q90 are within the RCP8.5 scenario, with one exception. In the 2050s there is a huge reduction (−706 $m^3 s^{-1}$) in Q10 for one of the RCP4.5 scenarios (model 3) simulated. In general, most of the scenarios show a wetter future, represented by the accumulation of changes in Q10 and Q90 in the top right quadrant (Figure 5.13).

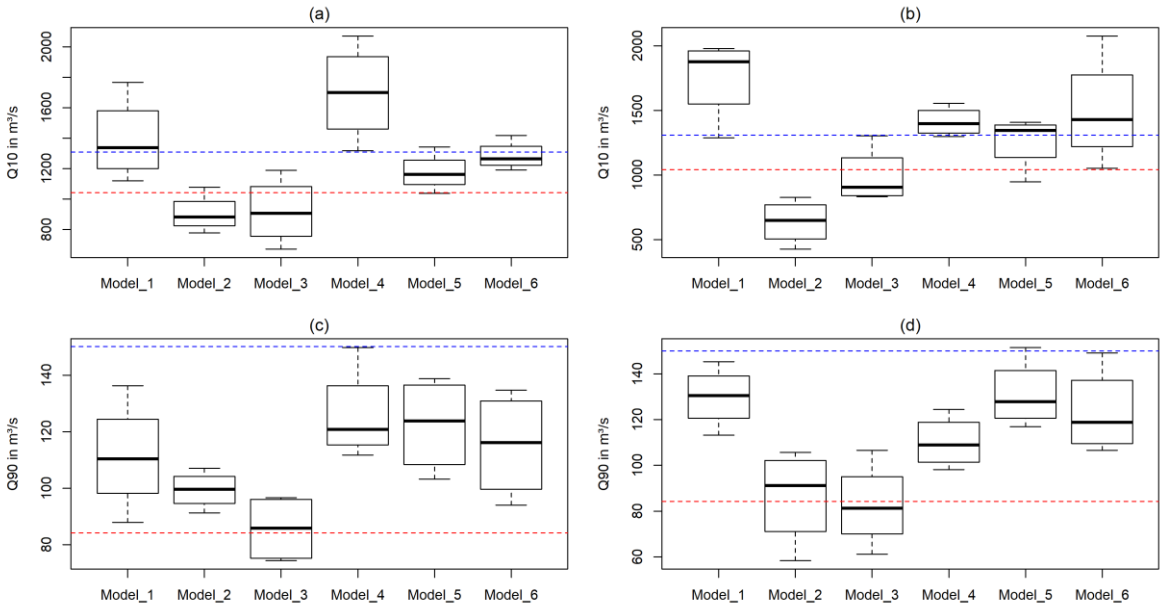

Figure 5.12 Boxplots showing the distribution of Q10 (a,b) and Q90 (c,d), representing the flow exceeded in 10% or 90% of the time for Q10 and Q90, respectively. The data in the left columns (a,c) is based on the model runs within the RCP4.5 scenario from 2010 to 2060, whereas the right columns display the modeling results within the RCP8.5 scenario. The dashed blue lines represent the measured historical Q10 and Q90 from 1958 to 1970 and the dashed red line represent the modeled historical Q10 and Q90 according to CORDEX Africa from 1951 to 2005, respectively.

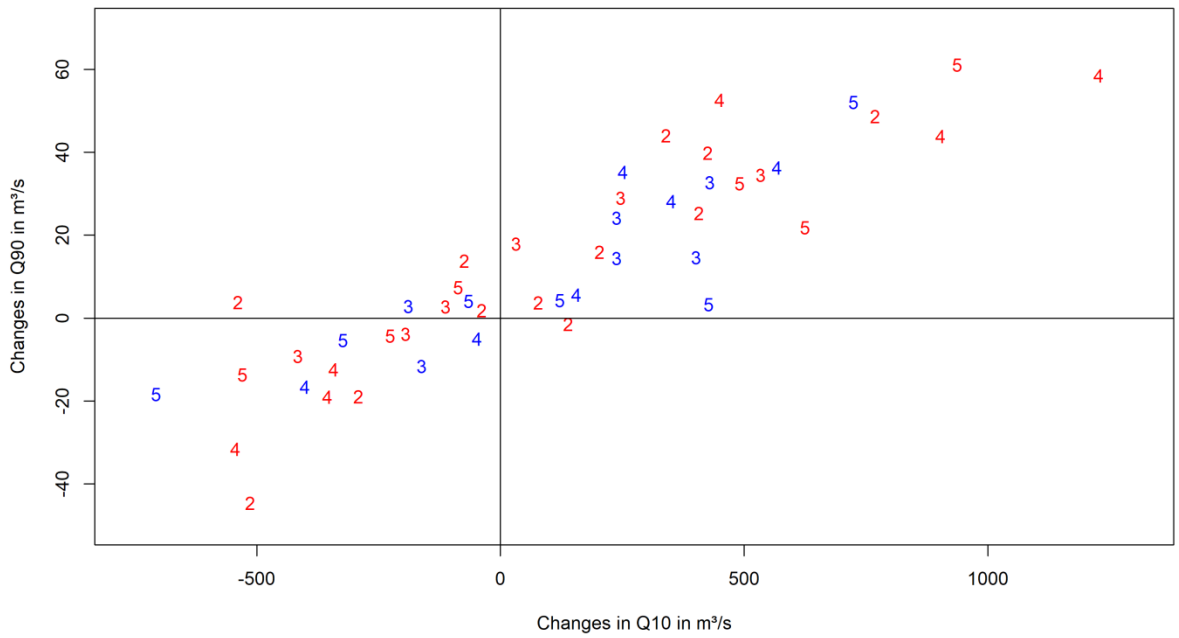

Figure 5.13 Scatterplot to visualize changes in Q10 and Q90 for each model and both RCP scenarios. Numbers represent the specific decades, whereas a "2" represents model simulations for the 2020s, continuing in this fashion up until the 2050s, represented with a "5". Blue numbers represent RCP4.5 simulations and red numbers RCP8.5 scenario simulations.

This general trend towards a wetter future is also represented in the results of smaller spatial scale (Figure 5.14). Figure 5.14 displays the comparison of the wettest and driest decade with their respective historical model run (1951–2005) for the overall water yield and evapotranspiration. Model 2 under the RCP8.5 scenario for the period 2020–2029 and model 6 under the RCP8.5 scenario for the period 2040–2049 were identified as the driest and wettest decades with regard to changes in discharge. This finding is based on the general hydrograph analysis (Figure 5.9) and the behavior of extreme discharge represented by Q10 and Q90 (Figure 5.13). The very pronounced increase of the overall water yield in the "wet scenario" (Figure 5.14a) is obvious, whereas the decrease in the "dry scenario" (Figure 5.14b) is less pronounced. The difference between the wet and dry scenarios with regard to evapotranspiration (Figure 5.14c,d) is more balanced and has a smaller magnitude. The changes in water balance components are less distinctive in the western part of the catchment for both scenarios compared to the eastern part of the catchment.

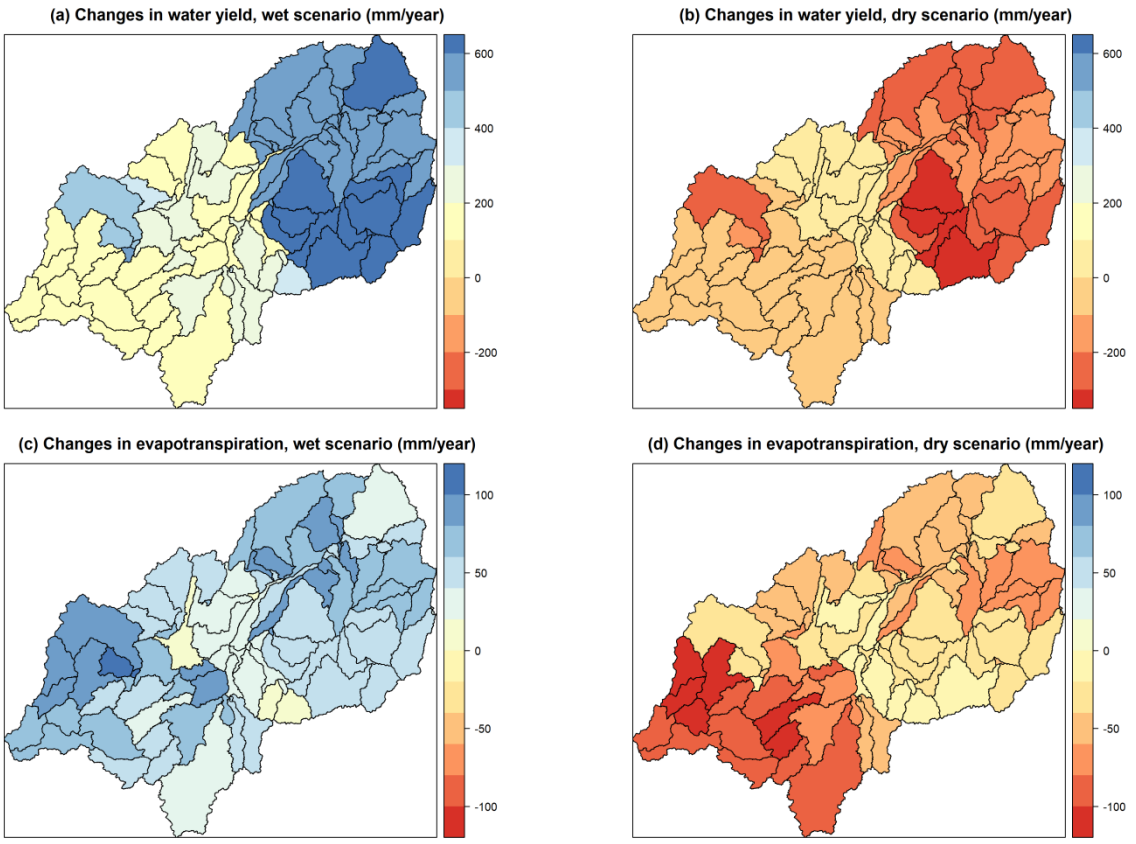

Figure 5.14 Average shifts in total water yield (a,b) and evapotranspiration (c,d) for the wettest and driest decade in comparison to their historical average (1951–2005). (a,c) Changes between the historical annual average of model 6 and the RCP8.5 scenario from 2040 to 2049 of model 6; (b,d) Changes between the annual historical average of model 2 and the RCP8.5 scenario from 2020 to 2029 of model 2.

5.4. Discussion

5.4.1.Model Performance and Bias-correction

The performance of the model and the arising uncertainties due to the data scarcity in the region are discussed in detail by Näschen et al. (Näschen et al., 2018). Hence, only a brief discussion on model performance is given here, whereas the main interest is drawn to the bias correction of the climate data, namely precipitation and temperature data.

The discharge pattern for the calibration and validation period (Figure 5.4) is captured well, with a good to very good statistical performance, according to Moriasi et al. (Moriasi et al., 2015). Deductions in statistical performance can be attributed to overestimations of discharge in some years (1959, 1961) and inaccuracies in simulating the discharge peaks (Näschen et al., 2018). During calibration, five out of the seven most sensitive parameters were related to groundwater (Näschen et al., 2018), indicating the importance of groundwater contribution for the catchment, which was also highlighted by other researchers (Burghof et al., 2017; Gabiri et al., 2018).

Bias-corrections with quantile mapping worked very well, as already proven by Teng et al. (Teng et al., 2015) in a comparison of several bias−correction methods. The seasonal variability for rainfall on monthly scale (Figure 5.5), as well as the exceedance probabilities of the bias-corrections, perform very well (Figure 5.6). The ensemble mean simulations of rainfall were neglected in this study due to their huge deviations compared to the single model outputs, with regard to the ranked rainfall distribution (Figure 5.6). Bias correction for temperature was also successful for all 21 CORDEX Africa datagrids, which is obvious by comparing Figure 5.7a–d, as well as Figures 5.A1 and 5.A2. The average annual temperature cycle (Table 5.3) displays a typical tropical daytime climate, indicated by more pronounced daily temperature amplitudes of up to 11.7 °C in September as an average of the whole period and all stations. However, the seasonal cycle is evident with Tmax and Tmin differences of up to 5.5 °C among the lowest and highest areal mean values within the considered period. Hence, it has to be considered that the bias correction was done from the period 2006 to 2100, but the analyses were only done until 2060 to find a compromise between the statistical variability of climate change projections and planning time-frames, such as the Tanzania Vision 2025.

The behavior of the areal mean monthly temperature of the catchment (Figure 5.7, Table 5.3) fits very well to the temporal precipitation patterns and the onset and ending of dry and rainy seasons (Koutsouris et al., 2016; Näschen et al., 2018). Minimum temperatures decrease from March until July, which can be attributed to cooling by evapotranspiration and shifts in the share of sensible and latent heat transport (Beven, 2012). In July, minimum temperature starts to rise again from about 14 °C to 19 °C, while maximum temperatures simultaneously increase from July until November, which is the onset of the short rains, where again cooling is achieved via evapotranspiration as well as more pronounced cloud coverage, and therefore less solar radiation (Tang et al., 2009). The increase of minimum and maximum temperatures starting in July also fits well with the declining impact of cooling by evapotranspiration within the catchment. It was shown (Näschen et al., 2018) that actual evapotranspiration and potential evapotranspiration diverge from July onwards due to a water deficit. This is exactly the month where minimum and maximum temperatures begin to rise, due to an increasing share of sensible heat in combination with decreasing cloud coverage. The reduced cloud coverage also implies a higher radiation and a positive feedback with regard to temperature in a drying system (Pokorny, 2019). The bias-corrected climate data, therefore, represent a sound behavior of a seasonal sub-humid tropical system. Moreover, water availability in the system is indirectly well-reflected by the shift in actual and potential evapotranspiration.

5.4.2.Impact of Climate Change on Water Resources

Overall, the modeled scenarios project a broad range of dry and wet conditions, whereas the distinction towards a wetter future for the catchment is more pronounced (Table 5.4, Figure 5.13). The annual average change in precipitation ranges between a reduction by 109 mm and an increase by 302 mm with respect to historical model runs, with an annual mean of 1336 mm. The rising temperature in all models, due to the adopted RCP scenarios, leads to consistently increasing potential evapotranspiration, while water availability is a temporally limiting factor due to the distinct seasonality in the catchment (Koutsouris et al., 2016; Nicholson, 2000).

This limitation of water is visible by looking at the changes in actual and potential evapotranspiration in the RCM projections. Potential evapotranspiration is increasing in all projections (Table 5.4), whereas the development of the actual evapotranspiration is more variable, indicating a spatio-temporal water deficit. On the one hand, dry scenario simulations (e.g., model 3 in RCP8.5; see Table 5.4) show increasing actual evapotranspiration, although precipitation is decreasing. This can be attributed to both increasing potential evapotranspiration and decreasing water yields. On the other hand, the increase of actual evapotranspiration is less distinctive in the wet scenarios (models 1, 5, 6) in comparison to the increase of precipitation (e.g., models 1 and 6 in both scenarios; see Table 5.4). In these scenarios, surface runoff increases by up to 67.8% and the overall water yield by up to 61.6%, indicating a shift in water balance, favoring water yield instead of evapotranspiration. This shift might be attributed to the temporal distribution of the precipitation. Figure 5.8 shows the increase of rainfall within the rainy season, while the temperature, and therefore the potential evapotranspiration, rises, especially in the dry season. Additionally, the aforementioned models 1, 5, and 6 show comparably high values of Q10 (Figure 5.12a,b), implying higher discharge peaks and heavy rainfall events. Furthermore, it was already shown that the system is energy limited throughout the rainy season, with actual evapotranspiration equal to potential evapotranspiration (Näschen et al., 2018). Otherwise, there is distinct water limitation throughout the dry season, with Q90 values below the historical measured value (Figure 5.12c,d).

An overall aggravation of seasonality is particularly challenging in (East) African countries because of the already existing high spatial and temporal variability of available water resources (McClain, 2013) resources mc. Considering the climatic feedback described in chapters 3.4 and 4.1, including the rising temperatures in combination with decreasing low flow and water availability in the dry season, drought-related risks might be aggravated in the region due to climate change. However, flooding intensity is more likely to increase (Figure 5.11b, Figure 5.13). This indicates an aggravation of severe floods in the rainy season in combination with the chance of an increasing drought risk in the dry season. Additionally, the discharge peak and the following inundation, which are important factors for the recession agriculture in the valley (CDM Smith, 2016; Koutsouris et al., 2016), are likely to shift from April to May from the 2020s onwards (Figure 5.9). This shift might be attributed to the changing precipitation patterns (Figure 5.8b) in combination with the comparably slow drainage for the overall catchment (Lyon et al., 2015). Therefore, wise catchment management is needed to adequately use and retain the potentially occurring water benefit in the rainy season and make it available during the more pronounced drought periods in the dry season. In contrast, poorly adapted catchment management will increase the risk of severe floods. Additionally, a shift in inundation dynamics needs to be communicated to ensure efficient agricultural production.

Although results show no clear signal towards an extension or shortening of the dry or wet seasons across all models, precipitation amounts primarily increase within the rainy season. In contrast, the dry season from June to October is consistent with regard to very low precipitation amounts (<20 mm per month on average) and increasing potential evapotranspiration due to increasing temperatures, even though some regional climate models predict increasing rainfall in September (Figure 5.8). However, a general consistency within the single scenarios regarding extreme events is observed, with an antagonistic trend of either a decrease of both Q10 and Q90 or the opposite trend, with only a few less-pronounced exceptions (Figure 5.13).

Nevertheless, the wide distribution of the decadal simulation results and also the RCM simulation results in Figure 5.13 show that the occurrence of a trend towards a wetter future with regard to Q10 and Q90 is more likely. However, the spread of the different models and the decadal distribution indicate a high uncertainty and no clear temporal trend. Especially, the span for extreme events, e.g., the 100-year return level, between the six models is extremely high (Figure 5.10, Table 5.5) and results have to be considered carefully. This span can be taken as a range of uncertainty, with a set of possible futures scenarios for the Kilombero Catchment. The knowledge of the performance of these climate scenarios and models can be very useful for management purposes of the catchment, e.g., the estimation of future inundation dynamics. Therefore, a hydraulic model for the agriculturally utilized parts of the catchment needs to be established to estimate the impacts of potential scenarios. The analyses in Figure 5.11a and Figure 5.12a,b suggest utilizing either model 1, 3, 4, or 6 in hydraulic flood models to prepare for possible future flooding events under wetter conditions and changing inundation dynamics, due to the high return levels and Q10 values. In contrast to that, model 2 and model 3 are suitable to prepare for dry conditions, for example in environmental flow assessments.

A more detailed analysis has already been undertaken by investigating the impact of particular wet and dry decades and their impact on water balance components (Figure 5.14). There exists a distinctive increase of the overall water yield in the wet scenario, resulting in an increase of about 50% within nearly all subcatchments compared to the status quo (Näschen et al., 2018). This change will have a huge impact on the overall hydrology of the catchment and its management. On the one hand, this is only the annual average of a whole decade, and therefore conceals intra- and interannual dynamics, which are even more pronounced. On the other hand, one has to keep in mind that this is the most extreme scenario out of many possible future scenarios. Nevertheless, the comparison of these extreme scenarios provides a sense of the uncertainty that water management has to deal with. The distinct influence of both the driest and wettest simulated decades on the eastern part of the catchment (Figure 5.14) can be attributed to the fact that the eastern part is, in general, more important for the water yield of the catchment due to the precipitation patterns and also the direction of flow of the Kilombero River towards the east (Näschen et al., 2018). Natkhin et al. (Natkhin et al., 2015) give an overview of studies investigating the impact of climate on discharge regimes. They also show diverging effects of climate change on discharge regimes, but most of the studies imply a decrease of discharge in the dry season in contrast to an increasing total runoff, which is in line with the insights in this study. Reasons for changes in the discharge regimes are changes in precipitations patterns (Githui, 2008; Yanda and Munishi, 2007), increasing evapotranspiration due to higher temperature (Githui, 2008), LULC changes (Yanda and Munishi, 2007), water abstractions (Githui, 2008; Kashaigili, 2008), and dam constructions (Mwamila et al., 2008).

These study results show that in addition to climate change analyses, manifold factors are influencing the hydrology within the catchment (Montanari et al., 2013). The method of land use and management, for example, exerts strong influence over soil hydraulic properties, and thus influences the amount of water retention, surface runoff, and flood generation (Giertz, 2004; Zimmermann et al., 2006). Particularly, agricultural land is characterized by high degrees of soil cultivation and low soil coverage by vegetation during parts of the year, which in general leads to an increase of surface runoff generation. Thus, a growth of the share of agricultural land, which is promoted through the SAGCOT initiative (Environmental Resources Management, 2013), might lead to an aggravation of flood events,

and hence intensify the negative effects climate change might exert on the regional water balance. Apart from the presumable effects on water balance, an increment in agricultural area might also lead to biodiversity losses within the Ramsar site (Behn et al., 2018; Daconto et al., 2018).

Still, the extent to which increasing agricultural production influences soil hydraulic properties depends on different regionally varying factors, such as soil type, cultivation, and irrigation schemes, and location within the catchment. The aforementioned factors need to be determined within proper field studies to assist in planning for the future water resource management of the Kilombero Catchment.

In general, LULC change (Msofe et al., 2019) and management change scenarios should be developed and included in future analyses to investigate their combined impact in combination with climate change on water resources. Moreover, this study concentrates only on water quantity, due to the lack of data on water quality, but it was already demonstrated that the impact of climate change could be amplified by LULC change with regard to soil erosion and the accompanied nutrient input into surface waters (Danvi et al., 2017; Op de Hipt et al., 2019).

5.5. Conclusions

The study clearly showed the broad range of possible future climate scenarios for the Kilombero Catchment according to the bias-corrected CORDEX Africa projections. The climate impact analysis on hydrology recommends adapting to more distinct seasonality due to shifting rainfall patterns. These shifting patterns will probably result in changing inundation dynamics and more severe flooding, while the likelihood of decreasing low flows is less pronounced. The designation of suitable arable land for the recession agriculture has to be adjusted in accordance with the respective hydrological patterns. Future agricultural management strategies should also take into account a delay of approximately one month in the inundation of the floodplain within the next decades, because of the common delay signal across all simulations (Figure 5.9). The presented modeling results should be taken as a range of possible futures, which could be applied following the precautionary principle to assess and prepare for possible future conditions. However, it is strongly recommended to use these climate change scenarios in combination with LULC change scenarios and management scenarios to have a more realistic representation of the hydrological conditions. These hydrological model results should be implemented into a well-established hydraulic model to get a better understanding of their possible impact on inundation extent, depth, and timing. This will facilitate and enhance the management of the floodplain and might assist in the designation of suitable areas for either conservation measures or agricultural production zones, also with regard to downstream water users and water-related infrastructure, such as the planned hydropower dam at Stiegler`s Gorge.

Author Contributions: K.N., B.D., and C.L. conceived and designed the experiments. K.N. performed the experiments. K.N. and B.D. analyzed the data. R.v.d.L. and L.S.S. downloaded and bias-corrected the climate data. K.N. wrote the article. All authors made revisions and improvements to the final version.

Funding: This study was supported through funding from the German Federal Ministry of Education and Research (FKZ: 031A250A–H) and German Federal Ministry for Economic Cooperation and Development under the “GlobE: Wetlands in East Africa” project.

Acknowledgments: The authors would like to thank the Rufiji Basin Water Board for data sharing and assistance in the field and Salome Misana for her administrative guidance and logistic assistance.

Conflicts of Interest: The authors declare no conflict of interest. The funding sponsors had no role in the design of the study; in the collection, analyses, or interpretation of data; in the writing of the manuscript; or in the decision to publish the results.

5.6. Appendix A

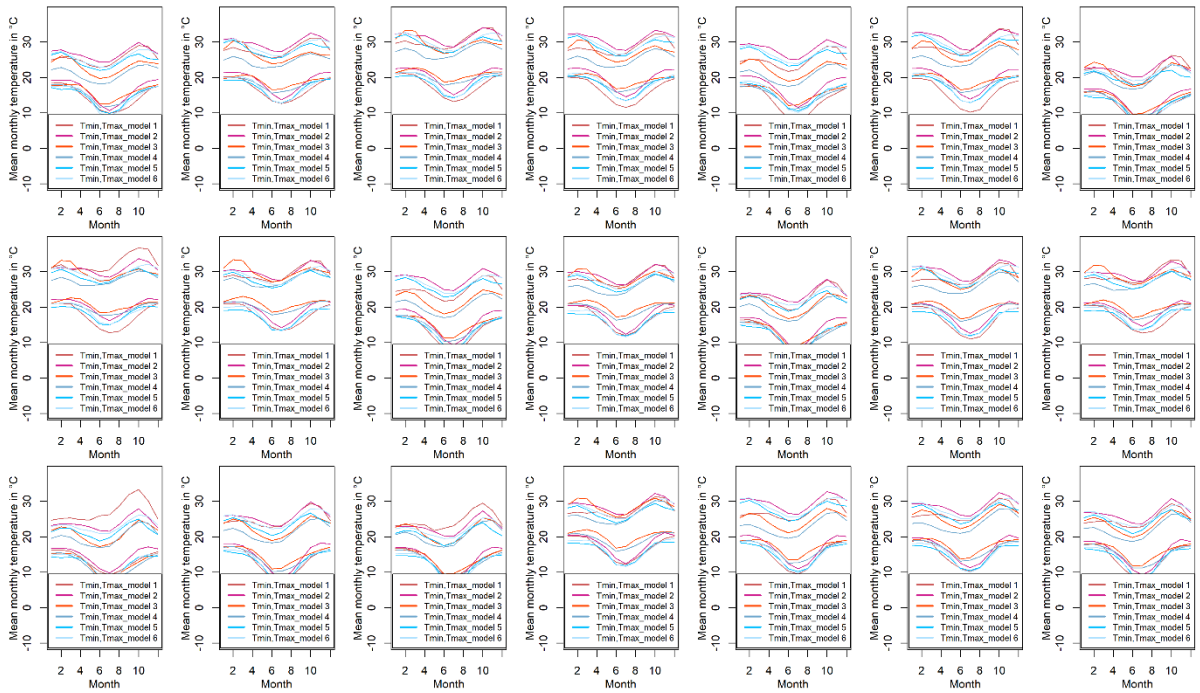

Figure 5.A1. Temperature from 1979-2005 for the 21 utilized CORDEX Africa datagrids before bias-correction. Each graph shows the average monthly temperature for all six models introduced in Table 5.2. Tmin and Tmax represent the mean monthly minimum and maximum temperatures respectively.

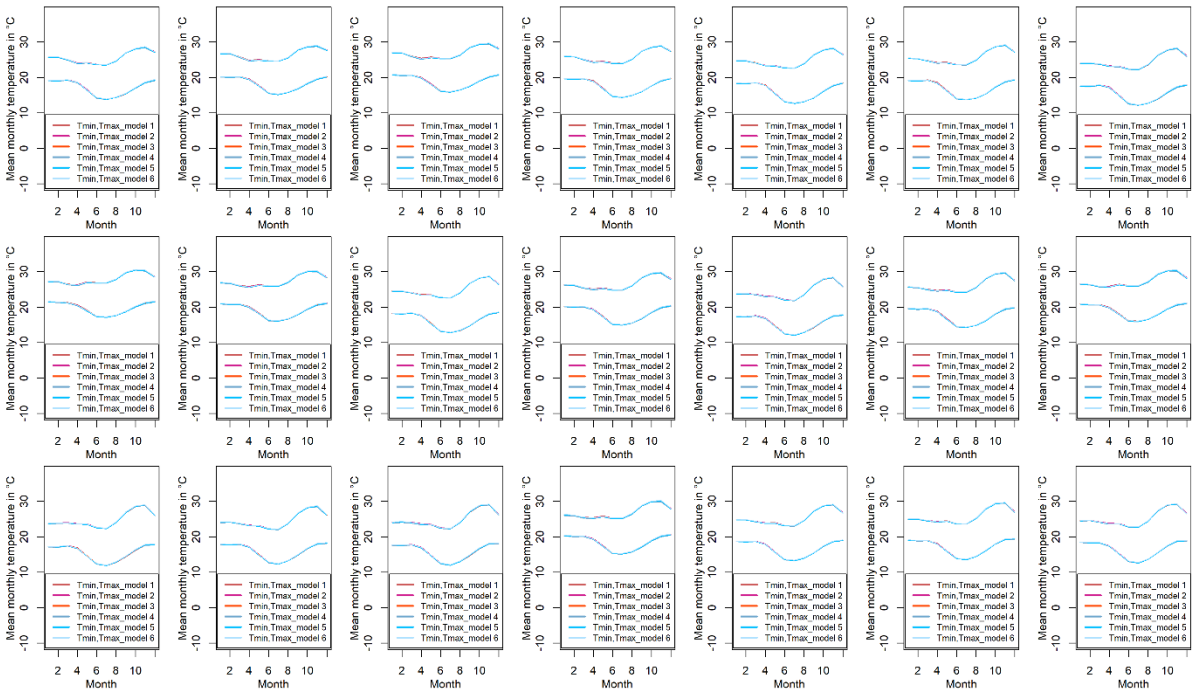

Figure 5.A2. Temperature from 1979-2005 for the 21 utilized CORDEX Africa datagrids after bias-correction with Era-Interim data. Each graph shows the average monthly temperature for all six models after bias-correction in Table 5.2. Tmin and Tmax represent the mean monthly minimum and maximum temperatures respectively.

6. The impact of land use/land cover change (LULCC) on water resources in a tropical catchment in Tanzania under different climate change scenarios

This chapter has been published as: Näschen, K., Diekkrüger, B., Evers, M., Höllermann, B., Steinbach, S., Thonfeld, F., 2019. The Impact of Land Use/Land Cover Change (LULCC) on Water Resources in a Tropical Catchment in Tanzania under Different Climate Change Scenarios. Sustainability 2019, Vol. 11, 7083. doi:10.3390/SU11247083
https://www.mdpi.com/2071-1050/11/24/7083

Abstract: Many parts of sub-Saharan Africa (SSA) are prone to land use and land cover change (LULCC). In many cases, natural systems are converted into agricultural land to feed the growing population. However, despite climate change being a major focus nowadays, the impacts of these conversions on water resources, which are essential for agricultural production, is still often neglected, jeopardizing the sustainability of the socio-ecological system. This study investigates historic land use/land cover (LULC) patterns as well as potential future LULCC and its effect on water quantities in a complex tropical catchment in Tanzania. It then compares the results using two climate change scenarios. The Land Change Modeler (LCM) is used to analyze and to project LULC patterns until 2030 and the Soil and Water Assessment Tool (SWAT) is utilized to simulate the water balance under various LULC conditions. Results show decreasing low flows by 6%−8% for the LULC scenarios, whereas high flows increase by up to 84% for the combined LULC and climate change scenarios. The effect of climate change is stronger compared to the effect of LULCC, but also contains higher uncertainties. The effects of LULCC are more distinct, although crop specific effects show diverging effects on water balance components. This study develops a methodology for quantifying the impact of land use and climate change and therefore contributes to the sustainable management of the investigated catchment, as it shows the impact of environmental change on hydrological extremes (low flow and floods) and determines hot spots, which are critical for environmental development.

Keywords: SWAT model; Land Change Modeler; Scenario analysis; Extreme flows; Tanzania; Kilombero

6.1. Introduction

Recent developments in sub-Saharan Africa (SSA) show an increasing trend of conversion of natural land cover into arable land (Brink et al., 2014; Brink and Eva, 2009; Gabiri et al., 2019; Guzha et al., 2018; Leemhuis et al., 2017; Marchant et al., 2018; Mucova et al., 2018; Näschen et al., 2018; Op de Hipt, 2018; Rosa et al., 2018; Yira et al., 2016). Drivers of change are manifold and can be directly linked to human activities such as population growth, economic development, and globalization (Kleemann et al., 2017; Marchant et al., 2018). Natural processes like floods, landslides, droughts and climate change affect land use and land cover change (LULCC) (Brink and Eva, 2009), although they are induced by anthropogenic activities to a certain degree. These conversions into arable land have an adverse impact on several ecosystem services as a trade-off for increased agricultural outputs such as food and timber production (Brink and Eva, 2009; Meijer et al., 2018). Several water-related targets of the Sustainable Development

Goals (SDGs) are at risk due to land conversions into arable land, especially with regard to SDG 6 (Clean Water and Sanitation) and SDG 15 (Life on Land) (Meijer et al., 2018; Nhemachena et al., 2018).

Several studies investigated the impact of LULCC and climate change on water resources separately (Faramarzi et al., 2013; Yira et al., 2016) or simultaneously (Notter et al., 2013; Op de Hipt et al., 2019). The results of the studies differ due to several reasons e.g., the type of LULCC, the regional focus, or the time period and model chosen to simulate climate change. However, many studies indicate an increased exposure to hydro-climatic extremes in Eastern Africa (Funk et al., 2008; Lyon and Dewitt, 2012; Shongwe et al., 2011; Williams and Funk, 2011). This study exemplarily analyzes LULCC compared to climate change in the Kilombero Catchment in Tanzania and how these affect water resources. The catchment itself is subject to aforementioned LULCC (Leemhuis et al., 2017; Meijer et al., 2018) and pressure on land resources in the valley is fostered by government plans to implement the Southern Agricultural Growth Corridor of Tanzania (SAGCOT) (Environmental Resources Management, 2013), which is accompanied by a growing population and migration of pastoralists into the valley (Msofe et al., 2019). SAGCOT follows a green growth approach covering three development clusters in Kilombero, Ihemi, and Mbarali, comprising one third of the mainland of Tanzania (Leemhuis et al., 2017; Milder et al., 2013; Steffens et al., 2019). On the one hand the key clusters are characterized by great agricultural potential and on the other hand they contain extensive forests, protected areas, and their infrastructure is poorly developed (Leemhuis et al., 2017). One of the key features of the SAGCOT initiative for the Kilombero cluster is the establishment of a sustainable agricultural intensification with irrigation schemes for rice and sugarcane as well as integrated crop-livestock-aquaculture systems in the catchment's wetland (Milder et al., 2013). These changes in LULC in combination with the effects of climate change complicate water resource management of the catchment. Yet, projections concerning water quantities are crucial to sustaining the socio-ecological system and long-term perspectives are especially essential for a responsible treatment of water resources under changing climatic conditions.

The dominant LULCC in the catchment is from grassland to cropland, which mainly occurs in its floodplain area (Leemhuis et al., 2017; Muro et al., 2018). The most important crop for this conversion is rain-fed rice, that is grown in the lowland areas (Kangalawe and Liwenga, 2005; Meijer et al., 2018). However, deforestation is becoming more important with the increasing population and the growing demand for timber, fuelwood and charcoal production (Johansson and Abdi, 2019). Other drivers of change are economic development, foreign agricultural investments, agro-technological advancements, favorable biophysical factors, policies, the aforementioned population growth, and increased migration of pastoralists into the valley (Johansson and Abdi, 2019; Msofe et al., 2019). These LULCC will affect ecosystem services and water resources in the catchment and scientific guidance is needed in order to enable a sustainable development of the catchment (Leemhuis et al., 2017; Meijer et al., 2018). Inhabitants of the catchment already report changing water dynamics, such as lower water levels and consequently depleted fish stocks (Johansson and Abdi, 2019). Paddy rice plays a specific role in this study due to its large-scale suitability in the catchment according to the SAGCOT plans (Environmental Resources Management, 2013) and additionally due to its high water demand and the resulting implications on water resources (Duku et al., 2016). The following goals of the study arose from this context:

(i) Develop scenarios for the LULC distribution for the Kilombero Catchment until 2030;
(ii) Analyze the impact of the different LULC scenarios on water resources at various temporal and spatial scales;
(iii) Investigate the impact of LULCC on low flow and high flow regimes;
(iv) Assess the combined impact of LULCC and climate change on water resources.

In order to reach these goals, observed patterns of change were correlated with various spatial features of the catchment using the digital elevation model (DEM), and were projected until 2030 by using the Land Change Modeler (LCM) (Eastman, 2016a, 2016b; Mas et al., 2014). Furthermore, the SWAT model was utilized to simulate the impact of the different LULC setups on water resources. Subsequently, the selected Global Climate Model-Regional Climate Model (GCM-RCM) developed for a previous study (Näschen et al., 2019) was integrated to estimate the combined effect of LULCC and climate change. Results show huge deviations in water balance components on a subcatchment scale and that especially high flow patterns vary among the different LULC scenarios.

An overview of abbreviations that are used within this study and their meanings is given in Table 6.1.

Table 6.1 List of abbreviations used in this study and their meanings.

Abbreviation	Meaning	Abbreviation	Meaning
CLMcom	Climate Limited-area Modeling Community	Q10	Flow exceeded in 10% of the specified period
CORDEX	Coordinated Regional Downscaling Experiment	Q90	Flow exceeded in 90% of the specified period
DEM	Digital elevation model	RCM	Regional climate models
EPIC	Erosion-Productivity Impact Calculator	RCP	Representative Concentration Pathways
GCM	Global Climate Model	RF	Random Forest
HRU	Hydrologic response unit	RBWB	Rufiji Basin Water Board
HWSD	Harmonized World Soil Database	SAGCOT	Southern Agricultural Growth Corridor of Tanzania
KGE	Kling-Gupta efficiency	SCS	Soil conservation service
LCM	Land Change Modeler	SDGs	Sustainable Development Goals
LULC	Land use/ land cover	SMHI	Swedish Meteorological and Hydrological Institute
LULCC	Land use/ land cover change	SRTM	Shuttle Radar Topography Mission
MLP	Multi-Layer Perceptron	SSA	Sub-Saharan Africa
MSS	Multispectral scanner	SWAT	Soil and Water Assessment Tool
NGO	Non-Governmental Organisation	TMA	Tanzania Meteorological Agency
NSE	Nash-Sutcliffe-Efficiency	UDSM	University of Dar es Salaam
PPP	Public-private partnership		

6.2. Materials and Methods

6.2.1.Study Site

The study site is located in the Morogoro region in south central Tanzania (Figure 6.1). It is enclosed by the Udzungwa Mountains in the north and west, whereas the Mbarika Mountains and the Mahenge Highlands demarcate the southern boundary of the catchment. The catchment is drained by the eponymous Kilombero River and comprises a total of 40,240 km² up to the confluence of the Kilombero River and the Luwego River (Näschen et al., 2018). From here downstream, the river is called Rufiji River and refers to the Rufiji Basin, which is the most important river basin of Tanzania (Daconto et al., 2018). The Rufiji Basin consists of three major tributaries and their respective catchments, which are the Great Ruaha, the Luwego, and the Kilombero. The Kilombero itself covers only 23% of the Rufiji Basin´s area, but it contributes 62% of total discharge and is therefore of particular importance with regard to water resources (Wilson et al., 2017). The Kilombero River itself has several perennial and seasonal tributaries, which mainly contribute inflow from the upland areas. However, this system is at risk, due to LULCC and water abstractions that affect the inflow of several tributaries and the maintenance of the environmental flows (CDM Smith, 2016; Daconto et al., 2018). The Kilombero river forms a complex braided and meandering river network in the central floodplain, which covers 7,967 km² and constitutes one of the most important African lowland fresh water wetlands (Mombo et al., 2011; Wilson et al., 2017). Since 2002 the floodplain has been designated as a Ramsar site and over 70% of the floodplain area is protected (Nindi et al., 2014).

The climate is a sub-humid tropical climate with a distinctive seasonality, which is characterized by a dry and a rainy season. The rainy season itself can be differentiated into the short rainy season from October until December/January (locally called “Masika”) and the long rainy season from March until May (“Vuli”) (Camberlin and Philippon, 2002; Zorita and Tilya, 2002). Nevertheless, this bimodal pattern only applies for the northern parts of Tanzania, whereas the south-western parts of Tanzania are characterized by a unimodal rainfall distribution and therefore one rainy season (“Msimu”) (Seregina et al., 2018). However, there are huge interannual, intraannual, and also spatial variabilities in the distribution of precipitation for the Kilombero Catchment recorded (Koutsouris et al., 2016; Näschen et al., 2019, 2018). This high variability can be attributed to the manifold factors influencing the local climate, such as remote forcings (e.g., Walker Circulation, Indian Ocean Dipole), regional circulations (e.g., Tropical Easterly Jet), but also local geographic factors (e.g., windward and leeward effects) (Nicholson, 2017). Annual mean areal precipitation is between 1200 and 1400 mm, whereas the mountainous parts receive up to 2100 mm and the valley 1100 mm, respectively (Koutsouris et al., 2016; Wilson et al., 2017). The mean annual temperature has an antagonistic pattern and varies between 24° C in the valley and around 17° C in the uplands of the catchment (Wilson et al., 2017).

Soils in the floodplain are largely heavy black cotton soils, with a good water content at field capacity, but also some patches of sandy soils (Msofe et al., 2019). According to the Harmonized World Soil Database (HWSD) most parts of the catchment are covered by acrisols, with some areas dominated by cambisols in the western part and nitisols in the Udzungwa mountains (Dewitte et al., 2013).

The land cover of the upper catchment embraces a mixture of natural vegetation like tropical rainforests, bush lands, and wooded grasslands with some patches of agricultural fields (Zemandin et al., 2011). The valley is surrounded by a *miombo* woodland belt with mainly *Brachystegia* spp., whereas the

floodplain itself is dominated by agricultural use and tall grasses such as *Penisetum purpureum*, *Panicum maximum*, *Hyparrhenia* spp., and *Phragmites mauritianus* with some isolated trees of *Ficus* spp. and *Kigelia africana* (Kato, 2007; Nindi et al., 2014). The most important crops grown in the valley are sugarcane (*Saccharum officinarum*), maize (*Zea mays*), paddy rice (*Oryza sativa*), and cassava (*Manihot esculata*) (Msofe et al., 2019). Rice production is dominated by small-scale farmers and rain-fed agriculture, although some small irrigations schemes do exist in the valley. Sugarcane is mainly grown as irrigated agriculture by a large-scale contractor (Kilombero Sugar Company) in the northeastern part of the catchment.

Recent developments show an increasing trend of conversion of wetland, forested areas, and grassland into arable land in the Kilombero Valley (Leemhuis et al., 2017; Näschen et al., 2018). The Kilombero area has to cope with many immigrants, including a high number of pastoralists, causing a population growth rate for the Kilombero area of 3.4% according to the national population census from 2012, which exceeded the national average of 2.8% (National Bureau of Statistics. United Republic of Tanzania, 2012). The SAGCOT growth corridor plans, including infrastructure developments like bridge construction and expansion of paved roads (Environmental Resources Management, 2013; Milder et al., 2013), as well as the planning of the Stiegler´s Gorge hydropower dam in the Selous Game Reserve downstream, might have a huge impact on the development of the catchment (Daconto et al., 2018).

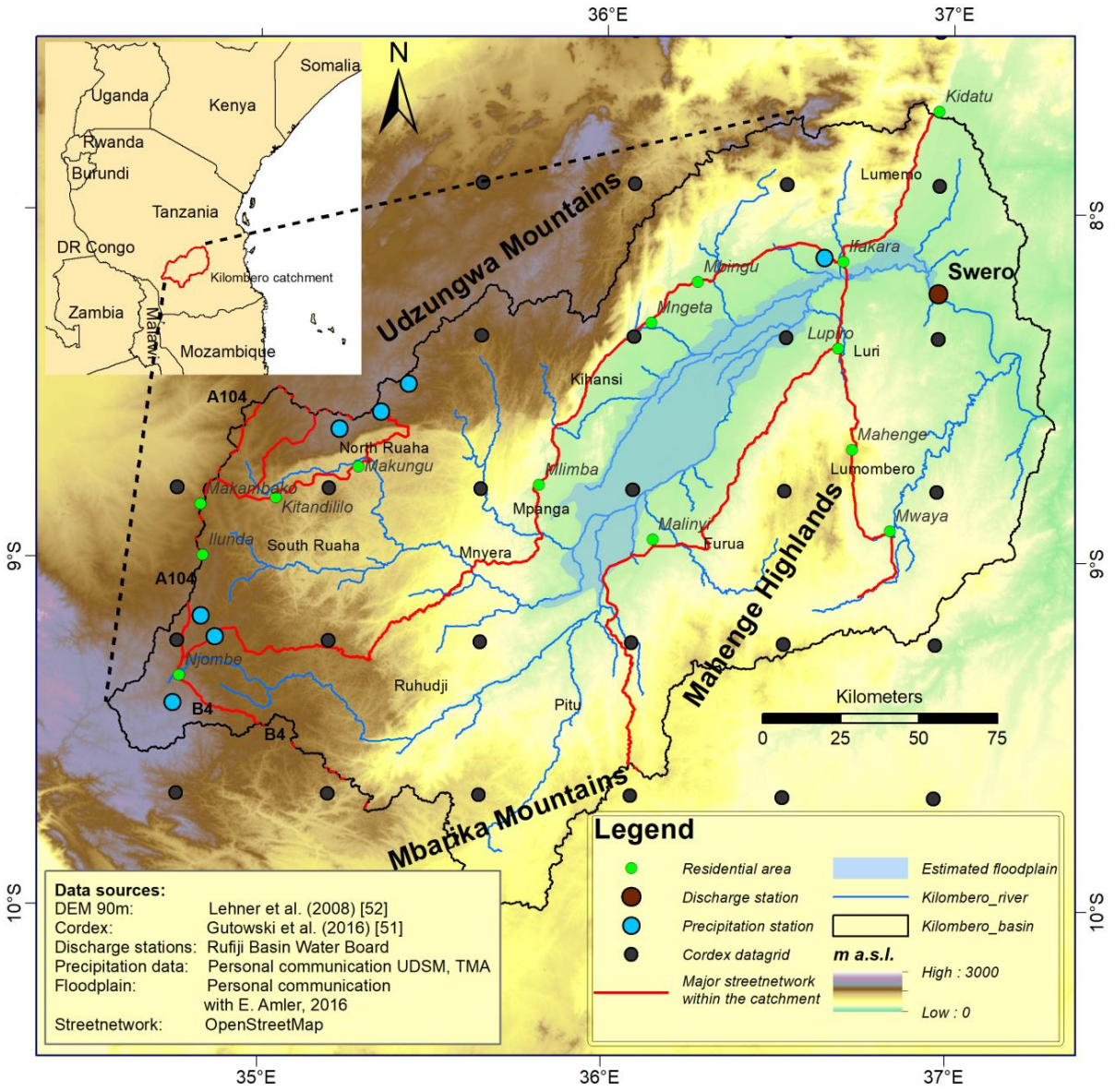

Figure 6.1 Overview map of the study area, including available precipitation and discharge stations (Swero). The estimated floodplain area is based on visual interpretation of Landsat images (modified after (Näschen et al., 2018)).

6.2.2.Input Data

The SWAT model for this study is based on the details already given by Näschen et al. (Näschen et al., 2018). The issue of data scarcity in the study region is solved by using freely available geodata in combination with data gathered from local partners in Tanzania (Table 6.2, (RBWB, 2014)). The most crucial but also most limiting data is discharge data, which has the longest time series at a downstream station ("Swero") near the outlet of the catchment but stretches in good quality only from 1958 to 1970. The station is currently being renewed and new stations are being set up in the catchment, nonetheless there is no time series and no rating curve for the new stations available up to today. Therefore, the historical discharge data was used to set up the hydrological model (Näschen et al., 2018). In addition,

LULC maps were produced from Landsat imagery for four different time steps. Due to extensive cloud cover, all available Landsat TM, ETM+, and OLI Surface Reflectance scenes within three-year periods around the years 1994, 2004, and 2014 were considered, and multi-temporal metrics (Mack et al., 2017) were calculated using different vegetation indices. Together with topographic indices based on the Shuttle Radar Topography Mission (SRTM) DEM, these were classified in a supervised Random Forest (RF) approach (Breiman, 2001; Näschen et al., 2018). The RF classifier was calibrated and validated using information from field visits, flight campaigns and Google Earth in a random sampling scheme. For the 1970s LULC map, due to the lack of suitable images, Landsat pre-Collection Level 1 images from the whole decade were cloud-masked, corrected for corrupted image lines, normalized to one master image, mosaicked, and classified. The spatial resolution of the early Landsat images (1970s) from the multispectral scanner (MSS) instrument is 60 m. The resulting maps were resampled to a 30 m pixel size in order to be complementary to the other Landsat products. Figure 6.2 shows the LULC maps as reclassified into SWAT LULC classes. The left configurations (a-d) include a barren class and an undifferentiated cropland class, whereas the right configurations (e-h) differentiate between cropland and rice as a specific plant (named “cropland-rice”). SWAT classes besides barren, cropland, and cropland-rice comprise forest evergreen, forest mixed, grassland, savanna, wetland, open water, and built-up.

Seven precipitation stations were used as input in combination with Coordinated Regional Downscaling Experiment (CORDEX) Africa data (Gutowski et al., 2016) for the other climate parameters (Table 6.2). For future climate scenarios GCM-RCM (Global Climate Models-Regional Climate Models) model combinations from CORDEX Africa were bias-corrected for temperature and precipitation. A more detailed description on the procedure can be found in Näschen et al. 2019 (Näschen et al., 2019). Two of these GCM-RCM scenario data sets were chosen for this study in order to represent a span of wet and dry scenarios covering increasing and decreasing annual precipitation amounts (Table 6.3, Table 6.4). Soil data was gathered from the Harmonized World Soil Database (HWSD) and the SRTM 90 m digital elevation model (DEM) was used for the SWAT model. A complete overview on all of the data sources utilized in this study is given in Table 6.2.

Table 6.2 Overview of the applied datasets, their resolution, sources, and the required parameters in this study.

Data set	Resolution/Scale	Source	Required Parameters
Digital elevation model (DEM)	90 m	Shuttle Radar Topography Mission (SRTM) (Lehner et al., 2008)	Topographical data
Soil map	1 km	FAO (Dewitte et al., 2013)	Soil classes and physical properties
Land use map	60 m (1970s), 30 m (1994, 2004, 2014)	Landsat Pre-Collection Level-1 (United States Geological Survey (USGS), n.d.), Landsat TM, ETM+, OLI Surface Reflectance Level-2 Science Products (USGS Department of the Interior, n.d., n.d.), SRTM (Lehner et al., 2008)	Land use/cover classes
Precipitation	Daily	Personal communication: Rufiji Basin Water Board (RBWB), University of Dar es Salaam (UDSM), Tanzania Meteorological Agency (TMA)	Measured precipitation
Climate	Daily/0.44 ° (1951-2060)	CORDEX Africa (Gutowski et al., 2016)	Temperature, humidity, solar radiation, wind speed, precipitation
Discharge	Daily (1958–1970)	RBWB (RBWB, 2014)	Discharge

Table 6.3 Overview of the Regional Climate Models (RCMs), their driving Global Climate Models (GCMs), and the assigned naming for the model combination within this study.

GCM	RCM	Institution	URL	In this study referred to as
CNRM-CM5	CCLM4-8-17_v1	Climate Limited-area Modeling Community (CLMcom)	https://esg-dn1.nsc.liu.se/	Dry model
MIROC5	RCA4_v1	Rossby Centre, Swedish Meteorological and Hydrological Institute (SMHI)	https://esg-dn1.nsc.liu.se/	Wet model

Table 6.4 Historical annual average precipitation according to the bias-corrected RCM simulations (1951–2005) and the absolute and relative changes of precipitation, actual evapotranspiration and overall water yield in SWAT simulations (2010–2060) according to the projections based on RCP4.5 and RCP8.5 scenarios. Numbers in parentheses represent the changes in percentage (modified after (Näschen et al., 2019)).

Climate Model	Historical Precipitation (after bias correction) in mm	RCP Precipitation changes in mm (%)	RCP actual evapotranspiration changes in mm (%)	RCP overall water yield changes in mm (%)
“Dry Model” (RCP4.5)	1311	−109 (−8.3)	-10 (-1.4)	-103 (-19.8)
“Wet Model” (RCP4.5)	1345	218 (16.2)	14 (1.5)	163 (42.1)
“Dry Model” (RCP8.5)	1311	−76 (−5.8)	11 (1.5)	-85 (-16.3)
“Wet Model” (RCP8.5)	1345	302 (22.5)	25 (2.7)	239 (61.6)

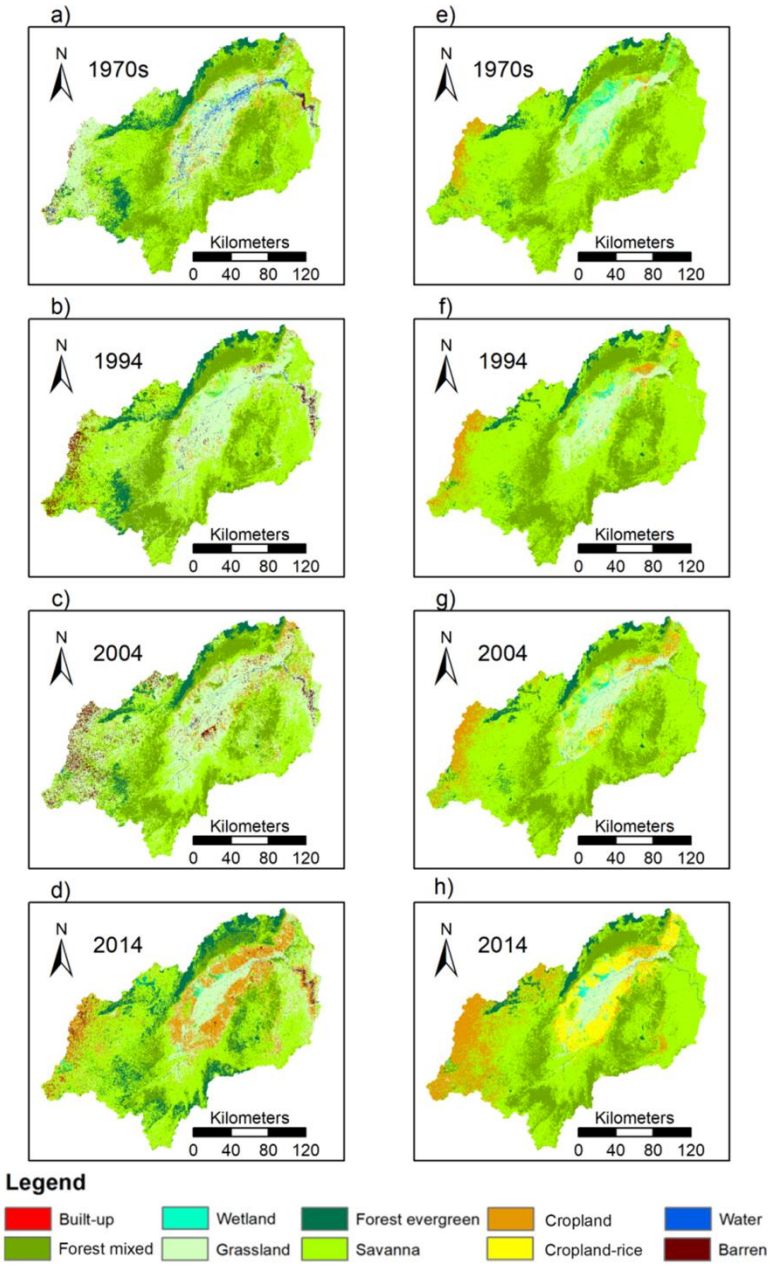

Figure 6.2 Land use and land cover classifications for four time steps ranging from the 1970s (a and e), 1994 (b and f), and 2004 (c and g) up to 2014 (d and h). Some differences among the LULC maps in the right and in the left column exist due to the classification process: Only the maps in the left column contain “barren” as a land use class, but they have only one LULC ”cropland”, whereas the maps in the right column differentiate in between “cropland” and “cropland-rice” as a specific crop.

6.2.3. Modeling Approach.

6.2.3.1. The SWAT Model

In this study the SWAT model (Arnold et al., 1998) was applied to simulate the hydrological processes on the catchment scale. SWAT is a semi-distributed and physically-based model which operates on a daily time-scale. The physically-based approach of SWAT with the incorporation of the Erosion-Productivity Impact Calculator (EPIC) model (Williams, 1995) allows to account for plant growth variations and is necessary to adequately simulate the impacts of land use changes on hydrological processes.

In a first step the SWAT model discretizes the catchment into subcatchments based on a threshold that defines the minimum drainage area to form a stream. Furthermore, these subcatchments are discretized into hydrologic response units (HRU), which are unique combinations of soil, slope, and land use within each of the subcatchments. These HRUs are the most important spatial unit for the calculation of hydrological processes within SWAT.

In general, the model differentiates between a land phase and a routing phase. The land phase considers most of the hydrological processes of the hydrological cycle, whereas the routing phase integrates the routing of water among the subcatchments and in-stream processes of water, sediments, nutrients, and organic chemicals. In the land phase the water balance equation is solved on HRU level and all HRU calculations are treated as the result of a subcatchment without considering routing among the single HRUs. Climate data input is given on the subcatchment scale, with the option to account for altitudinal effects on temperature or precipitation with so called elevation bands. These elevation bands modify temperature and precipitation to represent orographic effects in case of large altitudinal differences within the subcatchments (Neitsch et al., 2011). Precipitation can be intercepted by vegetation, enter the reach directly or hit the ground, where it might move as surface runoff, evaporate, or infiltrate into the soil based on the given physical conditions represented by the Soil Conservation Service (SCS) curve number and the climatic conditions (Monteith and Moss, 1977; Soil Conservation Service (ed.), 1972). Once water infiltrates into the soil, it is stored as soil moisture and can move among up to ten soil layers using a storage routing technique, which is based on the field capacity of the soil layers and the saturated hydraulic conductivity. Lateral flows in the soil are simulated with a kinematic storage model, which mainly depends on the slope of the area (Sloan and Moore, 1984). Groundwater is divided into two aquifers in SWAT: A shallow unconfined aquifer and a deeper confined aquifer. If water percolates from the soil through the unsaturated zone, it enters the shallow aquifer. From there, water might contribute as baseflow to the reach, move upwards as capillary rise due to LULC dependent water demand, or percolate deeper into the confined aquifer, where it is assumed to contribute to the regional water balance and is treated as being lost for the local catchment. However, both aquifers might contribute to the streamflow through different parameters (Liu et al., 2019). A detailed model description is given by (Arnold et al., 1998), (Neitsch et al., 2011), and (Arnold et al., 2012a).

6.2.3.2. Model Setup, Evaluation and Extreme Value Analysis (SWAT Model)

The SWAT model setup was done with ArcSWAT 2012 (revision664), whereas calibration and validation were performed with SWAT-CUP (version 5.1.6.2) and the SUFI-2 algorithm (Abbaspour, 2013) using the Kling-Gupta efficiency (KGE) as an objective function. The catchment was divided into 95 subcatchments and 1087 HRUs. Additionally elevation bands were integrated to adequately account for varying precipitation patterns due to high relief energy within the subcatchments (Näschen et al., 2018; Neitsch et al., 2011). The coefficient of determination (R^2) (Equation 6.1), the Nash-Sutcliffe-Efficiency (NSE) (Equation 6.2), and the aforementioned KGE (Equation 6.3) were some of the utilized evaluation criteria. A more detailed overview on the SWAT model setup and additional evaluation criteria is given by (Näschen et al., 2018).

$$R^2 = \frac{[\sum_{i=1}^{n}(O_i - \bar{O})(S_i - \bar{S})]^2}{\sum_{i=1}^{n}(O_i - \bar{O})^2 \sum_{i=1}^{n}(S_i - \bar{S})^2} \quad \text{(Equation 6.1)}$$

$$NSE = 1 - \frac{\sum_{i=1}^{n}(O_i - S_i)^2}{\sum_{i=1}^{N}(O_i - \bar{O})^2} \quad \text{(Equation 6.2)}$$

$$KGE = 1 - \sqrt{(r-1)^2 + (\sigma - 1)^2 + (\beta - 1)^2} \quad \text{(Equation 6.3)}$$

where *n* is the number of observations, O_i and S_i are the observed and simulated discharge values, respectively, and $\bar{O}$ and $\bar{S}$ are the mean of observed and simulated discharge values. *r* is the coefficient of correlation between observed and simulated data, σ is the ratio of the standard deviation of simulated and observed data, and β is the ratio of the means of simulated and observed data.

The results of the SWAT model were utilized to analyze changes in low flows and high flows for the different LULC setups separately and in combination with selected RCM-GCMs (Table 6.3). The extRemes 2.0 package (Gilleland and Katz, 2016) was utilized to calculate return levels from 2-year up to 100-year return levels using the generalized extreme value distributions (GEV) (Equations (6.4) and (6.5)) and the generalized maximum likelihood estimation (GMLE) method:

$$F(x) = exp\left[-\left\{1 + \gamma\left(\frac{x-\mu}{\alpha}\right)\right\}^{-1/\gamma}\right] \quad \text{(Equation 6.4)}$$

where γ is the shape parameter, μ the location parameter, and α the scale parameter of the probability distribution function with $\alpha > 0$ and $(1 + \gamma(x - \mu)/\alpha) > 0$. If $\gamma \to 0$, the function belongs to the Gumbel family and is as follows:

$$F(x) = \exp\left[-\exp\left\{-\left(\frac{x-\mu}{\alpha}\right)\right\}\right]. \quad \text{(Equation 6.5)}$$

Additionally, the Q10 index was applied, because it is less sensitive to outliers compared to the generalized extreme value analysis. The Q10 is defined as the daily discharge that is exceeded in 10% of all the simulations here. Moreover, the Q90 (Smakhtin, 2001; van Vliet et al., 2013) index was used to analyze low flows. In contrast to the Q10 index, the Q90 index is defined as daily discharge that is exceeded in 90% of all the simulations here. The Hydrostats package (Bond, 2018) in the statistical software R was applied for these analyses.

6.2.3.3. Land Use and Land Cover Change (LULCC) Scenarios

One of the main objectives of this article is to analyze the impact of LULCC on water resources until 2030. Therefore, scenarios of LULC for 2030 were developed using a mixed method approach containing land use change modeling, expert interviews, and a participatory mapping exercise in the framework of a workshop with local experts (Figure 6.3). The main goal of developing the 2030 scenarios was to identify implications of potential future LULC distributions on water resources in order to determine hot spots of change regarding water resources. In a first step, the historical LULC distributions from the 1970s until 2014 were derived from Landsat images (see chapter 2.2.). The Land Change Modeler LCM (Anand et al., 2018; Eastman, 2016b; Gashaw et al., 2018; Mas et al., 2014), within the Terrset Software Version 18.31 utilizing the IDRISI GIS System (Eastman, 2016b), was used to analyze the changes of LULC classes among the available historical products from the 1970s until 2014 ("Analysis of Change", Figure 6.3).

The next step consisted of a mixture of quantitative and qualitative methods to estimate potential drivers of change. The quantitative part analyzed the changes of all LULC classes between two time steps and finally identified potential explanatory factors for change. This was achieved by utilizing the evidence likelihood transformation integrated in the LCM to identify explanatory factors based on observed changes among the maps of 2004 and 2014. These time steps were identified as most suitable baseline for project changes for the period until 2030, because changes from the 1970s until 2004 are rather negligible (Figure 6.2). This procedure was done separately for the LULC maps covering cropland only, as well as for the maps that distinguish between cropland and cropland-rice (Figure 6.2c-d, and Figure 6.2g-h). The scenario with specific attention to rice was established due to the importance of rice crops for the catchment (Nindi et al., 2014; Wilson et al., 2017) and to assess the differences among cropland and cropland-rice scenarios with regard to their impact on water resources. Differences in cropland and cropland-rice within SWAT involve, among other factors, the plant's radiation-use efficiency, the growth rate, and the maximum leaf area index (Arnold et al., 2012).

Simultaneously, a qualitative component was performed to complement the quantitative results. Several experts in the region were interviewed and a workshop was held to perform a participatory mapping exercise. In this exercise experts from various disciplines were asked about recent hot spots of land use change and possible hot spots of land use change within the next 10 –20 years. The information was used to identify explanatory factors as well as to evaluate, revise, and contextualize the final maps for 2030 (see also chapter 4.1).

As spatial explanatory factors of change slope, elevation above sea level, distance to roads, rivers and settlements as well as the distance to former disturbances, so LULC conversions into cropland or rice were included in the modeling process. The processes involving distance to disturbances or settlements are driven by population growth in the valley and population growth is therefore integrated indirectly through these processes as a driver variable. Explanatory factors were also discussed within the workshop with local stakeholders from various fields (hydrology, ecology, social sciences, agronomy, district officers, NGO, and PPP representatives). On the baseline of these expert opinions and the observed patterns of historic LULCC (see Figure 6.2), it was assumed that conversion of a LULC class into cropland or rice is more likely close to roads, settlements, former conversions into agricultural land use or in flat areas, and lowlands that are especially suitable for rice production. Subsequently, the Multi-Layer Perceptron (MLP) neural network (Eastman, 2016b) was utilized to create the transition potentials in a transition model that simulates potential future LULC distributions using the built-in Markov Chain

Model (Adhikari et al., 2012; Eastman, 2016b). Based on observed change patterns and expert judgment, the resulting maps estimate the spread of either cropland or cropland-rice until 2030 and are used as input for the SWAT model to analyze the impact on water resources.

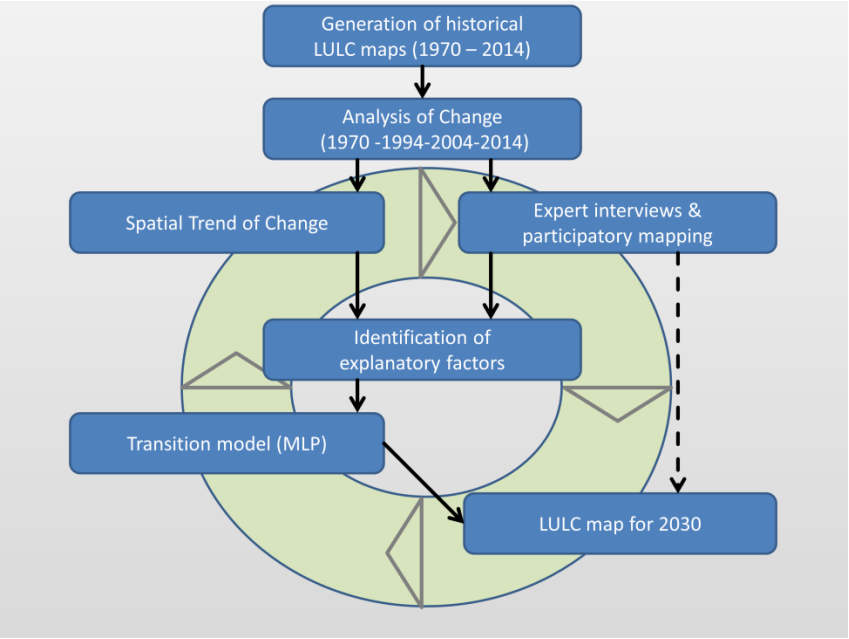

Figure 6.3 Flow chart indicating the major processes to generate the LULC maps for the 2030 scenarios.

For the purpose of training and evaluation, the MLP was given a set of pixels that were included in the transition model. In this specific case, a set of 10,000 pixels from the LULC setup of 2004 was taken. These pixels were chosen randomly fulfilling the following requirements: One half of the pixels changed from one of the other LULC classes into either cropland or cropland-rice in the LULC 2014 setup. The other half of the pixels consisted of pixels from all LULC classes from 2004 that were suitable to change either into cropland or cropland-rice (e.g., flat terrain or proximity to settlements or roads), but did not experience such change until 2014.

In a next step, these 10,000 pixels were randomly distributed into a training and a validation pixel group containing each half of the pixels. The training pixels were utilized to train the MLP and calculate the LULCC from 2004 to 2014, while the validation group was used to measure the accuracy of this training model to correctly predict persistence of LULC classes or their transition into cropland or cropland-rice from 2004 to 2014. Measure value for the performance of the transition model is the skill statistic with expected accuracy and skill measure (Equation 6 and 7):

$$E(A) = \frac{1}{(T + P)} \qquad \text{(Equation 6.6)}$$

where E(A) is the expected accuracy, T is the number of transitions in the submodel, and P the number of persistent classes.

$$S = \frac{(A - E(A))}{(1 - E(A))} \qquad \text{(Equation 6.7)}$$

where S is the skill measure ranging from -1 to 1, with values smaller 0 indicating a model worse than random chance and with value +1 indicating a perfect fit, while A is the measured accuracy, which accounts for the percentage of correct predictions (Eastman, 2016a).

The transition potentials for the single LULC classes gathered from this training and validation were later on transferred into a transition matrix, which was used to simulate the LULC maps for 2030.

All LULC scenario analyses with the SWAT model were performed with identical climate data to decouple the climate influence on water resources from the influence of LULCC. The MIROC5-RCA4_v1 model (Table 6.3) from 1958–2005 was chosen as baseline climatic data for the LULC analysis. The combined effects of climate change and LULC impacts on water resources are investigated in chapter 6.3.4 with two GCM-RCM combinations that show either dry (CNRM-CM5-CCLM4-8-17_v1, Table 6.3, 6.4) or wet (MIROC5-RCA4_v1, Table 6.3, 6.4) climatic conditions for the period of 2010–2060 (Näschen et al., 2019). The "dry model" is run with the RCP 4.5 scenario and the "wet model" with the RCP 8.5 scenario to account for uncertainties in climatic conditions by choosing the driest and wettest model already tested and bias-corrected for the region in a previous study (Näschen et al., 2019).

For the analyses on subcatchment scale (Figure 6.10, 6.12) the LULC setup of 1994 was used for the comparison instead of the setup of 1970. This was done because the setup of 2030 was projected based on changes to the setup from 2004 to 2014. Baseline data for the generation of these setups are Landsat 5, 7 and 8 images. Their band definitions are similar with only negligible differences (Vogelmann et al., 2016) and they all have the same resolution of 30 m. The 1970s setup is less suitable for comparison on subcatchment scale, since it was generated with pre-collection Level 1 60 m resolution data and conventional mosaicking (Näschen et al., 2018). The map from the 1970s is based on a decadal best pixel composite of images from different seasons and is therefore less consistent than the later maps, which are based on multi-seasonal multi-temporal metrics.

6.3. Results

6.3.1.Model Performances

A detailed overview of the model performance for the SWAT model is given by (Näschen et al., 2018). However, essential statistics on the model performance are presented in Table 6.5 and Table 6.6, referring to the equations stated in chapter 6.3.2.

Table 6.5 Summary of the quantitative model performance analysis for the calibration and validation period. R^2 is the coefficient of determination (Equation 1), *NSE* is the Nash–Sutcliffe efficiency (Equation 6.2) and *KGE* is the Kling-Gupta efficiency (Equation 6.3). A value of 1 indicates a perfect fit.

Simulation Period (Daily)	R^2	NSE	KGE
Calibration (1958–1965)	0.86	0.85	0.93
Validation (1966–1970)	0.80	0.80	0.89

The LCM performance is measured by the skill measure (Equation 6.7) and was satisfactory for both setups (Table 6.6).

Table 6.6 Skill measure (Equation 6.7) for both setups that modeled the transition of other LULC classes into cropland or into cropland-rice as a specific crop. Baseline data were observed transitions from 2004–2014, which were translated and extrapolated into LULC maps for the year 2030.

Transition	Skill measure
to cropland	0.69
to cropland-rice	0.77

6.3.2. Land Use Land Cover Change Scenarios

Figure 6.4 shows the result of the LCM for the year 2030. The maps show increasing density of agricultural activities at the fringe of the floodplain and an agricultural encroachment towards the river, whereas the central part of the floodplain is not converted. Other hot spots of change are the western parts of the catchment and the central northern parts, especially in Figure 6.4c. Figure 6.4a and 6.4c also show agricultural activities in the eastern parts along the Kilombero River.

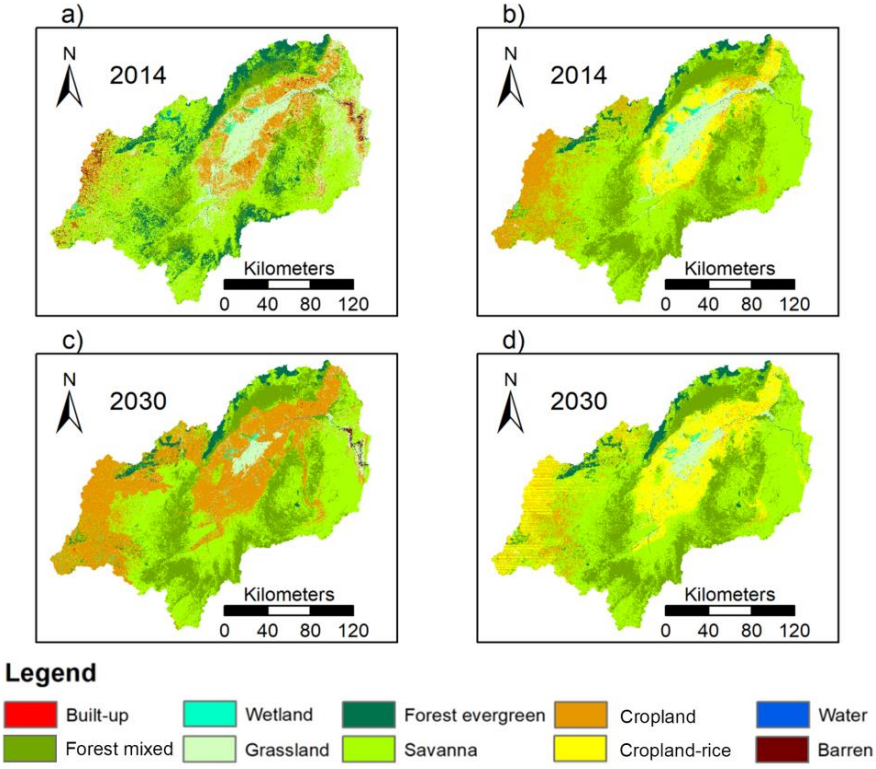

Figure 6.4 Land use and land cover classifications as modeled by the Land Change Modeler for the year 2030. For better comparison a) and b) show the setups for 2014 from Figure 6.2, c) displays the scenario based on the single cropland classification and d) illustrates the same scenario but distinguishes between cropland and cropland-rice land use class.

The percent share for all LULC types in the maps of Figure 6.2 and Figure 6.4 are displayed in Figure 6.5. The generic cropland setup distributions are shown on the left-hand side of Figure 6.5a to e and the maps with the differentiation of cropland and cropland-rice are displayed to the right-hand side of Figure 6.5f to j. The increasing share of cropland and cropland-rice classes from 2004 onwards for both

setups is noteworthy. The share of forest classes is quite stable, although there are fluctuations in between forest mixed and forest evergreen. The decreasing trend of savanna in the cropland-rice setup from 2004 is remarkable and more pronounced than in the cropland setup. However, the cropland setup generally has a higher share of grassland and a strongly declining share of grassland from 2004 onwards. Other classes are much less represented or disappear in the final HRU setup like the built-up class. However, the distribution of the HRU setup reflects the original LULC distribution well. The disappearance of the built-up class in the HRU setups can be attributed to the low share of residential areas (< 0.6%) in the baseline LULC setups from 1970 to 2014.

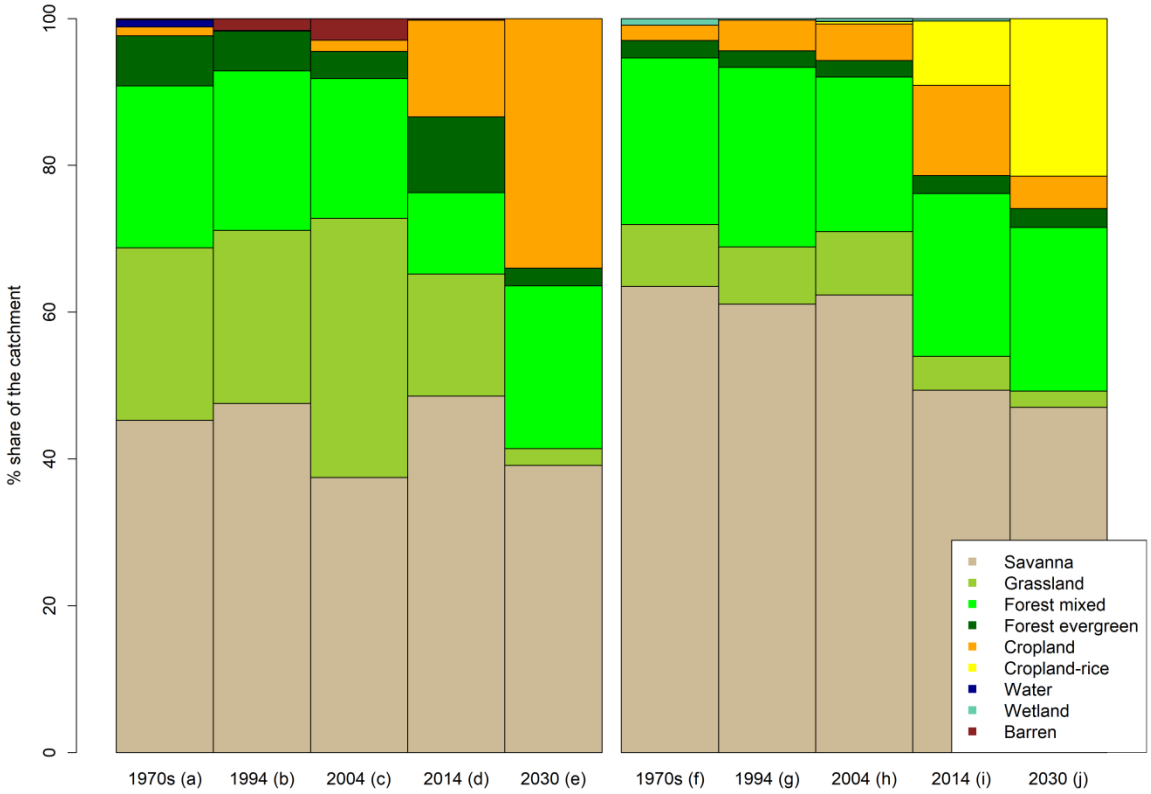

Figure 6.5 Observed and modeled (2030 (e and j)) share of the land use/land cover (LULC) classes within the Kilombero Catchment. (a) to (e) show the distribution from the 1970s to 2030 with a different classification method compared to (f) to (j). The built-up class dropped out in the final LULC distribution due to the low share of residential areas and the application of the HRU approach.

6.3.3.Impact of Land Use/Cover Changes on Water Resources

Figure 6.6a–b show that the overall annual discharge at the outlet is similar among all LULC setups. Nevertheless, a closer look at Figure 6.6c-d, which shows a zoom-in to the boxes, reveals differences between the two setups. On the one hand, the cropland setup (Figure 6.6c) shows an increasing trend for discharge from 1970 to 2030 with some fluctuations. These fluctuations are also reflected in fluctuations among the LULC classes in Figure 6.4. On the other hand, the setups that include rice

(Figure 6.6d) show a constantly decreasing trend of discharge at the outlet with an increasing share of rice (Figure 6.5).

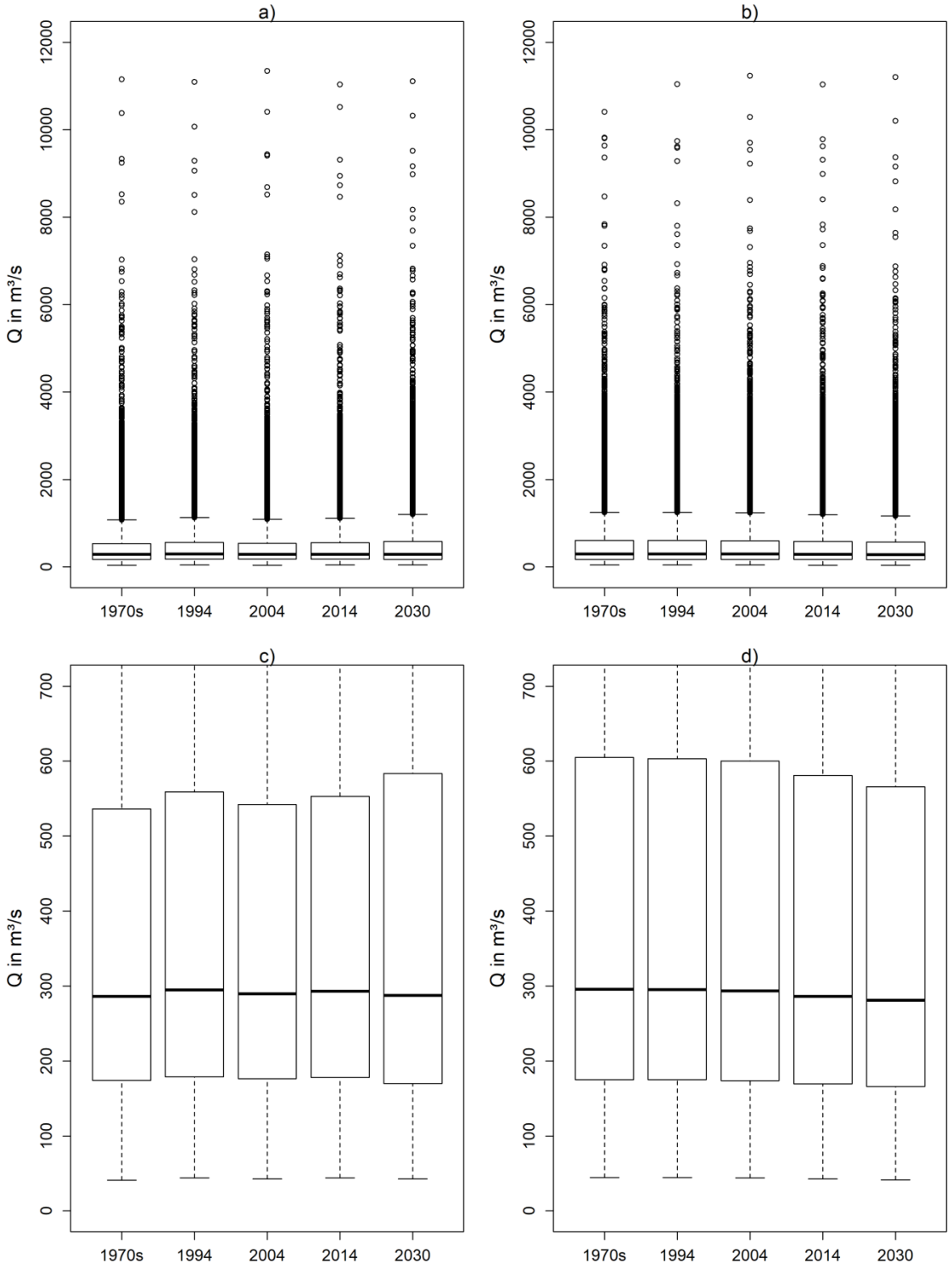

Figure 6.6 Box plots showing the annual discharge at the main outlet for the simulated period of 1958–2005. a) shows the discharge for the setups with cropland only and b) for the setup with the differentiation of cropland and cropland–rice. c) and d) show the very same information as a) and b), but zoom-in to the values of the boxes.

Figure 6.7 focuses on low flows (Figure 6.7a) and high flows (Figure 6.7b) for all setups. The general pattern for the low flows shows decreasing trends for the LULC setups including rice from the 1970s (Q90 of 119 m^3/s) to 2030 (Q90 of 112 m^3/s), which equals a drop of 6%. The cropland setups lack this trend, however the lowest Q90 value is again with the 2030 setup (114 m^3/s). The values for Q10 show an analogous picture for the cropland-rice setup, with decreasing trends from the 1970s setup (1430 m^3/s) to the 2030 setup (1320 m^3/s). The absolute changes (110 m^3/s) are more pronounced compared to the Q90 decrease, but the relative changes are comparable with 8%. The cropland setups show a different picture, with rather low absolute Q10 values from the 1970s (1118 m^3/s) up to 2014 (1169 m^3/s) and a sharp increase for the 2030 setup (1358 m^3/s), which equals an increase of 21% compared to the 1970s setup.

Figure 6.8 shows the discharge amount for return levels for all setups based on the GEV-GMLE analysis of 48 annual maximum values from the period of 1958 to 2005. The distribution is similar to the Q10 values presented in Figure 6.7b. The discharge of 2-year and 5-year return levels for the cropland setups increase from the 1970s setup (3260 m^3/s; 6310 m^3/s) to the 2030 setup (3566 m^3/s; 6595 m^3/s), whereas the cropland-rice setups show an opposing trend (1970s: 3655 m^3/s; 6663 m^3/s ; 2030: 3472 m^3/s; 6437 m^3/s). These trends are overcome by increasingly high return level values for both 2004 and 2014 setups. Furthermore, the relation of increasing return levels for the comparison of the 1970s setup and the 2030 setup with cropland is inverted from the 25-year return level onwards.

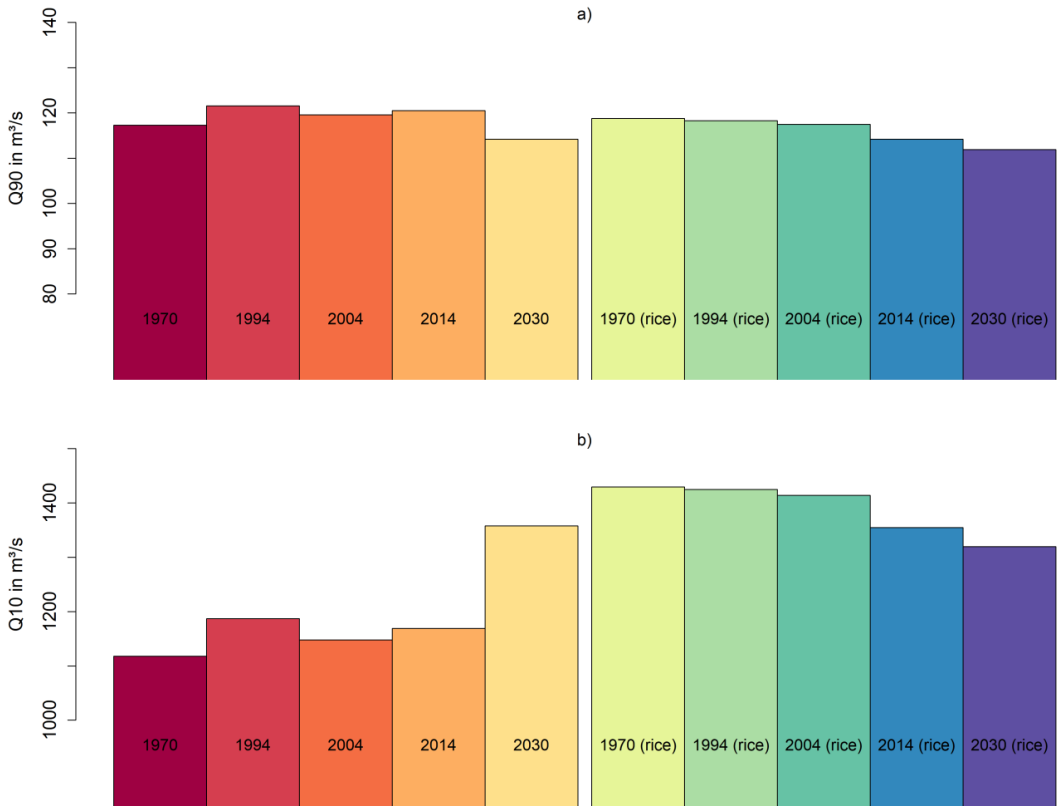

Figure 6.7 Distribution of Q90 (a) and Q10 (b), representing the flow exceeded in 90% or 10% of the time for Q90 and Q10, respectively. The reddish columns on the left represent the setups with cropland, whereas the blueish columns on the right display the modeling results for the setup with cropland and cropland-rice differentiated. Data is based on simulations from the period 1958–2005 and all inputs except for the LULC maps are not modified.

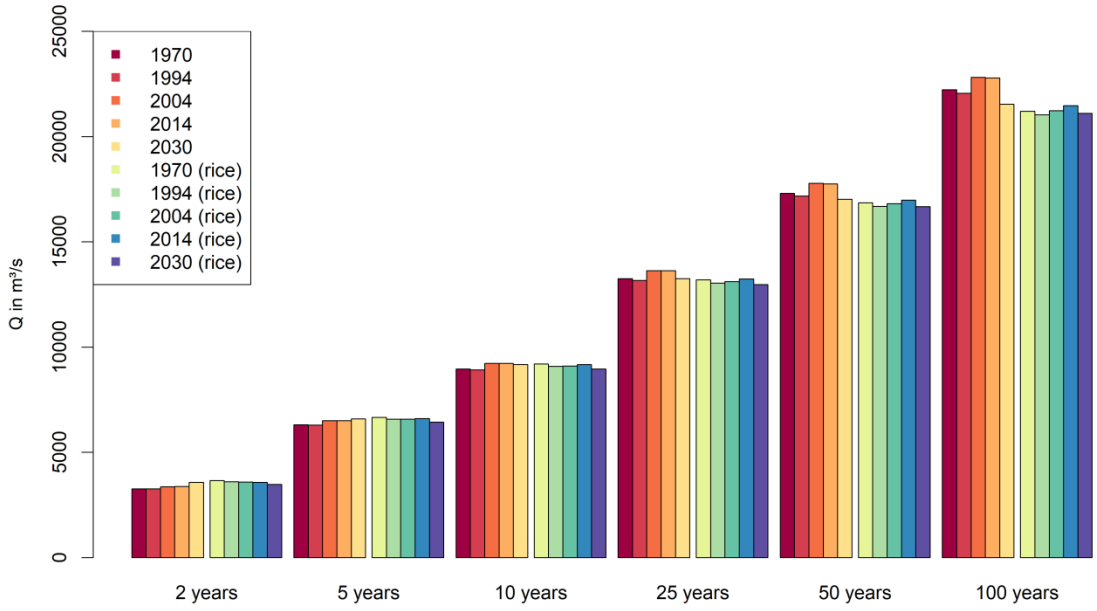

Figure 6.8 Return levels and respective discharge of flood events for all LULC setups. Return levels represent the discharge at the outlet for a 2-year, 5-year, 10-year, 25-year, 50-year, and 100-year event according to the generalized extreme value (GEV) model and the generalized maximum likelihood estimation (GMLE) method from the period of 1958 to 2005.

Figure 6.9 illustrates changes among LULC setups for selected water balance components, namely surface runoff, overall water yield and evapotranspiration on a monthly timescale for the whole simulation period from 1958–2005. All changes represent differences among the presented LULC setup and the basic setup from the 1970s. Hereby, all cropland setups (Figure 6.9a–d) are compared to the cropland 1970s setup and all cropland and cropland-rice setups (Figure 6.9e–h) are compared to the cropland and cropland-rice setup from the 1970s. Overall, the monthly changes are rather small, although water yield increases in the 2030 setup (Figure 6.9d) by an average of 22.3 mm per year in April, which equals 28.2% of the overall water yield for that month. Furthermore, evapotranspiration decreases nearly the whole year round (except for May and June) in that setup by up to 8.2 mm in average for the month of December, which equals 8.5% of the average evapotranspiration in that month. A different picture is shown for the rice scenarios (Figure 6.9e–h), where overall water yield decreases in the 2014 (Figure 6.9g) and 2030 (Figure 6.9h) setup for April and May. However, the average decrease ranges from 5.4 mm (5.1%; May, 2014 setup) to 8.1 mm (7.6%; May, 2030 setup) and is therefore less pronounced compared to the increases in the 2030 cropland setup.

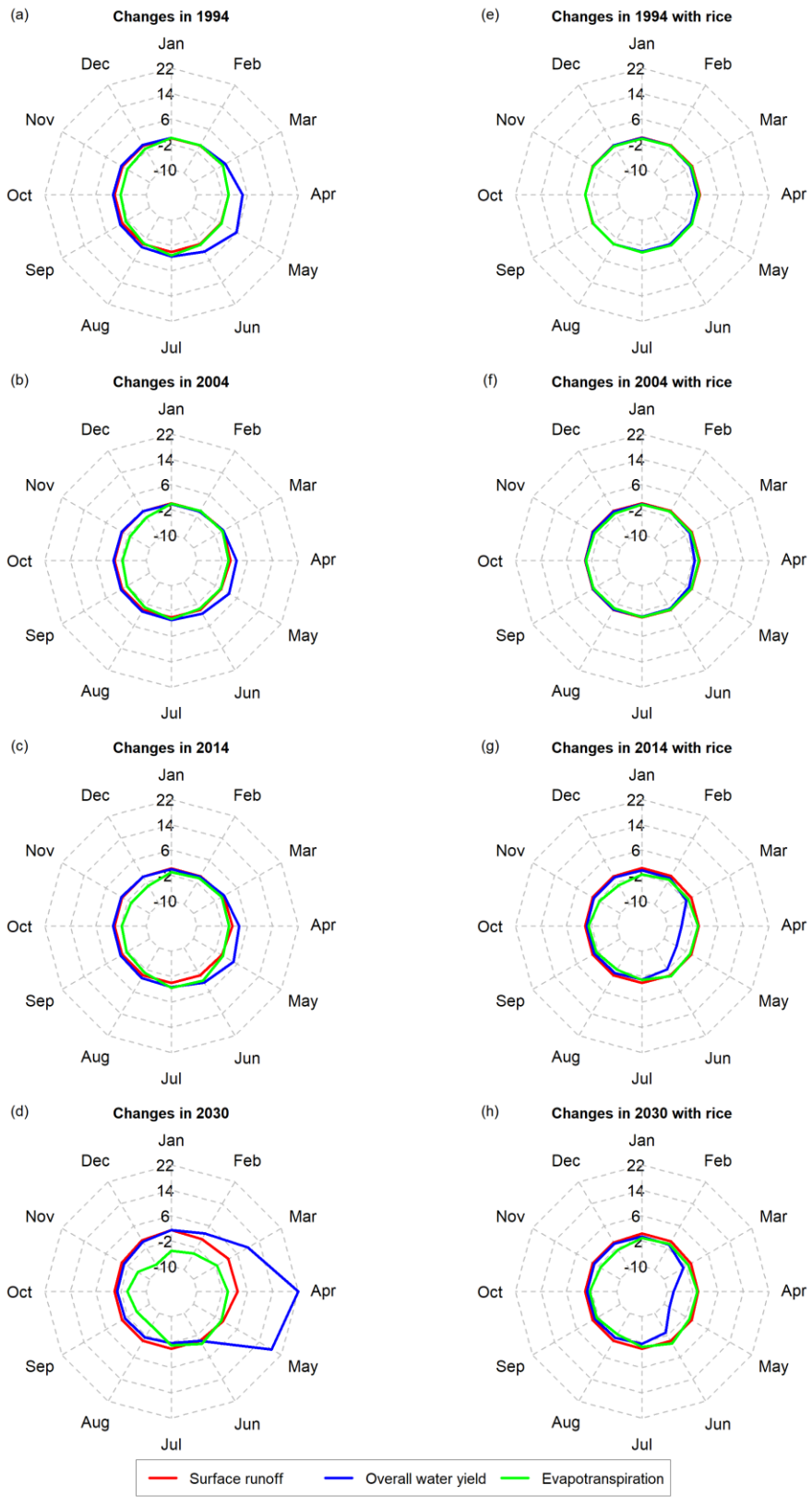

Figure 6.9 Average shifts (in mm) in selected water balance components for the entire catchment within the period from 1958 to 2005 compared to the 1970s setup with cropland (a-d), or cropland-rice (e-h). All inputs except for the LULC maps are not modified.

Variations of surface runoff, overall water yield, and evapotranspiration on subcatchment scale are shown in Figure 6.10. Figure 6.10(a–c) compares the annual water balance components' averages from the 2030 setup with the 1994 setup with cropland and Figure 6.10(d–f) compares the same with the cropland-rice setups, respectively. An increase of surface runoff and overall water yield is apparent (Figure 6.10a–b). The northeastern parts, and also the floodplain show increasing surface runoff values of 10 to 20 mm and increase in total water yield of more than 50 mm. Hence, evapotranspiration is decreasing in nearly all subcatchments, especially in the mountainous northwestern parts. The differences in the rice setups (Figure 6.10d–f) from 1994 to 2030 show a different pattern. Changes in surface runoff are less pronounced and most subcatchments show a slightly decreasing trend. Overall water yield is decreasing in many subcatchments by 50 mm and more, especially in the fringe of the floodplain, but also in some of the northwestern mountainous subcatchments. Furthermore, evapotranspiration is decreasing in many subcatchments, especially on the fringe of the floodplain and the western parts. However, slightly increasing trends of evapotranspiration are apparent e.g., in the northeastern subcatchments.

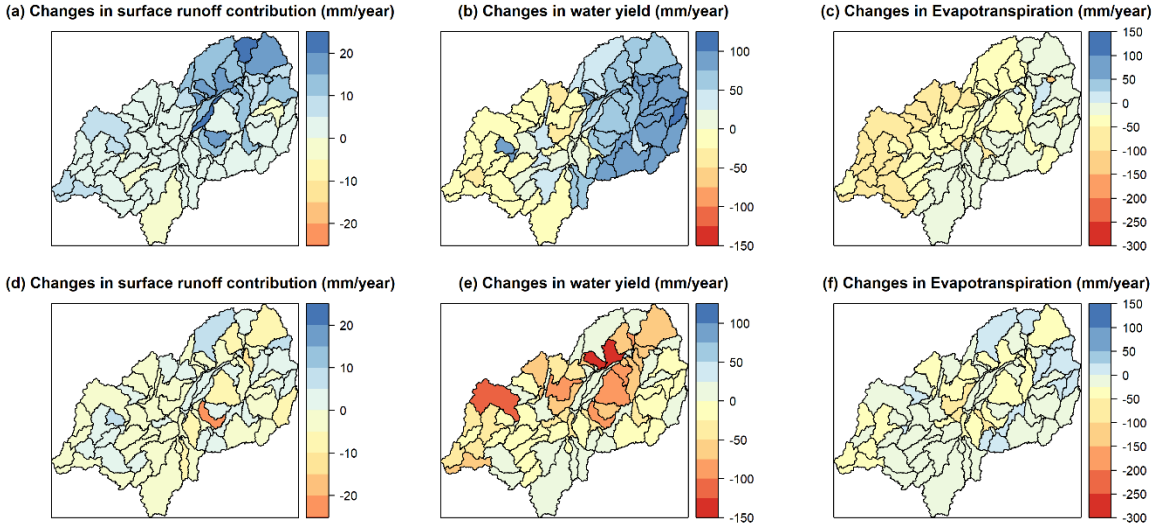

Figure 6.10 Average annual changes in selected water balance components on subcatchment scale. a–c) compares the cropland LULC maps of 1994 and 2030, while (d–f) compares the cropland-rice LULC maps of 1994 and 2030 on. All model runs used identic climate data from 1958 to 2005 and differences in water balance components refer only to changes in LULC.

6.3.4.Combined Effect of Land Use/Cover And Climate Change on Water Resources

The combined effect of LULCC and climate change on water resources is illustrated for a combination of distinctive wet and dry model combinations in Figure 6.11 and 6.12 in order to demonstrate the uncertainty and the span of possible future conditions according to the model combinations and their impact on water resources. Figure 6.11 displays the Q90 (Figure 6.11a) and Q10 (Figure 6.11b) modeling results for both LULC setups of 1994 and 2030, all driven by the climatic forcing of the "dry model" and the "wet model". Apparently, the span for Q10 and Q90 of the "dry model" and the "wet model" is more

pronounced in comparison to the differences among the LULC setups. The range of Q90 straddles from 101 m^3/s (2030, rice, “dry model”) to 162 m^3/s (1994, cropland, “wet model”). For Q10 the results span from 1310 m^3/s (1994, cropland, “dry model”) to 2416 m^3/s (1994, cropland-rice, “wet model”). These discrepancies represent a relative growth of 61% for Q90 and 84% for Q10, indicating a huge uncertainty for the future low flows and high flows with regard to a changing climate and LULCC. Furthermore, it is important to mention that all combined LULC and climate change scenarios for Q10 Figure 6.11b) show increasing values for Q10 compared to the LULC scenarios (Figure 6.7b), whereas Q90 values (Figure 6.7a) are lower for the dry climate scenario and higher for the wet climate scenario (Figure 6.11a).

Figure 6.12 illustrates a spatially more explicit dimension for the subcatchment scale by visualizing the deviations in surface runoff (Figure 6.12a), overall water yield (Figure 6.12b) and evapotranspiration (Figure 6.12c) between the cropland model setup of 1994 driven by the “dry model” and the cropland setup of 2030 driven by the “wet model”. The surface runoff component increases by more than 100 mm for some of the subcatchments in the annual average for the whole catchment and particularly for some of the subcatchments in the (north-) eastern part of the catchment. Unlike the western parts, which are mostly within the range of 0–20 mm increase. The pattern of the overall water yield is alike; however, it has another scale straddling from slightly decreasing trends in the western subcatchments to increasing values of nearly 600 mm in the eastern subcatchments. Water yield deviations increase towards the eastern parts, except for the floodplain, where this pattern is not as distinctive as for the surrounding mountainous areas. Evapotranspiration (Figure 6.12c) increases as well in the range of 100–200 mm for nearly all subcatchments and particularly for the northeastern floodplain and its fringe.

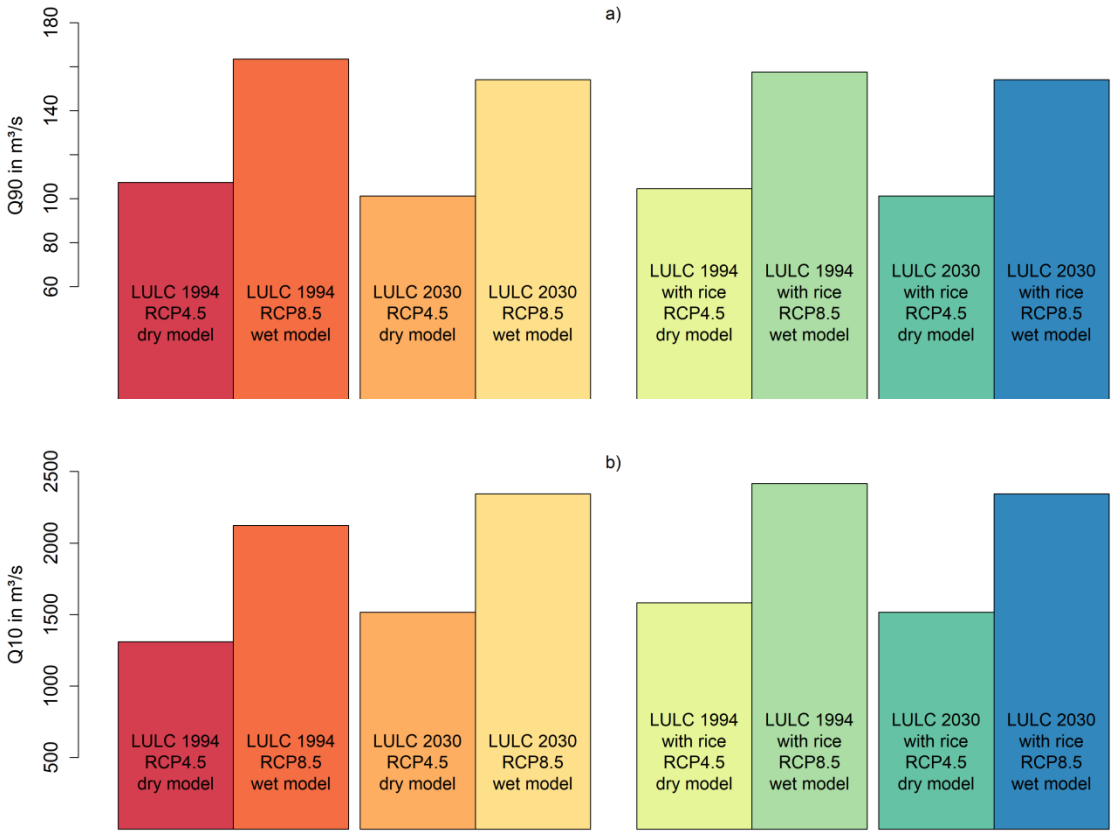

Figure 6.11 Bar plots showing the distribution of Q90 (a) and Q10 (b), representing the flow exceeded in 90% or 10% of the time for Q90 and Q10, respectively. The LULC setups of 1994 (cropland and cropland-rice) as well as the scenarios for 2030 (cropland and cropland-rice) are simulated with climate data of the period from 2010 to 2060 with the "dry" and the "wet" GCM-RCM model (Table 6.3).

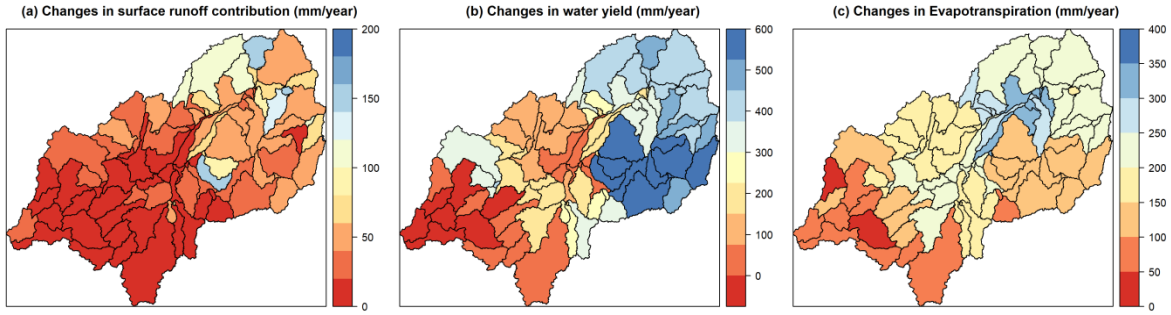

Figure 6.12 Average annual shifts in selected water balance components on subcatchment scale with a comparison of the LULC setup of 1994 and 2030 (both without consideration of rice). The LULC 1994 is using the "dry model" (Table 6.3) climatic data with the RCP 4.5 scenario as input, whereas the 2030 LULC setup is driven by the "wet model" (Table 6.3) and the RCP 8.5 scenario data. All model runs were performed with climate data for the period of 2010 to 2060. Differences in water balance components refer to changes in both LULC and climate change.

6.4. Discussion

6.4.1.Land Use Change Scenarios

This study focuses on changes from all LULC classes except built-up areas to either cropland or cropland-rice, although local studies in the catchment indicate the problem of deforestation as well (Johansson and Abdi, 2019). However, deforestation is not as pronounced for the entire catchment (Figure 6.4) (Leemhuis et al., 2017) and therefore only changes into agricultural LULC classes were explicitly modeled. Nevertheless, difficulties in the classification scheme among the different forest classes and open forest areas or savanna were apparent (Näschen et al., 2018). Natural classes in particular were prone to errors due to gradual differences in reflectance characteristics, although post-classification comparisons were mostly consistent and conform to historical maps. Yet, conversion into cropland was the focal LULCC and less prone to errors due to strong spectral changes (Näschen et al., 2018). Skill measures (Table 6.6) for both transitions to cropland or rice were satisfactory, nevertheless the exact distribution of LULC pixels in the 2030 scenarios should be interpreted carefully for several reasons. Firstly, the computed rate of change from 2004 to 2014 was transferred linearly until 2030. Secondly, this analyzed pattern is based on explanatory spatial factors like the altitude above sea level. Therefore, a saturation effect might occur due to limited space, e.g., in the wetland fringes surrounding the floodplain. The wetland fringes are nearly completely used as agricultural land in the setups of 2014 and 2030 (Figure 6.4). A growing demand for agricultural land in this area is a source of uncertainty, because the interaction with the enclosing landscape, and therefore agriculturally less suitable areas like upland forests or flood-prone areas, is a different process compared to the observed LULCC in the wetland fringes. Thirdly, alterations in demographic growth including natural birth rates and immigration are not included in this linear approach. However, the impacts of demographic growth on LULCC are indirectly integrated due to the transfer of observed changes from 2004 to 2014 to the year 2030. The demographic growth accelerated in the 90s and after 2000 due to the migration of mainly pastoralists into the valley (Msofe et al., 2019) and correlates with the growing share of cropland in the valley, which was increasingly converted from grassland and savanna into cropland to feed the growing population. We use these conversions into cropland as a proxy for demographic growth, due to the stagnating trends in rice yields in the area (Duvail and Hamerlynck, 2007; Kwesiga et al., 2019), although conversions into cropland might also be affected by investors from outside the valley and other factors. Lastly, the influence of politics and the economy is not included, but might change the LULC drastically by setting incentives for agricultural activities e.g., the SAGCOT initiative (Environmental Resources Management, 2013), changing the allocation or status of conservation areas or by developing the infrastructure. Furthermore, the spatial structure of the SWAT model and its HRU approach, which summarizes results for HRUs and neglects interactions among neighboring grid-cells within a subcatchment (Rathjens and Oppelt, 2012), has structural limitations compared to a fully distributed grid-based solution. However, SWAT is a well proven tool to determine impacts on water resources due to LULCC (Cornelissen et al., 2013; Martinez-Martinez et al., 2014; Niraula et al., 2015). Analysis of impacts on water resources on grid-cell scale is not the goal of this study, but rather to identify general trends of LULCC and their impact on specific areas prone to these LULCC in order to assist the local water resource management authorities to enable a sustainable use of the available water resources. Hence, a business as usual

scenario until 2030 was developed using the LCM and all analyses with regard to water resources were performed from catchment to the subcatchment scale.

The general distribution and spread of the modeled cropland/rice production area is reasonable. The hot spot of change for both scenarios is the fringe of the wetland. However, the center of the wetland is not transformed to agricultural fields on both setups, which is also reasonable due to the extended flooding and the threat to lose the harvest (Gabiri et al., 2018). Other areas of agricultural expansion are the western parts and the central northern parts, near the cities of Makambako and Njombe, and the main roads A104 and B4 (Figure 6.1). Although some rice is grown in the Njombe region, it is mainly an important production region for maize, Irish potato, tea, and flowers and therefore it is rather unlikely to dispense the income within these agriculturally suitable value chains for less suitable large scale rice production in this region. The southern part, which expanded from 2014 to the 2030 setups, was already confirmed by local experts in a participatory mapping exercise as a recent rice growing area in the framework of a stakeholder workshop in February 2019. The transformation of cropland to cropland-rice in the very northeastern parts is unlikely due to the existing and growing sugarcane fields of the Kilombero Sugar Company.

6.4.2.Land Use/Cover and Climate Change Impact Assessment on Water Resources

The impact of LULCC on average stream discharge seems to be negligible at the first glance (Figure 6.5). This is also in line with a former study on historical LULCC on cropland (Näschen et al., 2018), and was also observed in another catchment in Tanzania (Wambura et al., 2018) as well as in small catchments in West Africa with conversion of savanna into rice (Danvi et al., 2018). One important factor for the low impact at the main outlet is also the stable share and distribution of forest classes in the upland of the catchment (Figure 6.2, 6.4, 6.5 and (Näschen et al., 2018)). Yet, LULCC are still seen as the main driver for decreasing streamflow in Eastern and Southern Africa (Schäfer et al., 2015). These minor changes in streamflow at the main outlet due to LULCC detected in this study can be attributed to concealing effects for large catchments (Wagner et al., 2013) like the Kilombero Catchment. Therefore, it is important to analyze the water balance on several spatio-temporal scales like the subcatchment scale or monthly averages and also analyze changes in low- or high-flow patterns.

The Q90 as representative index for the low flows decreases for both scenarios – the cropland and the cropland-rice scenarios – by 6% or 8%, respectively, from 1970s to 2030. An environmental flow assessment found several parts of the catchment to be differently vulnerable to decreases in mean annual flows (CDM Smith, 2016). The upstream margin of the floodplain with a monthly recommended flow of 82.3% of the mean annual flow was defined as highly vulnerable concerning environmental flows (CDM Smith, 2016). Therefore, these decreasing trends of 6% and 8% of the Q90 at the outlet should be considered carefully for further analyses. Stakeholder interviews and discussions with local farmers revealed, that perennial tributaries of the Kilombero in the northeastern part of the catchment turned into seasonal tributaries in the last decades. This change is attributed to deforestation activities and expansion of cropland, and therefore needs to be taken seriously to maintain the socio-ecological system that depends on continuous availability of water resources and the transported sediments and attached nutrients (Johansson and Abdi, 2019; Wilson et al., 2017).

High flows are more distinct in the rice scenarios (Figure 6.6), although they decrease with an increasing share of rice (Figure 6.7b), especially in the months of April and May (Figure 6.9g–h). The

general differences among the cropland and cropland-rice scenarios arise from their different shares of all LULC classes (Figure 6.5). The rice setups have a lower share of forest classes for example and therefore a comparison that aims to determine the impact of a growing agricultural share should be done separately within the cropland-rice or cropland setups. Though, the decreasing high flows within the rice scenarios (Figure 6.6) can be attributed to the high water requirements of the rice plants (Duku et al., 2016).

The cropland scenario for 2030 (Figure 6.7b) displays a strong increase in the discharge amount of Q10, which is distributed to the months of March to May (Figure 6.9d). This might lead to aggravated flooding events, which could either endanger the farmer's harvest (Duvail and Hamerlynck, 2007; Kwesiga et al., 2019) their lives, critical infrastructure and their livelihood (National Bureau of Statistics. United Republic of Tanzania, 2017). Especially newly promoted, high yielding, but low growing improved varieties such as like SARO5 (TXD 306) might be negatively affected by these changes. These strong increases of water yield are accompanied by slightly decreasing evapotranspiration throughout the year (Figure 6.9d). These patterns with regard to LULCC and Q10 are aggravated by the effects of climate change. The combined effect of climate change and LULCC inherits an increase of 84% between the two scenarios comparing the lowest (LULC 1994, RCP4.5, dry model) and the highest (LULC 2030, RCP8.5, wet model) value for Q10 shown in Figure 6.11b. The effect of climate change outperforms the impact of LULCC, yet the contribution of LULCC to changes in Q10 is still substantial (Figure 6.7b). It is necessary to add that changes in management practices are not included in these LULCC, but several practices, like the establishment of year-round irrigation schedules, will further affect water resources (Reshmidevi et al., 2018; Reshmidevi and Nagesh Kumar, 2014). Furthermore, the uncertainty of the climate change signal, represented by the huge span in the GCM-RCM model runs (Näschen et al., 2019) (Figure 6.11), is much higher than in LULCC scenarios. While climate change models show diverging trends of more dry or more wet conditions and changes in the seasonality, the impact of conversion from natural LULC into agricultural utilized fields is more explicit (Danvi et al., 2018; Op de Hipt, 2018; Yira et al., 2016), although it still depends on the specific crops grown. Nevertheless, intensification of precipitation might foster groundwater recharge and therefore access to renewable water resources in the Kilombero Catchment as well as already described in other catchments in SSA (Cuthbert et al., 2019). This indicates a particular resilience to climate change and intensification of precipitation events. However, more observation-driven research is needed on the relation of surface water and groundwater resources on this topic (Cuthbert et al., 2019). Moreover, data availability on the hydrogeology of the Kilombero Catchment is still poor to be modeled precisely, although some data and a local conceptual model exists (Burghof, 2017; Burghof et al., 2017). Furthermore, the groundwater routines of the SWAT model are not sufficient for adequately modeling groundwater processes, because distributed parameters like the hydraulic conductivity and storage coefficients are disregarded in the linear reservoir approximations (Kim et al., 2008).

Overall, analyses on subcatchment scale (Figure 6.10, 6.12) show that the conversion into cropland leads to increasing surface runoff and overall water yield (Figure 6.10a–b), whereas a more diverse picture is shown for the rice setups (Figure 6.10d–e), due to the differences in LULC in the setups (Figure 6.5) and the aforementioned water demand of rice plants (Duku et al., 2016). Average annual evapotranspiration is decreasing in both agricultural setups in most of the subcatchments, especially where natural systems are converted into agricultural production zones, which is in line with other

studies from the tropics (Gabiri et al., 2019; Guzha et al., 2018; Yira et al., 2016). Still, there are studies that report increasing evapotranspiration due to conversion of forests to cropland (Mango et al., 2011). However, farming in the Kilombero Catchment is mainly done by low input rain-fed rice cultivation and only a few rice irrigation schemes do exist (Kashenge and Makoninde, 2017). Therefore, the rice setups were established using the default management plan from SWAT. A high input management setup would change the plant growth and consequently the evaporation of the plants (Danvi et al., 2018).

The scale dependency of hydrological processes and the spatio-temporal heterogeneity of water movement within the catchment are apparent by comparing the different characteristics of selected water balance components in the subcatchments (Figure 6.10, 6.12) and their monthly deviations for the entire catchment (Figure 6.9 and (Näschen et al., 2018)). The deviations that include the effects of climate change (Figure 6.12) are substantial, even though they compare the extreme situations concerning LULCC and climate change scenarios.

The manifold scenarios, inherited uncertainties and their implications on water resource management reveal the difficulties for local authorities and the need for further research in the area. The population in the catchment districts Kilombero and Ulanga has been and is currently increasing (National Bureau of Statistics. United Republic of Tanzania, 2012) and road infrastructure as well as the Stiegler's Gorge power station are being constructed. This will lead to further LULCC, and locally rapid deforestation has already been reported (Johansson and Abdi, 2019; Munishi-Kongo, 2013), consequently affecting the water balance (Yang et al., 2019). Forest protection against unregulated degradation is still problematic in Tanzania. There is a need to understand the social-ecological system to strengthen strategies, that ensure socio-economic benefits of local people, while preventing ecosystem degradation to allow a sustainable utilization and protection of the resource base (Rosa et al., 2018). The local scale and the understanding of the local communities that depend on the wetland resources and their adjacent mountain forests and savannas could be the key for the development of management policies in the Kilombero Catchment (Msofe, 2019). These could be for example the promotion of environmentally friendly sources of livelihood such as beekeeping, a sustainable forestry system accompanied by education on the socio-ecological system and improvements in the agricultural practices (Msofe et al., 2019). Still, migration into the valley and population growth are critical factors for the pressure on the ecological system (Johansson and Isgren, 2017; Msofe, 2019; Msofe et al., 2019). Further information on the flooding extent, timing and duration using a hydraulic model with regard to the LULCC and climate change scenarios should support to manage the floodplain under future conditions. Beyond that, there is still not sufficient data on water quality, especially with regard to the emerging use of fertilizers, herbicides, and pesticides (Msofe, 2019; Wilson et al., 2017).

6.5. Conclusions

The study shows different methods to develop LULC maps and how to utilize these methods for further LULC scenario development. Differences among these scenarios and their effects on water resources are shown. However, implications of LULCC and climate change impacts on various spatio-temporal scales are key aspects of this study. Results clearly show that it is not sufficient to analyze discharge only at the outlet in LULCC impact studies (Hrachowitz et al., 2013). It was shown that further analyses on different spatial scales and changes in low flows and high flow behavior are essential to

identify hot spots of change, obtain environmental flows and for flood protection. The scenario analysis shows a trend of decreasing low flows, especially until 2030 by 6% to 8%. These numbers should be taken seriously, as they represent only the catchment´s average, while several areas, e.g., the northwestern parts, show more pronounced declines in overall water yield and evapotranspiration. Since some rivers in the northwest that have already been subject to a shift from perennial to seasonal rivers management activities are crucial to maintaining and protecting the system. This study helps to identify areas that are essential for the maintenance of the social-ecological system with regard to water resources. However, these activities have to take part in collaboration with the involvement of local communities and might need the establishment of local management authorities to enable a sustainable management of the catchment (Daconto et al., 2018). Potential management activities could contain the protection of natural swamps within the valley or upland forests in combination with payment for ecosystem services to incentivize these protection zones for local communities. Other options include the exploration of more environmental friendly activities such as beekeeping or more sustainable forestry systems (Msofe et al., 2019). Additionally, information with regard to the endangered ecosystems and their importance for the farmer's fields should be communicated e.g., through extension officers to create mutual acceptance for these protection zones.

Conversely, high flows are more pronounced for the overall catchment with an increase of Q10 by up to 21% in 2030 compared to the 1970s due to LULCC only. These increases are associated with the months of March to May (the rainy season) and are remarkable for the town of Ifakara - a highly populated area with many small scale farmers, that frequently uses high yielding, but low growing rice varieties. Hence, the livelihood of the population in that area is at risk due to these LULCC, which are particularly fostered by climate change. Therefore, the retention capacities of natural systems like forests or swamps are indispensable for the maintenance of the social-ecological system.

Further analysis with specific crop and rice management parameterizations are recommended for more accurate projections. These projections should be utilized to run a hydraulic model for the flood areas in order to assist sustainable management with regard to water resources. The results of this study indicate a strong impact of changing climate on the water cycle, whereas the conversion of predominantly savanna and grassland to agricultural areas is less dramatic, yet remains important at the subcatchment scale.

Author Contributions: Conceptualization, K.N. and B.D.; formal analysis, K.N., S.S., F.T.; writing—original draft preparation, K.N.; writing—review and editing, K.N., B.D., M.E., B.H., S.S., F.T.;

Funding: This study was supported through funding from the German Federal Ministry of Education and Research (FKZ: 031A250A-H); German Federal Ministry for Economic Cooperation and Development under the GlobE: Wetlands in East Africa project; Deutsche Forschungsgemeinschaft (DFG) under the CRC/ Transregio 228: Future Rural Africa: Future-making and social-ecological transformation (Project number: 328966760).

Acknowledgments: The authors would like to thank Dr. Constanze Leemhuis for extensive academic exchange and administrative support. The authors also thank Larisa Seregina and Dr. Roderick van der Linden for downloading and bias-correction of the climate data. Additionally, the authors would like to thank Rufiji Basin Water Board for data sharing and assistance in the field and Prof. Salome Misana and Dr. Theobald Theodory for their administrative guidance and logistic assistance.

Conflicts of Interest: The authors declare no conflict of interest. The founding sponsors had no role in the design of the study; in the collection, analyses, or interpretation of data; in the writing of the manuscript, and in the decision to publish the results.

7. General conclusion

The major challenges for water resource management in the area, which are presented in the general introduction, have been addressed in this study on the Kilombero Catchment in Tanzania. The distribution of water resources, a central part of food security management, was presented on several spatio-temporal scales and for several scenarios that are relevant to local stakeholders. The interaction and dependence of the wetland system to the uplands was presented clearly for the catchment. In depth discussions and conclusions on these aspects are presented in the respective chapter 4, 5 and 6. However, a summary with regard to the research questions from the general introduction is provided in the following section, followed by the embedment in the broader context, the limitations of this study and an outlook.

7.1. Research questions and objectives

(i) How do the wetland and the catchment interact and what are the major hydrological processes?

A data base for the catchment was established in a first step to get a better understanding of the catchment's hydrology. Suitable data that fits to the mesoscale catchment were identified, either from local authorities, if possible, or otherwise from freely available global datasets. Additionally, climate data were bias-corrected and a new LULC classification with 30 m and 60 m resolution was developed. These data were utilized to set up, calibrate and validate a SWAT model based on historic discharge data. The setup of the model was successful and therefore a semi-distributed hydrological model was available to analyze the wetland-catchment interaction and the dominant hydrological processes. It was shown, that year-round base flow contribution from the uplands into the wetland is the dominant hydrological process that also preserves the wetland system and shows its dependence on the natural upland system. A first analysis of historic LULC maps from the 1970s to 2014 illustrated the scale dependency of hydrological processes in the catchment. The response on historical LULCC at the outlet of the catchment was negligible, whereas an analysis on subcatchment scale clearly showed shifts in water balance components due to LULCC. The study serves well as an example on how to utilize and combine local measurement data with freely available geodata and also how to use freely available geodata and to develop new products like LULC maps.

(ii) What are potential impacts of climate change on the hydrology of the catchment?

To answer this question six GCM-RCM model combinations from CORDEX Africa were chosen and later on corrected for bias based on local rainfall measurements and ERA-Interim reanalysis temperature data. At a first step the climate signal of the six model combinations was investigated for two RCP scenarios. The temperature showed a clear trend towards higher temperature throughout all models, whereas the precipitation pattern was much more diverse and complex. In the next step these climate data were used as input for the SWAT model to evaluate the impact on the hydrology. These analyses concentrated on subcatchment to catchment scale and from daily to decadal analyses ranging from 1951 to 2060. A general trend towards an aggravation of the seasonality was apparent, especially with regard to high flows (increase up to 67.8%), while decreasing low flows were less pronounced. Additionally, a

shift of the flooding season from April to May from 2020 onwards is a common signal across all simulations. Especially the shift in time and the changing magnitude of the flood is an essential information with regard to the agricultural utilization of the wetland for flood recession agricultural practices as well as for the risk assessment of flood prone areas.

(iii) What is the impact of LULCC on the hydrology of the catchment and what are potential future impacts and how do they interact with climate change?

As a first step the LCM was used in order to analyze the historical patterns of change from two sets of LULC classification maps ranging from 1970s until 2014. These classifications arise from different methodologies and concentrate either on generic cropland or additionally incorporate rice as a specific crop due to the importance of rice for the catchment. The spatial trends and the explanatory factors (e.g., altitude, slope or distance to disturbance) for these changes were identified and potential LULC distributions for 2030 were developed. Furthermore, these LULC distributions were contextualized and evaluated in the framework of a workshop and expert interviews with local stakeholders. Subsequently, the SWAT model was utilized to simulate the impact of these LULCC on hydrology on several spatio-temporal scales. At the outlet of the catchment the low flow (Q90) decreased by up to 8%, which is mainly occurring in the rainy season and the rice setup scenario. On subcatchment scale these deviations are more pronounced and environmental flows could be endangered. High flows are generally increasing, especially in combination with climate change scenarios with Q10 aggravated by an increase of 84% at the outlet. Several subcatchments close to Ifakara, which represents the most populated area, show an even more pronounced rise in Q10. Another study by (Hounkpè et al., 2019) in West Africa showed that flood risk due to LULCC and conversion of natural vegetation to agricultural land was underestimated by SWAT compared to WaSIM. Therefore, it is crucial to maintain on the one hand environmental flows for specific areas and seasons, while on the other hand retention capacities of natural systems are crucial to protect the livelihood of downstream riparians and to enhance the management of the flood recession agriculture. Potential hot spots of LULCC were identified like the fringe of the wetland and the western part of the catchment Also subcatchments that are susceptible to changes in hydrology (e.g., the area close to Ifakara) were identified by the subcatchment scale analysis.

7.2. Embedding in a broader context

This study contributes to water resource management in the Kilombero Catchment but also assists water resource management and water-related issues on several scales reaching from the catchment scale (i) to the country scale (ii) and is also applicable to the regional and continental scale (iii).

(i) Detailed and distributed information for the understanding of the hydrological system on the catchment level are presented, as well as an impact assessment of global change impacts on the catchment.

(ii) The results of the study might assist to plan for water resources beyond the Kilombero Catchment itself. The Kilombero River contributes the largest share of water to the Rufiji River, the largest river system of the country. The knowledge on water quantities that are leaving the catchment is on the one hand essential for dam management, power generation and therefore the recently increasingly promoted industrialization of the

country (Magufuli, 2015). On the other hand knowledge on water resources and the accompanied agricultural production is crucial for food security of the country with the Kilombero Catchment as one of the most productive rice producing areas in the region. In summary, knowledge on water resources is the connecting link among two of the most important subjects in the country that are agricultural production and the accompanied food security as well as industrialization.

Furthermore, water from the Kilombero River contributes to several unique ecosystems in the catchment, but also to downstream ecosystems that are internationally recognized for their high biodiversity and their endemic species (e.g., Selous Game Reserve). These systems serve beyond their intrinsic value as important factors to the tourism value chain and highly depend on water resources from the Kilombero Catchment. Therefore, quantitative analyses of the recent situation, but also for conditions under global change are essential to manage and preserve these ecosystems. A flexible approach for effective integral wetland-catchment conservation management was recently published by (Reis et al., 2019), which deals with the Amazon River basin and could serve as an example for further planning.

(iii) The framework provided here might also assist to make better informed management decisions with regard to water resources in other data-scarce catchments. The approach presented in this study is applicable to numerous catchments in SSA and beyond - if other, freely available precipitation products are utilized and bias-corrected as presented in the methodology of this manuscript. There are several products available to fill the gap of measured precipitation data e.g., CHIRPS[1] (1981-present) (Funk et al., 2015b), CMORPH[1] (1998-present) (Joyce et al., 2004), TAMSAT[1] (1983-present) (Tarnavsky et al., 2014) or TRMM[1] (1998-2015) (Huffman et al., 2007). An overview on the evaluation of precipitation products for Western Africa is provided by (Poméon et al., 2017). The interdisciplinary modeling framework of this study comprising methodologies from hydrology, meteorology and remote sensing allows to adequately represent a catchment's hydrology for historical, recent and future conditions. The bottleneck in hydrological modelling usually is the availability of discharge data, however the Global Runoff Data Base (GRDB) provides a database of more than 9,500 gauging stations worldwide. Many of these data sets from GRDB stop at 1990 or even before, which is not an issue if the users follow the approach presented on the LULC classification that allows to setup a hydrological model back until 1970. Following the approach presented in this manuscript it is possible to overcome data scarcity issues and utilize a mixture of available local measurements and freely available geodata. However, for smaller catchments it is important to use adequate data e.g. to represent the heterogeneity of soils also on a smaller scale. Therefore, the approach presented here is mainly feasible for meso and large scale catchments.

[1] See chapter VII List of Abbreviations for the full name

7.3. Research limitations

Nevertheless, this study still has some limitations that are within and beyond the common modeling uncertainties described by (Abbaspour et al., 2007) as "processes unknown to the modeler, processes not captured by the model and simplification of the processes by the model." Processes that are not fully captured by the SWAT model are for example the routing routines from HRUs within and to the next subcatchment, because the spatial allocation within a subcatchment is not considered by the model. A grid-based approach is available (Rathjens and Oppelt, 2012), but computationally not efficient for such a huge catchment. Furthermore, the plant growth parameters were taken from the SWAT database, because no parameters for the local varieties were available. An important issue with regard to hydrological modeling, especially in SSA, is the lack of groundwater data and the simple linear approaches for groundwater processes. However, until now hydrological modeling is the only option to quantitatively assess (ground)water resources in a cost efficient and comprehensive way in the region. Indeed, one of the reasons for choosing the SWAT model was the more simplistic groundwater approach that is used by the model, compared to other (ground)water models. The study tried to keep the groundwater model simple due to the lack of data, without losing spatial heterogeneity where it could be reflected (e.g., land use/land cover, topography etc.). Nevertheless, neglecting groundwater processes was not an option, due to the importance of groundwater processes reflected in the available conceptual model for the northeastern part of the catchment (Burghof et al., 2017). Additionally, the modeled water balance components were compared to the work of (Gabiri et al., 2018) and discharge was calibrated and validated to a gauging station downstream, which also integrates the features of the slow contribution of groundwater.

With regard to the scenario simulations presented in Chapter 5 clearly shows the inherent uncertainties with regard to climate change scenarios. Although the signal for temperature development is homogenous among the six model combinations, there are huge differences among the GCM-RCM combinations with regard to precipitation. Precise rainfall data as input for hydrological modeling in tropical regions is in any case a complicated issue due to the small-scale and patchy convectional rainfall events that are very difficult to represent accurately. Furthermore, it has to be considered, that SWAT does not model the evolution of the soil profile accurately e.g., the effect of soil erosion is not considered and could have huge impacts especially with regard to increasing surface runoff and aggravated soil erosion processes. Tipping points are another source of uncertainty. Following the principle of uniformitarianism potential tipping points or changes in the systems behavior that are not reflected in the modeling process, might be missed-out. This might include teleconnections and abrupt changes in the climate system, which are not covered by the GCM-RCM combinations in this study, feedbacks in the social-ecological system or water-related political decisions with extensive consequences. Therefore LULCC were modeled only until 2030 and until 2060 for climate change scenarios, as technological developments or other disruptures might affect these scenarios heavily and in unforeseen ways. Nevertheless, it is important for stakeholders to have scenario simulations available in order to plan for realistic future conditions, while considering intervention scenarios.

7.4. Outlook

The water-related perspectives of the Kilombero Catchment are coupled to several steering factors. One important aspect is the political agenda, that changes more and more from the „Kilimo Kwanza“ (Agriculture first) philosophy of the former President Jakaya Mrisho Kikwete to a more industrialization focused agenda of President John Pombe Magufuli. The overall consequences for the catchment, it´s residents and ecosystems are difficult to predict from the hydrological perspective alone. However, this study already gives valuable insights with regard to water resources. Interestingly, a review of (Jätzold and Baum, 1968) describes the development issues of the Kilombero Valley very similar to recent studies. They state, that the valley has been praised for its fertility, although it´s potential has not been properly used so far. This statement is very similar to those of recent stakeholders e.g., the SAGCOT initiative (Environmental Resources Management, 2013). An important pillar to gain acceptance for management plans is a broad acceptance across disciplines. One way to enhance acceptance and the role of local stakeholders, is collaborative modelling (Evers et al., 2012). The integration of local stakeholders in the modelling process in a next step could sharpen the model results by increased integrative and holistic thinking. This holistic thinking might be supported by the integration or coupling of models from other disciplines. One solution could be the coupling of the hydrological model with an agent-based economic model (Gebrekidan, unpublished) in order to simulate the behavior of local actors (here: farmers) with regard to their management practices. Actors will adapt their management practices with changing hydrological conditions and this will influence the hydrology vice versa, resulting in a feedback loop that hasn´t been modeled explicitly so far. Furthermore, the impact of changes in hydrology will affect the pattern of flooding, which will have a huge impact on local farming practices and residents. Examples for the coupling of 1D hydrodynamic and 2D hydrological models in the flood risk analysis do exist (Falter, 2016; Komi et al., 2017; Teng et al., 2017). However, data availability, especially with regard to the DEM and the representation of the river cross sections is often a bottleneck. Nevertheless, data on inundation extent from remote sensing applications are available, as well as water level data from piezometers (Gabiri et al., 2018). Additionally, more than 20 cross section measurements of the Kilombero River near the town of Ifakara were conducted by the author in order to determine the river depths. Next steps should therefore involve the application of a hydrodynamic model, the involvement of local stakeholders in collaborative modelling, and the coupling of the hydrological model with an agent-based economic model.

This study has shown, that the integration of remote sensing techniques in combination with hydrologic modeling allows to utilize historic discharge measurements for setting up a hydrologic model and also to simulate global change scenarios. However, the author emphasizes the need for in situ measurements and the importance of hydro-meteorological measurement networks. In situ measurements improve and guarantee the quality of remote sensing products and discharge data and additionally allow for small scale simulations and are therefore substantial part for all hydrological modeling activities.

8. References

Abbaspour, K.C., 2013. SWAT-CUP 2012. SWAT Calibration and Uncertainty Programs. Eawag, Dübendorf.

Abbaspour, K.C., Rouholahnejad, E., Vaghefi, S., Srinivasan, R., Yang, H., Kløve, B., 2015. A Continental-Scale Hydrology and Water Quality Model for Europe: Calibration and uncertainty of a high-resolution large-scale SWAT model. J. Hydrol. 524, 733–752. doi:10.1016/j.jhydrol.2015.03.027

Abbaspour, K.C., Yang, J., Maximov, I., Siber, R., Bogner, K., Mieleitner, J., Zobrist, J., Srinivasan, R., 2007. Modelling hydrology and water quality in the pre-alpine/alpine Thur watershed using SWAT. J. Hydrol. 333, 413–430. doi:10.1016/j.jhydrol.2006.09.014

Adhikari, S., Southworth, J., Adhikari, S., Southworth, J., 2012. Simulating Forest Cover Changes of Bannerghatta National Park Based on a CA-Markov Model: A Remote Sensing Approach. Remote Sens. 4, 3215–3243. doi:10.3390/rs4103215

Adjei, K.A., Ren, L., Appiah-adjei, E.K., Odai, S.N., 2014. Application of satellite-derived rainfall for hydrological modelling in the data-scarce Black Volta trans-boundary basin. Hydrol. Res. 1–15. doi:10.2166/nh.2014.111

Alemayehu, T., van Griensven, A., Bauwens, W., 2017. Improved SWAT vegetation growth module for tropical ecosystem. Hydrol. Earth Syst. Sci. Discuss. 21, 4449–4467. doi:10.5194/hess-2017-104

Amler, E., Schmidt, M., Menz, G., 2015. Definitions and Mapping of East African Wetlands: A Review. Remote Sens. 7, 5256–5282. doi:10.3390/rs70505256

Anand, J., Gosain, A.K., Khosa, R., 2018. Prediction of land use changes based on Land Change Modeler and attribution of changes in the water balance of Ganga basin to land use change using the SWAT model. Sci. Total Environ. 644, 503–519. doi:10.1016/j.scitotenv.2018.07.017

Andrew, S.M., Moe, S.R., Totland, Ø., Munishi, P.K.T., 2012. Species composition and functional structure of herbaceous vegetation in a tropical wetland system. Biodivers. Conserv. 21, 2865–2885. doi:10.1007/s10531-012-0342-y

Andrew, S.M., Totland, Ø., Moe, S.R., 2015. Spatial variation in plant species richness and diversity along human disturbance and environmental gradients in a tropical wetland. Wetl. Ecol. Manag. 23, 395–404. doi:10.1007/s11273-014-9390-2

Arnold, J.G., Allen, P.M., Muttiah, R., Bernhardt, G., 1995. Automated Base Flow Separation and Recession Analysis Techniques. Groundwater 33, 1010–1018.

Arnold, J.G., Kiniry, J.R., Srinivasan, R., Williams, J.R., Haney, E.B., Neitsch, S.L., 2012a. Soil & Water Assessment Tool: Input/output documentation, Texas Water Resources Institute, TR-439.

Arnold, J.G., Moriasi, D.N., Gassman, P.W., Abbaspour, K.C., White, M., Srinivasan, R., Santhi, C., Harmel, R.D., van Griensven, A., Van Liew, M.W., Kannan, N., Jha, M.K., 2012b. SWAT: Model use, calibration, and validation. Trans. ASABE 55, 1491–1508.

Arnold, J.G., Srinivasan, R., Muttiah, R.S., Williams, J.R., 1998. Large area hydrologic modeling and assessment part I: Model development. J. Am. Water Resour. Assoc. doi:10.1111/j.1752-1688.1998.tb05961.x

Baker, T.J., Miller, S.N., 2013. Using the Soil and Water Assessment Tool (SWAT) to assess land use impact on water resources in an East African watershed. J. Hydrol. 486, 100–111. doi:10.1016/j.jhydrol.2013.01.041

Barnett, T.P., Adam, J.C., Lettenmaier, D.P., 2005. Potential impacts of a warming climate on water availability in snow-dominated regions. Nature 438, 303–309. doi:10.1038/nature04141

Barnett, T.P., Pierce, D.W., Hidalgo, H.G., Bonfils, C., Santer, B.D., Das, T., Bala, G., Wood, A.W., Nozawa, T., Mirin, A.A., Cayan, D.R., Dettinger, M.D., 2008. Human-induced changes in the hydrology of the western United States. Science 319, 1080–3. doi:10.1126/science.1152538

Beck, A.D., 1964. The Kilombero Valley of Southcentral Tanganyika. East Afr. Geogr. Rev. 37–43.

Becker, A., Finger, P., Meyer-Christoffer, A., Rudolf, B., Schamm, K., Schneider, U., Ziese, M., 2013. A description of the global land-surface precipitation data products of the Global Precipitation Climatology Centre with sample applications including centennial (trend) analysis from 1901-present. Earth Syst. Sci. Data 5, 71–99. doi:10.5194/essd-5-71-2013

Behn, K., Becker, M., Burghof, S., Möseler, B.M., Willy, D.K., Alvarez, M., 2018. Using vegetation attributes to rapidly assess degradation of East African wetlands. Ecol. Indic. 89, 250–259. doi:10.1016/j.ecolind.2018.02.017

Benjaminsen, T.A., Maganga, F.P., Abdallah, J.M., 2009. The Kilosa Killings: Political Ecology of a Farmer-Herder Conflict in Tanzania. Dev. Change 40, 423–445. doi:10.1111/j.1467-7660.2009.01558.x

Beuel, S., Alvarez, M., Amler, E., Behn, K., Kotze, D., Kreye, C., Leemhuis, C., Wagner, K., Willy, D.K., Ziegler, S., Becker, M., 2016. A rapid assessment of anthropogenic disturbances in East African wetlands. Ecol. Indic. 67, 684–692. doi:10.1016/j.ecolind.2016.03.034

Beven, K.J., 2012. Rainfall-runoff modelling: the primer, Second Edi. ed, Rainfall-Runoff Modelling: The Primer. Wiley-Blackwell, Oxford, Chichester, Hoboken. doi:10.1002/9781119951001

Beven, K.J., Kirkby, M.J., 1979. A physically based, variable contributing area model of basin hydrology / Un modèle à base physique de zone d'appel variable de l'hydrologie du bassin versant. Hydrol. Sci. Bull. 24, 43–69. doi:10.1080/02626667909491834

Bonarius, H., 1975. Physical properties of soils in the Kilombero Valley (Tanzania). Schriftenr. der gtz 26 1–36.

Bond, N., 2018. Hydrostats: Hydrologic Indices for Daily Time Series Data.

Bossa, A.Y., Diekkrüger, B., Agbossou, E.K., 2014. Scenario-Based Impacts of Land Use and Climate Change on Land and Water Degradation from the Meso to Regional Scale. Water 6, 3152–3181. doi:10.3390/w6103152

Bossa, A.Y., Diekkrüger, B., Igué, A.M., Gaiser, T., 2012. Analyzing the effects of different soil databases on modeling of hydrological processes and sediment yield in Benin (West Africa). Geoderma 173–174, 61–74. doi:10.1016/j.geoderma.2012.01.012

Breiman, L., 2001. Random forests. Mach. Learn. 45, 5–32.

Brink, A.B., Bodart, C., Brodsky, L., Defourney, P., Ernst, C., Donney, F., Lupi, A., Tuckova, K., 2014. Anthropogenic pressure in East Africa—Monitoring 20 years of land cover changes by means of medium resolution satellite data. Int. J. Appl. Earth Obs. Geoinf. 28, 60–69. doi:10.1016/j.jag.2013.11.006

Brink, A.B., Eva, H.D., 2009. Monitoring 25 years of land cover change dynamics in Africa: A sample based remote sensing approach. Appl. Geogr. 29, 501–512. doi:10.1016/J.APGEOG.2008.10.004

Burghof, S., 2017. Hydrogeology and water quality of wetlands in East Africa. University of Bonn.

Burghof, S., Gabiri, G., Stumpp, C., Chesnaux, R., Reichert, B., 2017. Development of a hydrogeological conceptual wetland model in the data-scarce north-eastern region of Kilombero Valley, Tanzania. Hydrogeol. J. 26, 267–284. doi:10.1007/s10040-017-1649-2

Camberlin, P., Philippon, N., 2002. The East African March – May Rainy Season: Associated Atmospheric Dynamics and Predictability over the 1968 – 97 Period. J. Clim. 15, 1002–1019. doi:http://dx.doi.org/10.1175/1520-0442(2002)015%3C1002:TEAMMR%3E2.0.CO;2

CDM Smith, 2016. Environmental Flows in Rufiji River Basin Assessed from the Perspective of Planned Development in Kilombero and Lower Rufiji Sub-Basins. Report to the United States Agency for International Development.

Cornelissen, T., Diekkrüger, B., Giertz, S., 2013. A comparison of hydrological models for assessing the impact of land use and climate change on discharge in a tropical catchment. J. Hydrol. 498, 221–236. doi:10.1016/j.jhydrol.2013.06.016

Crist, E.P., 1985. A TM Tasseled Cap equivalent transformation for reflectance factor data. Remote Sens. Environ. 17, 301–306. doi:10.1016/0034-4257(85)90102-6

Crist, E.P., Cicone, R.C., 1984. A Physically-Based Transformation of Thematic Mapper Data---The TM Tasseled Cap. IEEE Trans. Geosci. Remote Sens. GE-22, 256–263. doi:10.1109/TGRS.1984.350619

Cuthbert, M.O., Taylor, R.G., Favreau, G., Todd, M.C., Shamsudduha, M., Villholth, K.G., MacDonald, A.M., Scanlon, B.R., Kotchoni, D.O.V., Vouillamoz, J.-M., Lawson, F.M.A., Adjomayi, P.A., Kashaigili, J., Seddon, D., Sorensen, J.P.R., Ebrahim, G.Y., Owor, M., Nyenje, P.M., Nazoumou, Y., Goni, I., Ousmane, B.I., Sibanda, T., Ascott, M.J., Macdonald, D.M.J., Agyekum, W., Koussoubé, Y., Wanke, H., Kim, H., Wada, Y., Lo, M.-H., Oki, T., Kukuric, N., 2019. Observed controls on resilience of groundwater to climate variability in sub-Saharan Africa. Nature 572, 230–234. doi:10.1038/s41586-019-1441-7

Daconto, G., Games, I., Lukumbuzya, K., Raijmakers, F., 2018. Integrated Management Plan for the Kilombero Valley Ramsar Site, Integrated Management. doi:10.1108/9781787145610

Dagg, M., Woodhead, T., Rijks, D.A., 1970. Evaporation in East Africa. Int. Assoc. Sci. Hydrol. Bull. 15, 61–67. doi:10.1080/02626667009493932

Daniel, S., Gabiri, G., Kirimi, F., Glasner, B., Näschen, K., Leemhuis, C., Steinbach, S., Mtei, K., 2017. Spatial Distribution of Soil Hydrological Properties in the Kilombero Floodplain, Tanzania. Hydrology 4, 57. doi:10.3390/hydrology4040057

Danvi, A., Giertz, S., Zwart, S.J., Diekkrüger, B., 2018. Rice intensification in a changing environment: Impact on water availability in inland valley landscapes in Benin. Water (Switzerland) 10. doi:10.3390/w10010074

Danvi, A., Giertz, S., Zwart, S.J., Diekkrüger, B., 2017. Comparing water quantity and quality in three inland valley watersheds with different levels of agricultural development in central Benin. Agric. Water Manag. 192, 257–270. doi:10.1016/j.agwat.2017.07.017

Dee, D.P., Uppala, S.M., Simmons, A.J., Berrisford, P., Poli, P., Kobayashi, S., Andrae, U., Balmaseda, M.A., Balsamo, G., Bauer, P., Bechtold, P., Beljaars, A.C.M., van de Berg, L., Bidlot, J., Bormann, N., Delsol, C., Dragani, R., Fuentes, M., Geer, A.J., Haimberger, L., Healy, S.B., Hersbach, H., Hólm, E. V., Isaksen, L., Kållberg, P., Köhler, M., Matricardi, M., McNally, A.P., Monge-Sanz, B.M., Morcrette, J.-J., Park, B.-K., Peubey, C., de Rosnay, P., Tavolato, C., Thépaut, J.-N., Vitart, F., 2011. The ERA-Interim reanalysis: configuration and performance of the data assimilation system. Q. J. R. Meteorol. Soc. 137, 553–597. doi:10.1002/qj.828

Dewitte, O., Jones, A., Spaargaren, O., Breuning-Madsen, H., Brossard, M., Dampha, A., Deckers, J., Gallali, T., Hallett, S., Jones, R., Kilasara, M., Le Roux, P., Michéli, E., Montanarella, L., Thiombiano, L., Van Ranst, E., Yemefack, M., Zougmore, R., 2013. Harmonisation of the soil map of africa at the continental scale. Geoderma 211–212, 138–153. doi:10.1016/j.geoderma.2013.07.007

Dinesen, L., 2016. Kilombero Valley Floodplain (Tanzania), in: Finlayson, C., Everard, M., Irvine, K., McInnes, R., Middleton, A.B., van Dam, A., Davidson, N.C. (Eds.), The Wetland Book. Springer Netherlands, Dordrecht. doi:10.1007/978-94-007-6172-8

Dixon, A.B., Wood, A.P., 2003. Wetland cultivation and hydrological management in eastern Africa: Matching community and hydrological needs through sustainable wetland use. Nat. Resour. Forum 27, 117–129. doi:10.1111/1477-8947.00047

Duku, C., Zwart, S.J., Hein, L., 2016. Modelling the forest and woodland-irrigation nexus in tropical Africa: A case study in Benin. Agric. Ecosyst. Environ. 230, 105–115. doi:10.1016/j.agee.2016.06.001

Duvail, S., Hamerlynck, O., 2007. The Rufiji River flood: plague or blessing? Int. J. Biometeorol. 52, 33–42. doi:10.1007/s00484-007-0105-8

Duvail, S., Mwakalinga, A.B., Eijkelenburg, A., Hamerlynck, O., Kindinda, K., Majule, A., 2014. Jointly thinking the post-dam future: exchange of local and scientific knowledge on the lakes of the Lower Rufiji, Tanzania. Hydrol. Sci. J. 59, 713–730. doi:10.1080/02626667.2013.827792

Eastman, J.R., 2016a. TerrSet Tutorial: Geospatial Monitoring and Modeling System. Clark University, Worcester.

Eastman, J.R., 2016b. TerrSet Manual. Geospatial Monitoring and Modeling System. Clark University, Worcester.

Economic Research Bureau University of Dar es Salaam, 2006. A Study to Establishing Mechanism for Payments for Water Environmental Services for the Rufiji River Basin in Tanzania. Dar es Salaam.

Eisner, S., Flörke, M., Chamorro, A., Daggupati, P., Donnelly, C., Huang, J., Hundecha, Y., Koch, H., Kalugin, A., Krylenko, I., Mishra, V., Piniewski, M., Samaniego, L., Seidou, O., Wallner, M., Krysanova, V., 2017. An ensemble analysis of climate change impacts on streamflow seasonality across 11 large river basins. Clim. Change 141, 401–417. doi:10.1007/s10584-016-1844-5

Elmqvist, T., Folke, C., Nyström, M., Peterson, G., Bengtsson, J., Walker, B., Norberg, J., 2003. Response diversity, ecosystem change, and resilience. Front. Ecol. Environ. 1, 488–494. doi:10.1890/1540-9295(2003)001[0488:RDECAR]2.0.CO;2

Environmental Resources Management, 2013. Southern Agricultural Growth Corridor of Tanzania (SAGCOT): Environmental and Social Management Framework (ESMF). Dar es Salaam.

Evers, M., Jonoski, A., Maksimovič, C., Lange, L., Ochoa Rodriguez, S., Teklesadik, A., Cortes Arevalo, J., Almoradie, A., Eduardo Simões, N., Wang, L., Makropoulos, C., 2012. Collaborative modelling for active involvement of stakeholders in urban flood risk management. Nat. Hazards Earth Syst. Sci. 12, 2821–2842. doi:10.5194/nhess-12-2821-2012

Falter, D., 2016. A novel approach for large-scale flood risk assessments : continuous and long-term simulation of the full flood risk chain. University of Potsdam. doi:10.13140/RG.2.1.2202.5844

FAO, 2001. World Soil Resource Reports 94: Lecture notes on the major soils of the world. Food and Agriculture Organization of the United Nations (FAO), Rome.

Faramarzi, M., Abbaspour, K.C., Ashraf Vaghefi, S., Farzaneh, M.R., Zehnder, A.J.B., Srinivasan, R., Yang, H., 2013. Modeling impacts of climate change on freshwater availability in Africa. J. Hydrol. 480, 85–101. doi:10.1016/j.jhydrol.2012.12.016

Federal Ministry of Education and Research (BMBF), 2011. National Research Strategy BioEconomy 2030 Our Route towards a biobased economy.

Feng, D., Beighley, E., Raoufi, R., Melack, J., Zhao, Y., Iacobellis, S., Cayan, D., 2019. Propagation of future climate conditions into hydrologic response from coastal southern California watersheds. Clim. Change 153, 199–218. doi:10.1007/s10584-019-02371-3

Funk, C., Dettinger, M.D., Michaelsen, J.C., Verdin, J.P., Brown, M.E., Barlow, M., Hoell, A., 2008. Warming of the Indian Ocean threatens eastern and southern African food security but could be mitigated by agricultural development. Proc. Natl. Acad. Sci. U. S. A. 105, 11081–6. doi:10.1073/pnas.0708196105

Funk, C., Nicholson, S.E., Landsfeld, M., Klotter, D., Peterson, P., Harrison, L., 2015a. The Centennial Trends Greater Horn of Africa precipitation dataset. Sci. Data 2, 150050. doi:10.1038/sdata.2015.50

Funk, C., Peterson, P., Landsfeld, M., Pedreros, D., Verdin, J., Shukla, S., Husak, G., Rowland, J., Harrison, L., Hoell, A., Michaelsen, J., 2015b. The climate hazards infrared precipitation with stations—a new environmental record for monitoring extremes. Sci. Data 2, 150066. doi:10.1038/sdata.2015.66

Gabiri, G., 2018. Multi-scale modeling of water resources in a tropical inland valley and a tropical floodplain catchment in East Africa Geofrey Gabiri.

Gabiri, G., Burghof, S., Diekkrüger, B., Steinbach, S., Näschen, K., 2018. Modeling Spatial Soil Water Dynamics in a Tropical Floodplain, East Africa. Water 10, 1–27. doi:10.3390/w10020191

Gabiri, G., Diekkrüger, B., Leemhuis, C., Burghof, S., Näschen, K., Asiimwe, I., Bamutaze, Y., 2017. Determining hydrological regimes in an agriculturally used tropical inland valley wetland in central Uganda using soil moisture, groundwater, and digital elevation data. Hydrol. Process. 32, 349–362. doi:10.1002/hyp.11417

Gabiri, G., Leemhuis, C., Diekkrüger, B., Näschen, K., Steinbach, S., Thonfeld, F., 2019. Modelling the impact of land use management on water resources in a tropical inland valley catchment of central Uganda, East Africa. Sci. Total Environ. 653, 1052–1066. doi:10.1016/j.scitotenv.2018.10.430

Gallant, J.C., Wilson, J.P., 2000. Primary topographic attributes, in: Wilson, J.P., Gallant, J.C. (Eds.), Terrain Analysis: Principles and Applications. John Wiley & Sons, New York, pp. 51–85.

Gardner, R.C., Finlayson, C.M., 2018. Global Wetland Outlook: State of the World´s Wetlands and their Services to People. Gland, Switzerland.

Gashaw, T., Tulu, T., Argaw, M., Worqlul, A.W., 2018. Modeling the hydrological impacts of land use/land cover changes in the Andassa watershed, Blue Nile Basin, Ethiopia. Sci. Total Environ. 619–620, 1394–1408. doi:10.1016/j.scitotenv.2017.11.191

Gebrekidan, B.H. (unpublished). Understanding the dynamics of land use and intensification in Kilombero Valley Floodplain: An Agent Based Modeling approach.

Gelfan, A., Gustafsson, D., Motovilov, Y., Arheimer, B., Kalugin, A., Krylenko, I., Lavrenov, A., 2017. Climate change impact on the water regime of two great Arctic rivers: modeling and uncertainty issues. Clim. Change 141, 499–515. doi:10.1007/s10584-016-1710-5

Giertz, S., 2004. Analyse der hydrologischen Prozesse in den sub-humiden Tropen Westafrikas unter besonderer Berücksichtigung der Landnutzung am Beispiel des Aguima-Einzugsgebietes in Benin. Diss. Math.-Naturw. Fak., Univ. Bonn. University of Bonn.

Gilleland, E., Katz, R.W., 2016. extRemes 2.0: An Extreme Value Analysis Package in R. J. Stat. Softw. 72, 1–39. doi:10.18637/jss.v072.i08

Githui, F.W., 2008. Assessing the Impacts of Environmental Change on the Hydrology of the Nzoia Catchment, in the Lake Victoria Basin. PhD thesis 203. doi:10.1109/NAPS.2012.6336347

GlobE Wetlands, 2013. GlobE - Wetlands in East Africa [WWW Document]. URL https://www.wetlands-africa.uni-bonn.de/ (accessed 10.29.19).

Goddard, L., Graham, N.E., 1999. Importance of the Indian Ocean for simulating rainfall anomalies over eastern and southern Africa. J. Geophys. Res. Atmos. 104, 19099–19116. doi:10.1029/1999JD900326

Godfray, H.C.J., Beddington, J.R., Crute, I.R., Haddad, L., Lawrence, D., Muir, J.F., Pretty, J., Robinson, S., Thomas, S.M., Toulmin, C., 2010. Food Security: The Challenge of Feeding 9 Billion People. Science 327, 812–8. doi:10.1126/science.1185383

Green, W.H., Ampt, G.A., 1911. Studies on soil phyics. J. Agric. Sci. 4, 1–24. doi:10.1017/S0021859600001441

Gupta, H.V., Sorooshian, S., Yapo, P.O., 1999. Status of Automatic Calibration for Hydrologic Models : Comparison With Multilevel Expert Calibration. J. Hydrol. Eng. 4, 135–143. doi:10.1061/(ASCE)1084-0699(1999)4

Gupta, H. V., Kling, H., Yilmaz, K.K., Martinez, G.F., 2009. Decomposition of the mean squared error and NSE performance criteria: Implications for improving hydrological modelling. J. Hydrol. 377, 80–91. doi:10.1016/j.jhydrol.2009.08.003

Gutowski, J.W., Giorgi, F., Timbal, B., Frigon, A., Jacob, D., Kang, H.S., Raghavan, K., Lee, B., Lennard, C., Nikulin, G., O'Rourke, E., Rixen, M., Solman, S., Stephenson, T., Tangang, F., 2016. WCRP COordinated Regional Downscaling EXperiment (CORDEX): A diagnostic MIP for CMIP6. Geosci. Model Dev. 9, 4087–4095. doi:10.5194/gmd-9-4087-2016

Guzha, A.C., Rufino, M.C., Okoth, S., Jacobs, S., Nóbrega, R.L.B., 2018. Impacts of land use and land cover change on surface runoff, discharge and low flows: Evidence from East Africa. J. Hydrol. Reg. Stud. 15, 49–67. doi:10.1016/J.EJRH.2017.11.005

Hargreaves, G.L., Hargreaves, G.H., Riley, J.P., 1985. Agricultural Benefits for Senegal River Basin. J. Irrig. Drain. Eng. 111, 113–124. doi:10.1061/(ASCE)0733-9437(1985)111:2(113)

Hastenrath, S., Nicklis, A., Greischar, L., 1993. Atmospheric-hydrospheric mechanisms of climate

anomalies in the western equatorial Indian Ocean. J. Geophys. Res. 98, 20219. doi:10.1029/93JC02330

Hecheltjen, A., Thonfeld, F., Menz, G., 2014. Recent advances in remote sensing change detection - a review., in: Manakos, I., Braun, M. (Eds.), Land Use and Land Cover Mapping in Europe. Practices & Trends. Springer, Dordrecht, Heidelberg, New York, London, pp. 145–178.

Heinkel, S.B., 2018. Therapeutic effects of wetlands on mental well-being. The concept of therapeutic landscapes applied to an ecosystem in Uganda. Bonn.

Hounkpè, J., Diekkrüger, B., Afouda, A.A., Sintondji, L.O.C., 2019. Land use change increases flood hazard: a multi-modelling approach to assess change in flood characteristics driven by socio-economic land use change scenarios. Nat. Hazards 98, 1021–1050. doi:10.1007/s11069-018-3557-8

Hrachowitz, M., Savenije, H.H.G., Blöschl, G., McDonnell, J.J., Sivapalan, M., Pomeroy, J.W., Arheimer, B., Blume, T., Clark, M.P., Ehret, U., Fenicia, F., Freer, J.E., Gelfan, a., Gupta, H.V., Hughes, D. a., Hut, R.W., Montanari, a., Pande, S., Tetzlaff, D., Troch, P. a., Uhlenbrook, S., Wagener, T., Winsemius, H.C., Woods, R. a., Zehe, E., Cudennec, C., 2013. A decade of Predictions in Ungauged Basins (PUB)—a review. Hydrol. Sci. J. 58, 1198–1255. doi:10.1080/02626667.2013.803183

Huffman, G.J., Bolvin, D.T., Nelkin, E.J., Wolff, D.B., Adler, R.F., Gu, G., Hong, Y., Bowman, K.P., Stocker, E.F., Huffman, G.J., Bolvin, D.T., Nelkin, E.J., Wolff, D.B., Adler, R.F., Gu, G., Hong, Y., Bowman, K.P., Stocker, E.F., 2007. The TRMM Multisatellite Precipitation Analysis (TMPA): Quasi-Global, Multiyear, Combined-Sensor Precipitation Estimates at Fine Scales. J. Hydrometeorol. 8, 38–55. doi:10.1175/JHM560.1

IUCN, UNEP-WCMC, 2019. The World Database of Protected Areas (WDPA) [WWW Document]. URL https://protectedplanet.net (accessed 6.21.19).

Jätzold, R., Baum, E., 1968. The Kilombero Valley (Tanzania) – characteristic features of the economic geography of a semihumid East African flood plain and its margins. Weltforum-Verlag GmbH, München.

Jenness, J., 2006. Topographic Position Index (tpi _jen.avx) extension for ArcView 3.x, Version 1.2.

Jew, E., Bonnington, C., 2011. Socio-demographic factors influence the attitudes of local residents towards trophy hunting activities in the Kilombero Valley, Tanzania. Afr. J. Ecol. 49, 277–285.

Johansson, E.L., Abdi, A.M., 2019. Mapping and quantifying perceptions of environmental change in Kilombero Valley, Tanzania. Ambio 1–12. doi:10.1007/s13280-019-01226-6

Johansson, E.L., Isgren, E., 2017. Local perceptions of land-use change: using participatory art to reveal direct and indirect socioenvironmental effects of land acquisitions in Kilombero Valley, Tanzania. Ecol. Soc. 22, 1–12. doi:https://doi.org/10.5751/ ES-08986-220103

Joyce, R.J., Janowiak, J.E., Arkin, P.A., Xie, P., Joyce, R.J., Janowiak, J.E., Arkin, P.A., Xie, P., 2004. CMORPH: A Method that Produces Global Precipitation Estimates from Passive Microwave and Infrared Data at High Spatial and Temporal Resolution. J. Hydrometeorol. 5, 487–503. doi:10.1175/1525-7541(2004)005<0487:CAMTPG>2.0.CO;2

Kangalawe, R.Y.M., Liwenga, E.T., 2005. Livelihoods in the wetlands of Kilombero Valley in Tanzania: Opportunities and challenges to integrated water resource management. Phys. Chem. Earth, Parts A/B/C 30, 968–975. doi:10.1016/j.pce.2005.08.044

Kashaigili, J.J., 2008. Impacts of land-use and land-cover changes on flow regimes of the Usangu wetland and the Great Ruaha River, Tanzania. Phys. Chem. Earth, Parts A/B/C 33, 640–647. doi:10.1016/J.PCE.2008.06.014

Kashenge, S., Makoninde, E., 2017. Perception and Indicators of Climate Change, Its Impacts, Available Mitigation Strategies in Rice Growing Communities Adjoining Eastern Arc Mountains. Univers. J. Agric. Res. 5, 267–279. doi:10.13189/ujar.2017.050503

Kato, F., 2007. Development of a major rice cultivation area in the Kilombero Valley, Tanzania. Afr. Study Monogr. 36, 3–18. doi:10.14989/68498

Kim, N.W., Chung, I.M., Won, Y.S., Arnold, J.G., 2008. Development and application of the integrated SWAT–MODFLOW model. J. Hydrol. 356, 1–16. doi:10.1016/j.jhydrol.2008.02.024

Kirimi, F., Thiong, K., Gabiri, G., Diekkrüger, B., 2018. Assessing seasonal land cover dynamics in the tropical Kilombero floodplain of East Africa. J. Appl. Remote Sens. 12, 1–23. doi:10.1117/1.JRS.12.026027

Kleemann, J., Baysal, G., Bulley, H.N.N., Fürst, C., 2017. Assessing driving forces of land use and land cover change by a mixed-method approach in north-eastern Ghana, West Africa. J. Environ. Manage. 196, 411–442. doi:10.1016/j.jenvman.2017.01.053

Kolding, J., Mombo, F., Temu, B., Nyanghura, Q., Cunliffe, R., 2017. Technical advisory services for biodiversity conservation and wetland management in Kilombero valley RAMSAR site, Tanzania. Dar es Salaam.

Komi, K., Neal, J., Trigg, M.A., Diekkrüger, B., 2017. Modelling of flood hazard extent in data sparse areas: a case study of the Oti River basin, West Africa. J. Hydrol. Reg. Stud. 10, 122–132. doi:10.1016/J.EJRH.2017.03.001

Kotze, D.C., Ellery, W.N., Macfarlane, D.M., Jewitt, G.P.W., 2012. A rapid assessment method for coupling anthropogenic stressors and wetland ecological condition. Ecol. Indic. 13, 284–293. doi:10.1016/J.ECOLIND.2011.06.023

Koutsouris, A., 2017. Building a coherent hydro-climatic modelling framework for the data limited Kilombero Valley of Tanzania. Diss. from Dep. Phys. Geogr. NV - 63. Stockholm University.

Koutsouris, A.J., Chen, D., Lyon, S.W., 2016. Comparing global precipitation data sets in eastern Africa: a case study of Kilombero Valley, Tanzania. Int. J. Climatol. 36, 2000–2014. doi:10.1002/joc.4476

Kwesiga, J., Grotelüschen, K., Neuhoff, D., Senthilkumar, K., Döring, T.F., Becker, M., 2019. Site and Management Effects on Grain Yield and Yield Variability of Rainfed Lowland Rice in the Kilombero Floodplain of Tanzania. Agronomy 9, 632. doi:10.3390/agronomy9100632

Lafon, T., Dadson, S., Buys, G., Prudhomme, C., 2013. Bias correction of daily precipitation simulated by a regional climate model: A comparison of methods. Int. J. Climatol. 33, 1367–1381. doi:10.1002/joc.3518

Lal, R., 1997. Deforestation effects on soil degradation and rehabilitation in western Nigeria. IV. Hydrology and water quality. L. Degrad. Dev. 8, 95–126. doi:10.1002/(SICI)1099-145X(199706)8:2<95::AID-LDR241>3.0.CO;2-K

Lalika, M.C.S., Meire, P., Ngaga, Y.M., Chang'a, L., 2015. Understanding watershed dynamics and impacts of climate change and variability in the Pangani River Basin, Tanzania. Ecohydrol. Hydrobiol. 15, 26–38. doi:10.1016/J.ECOHYD.2014.11.002

Lee, S., Yeo, I.-Y., Lang, M.W., McCarty, G.W., Sadeghi, A.M., Sharifi, A., Jin, H., Liu, Y., 2019. Improving the catchment scale wetland modeling using remotely sensed data. Environ. Model. Softw. 122, 104069. doi:10.1016/J.ENVSOFT.2017.11.001

Leemhuis, C., Amler, E., Diekkrüger, B., Gabiri, G., Näschen, K., 2016. East African wetland-catchment data base for sustainable wetland management. Proc. Int. Assoc. Hydrol. Sci. 374, 123–128. doi:10.5194/piahs-374-123-2016

Leemhuis, C., Thonfeld, F., Näschen, K., Steinbach, S., Muro, J., Strauch, A., López, A., Daconto, G., Games, I., Diekkrüger, B., 2017. Sustainability in the food-water-ecosystem nexus: The role of land use and land cover change for water resources and ecosystems in the Kilombero Wetland, Tanzania. Sustain. 9, 1513. doi:10.3390/su9091513

Legates, D.R., McCabe Jr., G.J., 1999. Evaluating the Use of "Goodness of Fit" Measures in Hydrologic and Hydroclimatic Model Validation. Water Resour. Res. 35, 233–241. doi:10.1029/1998WR900018

Lehner, B., Verdin, K., Jarvis, A., 2008. New Global Hydrography Derived From Spaceborne Elevation Data. Eos, Trans. Am. Geophys. Union 89, 93–104. doi:10.1029/2008EO100001

Liu, W., Park, S., Bailey, R.T., Molina-Navarro, E., Andersen, H.E., Thodsen, H., Nielsen, A., Jeppesen, E.,

Jensen, J.S., Jensen, J.B., Trolle, D., 2019. Comparing SWAT with SWAT-MODFLOW hydrological simulations when assessing the impacts of groundwater abstractions for irrigation and drinking water. Hydrol. Earth Syst. Sci. Discuss. 1–51. doi:10.5194/hess-2019-232

Lyon, B., Dewitt, D.G., 2012. A recent and abrupt decline in the East African long rains. Geophys. Res. Lett. 39. doi:10.1029/2011GL050337

Lyon, S.W., Koutsouris, A., Scheibler, F., Jarsjö, J., Mbanguka, R., Tumbo, M., Robert, K.K., Sharma, A.N., van der Velde, Y., 2015. Interpreting characteristic drainage timescale variability across Kilombero Valley, Tanzania. Hydrol. Process. 29, 1912–1924. doi:10.1002/hyp.10304

MacDonald, A.M., Bonsor, H.C., 2010. Groundwater and climate change in Africa: review of recharge studies. Keyworth.

Mack, B., Leinenkugel, P., Kuenzer, C., Dech, S., 2017. A semi-automated approach for the generation of a new land use and land cover product for Germany based on Landsat time-series and Lucas in-situ data. Remote Sens. Lett. 8, 244–253. doi:10.1080/2150704X.2016.1249299

Magufuli, J.P.J., 2015. Inauguration speech by John Pombe Joseph Magufuli [WWW Document]. United Nations Tanzania. URL https://tz.one.un.org/media-centre/statements/186-the-speech-by-h-e-john-pombe-joseph-magufuli-officially-inaugurating-the-11th-parliament-of-the-united-republic-of-tanzania (accessed 12.6.19).

Maltby, E., Acreman, M., 2011. Ecosystem services of wetlands: pathfinder for a new paradigm. Hydrol. Sci. J. 56, 1341–1359. doi:10.1080/02626667.2011.631014

Mango, L.M., Melesse, A.M., McClain, M.E., Gann, D., Setegn, S.G., 2011. Land use and climate change impacts on the hydrology of the upper Mara River Basin, Kenya: results of a modeling study to support better resource management. Hydrol. Earth Syst. Sci. 15, 2245–2258. doi:10.5194/hess-15-2245-2011

Marchant, R., Richer, S., Boles, O., Capitani, C., Courtney-Mustaphi, C.J., Lane, P., Prendergast, M.E., Stump, D., De Cort, G., Kaplan, J.O., Phelps, L., Kay, A., Olago, D., Petek, N., Platts, P.J., Punwong, P., Widgren, M., Wynne-Jones, S., Ferro-Vázquez, C., Benard, J., Boivin, N., Crowther, A., Cuní-Sanchez, A., Deere, N.J., Ekblom, A., Farmer, J., Finch, J., Fuller, D., Gaillard-Lemdahl, M.-J., Gillson, L., Githumbi, E., Kabora, T., Kariuki, R., Kinyanjui, R., Kyazike, E., Lang, C., Lejju, J., Morrison, K.D., Muiruri, V., Mumbi, C., Muthoni, R., Muzuka, A., Ndiema, E., Kabonyi Nzabandora, C., Onjala, I., Schrijver, A.P., Rucina, S., Shoemaker, A., Thornton-Barnett, S., van der Plas, G., Watson, E.E., Williamson, D., Wright, D., 2018. Drivers and trajectories of land cover change in East Africa: Human and environmental interactions from 6000 years ago to present. Earth-Science Rev. 178, 322–378. doi:10.1016/J.EARSCIREV.2017.12.010

Martinez-Martinez, E., Nejadhashemi, a. P., Woznicki, S. a., Love, B.J., 2014. Modeling the hydrological significance of wetland restoration scenarios. J. Environ. Manage. 133, 121–134. doi:10.1016/j.jenvman.2013.11.046

Mas, J.-F., Kolb, M., Paegelow, M., Camacho Olmedo, M.T., Houet, T., 2014. Inductive pattern-based land use/cover change models: A comparison of four software packages. Environ. Model. Softw. 51, 94–111. doi:10.1016/J.ENVSOFT.2013.09.010

Mashingia, F., Mtalo, F., Bruen, M., 2014. Validation of remotely sensed rainfall over major climatic regions in Northeast Tanzania. Phys. Chem. Earth 67–69, 55–63. doi:10.1016/j.pce.2013.09.013

McCartney, M., Rebelo, L.-M., Senaratna Sellamuttu, S., de Silva, S., 2010. Wetlands, agriculture and poverty reduction, IWMI Research Report 137. Colombo. doi:10.5337/2010.230

McClain, M.E., 2013. Balancing Water Resources Development and Environmental Sustainability in Africa: A Review of Recent Research Findings and Applications. Ambio 42, 549–565. doi:10.1007/s13280-012-0359-1

McFeeters, S.K., 1996. The use of the Normalized Difference Water Index (NDWI) in the delineation of open water features. Int. J. Remote Sens. 17, 1425–1432. doi:10.1080/01431169608948714

Meijer, J., Shames, S., Scherr, S.J., Giesen, P., 2018. Spatial scenario modelling to support integrated landscape management in the Kilombero valley landscape in Tanzania. The Hague.

Milder, J.C., Hart, A.K., Buck, L.E., 2013. Applying an Agriculture Green Growth Approach in the SAGCOT Clusters : Challenges and Opportunities in Kilombero, Ihemi and Mbarali. Dar es Salaam.

Mitsch, W.J., Gosselink, J.G., 2007. Wetlands, 4th ed. Wiley, New Jersey.

Mockus, V., 1972. Hydrology, in: National Engineering Handbook. p. 127.

Mombo, F., Speelman, S., Huylenbroeck, G. Van, Hella, J., Moe, S., 2011. Ratification of the Ramsar convention and sustainable wetlands management : Situation analysis of the Kilombero Valley wetlands in Tanzania. J. Agric. Ext. Rural Dev. 3, 153–164.

Montanari, A., Young, G., Savenije, H.H.G., Hughes, D., Wagener, T., Ren, L.L., Koutsoyiannis, D., Cudennec, C., Toth, E., Grimaldi, S., Blöschl, G., Sivapalan, M., Beven, K., Gupta, H., Hipsey, M., Schaefli, B., Arheimer, B., Boegh, E., Schymanski, S.J., Di Baldassarre, G., Yu, B., Hubert, P., Huang, Y., Schumann, A., Post, D.A., Srinivasan, V., Harman, C., Thompson, S., Rogger, M., Viglione, A., McMillan, H., Characklis, G., Pang, Z., Belyaev, V., 2013. "Panta Rhei—Everything Flows": Change in hydrology and society—The IAHS Scientific Decade 2013–2022. Hydrol. Sci. J. 58, 1256–1275. doi:10.1080/02626667.2013.809088

Monteith, J.L., Moss, C.J., 1977. Climate and the Efficiency of Crop Production in Britain. Philos. Trans. R. Soc. B Biol. Sci. 281, 277–294. doi:10.1098/rstb.1977.0140

Montzka, C., Canty, M., Kunkel, R., Menz, G., Vereecken, H., Wendland, F., 2008. Modelling the water balance of a mesoscale catchment basin using remotely sensed land cover data. J. Hydrol. 353, 322–334. doi:10.1016/J.JHYDROL.2008.02.018

Moriasi, D.N., Gitau, M.W., Pai, N., Daggupati, P., 2015. Hydrologic and Water Quality Models: Performance Measures and Evaluation Criteria. Trans. ASABE 58, 1763–1785. doi:10.13031/trans.58.10715

Moss, R.H., Edmonds, J.A., Hibbard, K.A., Manning, M.R., Rose, S.K., van Vuuren, D.P., Carter, T.R., Emori, S., Kainuma, M., Kram, T., Meehl, G.A., Mitchell, J.F.B., Nakicenovic, N., Riahi, K., Smith, S.J., Stouffer, R.J., Thomson, A.M., Weyant, J.P., Wilbanks, T.J., 2010. The next generation of scenarios for climate change research and assessment. Nature 463, 747–756. doi:10.1038/nature08823

Msofe, N.K., 2019. Socio-Ecological Drivers of Land Use Change and Wetland Conversion in Kilombero Valley Floodoplain, Tanzania. Am. J. Environ. Resour. Econ. 4, 1–11. doi:10.11648/j.ajere.20190401.11

Msofe, N.K., Sheng, L., Lyimo, J., 2019. Land use change trends and their driving forces in the Kilombero Valley Floodplain, Southeastern Tanzania. Sustain. 11, 1–25. doi:10.3390/su11020505

Mucova, S.A.R., Filho, W.L., Azeiteiro, U.M., Pereira, M.J., 2018. Assessment of land use and land cover changes from 1979 to 2017 and biodiversity & land management approach in Quirimbas National Park, Northern Mozambique, Africa. Glob. Ecol. Conserv. 16, e00447. doi:10.1016/J.GECCO.2018.E00447

Munishi-Kongo, S., 2013. Ground and Satellite-Based Assessment of Hydrological Responses To Land Cover Change in the Kilombero River Basin , Tanzania. University of KwaZulu-Natal.

Muro, J., 2019. Mapping intra- and inter-annual dynamics in wetlands with multispectral, thermal and SAR time series. University of Bonn.

Muro, J., Canty, M., Conradsen, K., Hüttich, C., Nielsen, A.A., Skriver, H., Remy, F., Strauch, A., Thonfeld, F., Menz, G., 2016. Short-Term Change Detection in Wetlands Using Sentinel-1 Time Series. Remote Sens. 8, 795. doi:10.3390/rs8100795

Muro, J., Strauch, A., Heinemann, S., Steinbach, S., Thonfeld, F., Waske, B., Diekkrüger, B., 2018. Land surface temperature trends as indicator of land use changes in wetlands. Int. J. Appl. Earth Obs. Geoinf. 70, 62–71. doi:10.1016/j.jag.2018.02.002

Mwamila, T.B., Kimwaga, R.J., Mtalo, F.W., 2008. Eco-hydrology of the Pangani River downstream of

Nyumba ya Mungu reservoir, Tanzania. Phys. Chem. Earth, Parts A/B/C 33, 695–700. doi:10.1016/J.PCE.2008.06.054

Näschen, K., Diekkrüger, B., Leemhuis, C., Seregina, L.S., Linden, R. van der, 2019. Impact of Climate Change on Water Resources in the Kilombero Catchment in Tanzania. Water 11, 859. doi:10.3390/W11040859

Näschen, K., Diekkrüger, B., Leemhuis, C., Steinbach, S., Seregina, L., Thonfeld, F., Linden, R. van der, 2018. Hydrological Modeling in Data-Scarce Catchments: The Kilombero Floodplain in Tanzania. Water 10, 599. doi:10.3390/W10050599

Nash, J.E., Sutcliffe, J.V., 1970. River flow forecasting through conceptual models part I — A discussion of principles. J. Hydrol. 10, 282–290. doi:10.1016/0022-1694(70)90255-6

National Bureau of Statistics. United Republic of Tanzania, 2017. The National Environment Statistics Report, 2017 (NESR, 2017) - Tanzania Mainland. Dar es Salaam.

National Bureau of Statistics. United Republic of Tanzania, 2012. 2012 Population and Housing Census Report. Dar es Salaam.

Natkhin, M., Dietrich, O., Schäfer, M.P., Lischeid, G., 2015. The effects of climate and changing land use on the discharge regime of a small catchment in Tanzania. Reg. Environ. Chang. 15, 1269–1280. doi:10.1007/s10113-013-0462-2

Ndomba, P., Mtalo, F., Killingtveit, A., 2008. SWAT model application in a data scarce tropical complex catchment in Tanzania. Phys. Chem. Earth, Parts A/B/C 33, 626–632. doi:10.1016/j.pce.2008.06.013

Neitsch, S.L., Arnold, J.G., Kiniry, J.R., Williams, J.R., 2011. Soil & Water Assessment Tool Theoretical Documentation Version 2009. Grassland, Soil and Water Research Laboratory, Temple.

Nhemachena, Charles, Matchaya, G., Nhemachena, Charity, Karuaihe, S., Muchara, B., Nhlengethwa, S., 2018. Measuring Baseline Agriculture-Related Sustainable Development Goals Index for Southern Africa. Sustainability 10, 849. doi:10.3390/su10030849

Nicholson, S.E., 2017. Climate and climatic variability of rainfall over eastern Africa. Rev. Geophys. 55, 590–635. doi:10.1002/2016rg000544

Nicholson, S.E., 2000. The nature of rainfall variability over Africa on time scales of decades to millenia. Glob. Planet. Change 26, 137–158. doi:10.1016/S0921-8181(00)00040-0

Nicholson, S.E., 1996. A review of climate dynamics and climate variability in Eastern Africa. Limnol. Climatol. Paleoclimatology East African Lakes.

Nindi, S.J., Maliti, H., Bakari, S., Kija, H., Machoke, M., 2014. Conflicts over Land and water resources in the Kilombero Valley Floodplain, Tanzania. Afr. Study Monogr. 50, 173–190. doi:10.1080/03056240902886133

Niraula, R., Meixner, T., Norman, L.M., 2015. Determining the importance of model calibration for forecasting absolute/relative changes in streamflow from LULC and climate changes. J. Hydrol. 522, 439–451. doi:10.1016/j.jhydrol.2015.01.007

Notter, B., Hurni, H., Wiesmann, U., Abbaspour, K.C., 2012. Modelling water provision as an ecosystem service in a large East African river basin. Hydrol. Earth Syst. Sci. 16, 69–86. doi:10.5194/hess-16-69-2012

Notter, B., Hurni, H., Wiesmann, U., Ngana, J.O., 2013. Evaluating watershed service availability under future management and climate change scenarios in the Pangani Basin. Phys. Chem. Earth 61–62, 1–11. doi:10.1016/j.pce.2012.08.017

Ntongani, W.A., Andrew, S.M., Ntongani, W.A., Andrew, S.M., 2013. Bird species composition and diversity in habitats with different disturbance histories at Kilombero Wetland, Tanzania. Open J. Ecol. 03, 482–488. doi:10.4236/oje.2013.37056

Ntongani, W.A., Munishi, P.K.T., More, S.R., Kashaigili, J.J., 2014. Local knowledge on the influence of land use/cover changes and conservation threats on avian community in the Kilombero wetlands, Tanzania.

Nyenzi, B.S., Kiangi, P.M.R., Rao, N.N.P., 1981. Evaporation values in East Africa. Arch. Meteorol. Geophys. Bioclimatol. Ser. B 29, 37–55. doi:10.1007/BF02278189

Op de Hipt, F., 2018. Modeling Climate and Land Use Change Impacts on Water Resources in the Dano Catchment. University of Bonn.

Op de Hipt, F., Diekkrüger, B., Steup, G., Yira, Y., Hoffmann, T., Rode, M., Näschen, K., 2019. Modeling the impact of climate change on water resources and soil erosion in a tropical catchment in Burkina Faso, West Africa. Sci. Total Environ. 653, 431–445. doi:10.1016/j.catena.2017.11.023

Peel, M.C., Finlayson, B.L., McMahon, T.A., 2007. Updated world map of the Köppen-Geiger climate classification. Hydrol. Earth Syst. Sci. 11, 1633–1644. doi:10.5194/hess-11-1633-2007

Penman, H.L., 1956. Evaporation: an introductory survey. J. Agric. Sci. 4, 9–29.

Piani, C., Haerter, J.O., Coppola, E., 2010. Statistical bias correction for daily precipitation in regional climate models over Europe. Theor. Appl. Climatol. 99, 187–192. doi:10.1007/s00704-009-0134-9

Pokorny, J., 2019. Evapotranspiration. Encycl. Ecol. 292–303. doi:10.1016/B978-0-12-409548-9.11182-0

Poméon, T., 2018. Evaluating the Contribution of Remote Sensing Data Products for Regional Simulations of Hydrological Processes in West Africa using a Multi-Model Ensemble. University of Bonn.

Poméon, T., Jackisch, D., Diekkrüger, B., 2017. Evaluating the performance of remotely sensed and reanalysed precipitation data over West Africa using HBV light. J. Hydrol. 547, 222–235. doi:10.1016/J.JHYDROL.2017.01.055

Priestley, C.H.B., Taylor, R.J., 1972. On the Assessment of Surface Heat Flux and Evaporation Using Large-Scale Parameters. Mon. Weather Rev. 100, 81–92. doi:10.1175/1520-0493(1972)100<0081:OTAOSH>2.3.CO;2

Ramsar, 2002. Information Sheet on Ramsar Wetlands (RIS) [WWW Document]. Ramsar. doi:10.1002/ardp.18471010230

Ramsar Convention Secretariat, 2016. An Introduction to the Ramsar Convention on Wetlands. Handbook 1 - International Cooperation on Wetlands, 5th Edition. Gland, Switzerland.

Rathjens, H., Oppelt, N., 2012. SWATgrid: An interface for setting up SWAT in a grid-based discretization scheme. Comput. Geosci. 45, 161–167. doi:10.1016/j.cageo.2011.11.004

RBWB, 2014. The Rufiji Basin Water Board (RBWB) discharge database.

Rebelo, L.M., McCartney, M.P., Finlayson, C.M., 2010. Wetlands of Sub-Saharan Africa: Distribution and contribution of agriculture to livelihoods. Wetl. Ecol. Manag. 18, 557–572. doi:10.1007/s11273-009-9142-x

Reddy, S.., Collins, A.., Mruma, A., 2003. Complex high-strain deformation in the Usagaran Orogen, Tanzania: structural setting of Palaeoproterozoic eclogites. Tectonophysics 375, 101–123. doi:10.1016/S0040-1951(03)00335-4

Refsgaard, J.C., Storm, B., 1995. MIKE SHE, in: Singh, V.P. (Ed.), Computer Models of Watershed Hydrology. Water Resources Publications: Highlands Ranch, Colorado USA, pp. 809–846.

Reis, V., Hermoso, V., Hamilton, S.K., Bunn, S.E., Linke, S., 2019. Conservation planning for river-wetland mosaics: A flexible spatial approach to integrate floodplain and upstream catchment connectivity. Biol. Conserv. 236, 356–365. doi:10.1016/J.BIOCON.2019.05.042

Reshmidevi, T.V., Nagesh Kumar, D., Mehrotra, R., Sharma, A., 2018. Estimation of the climate change impact on a catchment water balance using an ensemble of GCMs. J. Hydrol. 556, 1192–1204. doi:10.1016/J.JHYDROL.2017.02.016

Reshmidevi, T. V., Nagesh Kumar, D., 2014. Modelling the impact of extensive irrigation on the groundwater resources. Hydrol. Process. 28, 628–639. doi:10.1002/hyp.9615

Rienecker, M.M., Suarez, M.J., Gelaro, R., Todling, R., Bacmeister, J., Liu, E., Bosilovich, M.G., Schubert, S.D., Takacs, L., Kim, G.-K., Bloom, S., Chen, J., Collins, D., Conaty, A., da Silva, A., Gu, W., Joiner, J., Koster, R.D., Lucchesi, R., Molod, A., Owens, T., Pawson, S., Pegion, P., Redder, C.R., Reichle, R., Robertson, F.R., Ruddick, A.G., Sienkiewicz, M., Woollen, J., Rienecker, M.M., Suarez, M.J., Gelaro,

R., Todling, R., Julio Bacmeister, Liu, E., Bosilovich, M.G., Schubert, S.D., Takacs, L., Kim, G.-K., Bloom, S., Chen, J., Collins, D., Conaty, A., Silva, A. da, Gu, W., Joiner, J., Koster, R.D., Lucchesi, R., Molod, A., Owens, T., Pawson, S., Pegion, P., Redder, C.R., Reichle, R., Robertson, F.R., Ruddick, A.G., Sienkiewicz, M., Woollen, J., 2011. MERRA: NASA's Modern-Era Retrospective Analysis for Research and Applications. J. Clim. 24, 3624–3648. doi:10.1175/JCLI-D-11-00015.1

Riley, S.J., DeGloria, S.D., Elliot, R., 1999. A terrain ruggedness index that quantifies topographic heterogeneity. Intermt. Journcal Sci. 5.

Rosa, I.M.D., Rentsch, D., Hopcraft, J.G.C., 2018. Evaluating forest protection strategies: A comparison of land-use systems to preventing forest loss in Tanzania. Sustain. 10, 4476. doi:10.3390/su10124476

Ruszkiczay-Rüdiger, Z., Fodor, L., Horváth, E., Telbisz, T., 2009. Discrimination of fluvial, eolian and neotectonic features in a low hilly landscape: A DEM-based morphotectonic analysis in the Central Pannonian Basin, Hungary. Geomorphology 104, 203–217. doi:10.1016/j.geomorph.2008.08.014

Sakané, N., Alvarez, M., Becker, M., Böhme, B., Handa, C., Kamiri, H.W., Langensiepen, M., Menz, G., Misana, S., Mogha, N.G., Möseler, B.M., Mwita, E.J., Oyieke, H.A., Wijk, M.T., 2011. Classification, Characterisation, and Use of Small Wetlands in East Africa. Wetlands 31, 1103–1116. doi:10.1007/s13157-011-0221-4

Schäfer, M.P., Dietrich, O., Mbilinyi, B., 2015. Streamflow and lake water level changes and their attributed causes in Eastern and Southern Africa: state of the art review. Int. J. Water Resour. Dev. 0627, 853–880. doi:10.1080/07900627.2015.1091289

Scheffer, F., Schachtschabel, P., 2010. Lehrbuch der Bodenkunde, Geoforum. doi:10.1016/0016-7185(72)90096-6

Schneider, C., Laizé, C.L.R., Acreman, M.C., Flörke, M., 2013. How will climate change modify river flow regimes in Europe? Hydrol. Earth Syst. Sci. 17, 325–339. doi:10.5194/hess-17-325-2013

Schulla, J., 2017. Model Description WaSiM. Hydrology Software Consulting J. Schulla, Zürich.

Seibert, J., Vis, M.J.P., 2012. Teaching hydrological modeling with a user-friendly catchment-runoff-model software package. Hydrol. Earth Syst. Sci. 16, 3315–3325. doi:10.5194/hess-16-3315-2012

Seregina, L.S., Fink, A.H., van der Linden, R., Elagib, N.A., Pinto, J.G., 2018. A new and flexible rainy season definition: Validation for the Greater Horn of Africa and application to rainfall trends. Int. J. Climatol. 39, 989–1012. doi:10.1002/joc.5856

Sharpley, A.N., Williams, J.R., 1990. EPIC-Erosion Productivity Impact Calculator, 1. model documentation, Tech. Bull. ed. U.S. Department of Agriculture, Agricultural Research Service.

Sheikheldin, G.H., 2015. Ujamaa: Planning and Managing Development Schemes in Africa, Tanzania as a Case Study. J. Pan African Stud. 8, 78–96.

Shongwe, M.E., van Oldenborgh, G.J., van den Hurk, B., van Aalst, M., Shongwe, M.E., Oldenborgh, G.J. van, Hurk, B. van den, Aalst, M. van, 2011. Projected Changes in Mean and Extreme Precipitation in Africa under Global Warming. Part II: East Africa. J. Clim. 24, 3718–3733. doi:10.1175/2010JCLI2883.1

Sloan, P.G., Moore, I.D., 1984. Modeling subsurface stormflow on steeply sloping forested watersheds. Water Resour. Res. 20, 1815–1822. doi:10.1029/WR020i012p01815

Smakhtin, V.U., 2001. Low flow hydrology: A review. J. Hydrol. 240, 147–186. doi:10.1016/S0022-1694(00)00340-1

Soil Conservation Service (ed.), 1972. Hydrology, in: National Engineering Handbook.

Sommer, H., Kröner, A., Lowry, J., 2017. Neoproterozoic eclogite- to high-pressure granulite-facies metamorphism in the Mozambique belt of east-central Tanzania: A petrological, geochemical and geochronological approach. Lithos 284–285, 666–690. doi:10.1016/J.LITHOS.2017.05.010

Steffens, V., Hartmann, G., Dannenberg, P., 2019. Eine neue Generation von Wachstumskorridoren als Entwicklungsmotor in Afrika? Standort 43, 2–8. doi:10.1007/s00548-019-00565-6

Stevenson, N., Frazier, S., 1999. Review of wetland inventory information in Africa, in: Spiers, A.G.,

Finlayson, C.M. (Eds.), Global Review of Wetland Resources and Priorities for Wetland Inventory. pp. 105–201.
Strauch, M., Volk, M., 2013. SWAT plant growth modification for improved modeling of perennial vegetation in the tropics. Ecol. Modell. 269, 98–112. doi:10.1016/j.ecolmodel.2013.08.013
Tang, Q., Gao, H., Lu, H., Lettenmaier, D.P., 2009. Remote sensing: hydrology. Prog. Phys. Geogr. 33, 490–509. doi:10.1177/0309133309346650
Tang, Q., Oki, T., 2016. Terrestrial Water Cycle and Climate Change : Natural and Human-Induced Impacts. Wiley, Hoboken. doi:10.1002/9781118971772.ch6
Tarnavsky, E., Grimes, D., Maidment, R., Black, E., Allan, R.P., Stringer, M., Chadwick, R., Kayitakire, F., 2014. Extension of the TAMSAT Satellite-Based Rainfall Monitoring over Africa and from 1983 to Present. J. Appl. Meteorol. Climatol. 53, 2805–2822. doi:10.1175/JAMC-D-14-0016.1
Tenczer, V., Fritz, H., Bauernhofer, A., Hauzenberger, C., 2007. Two orogens – One shear belt: 1Ga of repeated deformation along the Central Tanzanian Shear Belt. J. Struct. Geol. 29, 1632–1649. doi:10.1016/j.jsg.2007.06.004
Teng, J., Jakeman, A.J., Vaze, J., Croke, B.F.W., Dutta, D., Kim, S., 2017. Flood inundation modelling: A review of methods, recent advances and uncertainty analysis. Environ. Model. Softw. 90, 201–216. doi:10.1016/j.envsoft.2017.01.006
Teng, J., Potter, N.J., Chiew, F.H.S., Zhang, L., Wang, B., Vaze, J., Evans, J.P., 2015. How does bias correction of regional climate model precipitation affect modelled runoff? Hydrol. Earth Syst. Sci. 19, 711–728. doi:10.5194/hess-19-711-2015
Themeßl, M.J., Gobiet, A., Heinrich, G., 2012. Empirical-statistical downscaling and error correction of regional climate models and its impact on the climate change signal. Clim. Change 112, 449–468. doi:10.1007/s10584-011-0224-4
Thonfeld, F., Steinbach, S., Muro, J., Hentze, K., Games, I., Näschen, K. Land use/ land cover change assessment in the protected areas of the Kilombero catchment, Tanzania. Unpublished.
Troch, P.A., Berne, A., Bogaart, P., Harman, C., Hilberts, A.G.J., Lyon, S.W., Paniconi, C., Pauwels, V.R.N., Rupp, D.E., Selker, J.S., Teuling, A.J., Uijlenhoet, R., Verhoest, N.E.C., 2013. The importance of hydraulic groundwater theory in catchment hydrology: The legacy of Wilfried Brutsaert and Jean-Yves Parlange. Water Resour. Res. 49, 5099–5116. doi:10.1002/wrcr.20407
Tucker, C.J., 1979. Red and photographic infrared linear combinations for monitoring vegetation. Remote Sens. Environ. 8, 127–150. doi:10.1016/0034-4257(79)90013-0
Ulrich, A., 2014. Export-Oriented Horticultural Production in Laikipia, Kenya: Assessing the Implications for Rural Livelihoods. Sustain. 6, 336–347. doi:10.3390/su6010336
United States Geological Survey (USGS), n.d. EarthExplorer [WWW Document]. URL earthexplorer.usgs.gov
USGS Department of the Interior, n.d. Product Guide Landsat 8 Surface Reflectance Code (LASRC) Product Version 4.1 [WWW Document]. Prod. Guid. Landsat 8 Surf. Reflectance Code Prod. Version 4.1. URL https://landsat.usgs.gov/sites/default/files/documents/lasrc_product_guide.pdf (accessed 4.18.18a).
USGS Department of the Interior, n.d. Product Guide - Landsat 4 - 7 Surface Reflectance (LEDAPS) Product Version 8.0 [WWW Document]. Prod. Guid. - Landsat 4 - 7 Surf. Reflectance Prod. Version 8.0. URL https://landsat.usgs.gov/sites/default/files/documents/ledaps_product_guide.pdf (accessed 4.18.18b).
van Vliet, M.T.H., Franssen, W.H.P., Yearsley, J.R., Ludwig, F., Haddeland, I., Lettenmaier, D.P., Kabat, P., 2013. Global river discharge and water temperature under climate change. Glob. Environ. Chang. 23, 450–464. doi:10.1016/J.GLOENVCHA.2012.11.002
Vogelmann, J.E., Gallant, A.L., Shi, H., Zhu, Z., 2016. Perspectives on monitoring gradual change across the continuity of Landsat sensors using time-series data. Remote Sens. Environ. 185, 258–270.

doi:10.1016/J.RSE.2016.02.060

Vörösmarty, C.J., McIntyre, P.B., Gessner, M.O., Dudgeon, D., Prusevich, A., Green, P., Glidden, S., Bunn, S.E., Sullivan, C.A., Liermann, C.R., Davies, P.M., 2010. Global threats to human water security and river biodiversity. Nature 467, 555–561. doi:10.1038/nature09440

Wagner, P.D., 2013. Impacts of Climate Change and Land Use Change on the Water Resources of the Mula and Mutha Rivers Catchment upstream of Pune, India. Thesis. Universität Köln.

Wagner, P.D., Kumar, S., Schneider, K., 2013. An assessment of land use change impacts on the water resources of the Mula and Mutha Rivers catchment upstream of Pune, India. Hydrol. Earth Syst. Sci. 17, 2233–2246. doi:10.5194/hess-17-2233-2013

Wahr, J., Molenaar, M., Bryan, F., 1998. Time variability of the Earth's gravity field: Hydrological and oceanic effects and their possible detection using GRACE. J. Geophys. Res. Solid Earth 103, 30205–30229. doi:10.1029/98JB02844

Wambura, F.J., Dietrich, O., Graef, F., 2018. Analysis of infield rainwater harvesting and land use change impacts on the hydrologic cycle in the Wami River basin. Agric. Water Manag. 203, 124–137. doi:10.1016/j.agwat.2018.02.035

Wambura, F.J., Ndomba, P.M., Kongo, V., Tumbo, S.D., 2015. Uncertainty of runoff projections under changing climate in Wami River sub-basin. J. Hydrol. Reg. Stud. 4, 333–348. doi:10.1016/j.ejrh.2015.05.013

Wilk, J., Hughes, D.A., 2002. Simulating the impacts of land-use and climate change on water resource availability for a large south Indian catchment. Hydrol. Sci. J. 47, 19–30. doi:10.1080/02626660209492904

Williams, A.P., Funk, C., 2011. A westward extension of the warm pool leads to a westward extension of the Walker circulation, drying eastern Africa. Clim. Dyn. 37, 2417–2435. doi:10.1007/s00382-010-0984-y

Williams, J.R., 1995. The EPIC Model., in: Computer Models of Watershed Hydrology. Highlands Ranch, CO., pp. 909–1000.

Williams, J.R., Hann, R.W., 1972. Hymo, A problem-oriented computer language for building hydrologic models. Water Resour. Res. 8, 79–86. doi:10.1029/WR008i001p00079

Wilson, E., McInnes, R., Mbaga, D.P., Ouedaogo, P., 2017. Ramsar Advisory Mission Report: United Republic of Tanzania, Kilombero Valley. Gland, Switzerland.

WREM International Inc., 2015. Rufiji Basin IWRMDP Final Report. Volume I: Rufiji IWRMD Plan. Georgia.

WREM International Inc., 2013. Rufiji Basin IWRMD Plan: Draft Interim Report II. Executive Summary: Preliminary Assessment Findings and Planning Recommendations.

WWAP (UNESCO World Water Assessment Programme), 2019. The United Nations World Water Development Report 2019: Leaving No One Behind, Unesco. Paris.

Yamamoto, K.H., Finn, M.P., 2012. Approximating Tasseled Cap Values to Evaluate Brightness, Greenness, and Wetness for the Advanced Land Imager (ALI).

Yanda, P.Z., Munishi, P.K.T., 2007. Hydrologic and land use/cover change analysis for the Ruvu River (Uluguru) and Sigi River (East Usambara) watersheds.

Yang, W., Long, D., Bai, P., 2019. Impacts of future land cover and climate changes on runoff in the mostly afforested river basin in North China. J. Hydrol. 570, 201–219. doi:10.1016/j.jhydrol.2018.12.055

Yawson, D.K., Kongo, V.M., Kachroo, R.K., 2005. Application of linear and nonlinear techniques in river flow forecasting in the Kilombero River basin, Tanzania. Hydrol. Sci. J. 50, 37–41. doi:10.1623/hysj.2005.50.5.783

Yeo, I.-Y., Lang, M.W., Lee, S., McCarty, G.W., Sadeghi, A.M., Yetemen, O., Huang, C., 2019a. Mapping landscape-level hydrological connectivity of headwater wetlands to downstream waters: A

geospatial modeling approach - Part 1. Sci. Total Environ. 653, 1546–1556. doi:10.1016/J.SCITOTENV.2018.11.238

Yeo, I.-Y., Lee, S., Lang, M.W., Yetemen, O., McCarty, G.W., Sadeghi, A.M., Evenson, G., 2019b. Mapping landscape-level hydrological connectivity of headwater wetlands to downstream waters: A catchment modeling approach - Part 2. Sci. Total Environ. 653, 1557–1570. doi:10.1016/J.SCITOTENV.2018.11.237

Yira, Y., Diekkrüger, B., Steup, G., Bossa, A.Y., 2017. Impact of climate change on hydrological conditions in a tropical West African catchment using an ensemble of climate simulations. Hydrol. Earth Syst. Sci. 21, 2143–2161. doi:10.5194/hess-21-2143-2017

Yira, Y., Diekkrüger, B., Steup, G., Bossa, A.Y., 2016. Modeling land use change impacts on water resources in a tropical West African catchment (Dano, Burkina Faso). J. Hydrol. 537, 187–199. doi:10.1016/j.jhydrol.2016.03.052

Zemandin, B., Mtalo, F., Mkhandi, S., Kachroo, R., McCartney, M., 2011. Evaporation Modelling in Data Scarce Tropical Region of the Eastern Arc Mountain Catchments of Tanzania. Nile Basin Water Sci. Eng. J. 4, 1–13.

Zimmermann, B., Elsenbeer, H., De Moraes, J.M., 2006. The influence of land-use changes on soil hydraulic properties: Implications for runoff generation. For. Ecol. Manage. 222, 29–38. doi:10.1016/J.FORECO.2005.10.070

Zorita, E., Tilya, F.F., 2002. Rainfall variability in Northern Tanzania in the March-May season (long rains) and its links to large-scale climate forcing. Clim. Res. 20, 31–40. doi:10.3354/cr020031

9. Publications

9.1. Peer reviewed journal articles

Näschen, K., Diekkrüger, B., Evers, M., Höllermann, B., Steinbach, S., Thonfeld, F., 2019. The Impact of Land Use/Land Cover Change (LULCC) on Water Resources in a Tropical Catchment in Tanzania under Different Climate Change Scenarios. Sustainability 2019, Vol. 11, 7083. doi:10.3390/SU11247083

Koubodana, D.H., Diekkrüger, B., Näschen, K., Adounkpe, J., Atchonouglo, K., 2019. Impact of the Accuracy of Land Cover Data sets on the Accuracy of Land Cover Change Scenarios in the Mono River Basin, Togo, West Africa. Int. J. Adv. Remote Sens. GIS 8, 3073–3095. doi:10.23953/cloud.ijarsg.422

Näschen, K., Diekkrüger, B., Leemhuis, C., Seregina, L.S. und R. van der Linden (2019): Impact of Climate Change on Water Resources in the Kilombero Catchment in Tanzania. Water 11, 859. doi:10.3390/W11040859

Op de Hipt, F., Diekkrüger, B., Steup, G., Yira, Y., Hoffmann, T., Rode, M., Näschen, K. (2019): Modeling the effect of land use and climate change on water resources and soil erosion in a tropical West African catchment (Dano, Burkina Faso) using SHETRAN. Science of The Total Environment. Vol. 653, Page 431-445, doi: 10.1016/j.scitotenv.2018.10.351

Gabiri G., Leemhuis, C., Diekkrüger, B., Näschen, K., Steinbach, S., Thonfeld, F. (2019): Modelling the impact of land use management on water resources in a tropical inland valley catchment of central Uganda, East Africa. Science of the Total Environment. Vol. 653, Page 1052-1066, doi: 10.1016/j.scitotenv.2018.10.430

Näschen, K., Diekkrüger, B., Leemhuis, C., Steinbach, S., Seregina, L., Thonfeld, F. & R. van der Linden (2018): Hydrological Modeling in Data-Scarce Catchments - The Kilombero Floodplain in Tanzania. Water 2018, Vol. 10, Page 599 10, 599. doi:10.3390/W10050599

Gabiri, G., Burghof, S., Diekkrüger, B., Steinbach, S. & K. Näschen (2018): Modeling Spatial Soil Water Dynamics in a Tropical Floodplain, East Africa. Water 10, 1–27. doi:10.3390/w10020191

Gabiri, G., Diekkrüger, B., Leemhuis, C., Burghof, S., Näschen, K., Asiimwe, I. & Y. Bamutaze (2018): Determining hydrological regimes in an agriculturally used tropical inland valley wetland in Central Uganda using soil moisture, groundwater, and digital elevation data. Hydrol. Process. 32, 349–362. doi:10.1002/hyp.11417

Daniel, S., Gabiri, G., Kirimi, F., Glasner, B., Näschen, K., Leemhuis, C., Steinbach, S. & K. Mtei (2017): Spatial Distribution of Soil Hydrological Properties in the Kilombero Floodplain, Tanzania. Hydrology 4, 57. doi:10.3390/hydrology4040057

Leemhuis, C., Thonfeld, F., Näschen, K., Steinbach, S., Muro, J., Strauch, A., López, A., Daconto, G., Games, I. & B. Diekkrüger (2017): Sustainability in the food-water-ecosystem nexus - The role of land use and land cover change for water resources and ecosystems in the Kilombero Wetland, Tanzania. Sustain. 9. doi:10.3390/su9091513

Leemhuis, C., Amler, E., Diekkrüger, B., Gabiri, G. & K. Näschen (2016): East African wetland-catchment data base for sustainable wetland management. Proc. Int. Assoc. Hydrol. Sci. 374, 123–128. doi:10.5194/piahs-374-123-2016

9.2. Conference contributions

Näschen, K., Diekkrüger, B., Leemhuis, C., Steinbach, S., Seregina, L.S., Thonfeld, F. & R. van der Linden (2018): Hydrological modeling of a data scarce catchment in East Africa. Poster presentation at: Summer School: "Sustainability in the FOOD-WATER-ECOSYSTEM Nexus in Sub Saharan Africa in support of the SDG's: Sustainable wetland use", 12.-18.03.2018, Kampala, Uganda.

Näschen, K., Diekkrüger, B., Leemhuis, C., Steinbach, S., Seregina, L., Thonfeld, F. & R. van der Linden (2017): Land use and climate changes in the Kilombero catchment and their potential impact on water resources. Oral presentation at: Water Management Workshop - The Kilombero case: From Catchment to Consumer, 09.-10.10.2017, Morogoro, Tanzania.

Näschen, K., Diekkrüger, B., Ermert, V., Leemhuis, C., Steinbach, S., Thonfeld, F. & R. van der Linden (2017): Applying the Soil and Water Assessment Tool (SWAT) to estimate impacts of land use and climate change on water resources in a data scarce catchment in Tanzania. Oral Presentation at: SWAT International 2017 Conference, 26.-30.06.2017, Warsaw, Poland.

Näschen, K., Beuel, S., Diekkrüger, B., Gabiri, G., Leemhuis, C., Müller, A. & M. Ziegler (2015): Hydrological modeling on multiple scales in a data scarce catchment in East Africa. Poster presentation at: Water Resources Assessment & Seasonal Prediction, 13.-16.10.2015, Koblenz, Germany.

Näschen, K., Diekkrüger, B. & C. Leemhuis (2015): Regional scale wetland-catchment interactions in East Africa. Oral presentation at: 12. PhD candidate Workshop "AG-HydMod", 28.-29.05.2015, Munich, Germany.